

UNIVERSITY OF MARIBOR
FACULTY OF MECHANICAL ENGINEERING

Doctoral Thesis

**SUSPENSION AND STEERING SYSTEM
DEVELOPMENT OF A FOUR WHEEL DRIVE AND
FOUR WHEEL STEERED TERRAIN VEHICLE**

March, 2013

M. Sc. Shpetim LAJQI



Univerza v Mariboru

Fakulteta za strojništvo

Doctoral Thesis

**SUSPENSION AND STEERING SYSTEM
DEVELOPMENT OF A FOUR WHEEL DRIVE AND
FOUR WHEEL STEERED TERRAIN VEHICLE**

March, 2013

Author: M. Sc. Shpetim LAJQI

Mentor: Assoc. Prof. Dr. Stanislav PEHAN

Co-mentor: Prof. Dr. Jože FLAŠKER

Author:	Shpetim LAJQI, M. Sc., B. Sc. Mech. Eng.
Title:	Suspension and Steering System Development of a Four Wheel Drive and Four Wheel Steered Terrain Vehicle
UDC classification:	629.373.027.2/.3(043.3)
Keywords:	terrain vehicle, suspension system, steering system, four wheel steering
Processing of text and graphics:	Shpetim LAJQI, M. Sc., B. Sc. Mech. Eng.
Proofreading:	George Yeoman, English Lector, MA.
Number of copies:	11

ACKNOWLEDGEMENTS

I would like to express my gratitude and appreciation to my mentor: Assoc. Prof. Dr. Stanislav Pehan and co-mentor: Prof. Dr. Jože Flašker for their continuing support and guidance throughout my years at the University of Maribor. I would also like to thank Assoc. Prof. Dr. Mark Kegl, for his constructive advice and effort. Special thanks to Mr. Jože Pšeničnik and his team at “RTC” Company in Maribor, where I was part of his project.

At the same time I would like to express my thanks to Prof. Dr. Mujë Rugova, former rector of the University of Prishtina and Prof. Dr. Musli Bajraktari, Dean of Faculty of Mechanical Engineering for my selection by the academic staff of the University of Prishtina to continue my doctoral studies at University of Maribor as part of an agreement between the two rectors of the University of Maribor and the University of Prishtina.

For financial support my thanks go to the Slovene Human Recourses Development Scholarship Fund, and the University of Maribor.

Further thanks go to my parents and family for their dedication, love and care. Finally, I would like to thanks my dearest wife Mirlinda and our children Enea, Dea, and Euron, who have always, be so patient and supportive throughout all the tough times.

CONTAINS

1 INTRODUCTION	1
1.1 Background.....	1
1.2 Problem definition.....	2
1.2.1 Methodology for examining problem	4
1.3 Expected original scientific contribution	4
1.4 Research objectives	5
1.5 Structure of the doctoral thesis.....	6
2 LITERATURE STUDY	8
2.1 Historical evolution	8
2.2 Function and classification of the suspension system.....	11
2.2.1 The solid axle suspension system.....	12
2.2.2 The independent suspension system.....	13
2.2.3 The controllability strategies for the damping system.....	15
2.3 Functions and classifications of the steering systems	16
2.3.1 Power steering system	17
2.4 Four wheels steering systems.....	18
2.4.1 Mechanical four wheels steering system	18
2.4.2 Hydraulic four wheels steering system.....	19
2.4.3 Electro-hydraulic four wheels steering system	19
2.4.4 Advantages of four wheels steering system.....	20
2.5 Current research into the suspension and steering systems.....	20
2.5.1 The current research being performed regarding suspension systems	21
2.5.2 The current researches on the steering systems.....	23
3 RESEARCH METHODOLOGY	25
3.1 Literature study.....	25
3.2 Design processes by applying CAD systems	25
3.2.1 Conceptual design.....	25
3.2.2 Preliminary design.....	26
3.2.3 Embodiment design	27
3.2.4 Detail design.....	27
3.3 Numerical analyses methods.....	28
3.4 Mathematic modeling and simulation	30
3.5 Optimization of the mechanical systems	31
3.5.1 Numerical optimization method.....	31
3.5.2 Optimization method based on a Genetic Algorithms.....	32
4 DEVELOPMENT OF THE SUSPENSION SYSTEM.....	33
4.1 Motivation, design requirement, constraints and terminology.....	33
4.1.1 Wheelbase of the vehicle l	35
4.1.2 Track width of the vehicle w	36
4.1.3 Sprung and un-sprung masses of the vehicle m_s and m_u	36
4.1.4 Design constraints and restrictions	36

4.2	Geometric parameters involved in the suspension system	37
4.2.1	Suspension geometry	37
4.2.2	Camber angle γ	38
4.2.3	Camber steer.....	40
4.2.4	Kingpin inclination angle and kingpin offset.....	41
4.3	Design process for developing of the suspension system.....	44
4.3.1	The first design concept.....	44
4.3.2	The second design concept.....	47
4.3.3	The final design concept.....	50
4.3	Discussing of the results	54
5	MODELING, SIMULATION AND OPTIMIZATION OF THE SUSPENSION MECHANISM FOR A TERRAIN VEHICLE	55
5.1	Kinematic modeling and analyses of the suspension mechanism.....	56
5.1.1	Displacement analysis of the suspension mechanism	56
5.1.1.1	Vector loops and vector position	57
5.1.1.2	Determining of the wheel path and other characteristic of the suspension mechanism	65
5.1.1.3	Comparison of the obtained results between developed program and the commercial Working Model Software.....	67
5.1.2	Velocities analysis of the suspension mechanism.....	69
5.1.4	Accelerations analysis of the suspension mechanism	70
5.2	Dynamic modeling of forces that acts on the suspension mechanism.....	71
5.2.1	Dynamic equation of the free bodies.....	75
5.3	Simulation of the terrain vehicle suspension mechanism.....	76
5.4	Optimization of the suspension mechanism.....	81
5.4.1	The problem of optimum design	81
5.4.2	The modeling of the suspension mechanism by the finite elements	83
5.4.3	The optimum design of the suspension mechanism	84
5.5	Discussing of the results	87
6	DESIGNS AND OPTIMIZATIONS OF PASSIVE, ACTIVE AND SEMI-ACTIVE SUSPENSION SYSTEMS FOR A TERRAIN VEHICLE.....	88
6.1	Mathematic modeling of the quarter vehicle suspension system	89
6.1.1	Passive linear and non-linear suspension systems.....	90
6.1.2	Active and semi-active non-linear suspension systems.....	92
6.2	Simulation of vehicle suspension by numerical methods	94
6.3	Verifying the reliability of the developed program	96
6.4	Optimization of the suspension parameters for passive, active, and semi-active suspension systems	98
6.4.1	Optimization of the suspension parameters for a passive linear suspension system	98
6.4.1.1	Genetic Algorithms	99
6.4.1.2	Multi-objective optimization process by using the Genetic Algorithms	101
6.4.1.3	Optimization of the passive linear suspension design parameters.	102
6.4.2	Optimization of the design parameters for the active and semi-active non-linear suspension systems.....	106

6.5	Simulation of the vehicle's suspension by using MATLAB/Simulink	107
6.6	Discussion of the results	112
7	DEVELOPMENT OF THE FOUR WHEEL STEERING SYSTEM FOR THE 4x4 TERRAIN VEHICLE.....	114
7.1	Kinematics of the two/four wheels steering system	115
7.1.1	Kinematics of the two-wheels steering system	115
7.1.2	Kinematics of the four-wheels steering system.....	117
7.2	Steering system for a terrain vehicle	119
7.2.1	Determining the steering wheel angles for the terrain vehicle in the 2WS mode	119
7.2.2	Determining of the steering wheel angles for the terrain vehicle in the 4WS mode	121
7.3	Design of the steering mechanism for a terrain vehicle.....	125
7.3.1	Design of the trapezoid steering mechanism for front wheels steering.....	126
7.3.2	Design of the vehicle steering mechanism with 2WS by using non-circular gears	129
7.3.2.1	Work principles of the steering mechanism with 2WS by using non-circular gears	134
7.3.3	Design of the vehicle's steering mechanism with 4WS by using non-circular gears	135
7.3.3.1	Work principles of the steering mechanism with 4WS by using non-circular gears	138
7.3.4	Design of the steering mechanism with 2WS/4WS for terrain vehicle	139
7.3.4.1	Work principles of the steering mechanism with 2WS/4WS	139
7.4	Discussion of the results	141
8	SUMMARY AND CONCLUSION	142
	LIST OF USED SOURCES	145
	APPENDICES	154
	Appendix A: Free body diagrams and forces that act in mechanism.....	155
	Appendix B: Simulation and optimization of the suspension parameters for passive, semi-active and active suspension systems for a terrain vehicle	166
	Appendix C: Design of the developed terrain vehicle	170
	Appendix D: Bibliography of the candidate	172
	Appendix E: Curriculum Vitae	178

LIST OF FIGURES

Figure 1.1:	Schematic presentation of the main dimensions for a new terrain vehicle	3
Figure 2.1:	Coach, constructed around 1650 years, exhibited in Automobile Museum in Turin	8
Figure 2.2:	Single rigid axle suspension system, invented by Elliot in 1804 years.....	9
Figure 2.3:	Steering mechanism for two axes coaches; a) steering by rotation of whole front axle, and b) steering by rotating only front wheels around the kingpin axis	9
Figure 2.4:	First automobile with an ICE, constructed by Karl Benz 1886.....	10
Figure 2.5:	Suspension and steering system for front axle.....	12
Figure 2.6:	A solid axle suspension system with leaf spring; a) front view, and b) side view.....	12
Figure 2.7:	The independent suspension system - front view	13
Figure 2.8:	Design of the independent suspension systems; a) MacPherson strut, b) double wishbone, and c) multi-link suspension system	14
Figure 2.9:	Quarter vehicle models; a) passive, b) active, and c) semi-active systems.....	15
Figure 2.10:	Mechanical front wheels steering system.....	16
Figure 2.11:	Hydraulic power steering system.....	17
Figure 2.12:	Electric amplifier system.....	17
Figure 2.13:	Mechanical four wheels steering system.....	18
Figure 2.14:	Hydraulic four wheels steering system	19
Figure 3.1:	Flowchart diagram showing the stages of the design process	26
Figure 3.2:	Modeling of a quarter of the suspension system by splitting into discrete portions - FE (modeling is performed by using Pro/Engineer and STAKx software).....	29
Figure 3.3:	Moving capabilities of FE mapping of nodes.....	29
Figure 3.4:	Flowchart diagram of FEA process.....	30
Figure 3.5:	Flowchart diagram of the mathematic modeling and simulation processes.....	31
Figure 4.1:	Terrain vehicle with four wheel drive and front wheel steering.....	34
Figure 4.2:	Basic geometric dimensions of the terrain vehicle	35
Figure 4.3:	Schematic model of a quarter of the vehicle's suspension system	36
Figure 4.4:	Suspension motions; a) bound, b) rest, and c) rebound	38
Figure 4.5:	Vertical wheel position; a) positive, b) zero, and c) negative camber angle	38
Figure 4.6:	Lateral tire forces as a function of positive camber angle	39
Figure 4.7:	Life expectancy of the tire as a function of camber angle.....	39
Figure 4.8:	Positive camber steer; a) front view, and b) plan view	40
Figure 4.9:	Principle of camber steer; a) negative camber steer, and b) positive camber steer	41
Figure 4.10:	Kingpin inclination angle and kingpin offset; a) side view, and b) front view ..	42
Figure 4.11:	The kingpin offset cases; a) positive, b) negative, and c) zero	43
Figure 4.12:	Front view of quarter double wishbone suspension system; a) longer, and b) shorter non-equal control arms.....	45
Figure 4.13:	Path of wheel for the suspension system with double wishbone longer and shorter non-equal control arms	46
Figure 4.14:	Vertical motion of the wheel as a function of the camber angle for suspension system with double wishbone longer and shorter non-equal control arms	47
Figure 4.15:	Front view of quarter double wishbone suspension system with longer equal control arms.....	48

Figure 4.16: Path of wheel for the suspension system with double wishbone longer non-equal length of control arm	49
Figure 4.17: Vertical motion of the wheel as a function of the camber angle for the suspension system with double wishbone longer non-equal and equal control arms	49
Figure 4.18: Final design of the 3D quarter suspension system for the terrain vehicle.....	51
Figure 4.19: Frontal view of the 2D quarter suspension system for the terrain vehicle	51
Figure 4.20: Path of wheel for the suspension system with double wishbone longer equal control arms and final design	52
Figure 4.21: Vertical motion of the wheel as a function of the camber angle for the suspension system with double wishbones longer equal control arms and final design	53
Figure 4.22: Final design of the terrain vehicle suspension system; a) 3D view, b) front view, and c) plane view.....	54
Figure 5.1: Kinematic linkages of the terrain vehicles suspension mechanism	56
Figure 5.2: Vector loops of four-bar links derived from the suspension mechanism.....	57
Figure 5.3: Output angular displacement θ_1 as a function of input angular displacement θ_3	60
Figure 5.4: Coupler angular displacement θ_2 as a function of input angular displac. θ_3	61
Figure 5.5: Vector loops of three-bar links derived from the suspension mechanism.....	62
Figure 5.6: Length of spring-shock absorber L_s as a function of input angular displacement θ_3	63
Figure 5.7: Output θ_9 as a function of input angular displacement θ_3	64
Figure 5.8: Vector loops of four-bar links derived from the suspension mechanism.....	64
Figure 5.9: Vertical motion of center of wheel $Z_M(\theta_3)$ as a function of input angular displacement θ_3	66
Figure 5.10: Lateral motion of center of wheel $Y_M(\theta_3)$ as a function of input angular displacement θ_3	66
Figure 5.11: Path of wheel regarding the suspension mechanism.....	67
Figure 5.12: Modeling of the suspension mechanism in WM environment	68
Figure 5.13: Working principles of the spring; a) compression, b) free, and c) extension.....	71
Figure 5.14: Convention sign used for a linear spring force as a function of spring length ..	72
Figure 5.15: Convention sign used for a linear damper force as a function of piston velocity	73
Figure 5.16: Free-body diagram of a vehicle during braking (longitudinal weight transfer) .	73
Figure 5.17: Simulation of ground configuration by using a hydraulic actuator	76
Figure 5.18: Ground excitation $z_r(t)$ and motion of wheel $Z_M(t)$ as a function of time.....	77
Figure 5.19: Kinematic results obtained in Working Model Software	81
Figure 5.20: Modeling of terrain vehicle suspension system by Finite Elements in STAKx software; a) side view, b) front view, c) plane view, and d) 3D view	83
Figure 5.21: Analyzing of vertical wheel motion by Finite Elements in STAKx	84
Figure 5.22: The optimization procedure for obtaining optimal design variables	84
Figure 5.23: Optimization procedure performed in iGOx environment	85
Figure 5.24: Path of wheel for initial and optimal designs variables of the terrain vehicle suspension mechanism.....	86
Figure 6.1: The passive linear and non-linear quarter-vehicle models.....	90
Figure 6.2: Skyhook concept for active and semi-active non-linear suspension systems	92
Figure 6.3: Flowchart diagram for solving differential equations of motion.....	95
Figure 6.4: Ground excitation represented by double cosine road bumps.....	96
Figure 6.5: Laboratory devices for determining suspension characteristics	97

Figure 6.6: a) Ground excitation, and b) vertical vehicle body displacements	97
Figure 6.7: GAs evaluation process.....	99
Figure 6.8: Genetic operators (crossover and mutation).....	101
Figure 6.9: Optimization process; a) Single point between two objective functions, and b) average distance between individuals as a function of generation	104
Figure 6.10: Percentage of generation as a function of criteria met over the forth runs	105
Figure 6.11: Initial and optimal values for objectives functions, as functions of vehicle speed: a) Vehicle's body acceleration - $\sigma_{\ddot{z}_s}$, and b) Dynamic tire forces - σ_{F_t}	105
Figure 6.12: Flowchart diagram for optimization design variables for damping force.....	106
Figure 6.13: Flowchart diagram for the simulation ground excitation, the vehicle's body accelerations, velocities, displacements, and tire forces as functions of time for passive linear suspension system	108
Figure 6.14: Flowchart diagram for simulation ground excitation, vehicle's body accelerations, velocities, displacements, and vertical tire forces as functions of time for non-linear active, semi-active, and passive suspension systems ...	108
Figure 6.15: Ground excitation as a function of time	109
Figure 6.16: Vehicle's body accelerations as a function of time for passive linear system .	109
Figure 6.17: Vehicle's body velocities as a function of time for passive linear system.....	110
Figure 6.18: Vehicle's body displacement as a function of time for passive linear system .	110
Figure 6.19: Vertical tire forces as a function of time for passive linear system	110
Figure 6.20: Vehicle's body accelerations as a function of time	111
Figure 6.21: Vehicle's body velocities as a function of time.....	111
Figure 6.22: Vehicle's body displacements as a function of time.....	111
Figure 6.23: Vertical tire forces as a function of time	112
Figure 7.1: Operation modes of the 4WS; a) counter steer, b) neutral steer, and c) same steer	114
Figure 7.2: Turning of the terrain vehicle towards the left side using the 2WS system.....	116
Figure 7.3: Turning of the terrain vehicle towards the left side using the 4WS system.....	117
Figure 7.4: Turning of the vehicle with 2WS; a) on the left side, and b) on the right side	120
Figure 7.5: Steering angle for the front wheels as a function of the steering wheel angle .	121
Figure 7.6: Turning of the 4WS system; a) towards the left side, and b) towards the right side.....	122
Figure 7.7: Steering angles for the front and rear wheels as a function of the steering wheel angle φ when the vehicle with 4WS turns; a) towards the left side, and b) towards the right side	123
Figure 7.8: Terrain vehicle's turning radius when operates in the 2WS and 4WS modes .	124
Figure 7.9: Vehicle turning radius as a function of steering wheel angles φ for 2WS and 4WS.....	124
Figure 7.9: Terrain vehicle's turning radius when operates in the 2WS and 4WS modes .	124
Figure 7.10: Road vehicle steering mechanism; a) rack and pinion, b) lever arm, c) drag link and d) multi-link	125
Figure 7.11: Trapezoidal steering mechanism; a) straight-ahead position, b) turning towards the left side.....	126
Figure 7.12: Comparison between functionality of the trapezoidal steering mechanism for different β and Ackermann steering condition	127
Figure 7.13: The error parameter e for concrete trapezoidal steering mechanism	128
Figure 7.14: Cases of the bump steering; a) toe-out, b) straight-ahead direction and b) toe-in	129
Figure 7.15: a) The non-circular gears, and b) pitch curves of the non-circular gears.....	130

Figure 7.16: Working position of the two pair's non-circular gears when the front wheels of the terrain vehicle are turning towards the: a) left side, b) straight-ahead, and c) right side	131
Figure 7.17: Radiiuses of the pitch curves as a function of input angular displacement δ_l ...	132
Figure 7.18: Angular displacements $\delta_2(\delta_l)$ obtained from the Ackermann steering geometry and the non-circular gears' as a function of angular displacement..	133
Figure 7.19: Pitch curves of the non-circular gear given by the movable coordinate system	134
Figure 7.20: Steering mechanism for terrain vehicle with 2WS by using non-circular gears	135
Figure 7.21: The front and rear; a) angular displacements $\delta_{2ForR}(\delta_{lForR})$ of the driven non-circular gears, and b) pitch curves in the (x_i, y_i) for driving and driven non-circular gears	137
Figure 7.22: Steering mechanism for the terrain vehicle with 4WS	138
Figure 7.23: Steering mechanism of the terrain vehicle with 2WS/4WS	140
Figure A.1: Free-body diagram; a) Body 1, and b) Body 2	155
Figure A.2: Free-body diagram; a) Body 3, b) Body 4, and c) Body 5	156
Figure A.3: Free-body diagram for dynamic analysis of the; a) Body 6, and b) Body 7....	157
Figure A.4: Spring, damper, spring & damper and wheel forces as a function of the time.	160
Figure A.5: Reaction forces in the joint A as a function of the time	160
Figure A.6: Reaction forces in the joint C ₂ as a function of the time.....	161
Figure A.7: Reaction forces in the joint B as a function of the time	161
Figure A.8: Reaction forces in the joint D ₆ as a function of the time.....	162
Figure A.9: Reaction forces in the joint C ₄ as a function of the time.....	162
Figure A.10: Reaction forces in the joint D ₄ as a function of the time.....	163
Figure A.11: Reaction forces in the joint E as a function of the time	163
Figure A.12: Reaction forces in the joint G as a function of the time.....	164
Figure A.13: Reaction forces in the joint I as a function of the time	164
Figure A.14: Reaction forces in the joint H as a function of the time.....	165
Figure B.1: Parts of the MATLAB codes for solving differential equations of motion for passive non-linear suspension system	166
Figure B.2: Parts of the MATLAB codes for solving differential equations of motion for non-linear semi-active suspension system.....	167
Figure B.3: Configuration MATLAB/Simulink parameters for solving the differential equations of motion.....	168
Figure B.4: Windows of Multi Objective Genetic Algorithms performed in MATLAB Optimization Tool	168
Figure B.5: Flowchart diagram of the optimization process utilized in MOGAs	169
Figure C.1: 2D/3D modeling of the terrain vehicle with four wheels drive and four wheels steering performed in Pro/ENGINEER environment	170
Figure C.2: 3D modeling of a front and rear suspension mechanism, engine and driver performed in Pro/ENGINEER environment	171
Figure C.3: 3D modeling of a front and rear suspension mechanism and driver performed in Pro/ENGINEER environment	171

LIST OF TABLES

Table 1.1: Check list with main design characteristics utilized for developing of the suspension and steering systems	3
Table 4.1: Description of the used symbols for the terrain vehicle model.....	34
Table 4.2: Joint points and main lengths of the double wishbone suspension mechanism with longer non-equal control arms.....	45
Table 4.3: Joint points and main lengths of the double wishbone suspension mechanism with shorter non-equal control arms.....	45
Table 4.4: Join point and main lengths of the double wishbone suspension mechanism with longer equal control arms.....	48
Table 4.5: Joint points and main length of the suspension mechanism links	52
Table 5.1: Vector representation of the four-bar linkages shown in Figure 5.2.....	58
Table 5.2: Vector representation of the three-bar linkages shown in Figure 5.5.....	63
Table 5.3: Vector representation of the four-bar linkages shown in Figure 5.8.....	65
Table 5.4: Comparison of the obtained results between the developed programs performed in MathCAD and the commercial Working Model Software	68
Table 5.5: Dynamic load for different driven condition.....	75
Table 5.6: Data for simulation of the suspension mechanism	78
Table 5.7: Results comparison for angular displacement, velocity & acceleration obtained by the developed program performed in MathCAD and Working Model Software	78
Table 5.8: Results comparison for length, relative velocity & acceleration of the spring & shock absorber, obtained by developed program and Working Model Software	79
Table 5.9: Results comparison for total and projection in y and z-axis of velocities for mechanism components, obtained by developed program and Working Model Software.....	79
Table 5.10: Results comparison for total and projection in y and z-axis of acceleration for mechanism components, obtained by developed program and Working Model Software	80
Table 5.11: Position of joints connection and design variables.....	85
Table 5.12: Initial and optimal values of design variables.....	86
Table 6.1: Description data for road bumps when the vehicle passed over them.....	96
Table 6.2: The MOGAs parameters performed in the MATLAB GAs toolbox.....	103
Table 6.3: Initial and optimal suspension design parameters	104
Table 6.4: Suspension parameters used for optimization of the active damping-force	107
Table 6.5: Initial and optimal design variables for the active damping force	107
Table 7.1: The geometric characteristics of the steering system with 2WS.....	120
Table 7.2: The geometric characteristics of the steering system with 4WS.....	122
Table 7.3: Parameters for modeling non-circular gears for steering system with 2WS.....	132
Table 7.4: Parameters for modeling non-circular gears for steering system with 4WS.....	137

SUSPENSION AND STEERING SYSTEM DEVELOPMENT OF A FOUR WHEEL DRIVE AND FOUR WHEEL STEERED TERRAIN VEHICLE

Keywords: terrain vehicle, suspension system, steering system, four wheels steering

UDC classification: 629.373.027.2/.3(043.3)

ABSTRACT

The key goal of doctoral thesis was to conceive, design, optimize, and analyze the suspension and steering systems for a four wheel drive and four wheel steered terrain vehicle. The common characteristic of a terrain vehicle is the greater motion of the wheels in order to protect the vehicle from rollover risk when running over rough terrain. Known suspension and steering systems have serious weaknesses. In order to ensure good driving comfort, efficient driving safety, and higher maneuverability, new principles of suspension and steering systems are proposed.

The proposed suspension system has been successfully derived from a classical double wishbone control arm. The control arms are long but both equal. Greater wheel motion has been ensured without reducing driving performance. In order to improve the comfort and safety an optimal active damping force has been determined by the active and semi-active systems. On the basis of comprehensive analysis, active system adequacy has been achieved. The proposed suspension design provides relatively small lateral wheel motion, zero camber angles, and it effectively absorbs the vibrations caused by ground configurations.

The goal of the developed steering system for this terrain vehicle was to design a new steering mechanism that would provide maneuverability at low speed and suitable stability at higher speed. This has been ensured by two modes of steering, all wheel steer and front wheel steer. The proposed steering mechanisms conform to Ackermann steering geometry for all modes and situations. A totally new steering concept has been developed. This effective design consists of special pairs of gears, known as 'non-circular gears'.

RAZVOJ OBES IN KRMILNEGA SISTEMA TERENSKEGA VOZILA S ŠTIRIMI GNANIMI IN ŠTIRIMI KRMILJENIMI KOLESI

Ključne besede: terensko vozilo, obes sistem, krmilni sistem, štirikolesno krmiljenje

POVZETEK

Cilj doktorske disertacije je zasnovati, oblikovati, optimizirati in analizirati sistem obes in krmilja za štirikolesno vozilo, ki ima pogon in krmiljenje na vsa kolesa. Značilnost terenskih vozil so veliki pomiki koles, da se vozilo ne prevrne, ko se giblje po neravnem terenu. Znani sistemi obes in krmiljenja imajo slabosti. Za zagotavljanje višje udobnosti, varnosti vozila, in odzivnosti je treba razviti nove koncepte obes in nov krmilni sistem.

Predlagan sistem obes je učinkovita modifikacija dvojnega A-mehanizma z enakima, a dolgima rokama, kar zagotavlja velike vertikalne pomike koles, brez poslabšanja voznih karakteristik. Optimalna sila dušenja, ki je potrebna za izboljšanje udobja in varnosti, se ustvarja z navideznim oziroma resničnim aktivnim sistemom, ki je dodan sitemu obes. Obširne analize dokazujejo upravičenost uporabe aktivnih sistemov. Predlagani sistem obes učinkovito absorbira vibracije zaradi neravnin in zagotavlja relativno majhno bočno pomikanje koles, brez nepotrebnega nagibanja.

Cilj je razviti takšen krmilni sistem terenskega vozila, ki bi zagotavljal učinkovito upravljanje vozila pri nizkih hitrostih in zagotavljal stabilnost pri večjih hitrostih. To je izpolnjeno s krmiljem, ki deluje na dva različna načina. Pri enem načinu sta so aktivna vsa štiri kolesa, pri drugem pa samo sprednja. Predlagani krmilni mehanizem z gonili in gredmi deluje tako, da v vseh situacijah povsem sledi zakonitosti Ackermannova. Prikazan je koncept povsem novega principa učinkovitega krmilnega sistema, ki temelji na posebnih gonilih s specialnimi pari zobnikov.

LIST OF USED SYMBOLS

Symbol	Unit	Explanation of the used symbol
A, B, C, D, E, F, G, H, I		Joint points of the suspension mechanism
$A(\theta_3), B(\theta_3),$ $C(\theta_3)$		Constants for determining output angular displacement θ_1
$D(\theta_3), E(\theta_3),$ $F(\theta_3)$		Constants for determining angular displacement θ_2
a_{12}	[mm]	Distance of the rotation center for the non-circular gears
a_i	[mms ⁻²]	Absolute accelerations for links of the suspension mechanism
a_{Ls}	[mms ⁻²]	Relative acceleration of the spring & shock absorber (slider link)
a_M	[mms ⁻²]	Absolute acceleration at the centre of wheel
a_{MY}, a_{MZ}	[mms ⁻²]	Acceleration components at the centre of wheel in y and z - axis
a_x	[ms ⁻²]	Longitudinal vehicle acceleration
a_{yi}, a_{zi}	[mms ⁻²]	Accelerations of the suspension mechanism links in y_i and z_i axis
b	[mm]	Tire width
\mathbf{b}		Design variables
b_i		Design variables of the suspension mechanism links
b_s	[Nsm ⁻¹]	Virtual shock-absorber damping coefficient at the sprung mass
b_u	[Nsm ⁻¹]	Virtual shock-absorber damping coefficient at the un-sprung mass
c	[mm]	Longitudinal distance between turning center and front axle
c_{sh}	[Nsm ⁻¹]	Shock absorber damping coefficient
c_{sh1}	[Nsm ⁻¹]	Shock absorber non-linear damping coefficient
c_{sh2}	[Ns ² m ⁻²]	Shock absorber non-linear square damping coefficient
d	[mm]	Longitudinal distance between turning center and rear axle
d	[mm]	Tire diameter
e	[deg]	Error of the trapezoidal steering mechanism
E_k	[kgm ² s ⁻²]	Kinetic energy
$f(x)$		Multi objective function
$f_0(\mathbf{b}, \mathbf{u})$		Objective function
$\{f\}$	[N]	Global nodal vectors of the applied forces
F_a	[N]	Active damping force
F_{dyn-l}	[N]	Dynamic linear force
F_{dyn-n}	[N]	Dynamic non-linear force
F_{FW}, F_{RW}	[N]	Vertical static forces acting in one tire (front or rear tires)

F_{Fx}, F_{Rx}	[N]	Braking forces acting in the front and rear tires
F_{Fz}, F_{Rz}	[N]	Vertical forces acting in the front and rear tires
F_j	[N]	Reaction forces of the suspension mechanism joints
F_s	[N]	Spring force
F_{sh}	[N]	Shock absorber damping force
F_{sh-l}	[N]	Shock absorber linear damping force
F_{sh-n}	[N]	Shock absorber non-linear damping force
F_{s-l}	[N]	Linear spring force
F_{s-n}	[N]	Non-linear spring force
F_{sta}	[N]	Vertical static force
F_{t-l}	[N]	Dynamic linear tire force
F_{t-n}	[N]	Dynamic non-linear tire force
F_w	[N]	Wheel force
F_y	[N]	Lateral tire force
F_{yj}, F_{zj}	[N]	Components of the reaction forces at the i^{th} joints; $i = A \dots H$
F_z	[N]	Vertical tire force
F_{z-l}	[N]	Vertical linear tire force
F_{z-n}	[N]	Vertical non-linear tire force
g	[ms ⁻²]	Gravitational acceleration (9.81 ms ⁻²)
H	[mm]	Height of the vehicle
$h(x)$		Constraint function
H_1	[m]	Amplitude of the first bump
H_2	[m]	Amplitude of the second bump
h_{CG}	[mm]	Height from ground surface of the vehicle center gravity
$h_j(\mathbf{b}, \mathbf{u})$		Constraint function
i		Steering gear ratio
\mathbf{i}, \mathbf{j}		Unit vectors in the Cartesian coordinative system
$i_{12}(\delta_1)$		Gear ratio of the non-circular gears for the 2WS
$i_{12F}(\delta_{1F})$		Gear ratio of the front non-circular gears for the 4WS
$i_{12R}(\delta_{1R})$		Gear ratio of the rear non-circular gears for the 4WS
i^{th}		Nodes
J_{ci}	[kg·m ²]	Mass moment inertia of the suspension mechanism links
$[k]$	[Nm ⁻¹]	Global stiffness matrix of a structure
$[k]^{-1}$	[mN ⁻¹]	Global inverse stiffness matrix of a structure
k_s	[Nm ⁻¹]	Spring stiffness linear coefficient

k_{s1}	[Nm ⁻¹]	Spring stiffness non-linear coefficient
k_{s2}	[Nm ⁻²]	Spring stiffness non-linear square coefficient
k_t	[Nm ⁻¹]	Tire stiffness linear coefficient
k_{t1}	[Nm ⁻¹]	Tire stiffness non-linear coefficient
k_{t2}	[Nm ⁻²]	Tire stiffness non-linear square coefficient
k_{t3}	[Nm ⁻³]	Tire stiffness non-linear cube coefficient
l	[mm]	Wheelbase of the vehicle
L	[mm]	Length of the vehicle
$L_1(x_1, y_1)$		Pitch curve of the non-circular gear1 for the 2WS
$L_2(x_2, y_2)$		Pitch curve of the non-circular gear 2 for the 2WS
l_F	[mm]	Distance from the front axle to the vehicle center gravity
l_R	[mm]	Distance from the rear axle to vehicle the centre gravity
L_s	[mm]	Spring free length
$L_s(def)$	[mm]	Spring length in compression or extension cases
m	[kg]	Total mass of the terrain vehicle
m_i	[kg]	Mass of the suspension mechanism links
m_{n12}	[mm]	Module of the non-circular gears for the 2WS
m_{n12F}	[mm]	Module of the front non-circular gears for the 4WS
m_{n12R}	[mm]	Module of the rear non-circular gears for the 4WS
m_s	[kg]	Vehicle's body mass (sprung mass)
m_u	[kg]	Wheel assembly mass (un-sprung mass)
n		Number of design variables
n_c		Number of constraints
n_{obj}		Number of objective functions
P_e	[kW]	Engine power
r	[mm]	Trapezoid offset arms
$r_1(\delta_1)$	[mm]	Radius of the pitch curve for the non-circular gear 1 of the 2WS
$r_2(\delta_2)$	[mm]	Radius of the pitch curve for the non-circular gear 2 of the 2WS
$r_{1F}(\delta_{1F})$	[mm]	Radius of the pitch curve for the front non-circular gear 1 of the 4WS
$r_{1R}(\delta_{1R})$	[mm]	Radius of the pitch curve for the rear non-circular gear 1 of the 4WS
$r_{2F}(\delta_{2F})$	[mm]	Radius of the pitch curve for the front non-circular gear 2 of the 4WS
$r_{2R}(\delta_{2R})$	[mm]	Radius of the pitch curve for the rear non-circular gear 2 of the 4WS
R_{2WS}	[mm]	Vehicle turning radius at the center of rear axle
R_{2WSmax}	[mm]	Maximal vehicle turning radius for the 2WS mode
R_{2WSmin}	[mm]	Minimal vehicle turning radius for the 2WS mode

R_{4WS}	[mm]	Vehicle turning radius at the vehicle center gravity
R_{4WS}	[mm]	Maximal vehicle turning radius for 4WS mode
R_{4WSmin}	[mm]	Minimal vehicle turning radius for 4WS mode
\mathbf{R}_i	[mm]	Vectors position of the suspension mechanism links ($i^{th} = 1 \dots 9$)
r_i	[mm]	Length of the suspension mechanism links ($i^{th} = 1 \dots 9$)
$s(\theta_3)$	[mm]	Relative displacement of the spring & shock absorber
t	[s]	Time
$\{\mathbf{u}\}$	[mm]	Global nodal vectors displacement
$\mathbf{u}_i, \mathbf{v}_i, \mathbf{w}_i$	[mm]	Vector displacement of i^{th} nodes
v	[kmh ⁻¹]	Vehicle speed
v_1	[kmh ⁻¹]	Vehicle speed over the first bump
v_2	[kmh ⁻¹]	Vehicle speed over the second bump
v_i	[ms ⁻¹]	Absolute velocities of the suspension mechanism links
$v_{Ls}(t)$	[mms ⁻¹]	Relative velocity of the spring & shock absorber
v_M	[mms ⁻¹]	Absolute velocity at the centre of the wheel
v_{MY}, v_{MZ}	[mms ⁻¹]	Velocity components at the center of the wheel in y and z - axis
v_{yi}, v_{zi}	[mms ⁻¹]	Velocities of the suspension mechanism links in y_i and z_i axis
w	[mm]	Track width of the vehicle
W	[mm]	Width of the vehicle
x		Design variables
x, y, z	[mm]	Cartesian coordinative system
x_1, y_1	[mm]	Movable axis of the non-circular gear 1 for the 2WS
x_2, y_2	[mm]	Movable axis of the non-circular gear 2 for the 2WS
x_{1F}, y_{1F}	[mm]	Movable axis of the front non-circular gear 1 for the 4WS
x_{1R}, y_{1R}	[mm]	Movable axis of the rear non-circular gear 1 for the 4WS
x_{2F}, y_{2F}	[mm]	Movable axis of the front non-circular gear 2 for the 4WS
x_{2R}, y_{2R}	[mm]	Movable axis of the rear non-circular gear 2 for the 4WS
x_i	[m]	Part of road for simulation ground excitations
Y_E, Z_E	[mm]	Position at the joint E
Y_M, Z_M	[mm]	Position at the centre of the wheel
Y_N, Z_N	[mm]	Position at the bottom of the tire
z_{max}	[mm]	Bound wheel position +250 mm
z_{min}	[mm]	Rebound wheel position -250 mm
z_{rest}	[mm]	Rest wheel position 0 mm
z_r	[m]	Ground excitation

z_s	[m]	Vertical displacement of the sprung mass
z_u	[m]	Vertical displacement of the un-sprung mass
$(z_s - z_u)$	[m]	Suspension travel
$(z_u - z_r)$	[m]	Tire deflection
$(\dot{z}_s - \dot{z}_u)$	[ms ⁻¹]	Relative velocity of the spring & shock absorber
\dot{z}_s	[ms ⁻¹]	Velocity of the sprung mass
\dot{z}_u	[ms ⁻¹]	Velocity of the un-sprung mass
\ddot{z}_s	[ms ⁻²]	Acceleration of the sprung mass
\ddot{z}_u	[ms ⁻²]	Acceleration of the un-sprung mass
γ	[deg]	Camber angle
σ	[deg]	Kingpin inclination angle
φ	[deg]	Steering wheel angle
μ	-	Coefficient of friction between tire and road surface
α	[deg]	Road slope angle
α_i	[deg]	Weight coefficient corresponding to the ground excitation
β	[deg]	Trapezoidal offset angle
ξ	[deg]	Trapezoidal coupler angle
$\Sigma F_{yi}, \Sigma F_{zi}$	[N]	Sums of the internal and external components of force in y_i and z_i axis
ΣM_{xi}	[N·m]	Sum of all moments acting in the suspension mechanism links
δz_s	[m]	Virtual displacement of the sprung mass
δz_u	[m]	Virtual displacement of the un-sprung mass
δW	[Nm]	Elementary work
δ_L	[deg]	Front steering angle of the left wheel for the 2WS
δ_R	[deg]	Front steering angles of the right wheel for the 2WS
δ_{LF}	[deg]	Front steering angles of the left wheel for the 4WS
δ_{LR}	[deg]	Rear steer angles of the left wheel for the 4WS
δ_{RF}	[deg]	Front steer angles of the right wheel for the 4WS
δ_{RR}	[deg]	Rear steer angles of the right wheel for the 4WS
δ_1	[deg]	Angular displacement of the non-circular gear 1 for the 2WS
$\delta_2(\delta_1)$	[deg]	Angular displacement of the non-circular gear 2 for the 2WS
δ_{1F}	[deg]	Angular displacement of the front non-circular gear 1 for the 4WS
δ_{1R}	[deg]	Angular displacement of the rear non-circular gear 1 for the 4WS
$\delta_{2F}(\delta_{1F})$	[deg]	Angular displacement of the front non-circular gear 2 for the 4WS
$\delta_{2R}(\delta_{1R})$	[deg]	Angular displacement of the rear non-circular gear 2 for the 4WS
θ_3	[deg]	Input angular displacement of the 4 th link

$\theta_i(\theta_3)$	[deg]	Angular displacements of the i^{th} suspension mechanism links
$\boldsymbol{\theta}_x, \boldsymbol{\theta}_y, \boldsymbol{\theta}_z$	[deg]	Rotational vectors of i^{th} nodes in axis x, y and z
$\omega_1(\delta_1)$	[s^{-1}]	Angular velocity of the non-circular gear 1 for the 2WS
$\omega_2(\delta_2)$	[s^{-1}]	Angular velocity of the non-circular gear 2 for the 2WS
$\omega_{1F}(\delta_{1F})$	[s^{-1}]	Angular velocity of the front non-circular gear 1 for the 4WS
$\omega_{1R}(\delta_{1R})$	[s^{-1}]	Angular velocity of the rear non-circular gear 1 for the 4WS
$\omega_{2F}(\delta_{2F})$	[s^{-1}]	Angular velocity of the front non-circular gear 2 for the 4WS
$\omega_{2R}(\delta_{2R})$	[s^{-1}]	Angular velocity of the rear non-circular gear 2 for the 4WS
$\omega_i(t)$	[s^{-1}]	Angular velocity of the i^{th} suspension mechanism links
ε	[deg]	Caster angle
$\varepsilon_i, \varepsilon_i(t)$	[s^{-2}]	Angular acceleration of the i^{th} suspension mechanism links
$\sigma_{\ddot{z}_s}$	[$m s^{-2}$]	Standard deviation of the vehicle's body acceleration
σ_{F_t}	[N]	Standard deviation of the dynamic tire forces

LIST OF USED ABBREVIATIONS

Abbreviations	Explanation of the used abbreviations
CAD	Computer Aided Design
CG	Center of gravity of the vehicle
CPU	Control Programming Unit
ECU	Electronic Control Unit
FE	Finite Element
FEA	Finite Element Analyses
FEM	Finite Element Methods
GAs	Genetic Algorithms
GM	General Motors
ICE	Internal Combustion Engine
MOGAs	Multi Objective Genetic Algorithms
QVM	Quarter vehicle model
RTC	Razvojno tehnološki center (Institute for Automotive Industry)
SAE	Society Automotive Engineering
SLA	Short-Long Arm
VSI	Vehicle Safety Institute
2D	Two dimensional view
2WD	Two wheels drive
2WS	Two wheels steering
4WS/2WS	Four wheels steering/ Two wheels steering
3D	Three dimensional view
4WD	Four wheels drive
4WS	Four wheels steering
4x4	Four wheel drive

1 INTRODUCTION

1.1 Background

The key issue for terrain vehicles is to ensure good tire contact with the ground's surface. In regard to specific ground roughness this can be assured by more or less comprehensive suspension and steering systems. The common characteristic of the terrain vehicle is greater motion of the wheels in order to protect the vehicle from rollover risk when it runs over rough terrain. When considering this fact, the existing suspension systems has shown weakness when the motion of the wheels is greater. In order to ensure good driving comfort, driving safety, and higher maneuverability, it is necessary to develop new suspension systems. A suspension system is considered ideal when it has the capability of isolating the vehicle's body from the vibration generated from road bumps, cornering, braking, and acceleration.

The suspension system physically connects the vehicle's chassis with its wheels, cushions all the ground loads to the vehicle, thus enabling the vehicle to be driven, brake, and steered in reasonable comfort and safety. The suspension system is fixed onto the vehicle's chassis and consists of the wheels with tires, springs, shock absorbers, and a few rods and linkages, as well as the steering system, Pehan et al. [1], Lajqi et al. [2 and 3].

The steering system is a decisional component for all types of vehicles. It represents a connection between driver and vehicle, Rill [4]. The main task of it is to steer a vehicle in the desired direction safely and under full control. Due to the importance of the steering system, it should be easily and safely done.

The traditional steering system design is usually a steering mechanism done by some kind of mechanical ways, Pehan et al. [1] and Rill [4]. By such a mechanism, safety is ensured. In general, the driver not only steers the vehicle but he gets a feedback from the road surface that is expressed by the contra torque on the steering wheel, Pehan et al. [1]. To avoid the complicated linkage between steering wheel and steered wheels, some prototypes of vehicles have been developed recently where the steering system is implemented by wire, [5]. At the current stage of the market the customers still highly prefer the mechanical steering mechanism helped by electric, hydraulic or electro-hydraulic amplifier. This is because of the safety reasons.

However, nowadays the steering mechanisms are developed enough to fulfill the expectations for most ordinary vehicles, but when it is a question of the terrain vehicle's situation it is different. The standard steering mechanisms are unable to follow Ackermann law in order to provide suitable stability as a result of greater wheels motion. Vertical greater wheel motion does not influence the contra torque on the steering wheel, but has the ability to rotate the steered wheels around its kingpin axles for minor angles. Thus causes the vehicle to decrease stability as a result of the bumps steering. These already described problems are multiplied by the greater wheels and shorter wheelbase, which is certainly characteristic of the modern development of terrain vehicles. Four wheel drives is an additional deepening problem of the terrain vehicle steering because of the shortage place. The power supply to the driven wheels, on the one hand, and the steering mechanism, on the other, now would be in the same place. The mass is complete when the four wheel drive and four wheel steering are requested at the same time.

1.2 Problem definition

The treated problem in this research project is the development of a suspension and steering systems for a terrain vehicle with four wheel drives and four wheel steering. The specific requirements that are necessary to respect during the design process are that the vehicle should provide suitable driving comfort, driving safety, and higher maneuverability. Driving comfort is, in relation to greater vertical wheels motion, driving safety dependent on the quality of contact by the tires with the road surface, and higher maneuverability requires big rotations of the wheels, around its kingpin axles.

Developing of the suspension and steering system is a result of the RTC Company in Maribor which is in the process of developing a new terrain vehicle. One of the sensibility parts that require particular attention are identified designing a new suspension and steering systems which should fulfill the requirement given previously. These firm requirements are as a result a designer of the RTC Company manufacturing a prototype of the terrain vehicle. These terrain vehicles were in operation, but during testing showed weakness in driving comfort, stability, and maneuverability. Therefore this approach tries to improve these weaknesses in order to design an effective suspension and steering systems. Some main dimensions (Figure 1.1), fundamental requirements and limits about a new terrain vehicle are presented by a check list, Table 1.1. These requirements are necessary to respect throughout the development process and for any eventually change should be given reasonable attention.

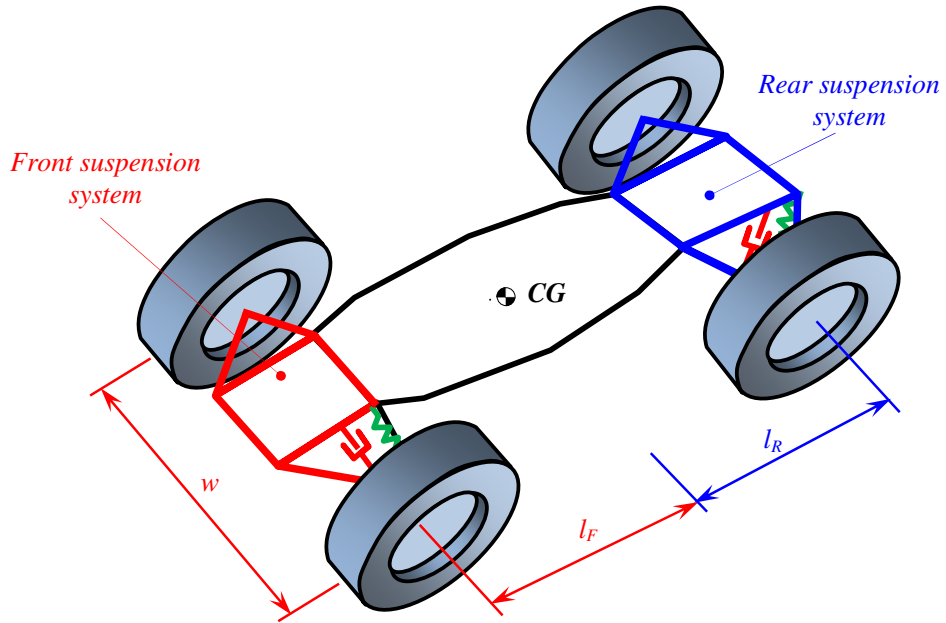


Figure 1.1: Schematic presentation of the main dimensions for a new terrain vehicle

Table 1.1: Check list with main design characteristics utilized for developing of the suspension and steering systems [6].

No.	Characteristics of a new terrain vehicle	Value	Unit	Remarks
1.	Engine: $P_e =$	~ 400	[kW]	Limit
2.	Power transmission: Gearbox	Mechanical		Request
3.	Vehicle speed: $v =$	$0 \dots 180$	[kmh ⁻¹]	Limit
4.	Maximal passing road slop angle: $\alpha =$	~ 50	[deg]	Wish
5.	Geometric dimensions: Wheelbase: $l =$ Track width: $w =$ Distance: $l_F =$ Distance: $l_R =$	2800 2100 1400 1400	[mm]	Limit
6.	Total mass of the terrain vehicle: $m =$	1150	[kg]	Limit
7.	Dimensions of the front and rear wheels: Tire diameter: $d =$ Tire width: $b =$	800 250	[mm]	Request
8.	Number of seats: $n =$	2	[place]	Request
9.	Camber angle: $\gamma =$	~ 0	[deg]	Limit
10.	Minimal vehicle turning radius: $R_{min} =$	2.5	[m]	Limit
11.	Suspension system design: Front and rear axles:	Independent suspension		Request
12.	Steering system design:	Mechanical		Request
13.	Maximal vertical wheel motion: Rebound: $z_{min} =$ Rest position: $z_{res} =$ Bound: $z_{max} =$	- 250 0.0 + 250	[mm]	Request

In Table 1.1 obviously shown that, the new suspension and steering systems require the vertical wheel motion to be ± 250 mm, zero camber angle, and a minimal turning radius 2.5 m. All these characteristics have affects in comfort, safety, and maneuverability.

1.2.1 Methodology for examining problem

On the basis of previous experiences, it was known that, for the suspension and steering systems, it would be impossible to satisfy all the requirements shown on the check list, Table 1.1. Therefore, the new design for both systems it is necessary.

The suspension system is developed by analyzing several designs of the suspension mechanism. In order to evaluate performances that provides known systems, the lateral wheel motion and camber angle are taken in consideration. Perfect results have been shown for the proposed design, which is derived from double wishbone with long equal control arms. To improve the comfort and safety, the active and semi-active systems were proposed. On the basis of comprehensive analysis, it is shown that active systems provide better behavior compared with semi-active or passive ones. The developed suspension system offers relatively small lateral wheel motion, zero camber angle, and effectively absorbs vibrations caused by ground excitation. Therefore, it is ensures an improvement in driving comfort and driving safety due to better absorbs vibration and quality contact of the tires with the ground.

In order to develop a proper steering mechanism it was foreseen to design a special steering gearbox and transmissions that would fit into each kingpin axis of the steerable wheel. The steering gearbox consists of planetary gears, bevel gears, and several pairs of non-circular gears that provide variables gear ratio. The non-circular gears are designed to follow Ackermann steering geometry. The wheels' transmission consists of a pair of bevel gears. The driver effort is transmitted from steering gearbox into front and rear steerable wheels through the steering propeller shafts. All the mentioned components are rarely used in steering systems but in the case of terrain vehicles these components are necessary in order to provide maneuverability at low speed and suitable stability at higher speed. This is ensured by two modes such as all wheels steering and front wheels steering. The proposed steering mechanisms follow the Ackermann steering geometry in all modes and situations.

1.3 Expected original scientific contribution

The objectives of this approach are conceiving, designing, optimizing and analyzing of the suspension and steering systems for a four wheel drive and four wheel steered terrain vehicle. Known solutions have shown serious weaknesses regarding common characteristics that

terrain vehicles have. In order to ensure good driving comfort, driving safety, and higher maneuverability and new principles of suspension and steering systems are proposed.

The proposed suspension system was successfully derived at from a classic double wishbone control arms. The control arms are long but both equal. Greater wheel motion is ensured without reducing driving performance. To improve the comfort and safety, an optimal active damping force is determined by employing an active or semi-active system. On the basis of comprehensive analysis it is shown that active systems are more adequate. The proposed suspension design provides relatively small lateral wheel motion, zero camber angle and it effectively absorbs the vibrations caused by ground configuration.

The developed steering system for the terrain vehicle provides good maneuverability at low speed and suitable stability at higher speed. This is ensured by two modes of steering, all wheel steering and front wheel steering. The proposed steering mechanisms follow the Ackermann steering geometry in all modes and situations. A totally new steering concept has been developed. Effective design is obtained by utilizing special pairs of gears, known as non-circular gears, in order to follow Ackermann law.

1.4 Research Objectives

The objectives of this research were focused as follows:

- i. Detailed analyses of requirements and limits given for the project as shown by the check list for the terrain vehicle, in order to satisfy all the detailed tasks of the project, as far as possible,
- ii. Investigate and carefully analyze many original and new concepts regarding suspension and steering systems,
- iii. Development of completely new suspension mechanism and control strategies for determining adequate damping force in order the terrain vehicle to provide suitable driving comfort and driving safety when moving over various terrain,
- iv. Development of a completely new steering system that would enable the steering of all wheels/front wheels in mechanical ways. Therefore, the developed system would provide good maneuverability at low speed and suitable stability at higher speed.
- v. The development process would be accomplished by using various research methods and optimization in order to obtain an optimal solution and
- vi. Achieved results regarding suspension and steering system will be checked and discussed in very detail.

1.5 Structure of the doctoral thesis

The Doctoral thesis is organized into eight chapters.

Chapter 1 presents the introduction about the suspension and steering systems for a terrain vehicle, problem definition, expected original scientific contributions and research objectives that are carried out in the doctoral thesis.

Chapter 2 presents the literature study for the suspension and steering systems. A brief history of their development, functions, classifications, advantages and disadvantages, controllability strategies, four wheel steering are outlines in this chapter. At the end of this chapter the current research, related to the suspension and steering systems as well as scientific contribution which differ from others are summarized.

Literature studies, designing by application of the CAD systems, analytical and numerical simulation methods as well as optimization of the mechanical systems, are some of the used research methods shown in Chapter 3.

Chapter 4 introduces the designing process regarding the development of the suspension system. In order to fulfill the requirement about driving comfort, driving safety and maneuverability, firstly, the design requirements, limitations and terminologies are presented. Secondly, an introduction to the geometric parameters involved in the suspension system such as *camber angle*, *caster angle*, *kingpin inclination* and *kingpin offset* are given. Furthermore, several design concepts are analyzed in detail for deriving the final design of the suspension mechanism. For each design, the obtained results, presented by diagrams for camber angles and the lateral wheel motion as a result of the vertical wheel motion, are discussed.

In the chapter 5 the mathematical expressions for kinematic and dynamic behavior of the developed suspension mechanism are derived. The mathematical expressions for several suspension links of the mechanism are solved by employing numerical methods. For each movable link of the suspension mechanism the expressions are derived by utilizing vector loops and free body diagrams. The obtained results from the analytical approach are compared with comprehensive commercial software the so-called Working Model Software. The suspension mechanism behaviors are analyzed also with Finite Element Methods, performed by the *STAKx* software. An optimization of the suspension mechanism links, with the objective to obtain less lateral wheel motion, is performed by employing the *iGOx* optimizer.

Chapter 6 introduces the procedures for design and optimization of the passive, active, and semi-active linear and non-linear suspension systems of a terrain vehicle. The developed procedure gives the ability to analyze vehicles' suspension performances, resulting from passive, active, or semi-active systems. The vehicle suspension system is represented by a mathematical model, and the equations of motion are derived and solved by using MATLAB/Simulink software. In order to verify the reliability of the derived computer program, a comparison is made to measured experimental data. The decisional suspension parameters for passive linear systems are optimized by utilizing the Multi-Objective Genetic Algorithms. The parameters that determine active damping forces are optimized by using the Hooke-Jeeves method which is based on non-linear programming. The performance of the passive linear suspension systems is evaluated for initial and optimal design parameters. The usefulness of the treated active and semi-active systems on an actual terrain vehicle is presented and compared with the passive ones.

The design of the new steering system of a terrain vehicle with all wheels steer is discussed in chapter 7. Some known steering systems are investigated and analyzed in detail in order to find a suitable solution. The developed steering system is designed to operate by two modes. In the first operation mode, when the vehicle moves at lower speed, the vehicle steers all wheels thus ensuring higher maneuverability. In the second operation mode, at the higher speed, the vehicle steers only the front wheels by locking the rear wheels thus providing better driving safety. The mathematical expressions for determining the steering characteristics are determined for all operation modes. The simulation result for all operation modes are presented in suitable graphical format. Particular care is devoted to design of the steering gearbox which provides exact Ackermann steering geometry. This is achieved by a development of a special pairs of non-circular gears.

The summary and conclusion of the research work is presented in Chapter 8. The obtained results regarding the development of the suspension and the steering systems are presented and discussed. On the basis of comprehensive analysis, it is shown that the developed suspension and steering system for terrain vehicles with four wheel drives and four wheels steer have successfully fulfilled all the requirements given in the check list and; the developed systems ensure driving comfort, driving safety, and good vehicle maneuverability.

Some of the additional materials pertaining to relevant results of the study, drawing, diagrams, flowcharts, and publications relating to the doctoral thesis are enclosed in the appendices.

2 LITERATURE STUDY

Chapter 2 presents the literature study for the suspension and steering systems. A brief history of their development, functions, classifications, advantages and disadvantages, controllability strategies, four wheel steering are outlines in this chapter. At the end of this chapter the current research, related to the suspension and steering systems as well as scientific contribution which differ from others are summarized.

2.1 Historical evolution

Transportation of passengers and goods before the advent of vehicles was horse-driven by coach, then steam machines, and later by Internal Combustion Engines (ICE). So, suspension function and its importance have been known since that time. To prove this fact, the Automobile Museum in Turin exhibits an interesting example of a horse coach constructed around 1650, which shows the existence of a suspension system. The body of the coach was connected with a fourth leaf spring, such as shown in Figure 2.1. There is identification of any damping device, probably the internal friction produced from the leaf springs and belts provided the expected leaver of comfort, Genta and Morello [7].

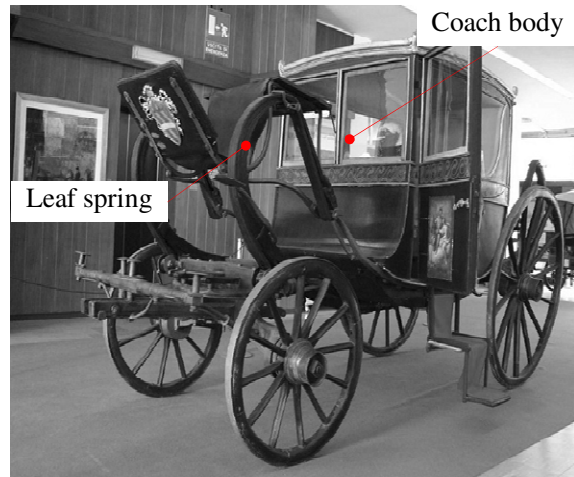


Figure 2.1: Coach, constructed around 1650, exhibited in Automobile Museum in Turin, Genta and Morello [7]

An Englishman Obadiah Elliot, in 1804 invented the single rigid axle suspension by using the elliptical steel leaf spring shown in Figure 2.2. This suspension was used for horse coaches as well as adapted for use in the first steam road vehicle, in the nineteen century, before the invention of the internal combustion engine.

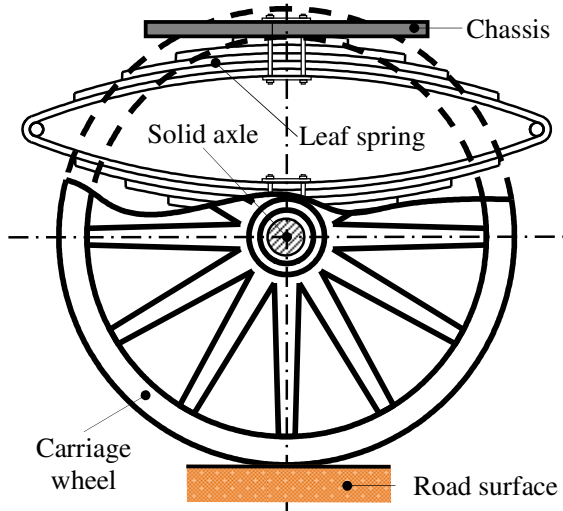


Figure 2.2: Single rigid axle suspension system, invented by Elliot in 1804 years

For heavier two axes coaches destined for the transport of goods, inventors tried to find a solution for constructing a kind of steering mechanism. Initially this was achieved by a simple solution, where front axle rotates together with the wheels, Figure 2.3.a.

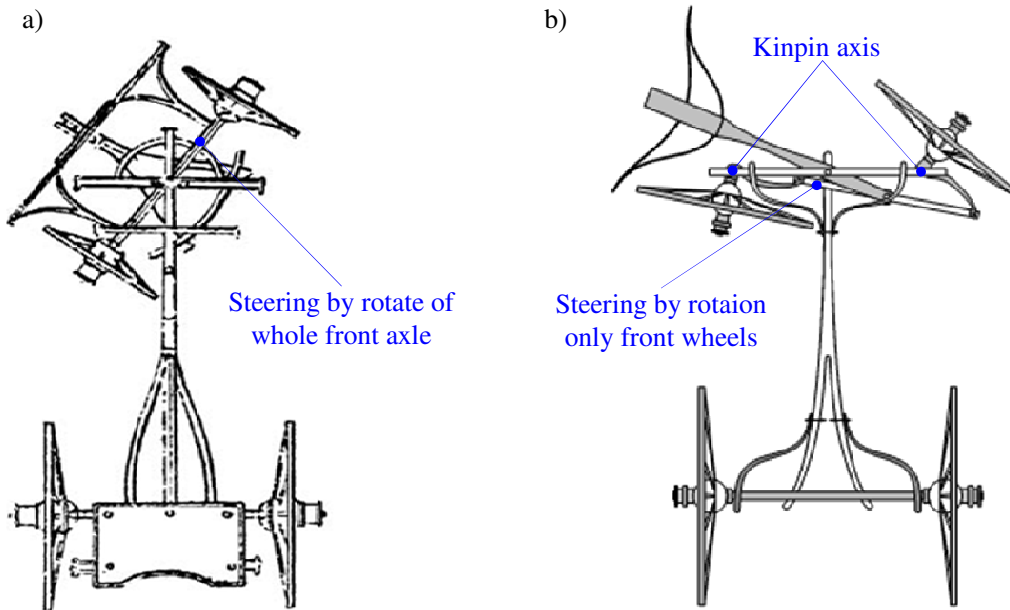


Figure 2.3: Steering mechanism for two axes coaches; a) steering by rotation of whole front axle, and b) steering by rotating only front wheels around kingpin axis, Dixon [8], Jazar [9]

Steering by rotation of the whole axle provides good geometric positioning of the wheels, but the rotation axles require larger operational space. To avoid this weakness, in 1816 Längensberger in Germany patented his steering mechanism where the front axle always stay parallel in regard to the rear axle, but each wheels rotates around its kingpin axis, as shown in Figure 2.3.b, Dixon [8] and Jazar [9]. Such a mechanism enables each wheel to be

steered through different angles, which greatly reduces the resistance to motion during firm turns. Later, in 1818 Rudolf Ackermann filed a British patent, Dixon [8]. This patent describes the steering geometry law for two wheels in order for the wheels to roll correctly. A considerable number of vehicles still use the Ackermann steering principle.

The first automobile with an ICE was a tricycle invented by Karl Benz 127 years ago, but there is no evidence about the design of the suspension system, Figure 2.4. This maybe is a result of this genius focusing on developing his internal combustion engine as a priority of his work. Therefore, from 1886 a new epoch started for vehicles.

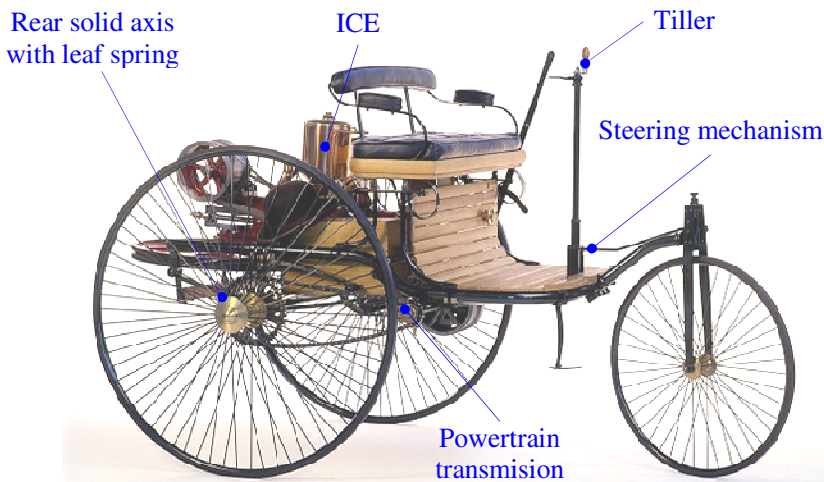


Figure 2.4: First automobile with an ICE, constructed by Karl Benz 1886, [10]

In 1893 Karl Benz obtained a German patent for a steering mechanism that followed the Ackermann steering principle, the same steering system as La Macelle in 1878. In 1897 Benz introduced the steering wheel for cars, a much superior system compared to the tiller. This steering wheel was adopted by all manufacturers and was used in all ground vehicles [10].

Some years later, Gottlieb Daimler and some European vehicle manufacturers applied coil springs for suspension systems. However, most manufacturers focused on leaf springs that were less costly, and easier to manufacture and assemble, Mohd [11].

The first shock absorbers appeared around 1910, fitted in vehicles only by customers' requests for sporty driving after the vehicle was sold. Many solutions were shown. Mostly of these had friction shock absorbers which worked in extension stroke, as well as some that worked in compression stroke. Hydraulic shock absorbers were used later.

Nowadays, several different designs of suspension and steering systems have been introduced over past years, as a result of each designer wanting its vehicle to have the best characteristics in terms of comfort, stability, and maneuverability.

2.2 Function and classification of the suspension system

The primary function of the vehicle's suspension system is to keep quality contact between the tires and the road surface, as well as to isolate the vehicle's body from vibration coming from road disturbances. The suspension system physically connects the vehicle's chassis with its wheels, and consists of wheels with tires, springs, shock absorbers, and a few rods and linkages, as well as the steering system, Pehan et al. [1], Lajqi et al. [2 and 3].

According to Genta and Morello [7], Gispelle [12], and Duffy and Krick [13], the secondary functions of the suspension system are identified as follows:

- Suspension mechanism should follow the motion of the wheels during upward and downward motions in order to avoid undesired wheel motions such as bump steering (toe-in or toe-out), camber angle, track variation, wheelbase variation, etc.,
- Support the weights of the chassis, vehicle body, engine, power train system, as well as passengers with their baggage,
- Allow the wheels to go upwards and downwards, thus causing minimal motion of the vehicle's body,
- Ensure the steering system to keep the wheels in correct alignment, and
- Allows for rapid cornering of the vehicle without extreme body roll.

Generally speaking, the designs of the suspension system are classified into two main group's, *solid axle* and *independent suspension system*, Pehan et al. [1], Lajqi et al. [3], Gillespie [12], Eslaminasab [14]. Both systems are used on ordinary and commercial vehicles.

Figure 2.5 introduces the basic elements that constitute the independent suspension system, used in most front axles of ordinary vehicle, such as:

- *Coil spring* – is used widely in independent suspension systems. The main characteristic is spring stiffness which is related to the diameters of the wire and coil, number of coils, and the shear modulus of the material. The coil spring stores energy and provides flexibility during wheel motion caused by irregularity of the road surface,
- *Shock absorber* – effectively dissipate energy after spring compression/extension and damp vibration on the vehicle's body. Shock absorber is a telescopic device with hydraulic fluid that usually is fitted in parallel with the coil spring. Without shock absorber, the vehicle body strongly oscillates, caused by road irregularity.
- *Control arm* – holds the steering knuckle, the wheel hub and moves upward and downwards with wheels,

- *Steering knuckle* – provides bearing support for the wheel hub, bearings, and the wheel assembly.

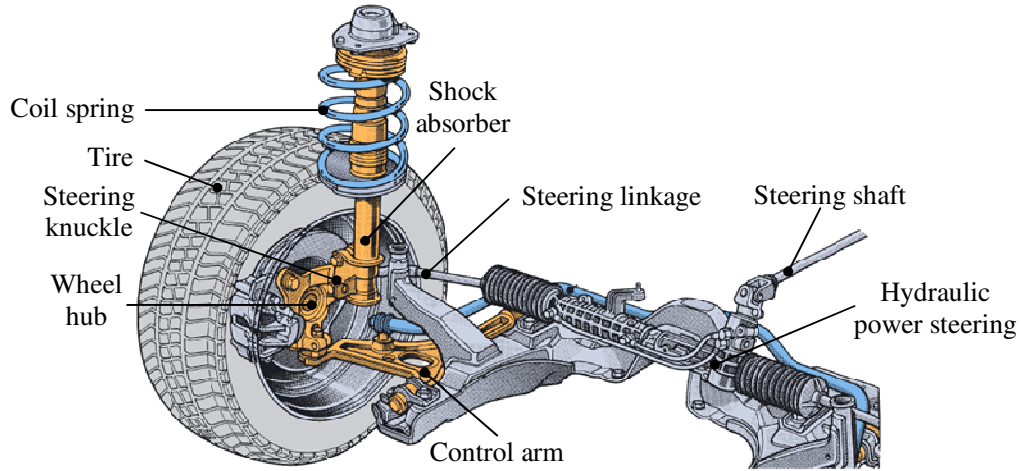


Figure 2.5: Suspension and steering system for front axle, Fisher et al. [15]

2.2.1 The solid axle suspension system

The solid axle suspension system is also known as the dependent suspension system. Connections of the left and right wheels are on the same solid axle, Figure 2.6. In this situation, any movement of wheels will be transmitted to the opposite wheels causing them to camber together. Solid drive axles are used usually on the rear axles of many passenger cars, trucks and, on the front axle in many four wheel drive vehicles.

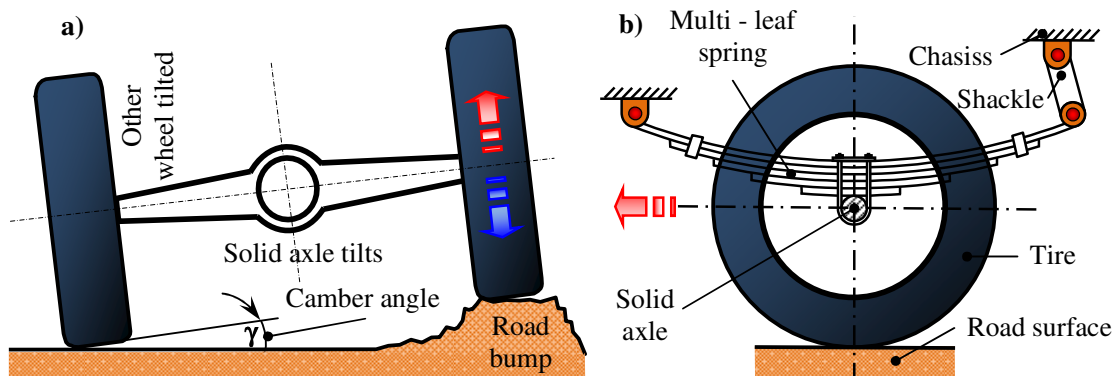


Figure 2.6: A solid axle suspension system with leaf spring; a) front view, and b) side view

The advantage of solid axles is considered to be the camber angle which is unaffected by the rolling of the vehicle's body. Therefore, it produces little camber when cornering. In addition, wheel alignment is readily maintained, which contributes to minimizing tire wear. The disadvantage of solid steerable axles is their susceptibility to shimmy steering vibrations, heavy mass, etc. The better known types of solid axles are: Hotchkiss, Four link and De Dion.

2.2.2 The independent suspension system

The independent suspension system, allows one wheel to move upwards and downwards with a minimum effect on the other wheels, Figure 2.7. Most passenger cars and light truck with a front axle use this type of suspension system because it provides more space for installing the engine, allows effective vertical wheel motion, offers better resistance to steering vibrations, as well as providing good driving comfort. Although this suspension system has better suspension capabilities for some vehicles, it does not satisfy, in general, the requirements for terrain vehicles.

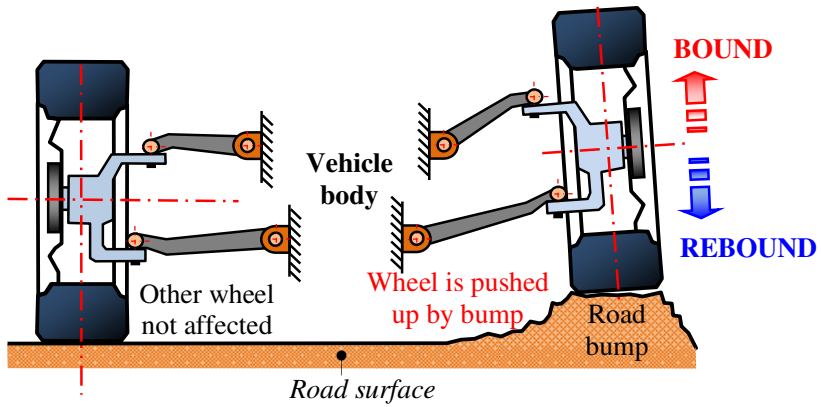


Figure 2.7: The independent suspension system - front view

The disadvantages of the independent suspension system are considered to be the complexities of the design and the manufacturing costs due to the greater number of parts.

Over the years, many types of independent suspension systems have been developed such as MacPherson, double wishbone, multi-link, trailing arm, and swing axle. Many of them have been discarded for different reasons. The MacPherson strut, double wishbone, and multi-link suspension systems have found applications in many types of the vehicles.

The *MacPherson strut* suspension consists of a single control arm and a strut assembly (spring and shock absorber) which allows the tire and wheel to move upward and downward. The major components of the MacPherson strut are shown in Figure 2.8.a. Such configurations can be used for front and rear axles. This suspension has a lesser number of parts, lower mass, and providing considering smooth driving comfort. The McPherson strut, regarding manufacturing cost, offers reasonable performance, but never matches the requirements fulfilled by the double wishbones or multi-link suspension. Furthermore, this type of suspension requires more vertical space and robust connection with vehicle body.

The *double wishbone* suspension in the United States of America is called “A-arms”, and “Double Wishbones” in the United Kingdom, Figure 2.8.b.

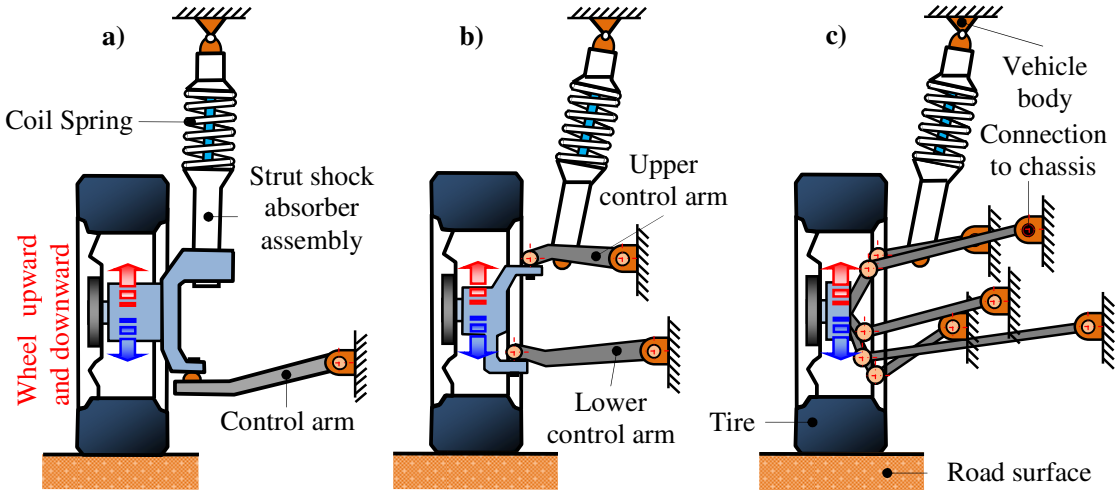


Figure 2.8: Design of the independent suspension system;

a) MacPherson strut, b) double wishbone, and c) multi-link suspension system

Double wishbone suspension systems are applied to luxury sedans and sports cars because their design of elastic-kinematic parts allows for the provision of an optimum compromise between handling and comfort, Genta and Morello [7]. The double wishbone uses two control arms to hold the wheel during ground excitation. The upper and lower control arms usually have non-equal lengths, from which the acronym SLA (short-long arm) gets its name. During the design process of double wishbone careful analyses is required to give good performance, Gillespie [12], Güler [16]. The disadvantages of double wishbone compared with the MacPherson strut suspension is in the complexities of the design and the manufacturing costs due to the increased number of parts.

The *multi-link* suspension system belongs to the group of independent systems shown in Figure 2.8.c. It is used on both front and rear suspension systems and was derived at by improving double wishbone. It uses three or more lateral arms and one or more longitudinal arms that are not required to be of equal length. Recently, the multi-link suspension system seems to have become the best independent system for vehicles because it offers the best compromise between comfort, stability, and maneuverability, [17]. Moreover, such a suspension system allows vehicles to obtain better performance compared with other types. By taking into consideration all of these good things, the multi-link suspension system naturally has a higher price for designing and manufacturing. In fact, the suspension geometry needs to be checked carefully using design analysis software for obtaining better performance of the vehicle. Except for the costs and higher complexity when designing and manufacturing, this solution is considered suitable when developing such systems for terrain vehicles.

2.2.3 The controllability strategies for the damping system

Suspension systems regarding controllability strategies are categorized as passive, active, and semi-active systems, Eslaminasab [14], Lajqi et al. [18] and Senthil [19], Figure 2.9.

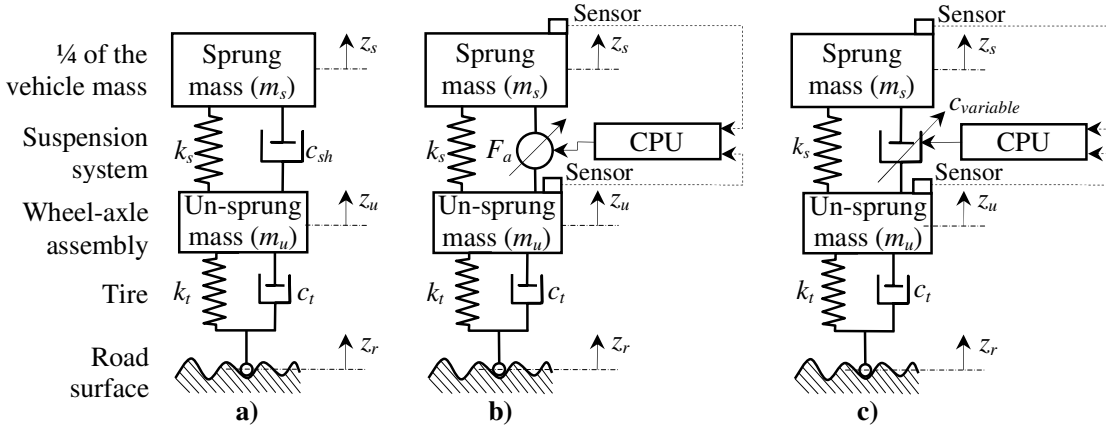


Figure 2.9: Quarter vehicle models; a) passive, b) active and c) semi-active systems

The *passive suspension system* includes, besides the mechanism, at least one of the conventional spring and shock absorber, Figure 2.9.a. The spring has linear or nonlinear characteristics, whilst the shock absorber exhibits a non-linear relationship between force and relative velocity. In general, the hydraulic shock absorbers are used in most vehicles. They work on the principle of fluid friction, Eslaminasab [14]. The damping effect in a hydraulic shock absorber is created by fluid-flow through orifices that are small holes in the shock-absorber's piston. The characteristics of the spring and shock absorber are immutable and cannot be adapted to any momentary operational condition of the vehicle. Thus the vehicle's performance is very limited and any improvements can only be done by the optimization of springs' and shock absorbers' characteristics. Even though these suspension systems do not fulfill all expectations regarding comfort and safety, they are widely used. For better control under various operational conditions, an active system can be used, Figure 2.9.b.

This *active suspension system*, in addition to the already described components, is also comprised of an actuator, sensors, and a control programming unit (CPU). Actually the shock absorber is replaced by an active force actuator. The operational conditions of the vehicle are continuously controlled by sensors that measure the velocities of the sprung and un-sprung masses and lead it to the CPU that ensures correct impulses for the actuator, which creates the desired active damping forces when required. To ensure adequate damping forces within active systems, hydraulic actuators are used because they act strongly, provide sufficient accuracy during operation, are simple in design, and have lower costs.

The *semi-active suspension system* is based on passive and active systems. This system presents one that contains a passive shock absorber instead, and a variable shock absorber as an active damping force that is automatically controlled by an integrated regulator. The damping force is modulated in accordance with the operational conditions, which are continuously controlled by sensors connected to CPU. The correct damping force can be ensured by adjusting the orifice area within the shock absorber, by which the resistance of fluid-flow is adapted, Wong [20]. Most of the variable shock absorbers' work is based on the electro-rheological or magneto-rheological fluids effects, Nekoui and Hadavi [21]; others include servo-valves, and solenoid valves. The servo-valves are excellent devices for changing the damping characteristics that likely work well but they are unfortunately very expensive and complicated devices compared to solenoid. The semi-active system offer good advantages under extreme driving conditions. When compared with the fully-active system, the semi-active suspension system requires less energy, is cheaper, the simplest in design, and provides other competitive performances when compared to passive systems, Lajqi et al. [18], Karnopp et al. [22], Pajaziti [23], Lin and Kanellakopoulos [24], Yi and Song. [25], Hong et al. [26], Turnip et al. [27].

2.3 Functions and classifications of the steering systems

The steering system consist of several components such as the steering wheel that is operated by the driver, the steering shaft that transmits the driver's commands to the steering gearbox, the steering linkages are connected to the steering wheels in order to steer the vehicle along the desired path, Figure 2.10.

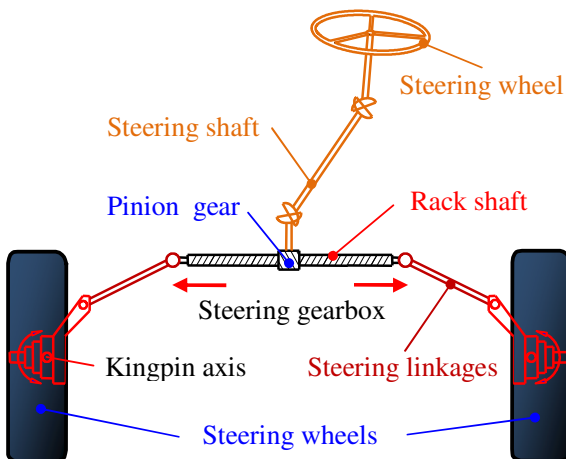


Figure 2.10: Mechanical front wheels steering system

The steering gearbox is used to provide mechanical advantage as a result of gear ratio, in order to help the driver to steer the vehicle more easily due to friction between the tires and the road surface. To date many types of steering gearbox have been developed. Most of the standard steering gearboxes are: rack and pinion, recirculation ball, worm and roller, articulated steering, steering by wire, etc.

Rack and pinion is widely used in most common types of steering systems for ordinary vehicles due to its low cost and easy manufacture, Figure 2.10. When the driver turns the steering wheel, the pinion gear rotates and moves the rack shaft in the right or left direction. Then through the steering linkages to steering the front wheels.

2.3.1 Power steering system

The power steering system has become more widely used over recent years due to the increasing vehicle weight affecting steerable axles. In order to reduce the driver's steering effort, a power amplifier is applied to the existing steering systems. The most common power amplifier is hydraulic, sometimes integrated within an electro-hydraulic device with electronic control, to adjust steering effort according to the vehicle's speed, Figure 2.11.

The power amplification is known as ***power steering***. This system requires a power steering pump attached to the engine and other necessary components. For safety reason all power steering systems are designed in this way, the vehicle can be steered manually when the engine is not running or if any failure occurs within the power amplifier. Most vehicle manufacturers have started substituting hydraulic amplifiers with electric ones, Figure 2.12. This is only for efficiency reasons, because the electric amplifier only needs to assist the driver when the steering wheel is turned, whereas the hydraulic pump must run constantly and the fuel consumption of the engine increases by about 2-3 %, Genta and Morello [7].

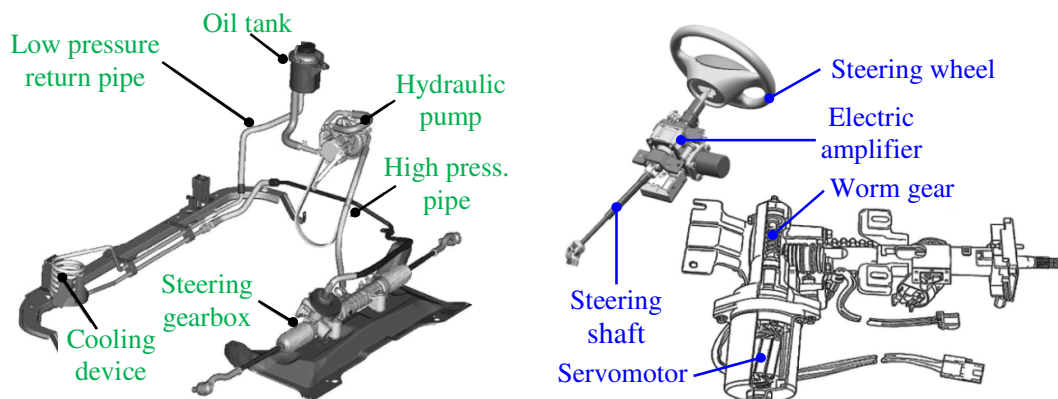


Figure 2.11: Hydraulic power steering system, Genta and Morello [7]

Figure 2.12: Electric amplifier system, Genta and Morello [7]

2.4 Four wheels steering systems

A vehicle with a four wheels steering (4WS) systems manifests itself when the driver through steering wheel is able to turn both the front and rear wheels of the vehicle during the same steering input. The concept for equipping vehicles with 4WS systems has been a hot topic in vehicle dynamics since from the 1980's, leading to the production of several vehicles equipped with this type of technology in the early 1990's. Since then, there has been a growth of interest in researching and developing 4WS systems. There are many necessary reasons for researching 4WS such as improving the maneuverability, stability of the vehicle, and increasing driving comfort for drivers and passengers.

Even though 4WS has advantages over the front wheel steering, it is more complex and expensive. Currently the cost of a vehicle with 4WS is more than the front wheel steered. There are three types of 4WS systems: *mechanic*, *hydraulic*, and *electro-hydraulic*.

2.4.1 Mechanical four wheels steering system

Mechanical 4WS systems use twin steering gearboxes. The first one is to steer the front wheels, whilst the second steers the rear wheels. Connection between the front and rear steering gearboxes is performed by using propeller shafts, Figure 2.13.

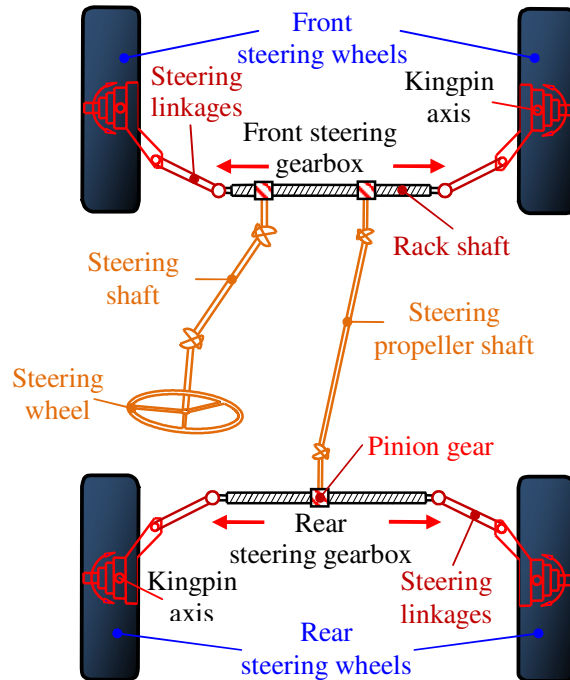


Figure 2.13: Mechanical four wheels steering system

The mechanical 4WS system is insensitive to the vehicle speed, Erjavec [28].

2.4.2 Hydraulic four wheels steering system

The hydraulic 4WS system uses a hydraulic working principle and is one of the simplest designs. A hydraulic 4WS system as designed for a model of vehicle produced by Mitsubishi Motors is shown in Figure 2.14. The main weakness of this system is that the driver does not feel feedback caused from road disturbances and, in some cases, this has a negative influence on driving safety.

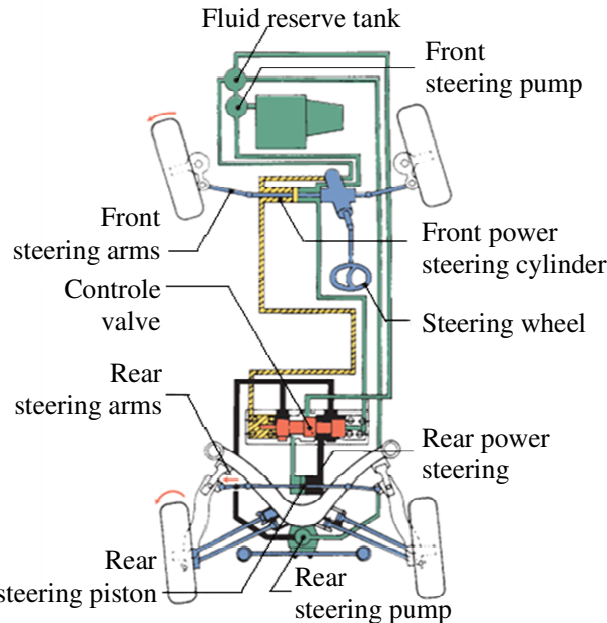


Figure 2.14: Hydraulic four wheels steering system, Erjavec [28].

Two way hydraulic cylinders are installed in the front and rear axles, thus making it possible to turn the wheels towards the right and left sides. When driver turns the steering wheel the steering hydraulic pumps in the front and rear side of the vehicle supply fluid to the front and rear hydraulic cylinders.

2.4.3 Electro-hydraulic four wheels steering system

The electro-hydraulic 4WS is a system that combines an electronic control unit (ECU) with hydraulic devices. This system provides the possibility for the vehicle to be sensitive regarding adequate wheel steering angles and vehicle speed. The sensitivity with speed provides the opportunity to optimize the vehicle's dynamic characteristics at any speed, thereby producing enhanced stability at higher vehicle speed, and maneuverability at lower speed. In this system, a speed sensor and the steering wheel's angle sensor feed information to the ECU. By processing the received information, the ECU commands the hydraulic system to steer the rear wheels.

2.4.4 Advantages of four wheels steering system

The 4WS system is a serious effort on the part of automotive design engineers in order to provide steering of the vehicle near the neutral steering. By advancing technology, 4WS systems can operate fully electronically steer-by-wire, equal steer angles for front and rear wheels, and sensors for monitoring the vehicle's dynamics and adjusting the steering angles in real time. By such systems, stability at high speed is improved and any negative effects of road irregularities are minimized. By steering the rear wheels in the opposite direction to the front wheels at low speed, the vehicle's turning radius is greatly reduced. Therefore, vehicle maneuvering on narrow roads and when parking, becomes easier, Erjavec [28].

Generally speaking, 4WS's advantages include cornering capability, steering response, straight-line stability, and lane changing and maneuverability at low-speed. In 2008, a Renault Laguna Coupe, being the first European model, arrived on the market equipped with all wheel steering, followed by BMW 7-series in 2009. These systems are controlled electronically and therefore provide extended possibilities. Other models of vehicles with 4WS are: Chevrolet Suburban 2500, GM Concept truck, Jeep Hurricane, etc.

Although such a complex 4WS system has not been designed for massive production, a number of prototypes with some of these technologies have been built and tested successfully.

2.5 Current research into the suspension and steering systems

Much of the current research regarding suspension and steering systems can be found in technical papers published by the Society Automotive Engineers (SAE), particularly from vehicle dynamics conferences. Other sources that help this approach are books, monographs, journals for automotive engineering, proceeding paper, notes, and theses in order to collect necessary information. Recently, research into suspension and steering systems has included a wider array of the subject:

- Active controls strategies for the suspension and steering systems,
- Materials and manufacturing techniques regarding suspension and steering systems,
- Modeling, optimization and testing techniques in order to improve performances of the suspension and steering systems,
- Improving known suspension and steering systems, and
- Developing new design for the suspension and steering systems.

The referred to papers in this thesis are proofing regarding the actual orientation of researcher towards vehicle suspension and steering systems. The active control strategies for

suspension and steering systems display the great interest from researchers in order to advance the driving comfort and maneuverability of a vehicle. Other researchers focus on analyses for improving current systems and their designs, for better performance. Whilst, for developing new designs for suspension and steering systems there are limited research sources, probably due to the secrecy of manufacturer's. The objective of this approach is not to improve current systems but to design an innovative concept regarding a suspension and steering systems for a terrain vehicle.

2.5.1 The current research being performed regarding suspension systems

Lajqi et al. [18] describe a simplified method for determining suspension parameters for different types of passenger cars equipped with passive suspension systems. These parameters are obtained by mathematical modeling of the quarter vehicle model and the experimental measuring displacement of vehicle body and force actions between tires and road surfaces.

Mokhlespour et al. [29] in their research, present an optimization procedure for a double wishbone suspension system with variable camber angle adjusting of hydraulic mechanism. This system adjusts the camber angle within the range from -5.5 ... 5.5 degrees. Such optimization and control of the camber angle in addition to the vehicle stability is effective in the tires' adhesion on road, and improves the service life of the tire when the camber is zero.

Allred [30] explores how a compliant mechanism can be used within vehicles' suspension system. Such a mechanism has advantages regarding the questions of space requirements, lower number of joints, rigid links, and simpler design for manufacturing and assembly. Fatigue failure has been found to be a limiting design constraint that competes with space and weight constraints. As the advantage of this concept is lower weight, it does not require precise vehicle handling characteristics, and when comparing cost with performance give reasonable results.

Heo et al. [31] have developed a method for computing kingpin geometry which is an important design feature of vehicle suspension geometry. It determines the steering feelings of drivers, the handling performance, and the steering stability of a vehicle. The idea of a geometric kingpin axis has been used to design a relatively simple suspension mechanism such as a double wishbone type, and various techniques have been developed for designing the kingpin axes of multi-link suspensions. However, a kingpin axis for a real vehicle has been unknown because there has been no method for measuring or computing it.

Maher [32] has identified control strategies for vehicle suspension system by measuring operational data. Finding methods for identifying the values of suspension parameters has

considerable interest, in practice. For facilitating experimental suspension system data, a quarter car suspension test rig has to be constructed. A combination of time and frequency domain methods are used to identify suspension parameters, extract sprung mass, linear stiffness, and non-linear damping model.

Bouzara and Richard [33] have analyzed the effects of vibrations on the driving comfort and driving safety observed by a variation of different suspension coefficients, road disturbances, and seating positions. In their study they developed a mathematical model for simulating the dynamic behavior of a 3-D vehicle. By using this model, various types of non-linear suspensions with semi-active and active systems can be investigated.

Gobbi and Mastinu [34] have used a simple linear model to derive at a number of analytical formulas that describe the dynamic behavior of the passive suspension system. They have introduced an optimization method, based on Multi-Objective Programming and Monotonicity analysis featuring the best compromises between those conflicting objective functions that indicate improved driving comfort, driving safety, and suspension travel.

Baumal et al. [35] demonstrated numerical optimization methods for partially automating the design process. A global optimization technique such as Genetic Algorithms is used to determine vehicle suspension parameters. The objective was to minimize the movement of the passenger's seat, subject to constraints representing driving safety and suspension travel. Genetic Algorithms are also used to compare obtained results from cited literature based on a gradient projection method.

Alkhatib et al. [36] has used the Genetic Algorithms method for optimizing the problem of a linear vibration isolator. This method was extended to optimize a linear quarter vehicle model. An optimal relation was found between the root mean square of the absolute acceleration and the relative displacement. The optimal solution was obtained numerically by Genetic Algorithms and by employing a cost function that contributes to minimizing the absolute acceleration and displacements of the vehicle body.

Yu and Yu [37] describe a procedure for obtaining an optimal vehicle suspension design on a quarter vehicle dynamic model. Two objective functions were used for minimizing the acceleration of the sprung mass and suspension travel, subject to a number of constraints. In solving this problem, the Genetic Algorithms have been used and consistently found to be near optimal solutions within specified parameter ranges for several independent runs.

The proposed suspension system for the terrain vehicle was successfully derived at from a classic double wishbone control arm. The control arms are long but both equal. Larger wheel motion is ensured without reducing driving performance. To improve the comfort and

safety an optimal active damping force is determined by the active and semi-active systems. Optimization of the suspension parameters for passive ones is performed by Multi Objective Genetic Algorithms, whilst for active damping force by employing Hooke-Jeeves non-linear programming method. On the basis of comprehensive analysis it is shown the active systems are more adequate. The proposed suspension design provides relatively small lateral wheel motion, zero camber angles, and effectively absorbs the vibrations caused by road excitation.

2.5.2 The current researches on the steering systems

Manufacturers producing Honda vehicles have developed a 4WS system in a mechanical way. The turn of the rear wheels are depends from the steering of the front wheels. This system provides two steering characteristics, Heisler [38]. One characteristic is when the vehicle moves at high speed, the rear wheels steer over a small angle in the same direction as the front wheels, and in the other when the vehicle's moves at low speed and the rear wheels steer in the opposite direction the front wheels. These characteristics were made possible from an epicyclic gear set consisting of a fixed internally toothed annular ring gear in which a planetary gear driven by an eccentric shaft revolves. This unit is incorporated within the rear steering gearbox which controls the rear wheels' turns.

Mazda manufacturers of these vehicles have designed a 4WS by using a hydraulic power unit, which is controlled electronically in accordance with the steering wheel angle and vehicle speed. This design seems to be more complicated than the Honda 4WS. This system incorporates suitable fail-safe for trouble-free operation. In the case of hydraulic or electronic system failure then the rear wheels are locked and the vehicles operate as normal. For speeds of less than 35 km/h, the rear wheels are steered in the opposite direction to the front wheels. If the speed reaches 35 km/h, the rear wheels are turned to the straight-ahead position. More than this speed and the rear wheels are steered in the same direction as the front wheels with an angle limited to 5° [39].

Pehan et al. [1] have presented the modeling and simulation of an off-road vehicle with a four wheel steering system. Research focused on developing a steering and suspension system which provides reasonable driving comfort, driving safety, and maneuverability. Based on their approach, a new mechanical steering mechanism has been introduced by which the steering mechanism ensures good maneuvering for an off-road vehicle at low speed and, on the other hand, a mechanism with satisfactory stability requirements at higher speeds. Their conclusion is that the vehicle with 4WS produces better maneuverability than front wheel steering for cases when the rear wheels are steered in the opposite direction to the front

ones. The stability of this vehicle at high speed is obtained by locking the rear wheels and turning them into the straight-ahead position.

Alter [40] has investigated the performance benefits of four wheels steering in passenger vehicles at driving speeds of around 50 km/h. The objective of the research was to compare the performance of 4WS with 2WS under steady-state skidpan and transient lane-changing conditions. Steady-state results prove to be nearly identical between the 4WS and 2WS runs of each vehicle. The transient effect of 4WS was to transfer a larger percentage of the cornering force load onto the front tire.

Spentzas et al. [41] have reviewed some aspects of the kinematical theory regarding four wheels steering vehicles and have presented some new results and conclusions. The kinematic analyses of the vehicle with 4WS allowed for Ackermann's law for vehicles with 2WS. The kinematic theory for vehicles with 2WS vehicles is a sub-case of generalized kinematic theory for vehicles with 4WS.

Brabec et al. [42] have developed a control system for vehicles with four wheels steering and then building a model of the vehicle with 4WS in the scale 1:5 which allows for the following behavior of the vehicle with 4WS. By means of the control computer in the model, they will be able to assess several types of the algorithms for steering rear wheels. These algorithms will be optimized according to lateral acceleration, and the yawing velocity.

Lee [43] has made a realistic application for the sensitive analysis of a four wheel steering vehicle with complete suspension system, and with a comprehensive analytical tire model implemented. A steering control strategy is developed for vehicle simulation to follow a prescribed path. The simulation results using the optimal steering ratio are compared against the results of the conventional two wheel steering based on the linear bicycle model.

Emura and Arakawa [44] have investigated a steering mechanism using elliptical gears for a virtual two-wheeled vehicle. They have also developed and test a steering mechanism for four wheeled robots that could be used in industry. The developed steering mechanism has shown suitable results regarding wheeled robotic maneuverability.

The developed steering system for the terrain vehicle is a totally new concept from other steering mechanisms. This system provides maneuverability at low speed and suitable stability at higher speed. This is ensured by two operation modes of steering: all wheels steer, and the front wheels steer. The proposed steering mechanism follows the Ackermann steering principle in all modes and situations. A totally new steering concept has been developed. This effective design consists of special pairs of gears, known as non-circular gears. Therefore, the developed design offers higher maneuverability and ensures good driving safety.

3 RESEARCH METHODOLOGY

This chapter discusses the research methodologies utilized for developing a suspension and steering system for a four wheel-drive and four wheel-steered terrain vehicles. The main research methods employed during this thesis can be identified as *literature studies; design processes by applying CAD systems, numerical analyses methods, mathematical modeling and simulation, optimization of the mechanical systems*, as well as the *comparison, analysis, and evaluation of the obtained results*. The main aim is to introduce how these methods can be used to solve treated problems in order to fulfill, as far as possible, the predefined requirements given by the check list.

3.1 Literature study

A significant amount of literature, scientific papers, patents, many original and innovative concepts regarding suspension and steering systems [1-112] have been studied and analyzed carefully. These investigations made it possible to find suitable solutions and to fulfill as much as possible the requirements given in the check list (Table 1.1). Research started by exploring the development history, classifications, functions, advantages and disadvantages, controllability and configuration of suspension and steering systems, such as presented in Chapter 2. By studying recent literature it was possible to collate new and relevant information from what others have done within the same field, in order to find favorable solutions for the suspension and steering systems of terrain vehicles.

3.2 Design processes by applying CAD systems

Design processing forms a major part of research and development activities. This process covers the activities of preparing drawings, detailed technical specifications, as well as necessary information for manufacturing products in order to satisfy customer requirements.

Generally speaking, the task of each engineer is to apply his/her scientific and engineering knowledge to find one or more suitable solutions for specific design problems. In addition to the basic design, it is necessary to optimize it according to requirements and constraints; such are materials, technological possibilities, reasonably cost, legal restrictions, and environmental and human source-related considerations.

The design task becomes clearer after recognition of the problem and defining the criteria and requirements that engineers have to adopt and apply in order to design for production. According to Pahl et al. [45], Mastinu et al. [46] the four stages of the design process can be defined as is shown in Figure 3.1.

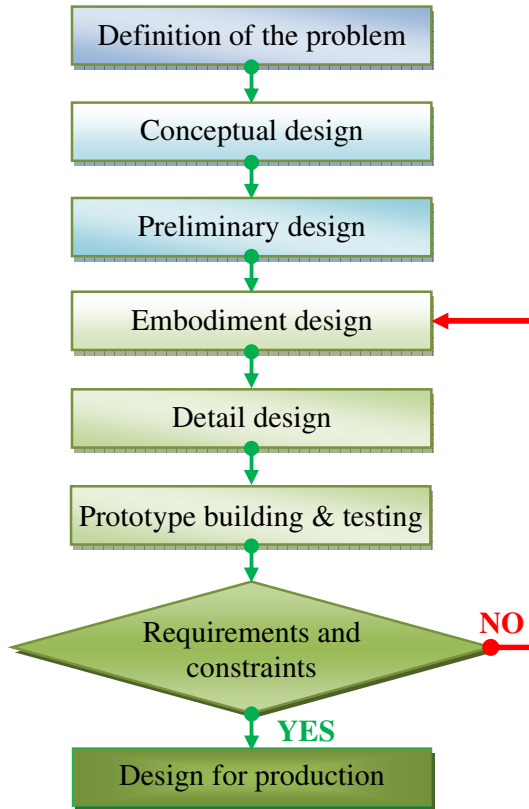


Figure 3.1: Flowchart diagram showing the stages of the design process

3.2.1 Conceptual design

Conceptual design is the part of the design process that determines the method of solving and treating a problem. At this stage it is necessary to identify the essential problems, establish the functions, and find working principles for the problem. The basic solution could be reached by examining the working principles of the problem and combining them with real possibilities, in order to find a solution.

3.2.2 Preliminary design

Preliminary design is the second stage of the design process, also known as feasibility design, and is considered as part of the conceptual design. The preliminary design is obtained by refining the conceptual design according to the design specifications regarding the best choice for the preliminary design.

3.2.3 Embodiment design

Embodiment design starts from preliminary layouts, selecting the most desirable preliminary layouts, the working concepts of a technical product, and again refining and evaluating using technical and economic criteria. Much work is then done to refine the concept. The geometry, shapes, weights, and interactions are determined during this stage.

3.2.4 Detail design

The detail design is the final stage of the design process that combines the embodiment of technical products with final instructions for manufacturing. This stage of design includes detailed explanations about the drawings, dimensions, tolerances, sizes, forms, surface properties of all the individual components, specifications of the materials, operating procedures, manufacturing costs, etc.

The classification of the design process as four stages is not a unique one and is in fact a general classification when considering complex mechanical systems. Nowadays, CAD systems are employed for implementing the design phases mentioned previously. The more up-to-date the greater those applications concerning CAD systems utilize computer software's such as AutoCAD, CATIA, Pro/ENGINEER, SolidWorks, etc.

The working principles of CAD systems are based on interactive computer graphics. The users of CAD systems are designers who use data for executing commands via various input devices of the computer, and develop images on the output device (monitor screen, printer) for faster and easier designing. The designer with his conceptual design performs a part of the design process, whilst the computer carries out the task most suited to its capability, such as fast calculations, searching, sorting, routine operations, displaying on a monitor, analyses of structural design, printing drawings, Balic [47].

The CAD system has many advantages compared with traditional manual design. It improves the efficiency and quality of work, saves money during design, as well as the manufacturing process. The other advantages of the CAD system could be hard to measure but some of them are: increasing the productivity of design, easy corrections of drawings, repetitive parts of a drawing, virtual reality simulation of the structural design, reducing storage space, etc. In addition to advantages, CAD systems also have some drawbacks, such as a high initial cost, requires adequate training and education of staff for efficient usage, reduction of human resources, etc.

3.3 Numerical analyses methods

Nowadays, as also in past, numerical analysis through Finite Element Methods (FEM) is significantly used in different engineering fields, such as aerospace, automotive, heavy equipment and machinery, civil engineering, etc. Analysis by mechanical systems often presents difficult engineering tasks because of the high complexities of their geometry on the one hand, and the different applied loads (dynamic load, stiffness, etc.), on the other. The behavior of these systems can be analyzed by setting the differential equations as a basic principle of the mechanics. The solving of differential equations in many cases is impossible, except in those cases where the geometrical, loading, and boundary conditions of the problem are very simple, and makes possible direct integration, Mecitoglu [48]. On the other hand, the solving of a mechanical problem where the geometry and loading condition are relatively complex is impossible to solve by analytical methods. This problem successfully can be solved by employing numerical methods. FEM belongs to the class of numerical methods and is one of the more powerful methods for solving a wide-spectrum of engineering problems.

The exact period of early development regarding FEM is very difficult to determine, Sorić [49]. In 1943 it was discovered that the mathematician R. Courant had developed Finite Element Analyses for obtaining approximate solutions for vibration systems, Mohd [11]. The first publication on FEM appeared from J.H. Argyris in 1954. The number of publications referring to FEM is relatively large. Between 1967 and 1999, a total of 467 books were published regarding FEM, Mackerle [50]. According to Sorić [49] and Mackerle [50] the first computer program based on Finite Elements was introduced between 1960 and 1970 and by 2002, 1538 FE codes had been registered.

The design task utilized by Finite Element Analysis (FEA) is to investigate the behavior of a structure which is subjected to specific boundary conditions and loads. In order to make an analysis of the mechanical structures using FEA, the real geometry of the structure first needs to be split into discrete portions, which are known as **Finite Elements** (FE). Each FE is formed by joining points known as **nodes**. FE and nodes form a grid so-called a **mesh**. This mesh is programmed to contain the structural properties of selected materials which then define how the structure will react according to certain loadings. The quarter suspension system of the terrain vehicles performed by discrete FE is shown in Figure 3.2.

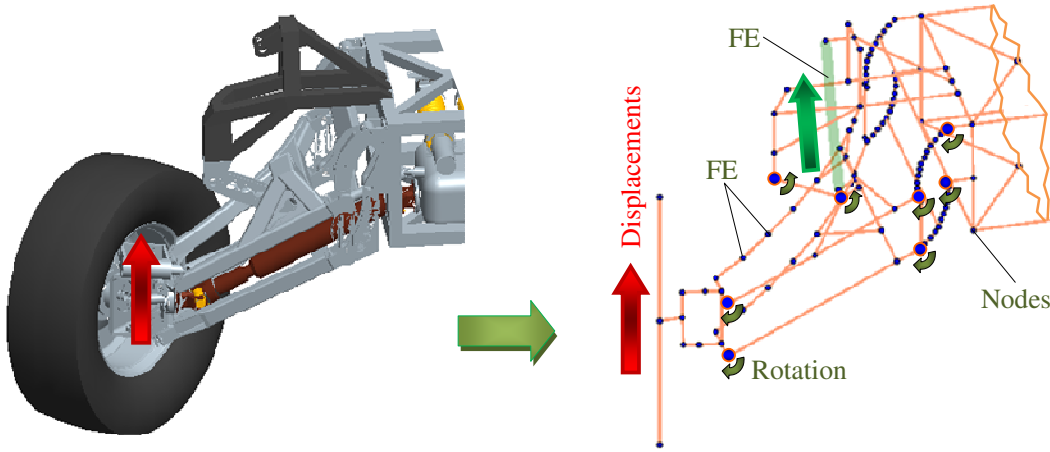


Figure 3.2: Modeling of a quarter of the suspension system by splitting into discrete portions - FE (modeling is performed by using Pro/Engineer and STAKx software)

Usually a FE is a non-linear formed by the joining of two nodes. Each node has the capability to move within six degrees of freedom (when three are *displacements* and three are *rotations*), Figure 3.3.

The relation between the stiffness matrixes, vector displacement, and the applied force in nodes is determined by the global equation of FE. The global equation of FE is described by the following expression:

$$[k] \cdot \{u\} = \{f\}, \quad (3.1)$$

where $[k]$ denotes the global stiffness matrix of a structure, $\{u\}$ is the global nodal vectors displacement, $\{f\}$ introduces the global nodal vectors of the applied forces, u_i, v_i, w_i are the termed vectors displacement of nodes i^{th} , $\theta_x, \theta_y, \theta_z$ define the rotational vectors of nodes i^{th} in the axes x, y and z and $i = 1, 2, \dots, n$ are the presented nodes.

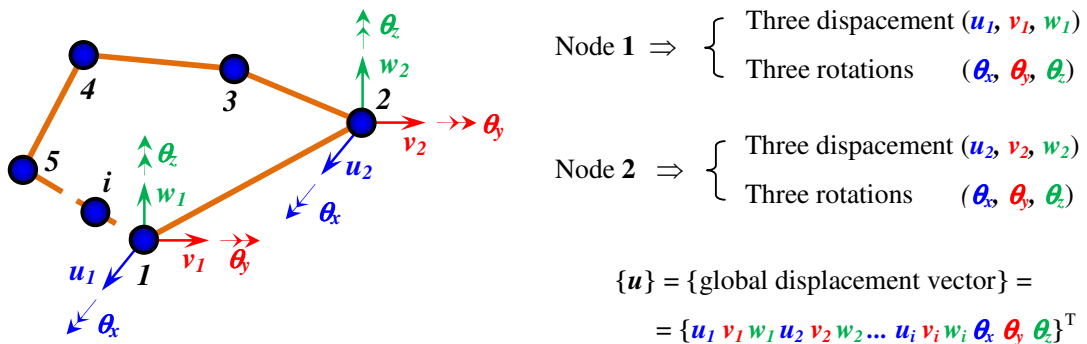


Figure 3.3: Moving capabilities of FE mapping of nodes

Recently, an improved performance by computers has allowed the rapid development of software packages for solving mechanical problems that are based on FEM. This software

enables modeling, analysis, and optimization, as well as modifications of designs for various engineering problems over a short time. Numerical analysis, dynamic simulation, and optimization can be performed by employing software packages such as STAKx, MATLAB, Working Model, MathCAD, iGOx-i, etc. The tasks of each FEA software is based on FEM formulation of a model, and the correct defining of input data. In practice, FEA software is usually divided into three parts: **pre-processing**, **processing**, and **post-processing**. A flowchart showing the organization of FEA software, is shown in Figure 3.4.

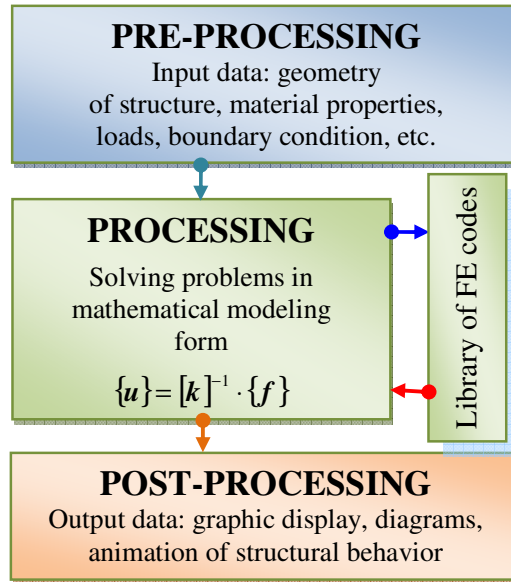


Figure 3.4: Flowchart diagram of FEA process, Mecitoglu [48], Sorić [49], Roylance [51]

where $[k]^{-1}$ denotes the global inverse stiffness matrix of a structure.

The pre-solver formulates the mathematical model by reading data from pre-processor, the processor computes solution by solving global equation of FE, while in the post-processing stage are presented obtained results and their interpreting.

3.4 Mathematic modeling and simulation

The mathematical modeling and simulation is an important process in the automotive and other parts of engineering. They present the basic methods for designing and analyzing a mechanical system. Basically, the mathematical modeling is performed in mathematical language to represent and describe the existing model or a model that is going to be constructed. During the modeling process, the researchers have to make several attempts in order to be sure that the simulation results are suitable and accurate, Figure 3.5. In general, researchers and engineers before the final production design perform the mathematical

modeling and simulation. Unfortunately, it is impossible to build an adequate model for analyzing. Always exists Problems always exist that are impossible to model.

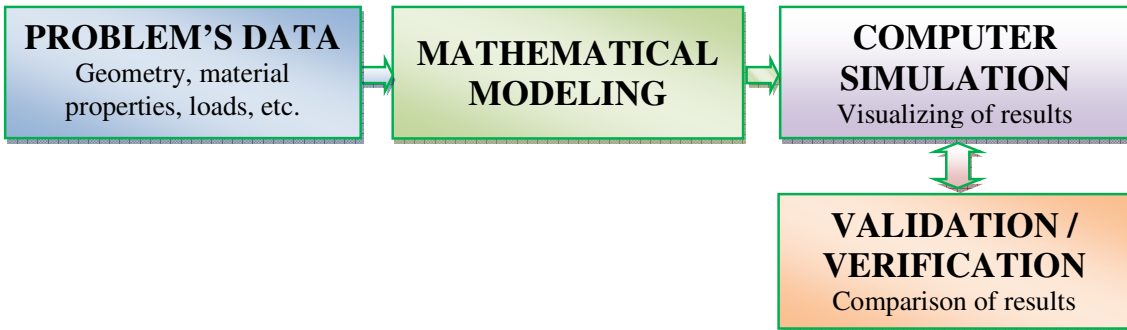


Figure 3.5: Flowchart diagram of the mathematical modeling and simulation processes

For that reason it is necessary to make some assumptions and modifications. Although mathematical modeling describes just a part of the reality it can be very useful for analyses and design. In most cases when modeling and simulating mechanical systems described using mathematic expressions, software packages such MATLAB/Simulink, MathCAD are used.

3.5 Optimization of the mechanical systems

Optimization techniques for mechanical systems play an important role. The purpose of this is to find the best ways of deriving maximum benefit from available resources. Over recent years, several optimization methods have been developed (e.g. Gradient, numerical, Genetic Algorithms, etc.). Optimization methods based on Gradient platform are widely used in mechanical optimization systems. These methods have favorable convergence properties and computation effort is very small. However, the optimization method based on Genetic Algorithms is a stronger tool for finding the global optimal point without any requirement on the gradient and the Hessian Matrix.

As discussed in Chapter 2, *driving comfort*, *driving safety* and *maneuverability* of the vehicle can be achieved by designing an efficient suspension and steering system. Optimization of these systems can be done by employing so-called *iGOx* optimizer software which works in Gradient platform. While optimization of the suspension parameters can be done by employing Multi Objective Genetic Algorithms, and the Hooke-Jeeves methods.

3.5.1 Numerical optimization methods

Numerical optimization methods that are used in engineering are usually divided into the following three groups, Lenart [52]: *conventional*, *shape* and *topology* optimization methods.

The *conventional* optimization method is a numerical method and is one of the more popular optimization methods due to its easy usage. This method is based on a modest modification such as the geometric parameters of individual finite elements (e.g. cross-section, thickness, etc.). In other hand, the *topology* optimization methods are probably the most complex methodology for optimizing mechanical systems and when working intensively to develop. Sometimes shape organization is used between *conventional* and *topological* optimization methods. The key problem before shape optimization is the selection of suitable ways for geometric parameterization. The parameterization process used for the optimization of a suspension system is already complex enough. The main reason for this is the fact that the conventional optimization process does not require substantial changes in preparation data for the analysis of the structure. The situation is totally different when optimizing the shape of the suspension mechanism or other structure. Automatically changing FE mesh requires a different concept for preparing geometric data. In this situation, it is necessarily to have several FE codes that have been tested and applied in various applications, and will be used for optimizing the geometry of the suspension mechanism. In this case, the geometric data prepared for modeling the suspension mechanism are so-called project elements obtained from FE codes. These project elements are prepared in ways that depend on the design variables. Design variables, within this context, can therefore be considered as a form of parameterized FE mesh, and the whole approach is called the concept of suspension mechanism parameterization.

3.5.2 Optimization method based on a Genetic Algorithms

The Genetic Algorithms (GAs) used for optimization of the mechanical system are stronger tools for finding the global optimal point without any requirement on the gradient and the Hessian Matrix. GAs are used for global search methods that are based on Darwin's principle of natural selection and genetic modification. GAs consists of *initial population, fitness function, selection function, crossover, and mutation*.

Therefore, based on the wider number of publications and the research done regarding GAs, it can be concluded that optimization of the suspension parameters based on the GAs platform provides suitable results, Likaj et al. [53]. The multi-objective GAs optimization method is employed for optimization of passive suspension parameters such as spring stiffness, damping coefficient, tire stiffness, sprung and un-sprung masses of the terrain vehicle.

4 DEVELOPMENT OF THE SUSPENSION SYSTEM

Nowadays, as well as in the past, the development of suspension systems for vehicles attracts great interest by the designers and manufacturers of those vehicles. In general, the optimal design of a vehicle's suspension system has an influence on improving: driving comfort, driving safety, maneuverability, and the service-lives of the vehicle's components.

This chapter identifies the more important suspension geometric characteristics that have an influence on the final design and performance, thus ensuring a reliable suspension system. Each suspension characteristic such as wheelbase, track width, camber angles, camber steering, kingpin inclination, and kingpin offset, is adequately explained.

Particular interest is concentrated on the camber angles, the kingpin inclination, and the kingpin offset, which contribute towards driving safety as a result of better contact of the tire with the road surface. In addition to this feature, consideration should also be given when developing a suspension system to those design requirements and constraints shown on the check list. Some conceptual designs are analyzed in detail, and after refining them a conceptual design could be obtained for a suitable final design of the terrain vehicle's suspension system that fulfills the design criteria.

4.1 Motivation, design requirement, constraints and terminology

Developing a terrain vehicle is a process carried out by the RTC Company in Maribor [6]. The main sensitive parts of the terrain vehicle, such as the suspension and the steering system, are treated here. The motivation for developing this project stems from the example given by the RTC Company. They have designed and manufactured a terrain vehicle for sport and recreation purposes. The design and view of it is presented in Figure 4.1. It appeared to have some problems with stability and maneuverability. These problems could be quantified with some available information at our disposal. The vertical motion of the wheels was insufficient to protect the vehicle from roller risk when performing on uneven terrain. The suspension components provided unsuitable driving comfort, and the vehicle's maneuverability was limited. The existing geometric dimensions provided insufficient stability, etc.

In order to avoid these weaknesses it was necessary to make a detailed scientific study of the suspension and steering systems. On the other hand, this project for the terrain vehicle was completely new and it was insufficient to make only small modification.

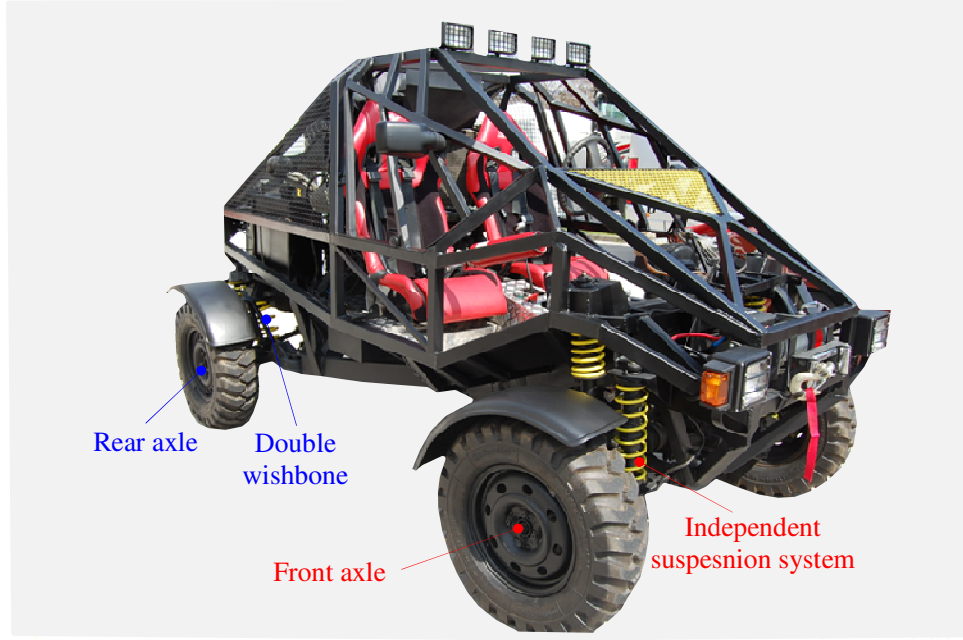


Figure 4.1: Terrain vehicle with four wheel drive and front wheel steering [6]

A completely new suspension and steering system needed designing in order to fulfill the design criteria. The new designs had to avoid the problems mentioned previously. The design requirements and constraints given by the check list in Table 1.1 had to be considered during the development process. The newly-developed terrain vehicle's suspension and steering system would have to satisfy requirements relating to *driving comfort*, *driving safety*, and *maneuvering* capabilities. These would ensure the terrain vehicle had better performance and enable mass production, of course, after prototyping and testing. Figure 4.2 introduces the basic model of the developed terrain vehicle with all its necessary geometric dimensions in order to provide more clarity and practically during the development process, whilst Table 4.1 provides an explanation of the used symbols shown in Figure 4.2.

Table 4.1: Descriptions of the used symbols for the terrain vehicle model

Symbols	Descriptions of used symbols
CG	Center of Gravity of the vehicle
h_{CG}	Height from the Center of Gravity of the vehicle to the ground
H	Height of the vehicle
l	Wheelbase of the vehicle
L	Length of the vehicle
l_F	Distance from the front axle to the Center of Gravity of the vehicle
l_R	Distance from rear axle to the Center of Gravity of the vehicle
w	Track width of the vehicle
W	Width of the vehicle

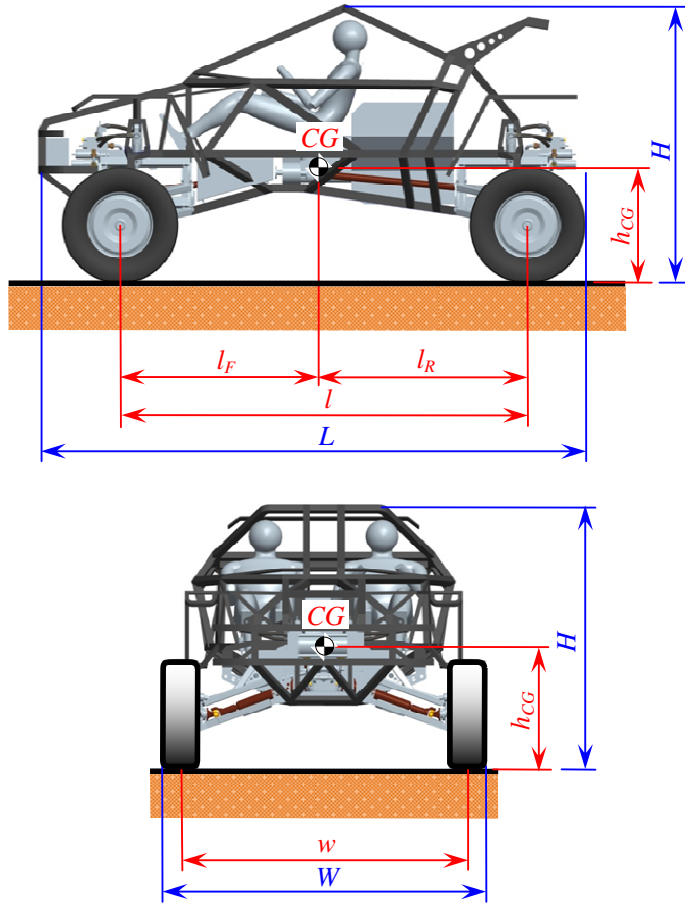


Figure 4.2: Basic geometric dimensions of the terrain vehicle

A lot of terminology exists relating to the suspension system's design. The follow describes only those that were important for usage during the development process.

4.1.1 Wheelbase of the vehicle l

The *wheelbase* of the vehicle l is the longitudinal distance between the centers of the front and rear axles, as shown in Figure 4.2. The wheelbase of the vehicle has a greater influence on the distributions of the longitudinal axle loads. If the wheelbase of the vehicle is longer the load distribution is lower between the front and rear axles and provides more space for fitting a vehicle's device, whilst a vehicle with a shorter wheelbase provides greater load distribution during the acceleration and braking processes, as well as during cornering situations.

A vehicle with a longer wheelbase offers more opportunity for fitting softer springs resulting in an increased level of driving comfort. On the other hand, a vehicle with a shorter wheelbase has more advantage regarding lower turning radius for the same steering input, Reimpell et al. [54]. The value of the wheelbase when developing a terrain vehicle is $l = 2800$ mm and all four tires have outside diameter $d = 800$ mm by width $b = 250$ mm.

4.1.2 Track width of the vehicle w

The *track width* of the vehicle w is the distance between the centerlines of the right and left wheels when viewed from the front or rear side, Figure 4.2. The track width is another important factor. It has a direct influence on a vehicle's cornering behavior and tendency to roll, Reimpell et al. [54]. A vehicle with a larger track width has advantage over the smaller lateral load distribution but, on the other, has disadvantages because it requires more lateral motion in order to avoid obstacles when turning.

In general, a vehicle with wider track width will provide more stability than a vehicle with narrow track width. The track width of the developed terrain vehicle is $w = 2100$ mm. The front and rear wheels are along the same line. This size of track width provides more stability when cornering and when a vehicle moves over terrains with higher slope.

4.1.3 Sprung and un-sprung masses of the vehicle m_s and m_u

The *sprung mass* of the vehicle m_s is a mass which is carried by suspension springs (frame, engine, transmission, body, etc.), whilst the *un-sprung mass* m_u is a mass that is unsupported by a suspension spring (wheel axles, wheel hub, tires, wheel bearings, spring, dampers, etc.). When the vehicle moves over bump or road holes, the un-sprung mass is rapidly accelerated and must be decelerated by the suspension damping devices. Figure 4.3 shown a quarter model of it by introducing the sprung and un-sprung masses of the vehicle.

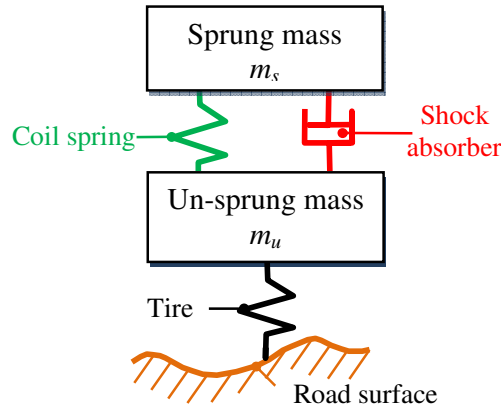


Figure 4.3: Schematic model of a quarter of the vehicle's suspension system

The total mass of the terrain vehicle m would be $m = m_s + m_u = 1150$ kg.

4.1.4 Design constraints and restrictions

Some of the requirements and restrictions were given by the RTC Company according to the European Commission Directive on Design Rules. During the designing processes of the

suspension and steering systems consideration should be given to a consideration of the materials' properties, available parts, weight, cost as well as the possibilities for manufacture. Although all of these are important for evaluating the design, compromises are often necessary. In this case the criteria had to be addressed and a solution obtained that ensured most of the requirements regarding the treated problem.

The basic condition during the conception and designing of the suspension and steering system is knowledge regarding the vehicle's main characteristics. Such characteristics are the considered total mass, vehicle speeds, geometric dimensions, minimal turning radius, maximal gradients of road slopes, dimensions of tires, and many other parameters that affect the accuracy of the design. The required design data was available.

Restrictions placed limitations on adequate software, prototypes, experimental results, small errors and deviations in design and manufacturing, the limitations of ECE regulations, adjustments to the rear wheels, etc.

4.2 Geometric parameters involved in the suspension system

The function of the suspension system is to keep, as much as possible, the positions of the tires relatively constant regarding the road surface throughout the motion of the suspension mechanism. When designing it, it was very important to identify how the vertical motion of wheel would be, in order to design a suitable suspension mechanism that would ensure such wheel motion.

4.2.1 Suspension geometry

When speaking about the suspension geometry, this means how the un-sprung mass of the vehicle would be connected to the sprung mass. These connections not only dictate the path of the wheel, but also control those forces transmitted between the un-sprung and sprung masses.

The designing of a terrain vehicle's suspension geometry is the same for both the front and rear axles as an advanced model of the double wishbone. This advanced model could be ranked as a multilink suspension system. The following provides more information and details about its characteristics.

The critical criterion concerning the designing of this suspension system was the ensuring of much higher vertical wheel motion in order for the tires to negotiate terrain roughness. If the suspension mechanism does not provide efficient motion of the wheels then when the wheels contact bumps or road holes, the wheels will continue their upward motion,

taking the chassis with them at the same high velocity, and causing greater acceleration by the driver. The main task was to design a fully operational suspension system which would allow efficient vertical wheel motion and thus the vehicle would provide suitable driving comfort and driving stability during movement over various terrains. The check list required the wheel stroke to be 500 mm, where the wheel position in *bound* is +250 mm - Figure 4.4.a, *rest* is 0 mm - Figure 4.4.b and *rebound* is -250 mm - Figure 4.4.c.

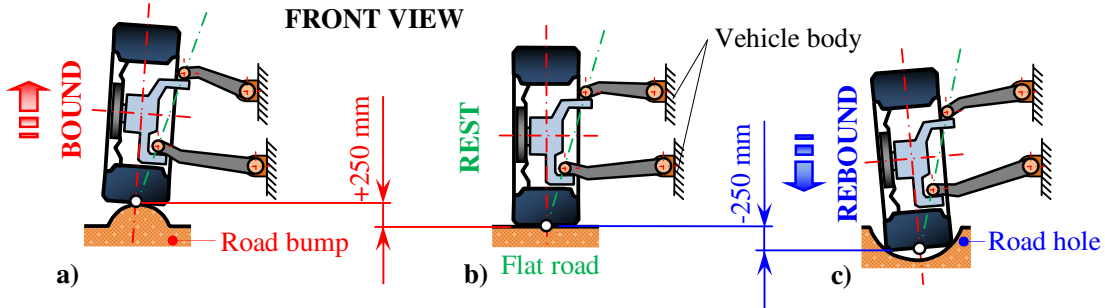


Figure 4.4: Suspension motions; a) bound, b) rest, and c) rebound

When the vehicle's wheels move over bumps or road holes causing bound or rebound motion, they must not come into contact with any part of the chassis or the vehicle body.

4.2.2 Camber angle γ

Some types of vehicles when moving over various terrains such as bumps and holes as well as cornering, change the centers of the vertical positions of the wheels which is the so-called *camber angle* γ . The camber angle is an angle between the vertical axis of the wheels and the vertical axis of the vehicle when viewed from the front or rear. According to the configuration of the suspension system, the camber angle has three possible positions such as *positive camber*, *zero camber*, and *negative camber*, as shown in Figure 4.5.

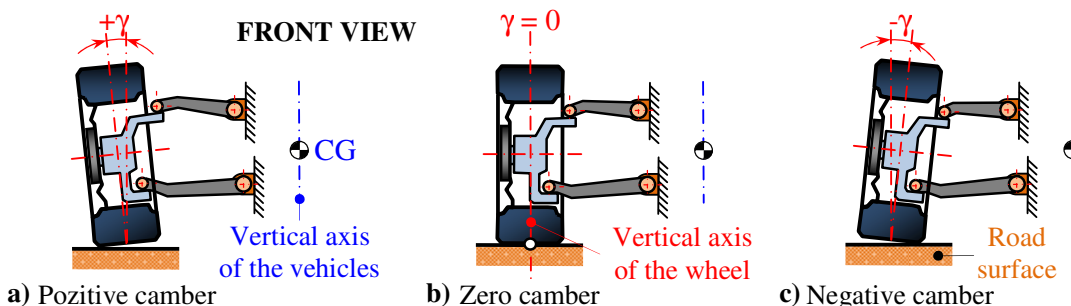


Figure 4.5: Vertical wheel position; a) positive, b) zero and c) negative camber angle

The camber angle is termed *positive camber* $+\gamma$ if the top of the wheel is further out than the bottom, Figure 4.5, a *zero camber* $\gamma = 0$ is the case where the top and bottom of the wheel

are in the same centerline as the vehicle, Figure 4.5.b. It is called *negative camber* - γ when the bottom of the wheel is further out than the top, Figure 4.5.c.

Any camber angle increase will therefore reduce the stability and traction of the vehicle as a result of a small contact of the tire with the road surface. The camber angle causes the lateral tire forces so-called *camber thrust force*, as shown in Figure 4.6. If the camber angle increases continuously, then the lateral tire force F_y also increases, which affects life-expectancy of the tire, and the vehicle's stability.

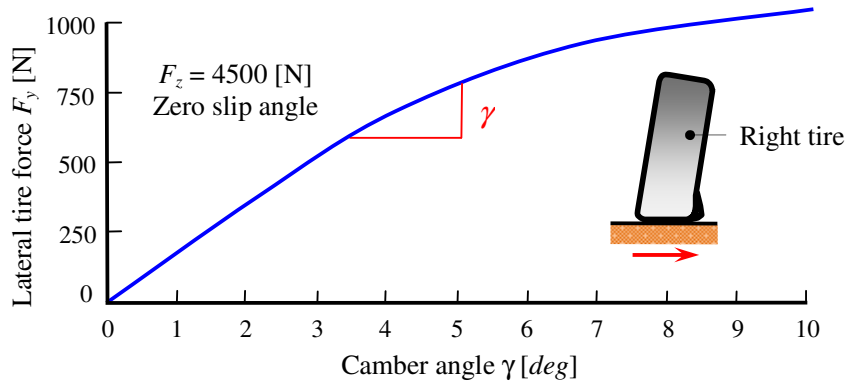


Figure 4.6: Lateral tire forces as a function of positive camber angle, Gillespie [12]

Studies have shown that *zero camber* leads to better life-expectancy when tire wear is smaller. Positive camber would lead to more pronounced wear on the outer shoulder and negative camber to more pronounced wear on the inside of the tire, Figure 4.7, Reimpell [54].

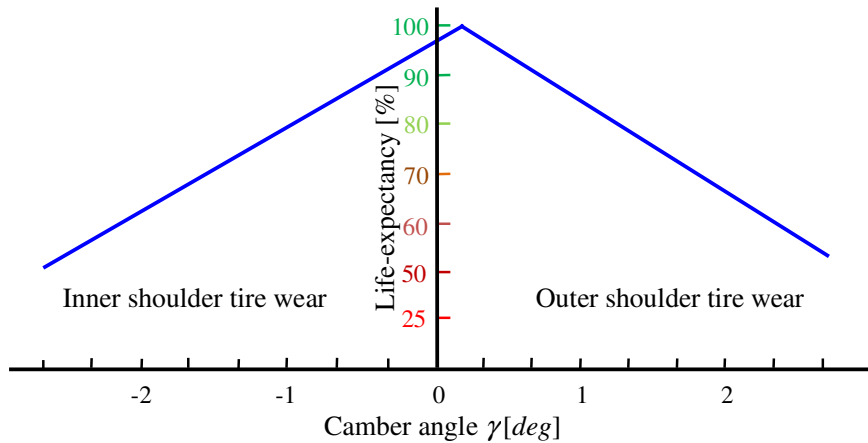


Figure 4.7: Life-expectancy of the tire as a function of camber angle, Reimpell [54]

When considering the advantages that suspension systems' with zero camber angles provide e.g. better contact of tire with ground surface and the life-expectancy of the tire is higher, it was decided to design a suspension mechanism for our terrain vehicle that would offer zero camber angles during the bound or rebound motion of the wheel.

4.2.3 Camber steer

When the wheels of a vehicle are cambered from the vertical centerline axis, the rolling radius is smaller on one side than the other. The tire then forms part of a cone and tries to rotate about its apex, as is shown in Figure 4.8.

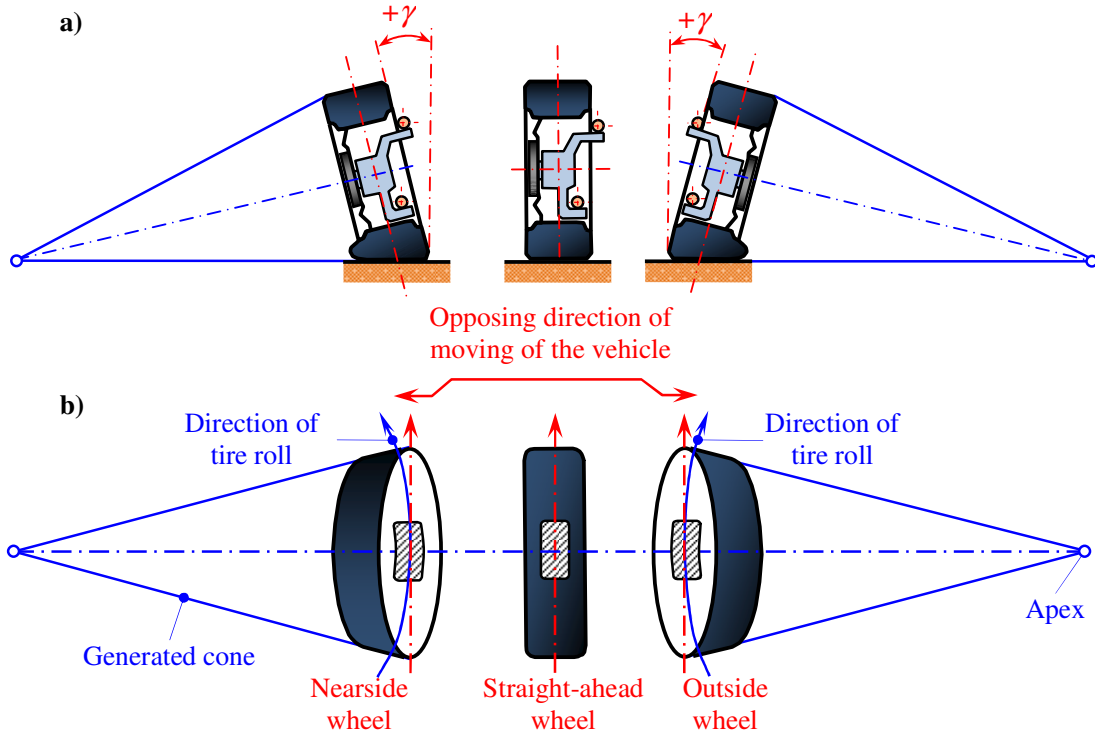


Figure 4.8: Positive camber steer; a) front view, and b) plan view

If an over tire-roll, a point on the larger side of the tire moves further by more than a point on the smaller side, this causes the wheel to deviate from the straight ahead direction and produce *camber steer*. Positive camber steer will push wheels into turning away from each other and produce *toe-out*, Figure 4.8, whilst negative camber on each side pushes the wheels to turn towards each other, thus causing *toe-in*, Figure 4.9, Heisler [38]. Toe setting affects three major issues regarding a vehicle's performance, such are: tire wear, straight line stability, and corner-entry handling characteristics. Toe-in improves the directional stability of a car and reduces the tendency of the wheel to shimmy, Rill [4]. When the camber angle is negative, negative camber steer assists the steering of the vehicle because the tires want to follow the natural direction path created by the generated cone. Conversely, positive camber angle hinders the steering of the vehicle as a result the tires being obligated to follow a forced path which is different from the natural direction of tire roll, Figure 4.9.

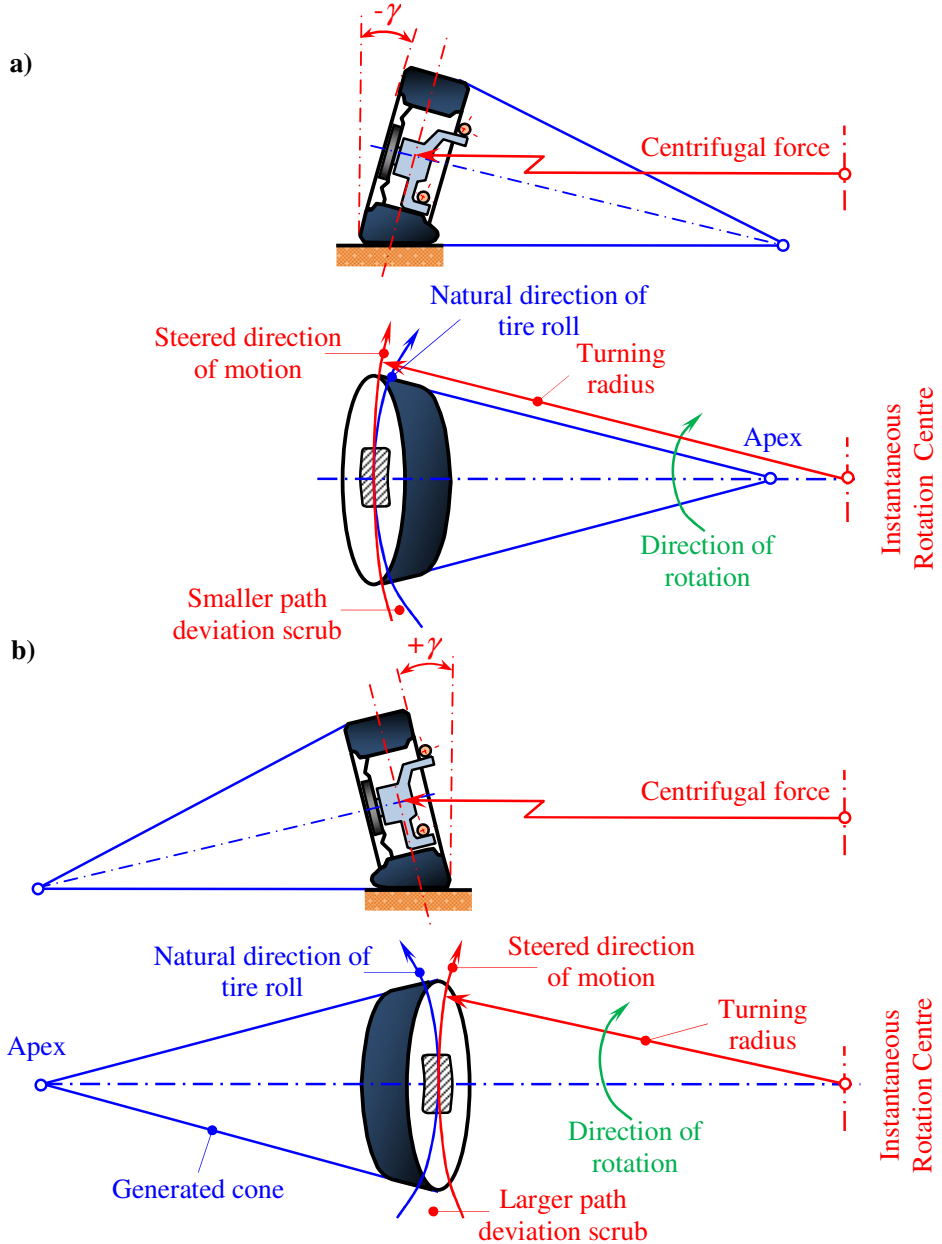


Figure 4.9: Principle of camber steer; a) negative camber steer, and b) positive camber steer

4.2.4 Kingpin inclination angle and kingpin offset

Kingpin geometry is also an important factor for designing vehicle suspension geometry. It determines the steering feelings of drivers, the driving performance, and the steering stability of the vehicle. The caster angle ε is the angle formed between the steering axis and the vertical axis of the wheel, viewed from the side of the vehicle, Figure 4.10.a. The caster angle for each wheel on an axle should be equal and provide steering stability, Dixon [8]. The kingpin inclination angle σ is the angle that arises between the steering axis and vertical axis

of the wheel, viewed from the front of the vehicle, Figure 4.10.b. It is also known as steering axis inclination and usually has a range from 0 to 20°, Lee [43].

The kingpin angle helps offer space for fitting brakes. If the kingpin inclination is determined correctly, then driver steering effort will be reduced by providing drivers with good feeling. If the kingpin inclination angle is zero, it is called centerline steering. The kingpin inclination axis is usually neither vertical nor centered on the tire contact patch for reasonable issues regarding the steering stability of the vehicle.

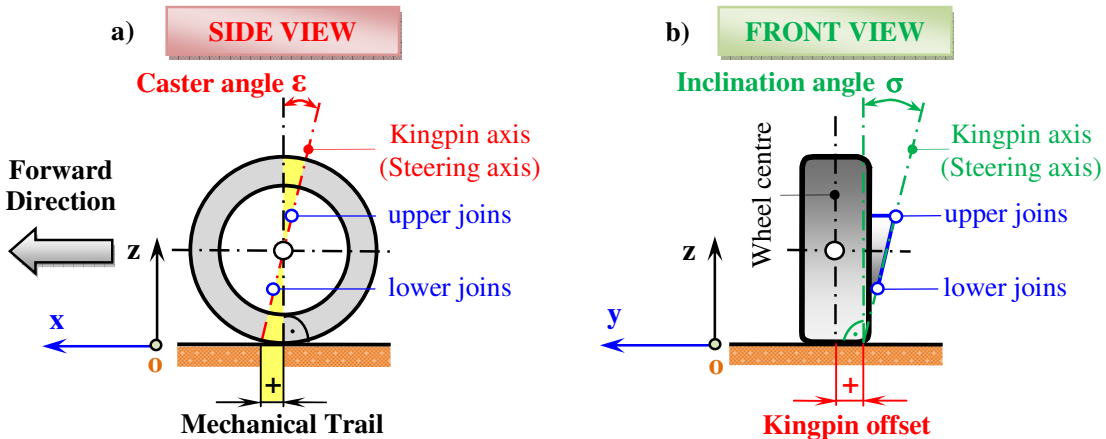


Figure 4.10: Kingpin inclination angle and kingpin offset; a) side view, and b) front view

The *kingpin offset* is the horizontal distance measured from the steering axis to the intersection point with the ground and wheel center contact with ground as shown in Figure 4.10 and Figure 4.11. The kingpin offset is also known as the scrub radius which can be positive, negative and zero offset, Figure 4.11. The kingpin offset is positive when the contact center of the wheel is outside the steering axis intersection point on the ground, Figure 4.11.a. If the contact center of the wheel is inside the steering axis intersection point to the ground then the kingpin offset is negative, Figure 4.11.b. It is zero when the contact center of the wheel is at the same point of steering axis intersection on the ground, Figure 4.11.c. The larger kingpin inclination angles result with a smaller or negative kingpin offset.

When a driver accelerates or stops a vehicle then the vehicle's wheels will produce driving or braking forces (at the ground). These forces are transmitted through the steering mechanism's additional steering torques to the steering wheel, which is proportional to the offset distance. If the driving or braking force is different on the left than on the right wheels then there will be a net steering torque felt by the driver (assuming that the steering system has good enough reverse efficiency). When the wheels have a tendency to stop or accelerate during the braking or acceleration processes, the positive kingpin offset distance and the

inertia force of the vehicle produce a turning moment which force the wheels to turn about the contact patch center in an outward direction at the front, Figure 4.11.a. Therefore the positive kingpin offset compounds the natural tendency for the vehicle to deviate towards the left if the right wheel slips instead of continuing on a stable straight ahead path, Heisler [38].

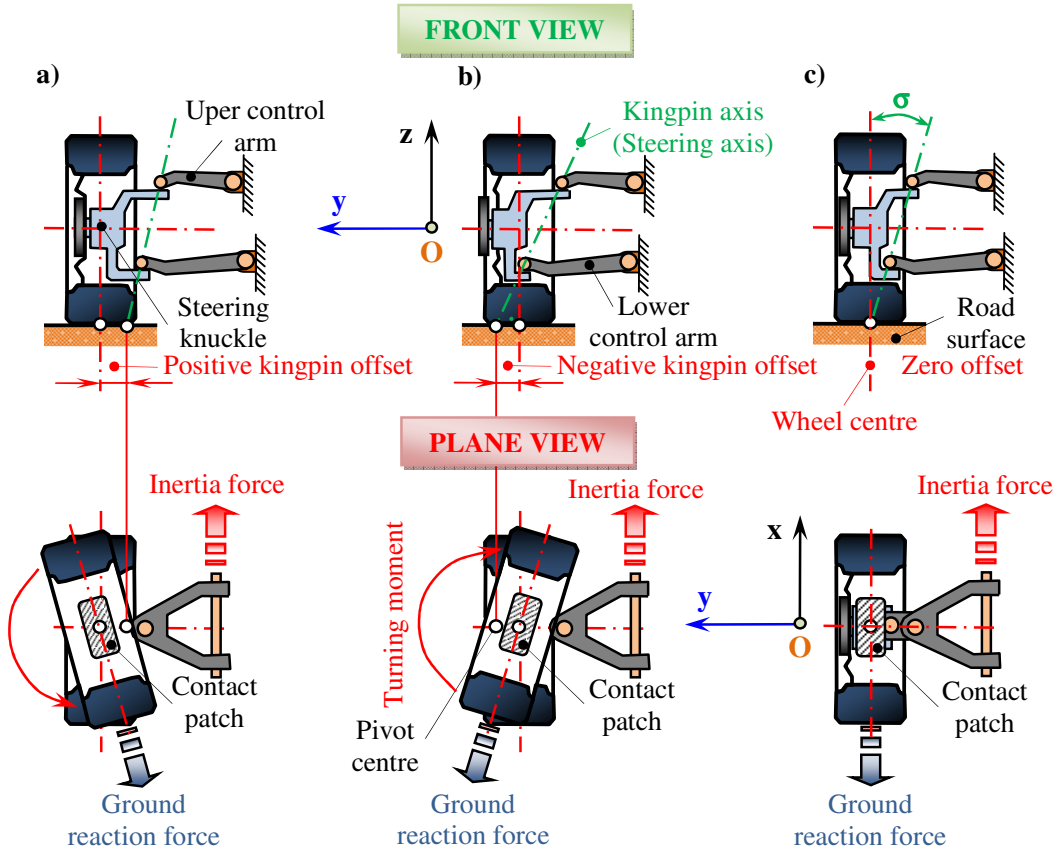


Figure 4.11: The kingpin offset cases; a) positive, b) negative, and b) zero

With negative kingpin offset the inertia force of the vehicle will produce a turning moment that forces the wheels to turn inwards at the front about the contact path center, Figure 4.11.b. The consequence of negative kingpin offset is that the effective braked wheels rotate in the opposite direction to which the vehicle tends to turn and so counteracts the deviation tendency, enabling the vehicle to stay in a stable straight ahead direction. Sometimes a negative offset is used, thus giving straighter braking when the surface friction varies between tracks, Dixon [8].

The only case when turning moment (additional steering torque) will not be produced from the wheels of the vehicle will be when the kingpin offset is zero, because there is no turning moment, Figure 4.11.c. When developing a suspension system for a terrain vehicle the tendency is to design the kingpin offset to be zero.

4.3 Designing process for developing of the suspension system

After a detailed study of the literature and by taking into consideration the advantages and disadvantages concerning various suspension systems such as respecting the criteria and constraints, sufficient knowledge had been developed to effectively design a suspension system for the terrain vehicle. It was found that the best response to fulfilling the design task was to install an independent suspension system. This independent suspension system would make it possible for each wheel to have independent motion.

In order for the terrain vehicle to provide good performance a suspension system would be required that would allow greater wheel motion in a vertical direction, whilst in passenger cars such movements are considerably smaller due to the rollover risk. In order to ensure greater motion of the wheel, the suspension system should continuously maintain contact between tires and ground surface. Based on previous experience these requirements could be obtained if the suspension system provides a zero camber angle. It was foreseen that an adequate solution would be a sophistication of the double wishbone suspension system.

The following were the examined kinematics of the double wishbone suspension systems, where the lengths of the control arms will be both equal and unequal. The developed design is derived from double wishbone. For analyzing the suspension performance when a vehicle passed over bumps, a comparison was carried out of the behavior of the wheel motion when wheels moved from their static positions (rest positions – 0) to their upward limits (bound positions +250 mm) and to their downward limits (rebound positions -250 mm).

Many authors within this research area have only analyzed the quarter vehicle suspension system. Therefore, it seemed to be sufficient to analyze only the quarter of it. This justification was a result of the fact that the terrain vehicle has the same suspension mechanism on all its wheels.

4.3.1 The first design concept

The first design concept was started by analyzing the double wishbone with the unequal control arms introduced in Figure 4.12. Figure 4.12.a shows a frontal view of the double wishbone suspension system with equal longer arms, whilst Figure 4.12.b show unequal shorter control arms. If the vehicle has large track width w it is better to start from the premise that the longer control arms of the double wishbone are better than the shorter. The double wishbone suspension system expect their current popularity, longer control arms allow a relatively large vertical motion of wheel which corresponding by small changes of its

characteristics. The suspension system with shorter control arms works reasonably well around a limited range of motions and after that drastically changes its characteristics when it is near the end of its motion.

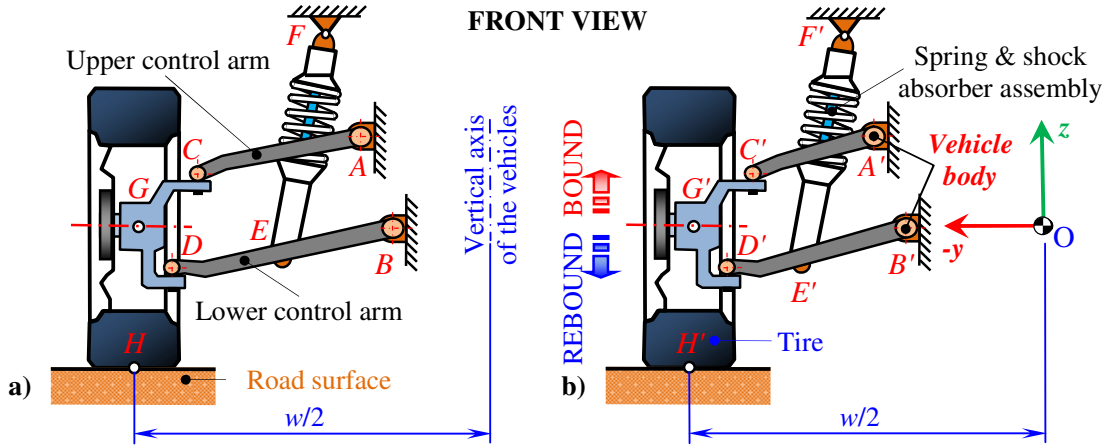


Figure 4.12: Front view of the quarter double wishbone suspension system;

a) longer and b) shorter non-equal control arm

In order to confirm the statement that the suspension system with longer control arms has better kinematics behavior compared with the shorter ones, the following necessary data for the modeling of suspension systems with longer and shorter non-equal control arms, is presented in Tables 4.2 and 4.3.

Table 4.2: Joint points and main lengths of the double wishbone suspension mechanism with longer non-equal control arms

Axis	Joint positions and length of links [mm]												
	A	B	C	D	E	F	G	H	\overline{AC}	\overline{BD}	\overline{CD}	\overline{BE}	
y_i	-323	-273	-767	-849	-561	-500	-992.5	-992.5	500	650	270	325	
z_i	85	-85	-126	-386	-236	300	-250	-650					

The data presented in Table 4.2 is used for modeling the suspension system with longer non-equal arms, whilst Table 4.3 introduces data for modeling the suspension system with shorter non-equal upper and lower control arms.

Table 4.3: Joint points and main lengths of the double wishbone suspension mechanism with shorter non-equal control arms

Axis	Joint positions and length of links [mm]												
	A'	B'	C'	D'	E'	F'	G'	H'	$\overline{A'C'}$	$\overline{B'D'}$	$\overline{C'D'}$	$\overline{B'E'}$	
y_i	-450	-400	-755	-826	-613	-500	-990	-990	350	500	270	250	
z_i	85	-85	-87	-347	-216	300	-250	-650					

Relative motions of the wheels can be in: longitudinal x , lateral y , and vertical z directions. During the braking and acceleration processes of the vehicle in the longitudinal direction, caster angle and mechanical trail appear. Lateral and vertical motions of the wheels occur when the vehicle moves over uneven terrain by producing bound and rebound positions.

Researches so far have indicated that for kinematic analyses of the wheels motion it is suitable to consider only the vertical and lateral motions. For comparison, kinematic advantages that provide the suspension system with double wishbone longer and shorter non-equal control arms are simulated in Working Model environments, the results are shown by the diagrams.

Figure 4.13 present the path of the wheel for the suspension system with double wishbone longer and shorter non-equal lengths of the control arms. It is indicated that during the vertical motion of the wheel in rebound for -220 mm and rest positions 0, the path of the wheel has the same lateral displacement by intersection at the same point.

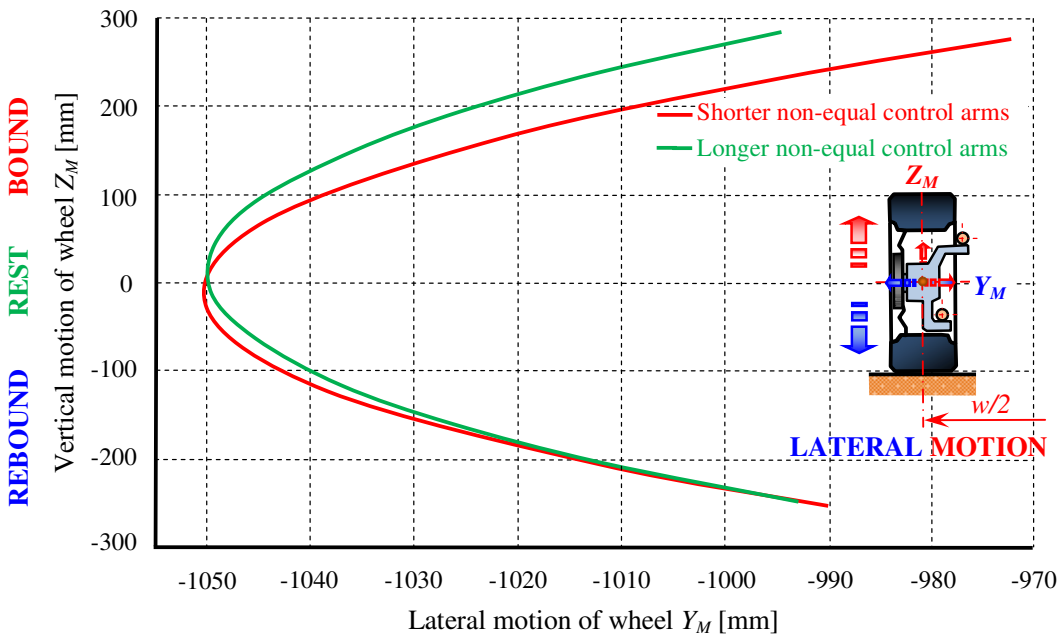


Figure 4.13: Path of wheel for the suspension system with double wishbone longer and shorter non-equal control arms

Figure 4.14 introduces how the camber angle for longer and shorter non-equal control arms changes as a result of motion of the wheel from its rest position. It is observed that when the wheel moves upward from the rest position, the camber angles drastically increase by producing negative camber angle, whilst when the wheel moves downward the camber angle becomes more positive with smaller values than the upward motion. Also the suspension

system with shorter control arms produces more camber angle compare with the longer control arms. The higher values for the camber angles are a result of the upper and lower control arms not having equal lengths. Higher values of camber angles have an influence on vehicle stability as a result of poor contact of the tires with the road surface.

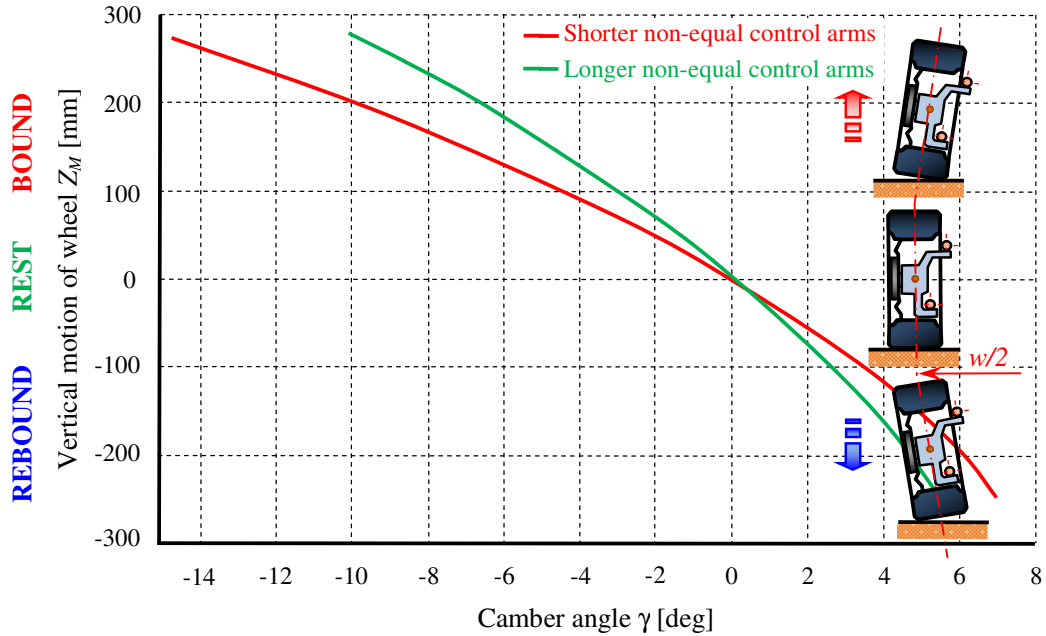


Figure 4.14: Vertical motion of wheel as a function of camber angle for the suspension system with double wishbone longer and shorter non-equal control arms

It can obviously be seen that the suspension system with double wishbone shorter control arms has lower performances compared with the longer control arm. This confirms when with wheel motion in the boundary positions, the suspension system with shorter non-equal control arms obtains greater displacements and camber angle, and consequently influences the life expectancy of the tires, and vehicle stability. Therefore, in the second design concept and the final design, the suspension system of the terrain vehicle was designed a longer length of control arm. The only significant disadvantage of the double wishbone suspension system with longer control arms is their relatively low stiffness. This potential problem can be overcome by using a slightly larger tube with a thicker wall.

4.3.2 The second design concept

The second design concept was an advancement of the first design concept, Figure 4.15. So, the design of the suspension system in this case was based on the fact that the double wishbone with longer control arms offered better features compared to the shorter. This argument was proven during the first design concept. What differentiates from the first design

concept is that the upper and lower control arms have equal lengths. The comparison reference is used double wishbone with longer non-equal control arms. Figure 4.15 introduces the frontal view of the quarter double wishbone suspension system with longer equal control arms. Table 4.4 gives the necessary data for modeling the suspension system with longer equal upper and lower control arms.

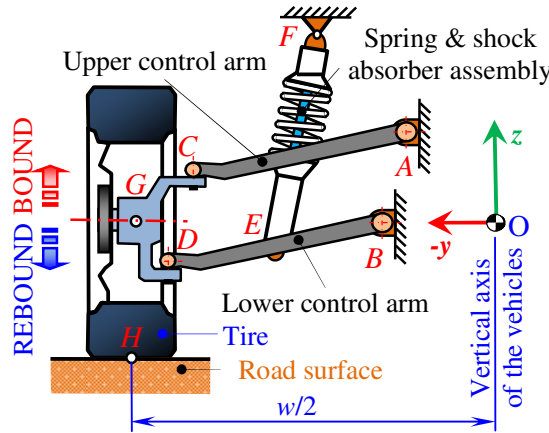


Figure 4.15: Front view of quarter double wishbone suspension system
with longer equal control arms

Table 4.4 Joint points and main lengths of the double wishbone suspension mechanism with longer equal control arms

Axis	Joint positions and length of links [mm]												
	A	B	C	D	E	F	G	H	\overline{AC}	\overline{BD}	\overline{CD}	\overline{BE}	
y_i	-273	-313	-816	-856	-584	-500	-992.5	-992.5	600	600	175	300	
z_i	85	-85	-171	-342	-213	300	-250	-650					

The data presented in Table 4.4 will be used for modeling the suspension system with longer equal control arms within the Working Model environments. The results are presented in the following diagrams.

Figure 4.16 shows the path of wheel for the double wishbone suspension system with longer non-equal and equal control arms. It is shown that during rebound the motions of the wheel curves seem to be similar to the non-equal and equal control arms. For the rest position, both systems have the same wheel path. However, when the wheel is in bound motion, the difference between the non-equal and equal control arms is very small. In other words this small difference in lateral wheel displacement cannot be considered either as an advantage or disadvantage that provides the suspension system with longer non-equal and equal control arms.

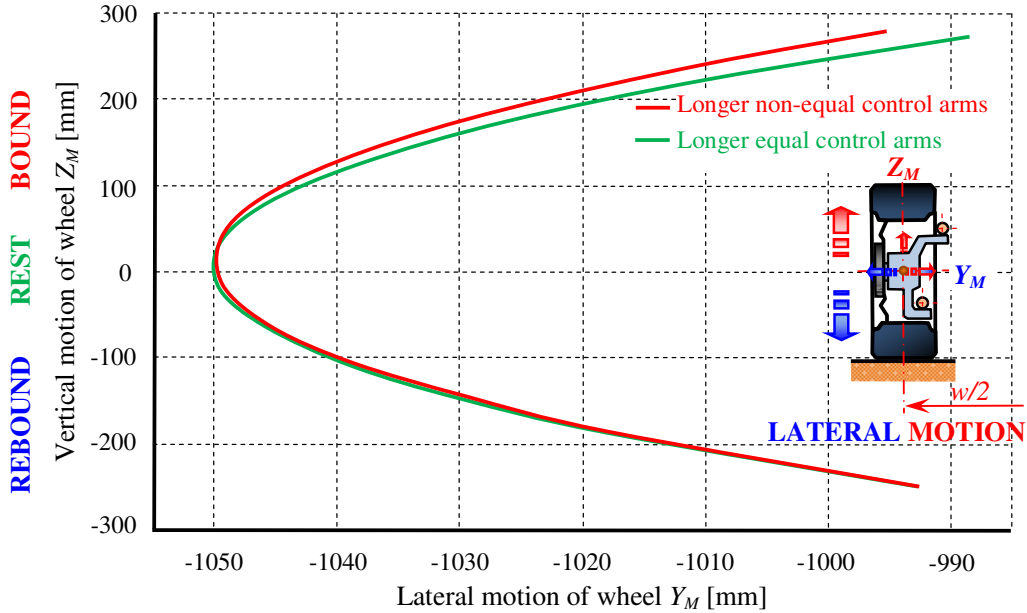


Figure 4.16: Path of wheel for the suspension system with double wishbone longer non-equal and equal control arms

Figure 4.17 introduces how the camber angle for longer non-equal and equal control arms changes as a result of the motion of wheel from its rest position. It can be observed that when the wheel moves upward or downward from the rest position, the camber angle obtain higher values for the double wishbone with longer non-equal control arms. The situation is totally different for the double wishbone with longer equal control arms where the change of the camber angle from rest position is approximately zero.

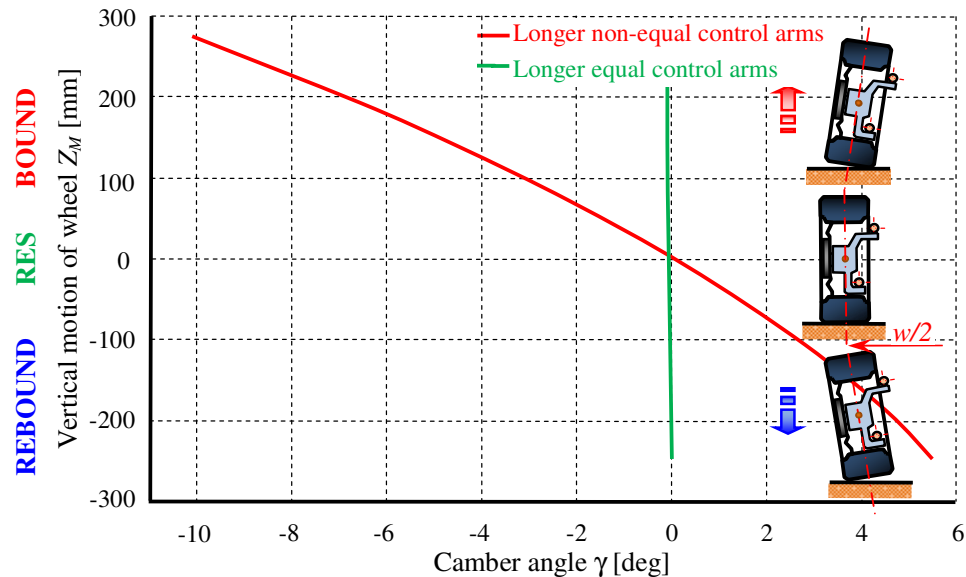


Figure 4.17: Vertical motion of the wheel as a function of the camber angle for the suspension system with double wishbone longer non-equal and equal control arms

As a result of the characteristics shown in Figures 4.16 and 4.17 for the suspension system with longer equal control arms, it can be concluded that this suspension system had the better advantages when compared to the longer non-equal control arms. Even though it can be considered that such a suspension system offers better performance than others, in the boundary position the wheel (bound and rebound) from the rest position still has a large displacements of the wheel in the lateral direction of around 58 mm left and 58 mm right for the wheel, a total of 116 mm. Such a displacement would be expected to affect the life-expectancy regarding driving stability by causing additional loads on the suspension mechanism. Therefore, in the final design of the suspension system, the development of it focused on the sophistication of the second concept design but with a new design to fulfill the requirement that camber angle and lateral wheel motion should have smaller values as far as possible.

4.3.3 The final design concept

The state-of-the-art for final design concept of the terrain vehicle's suspension system is based on three fundamental principles:

- a suitable design for robust performance,
- using the best proven performance provided by the reviewed suspension, and
- continuous refining of the design until it is optimized for fulfilling the submitted requirement.

Actually, the advent the personal computer made it possible to analyze the suspension geometry without cutting and welding its structures. By applying the available knowledge for using computer simulations, it was possible to attain the predefined requirements. The only thing still required to do was to decide what the suspension system needed to function well and then run the computer to proceed with the variables and obtain the desired design.

The final design of the suspension system was derived at by refining the double wishbone suspension system with a longer equal control arm, Figure 4.18.

This suspension system is categorized as a multi-link suspension system that is rather more complicated than other systems, and 3D of quarter of it is shown in Figure 4.18. This design allows for relatively large vertical motion of wheel by using correspondingly small undesired suspension characteristics. The further development process focused on the lateral motion of the tire and camber angle having, as far as possible, smaller values for the boundary positions when the wheel motion is in bound and rebound. The design of the quarter suspension system in 2D (y and z - axis) with necessary parameters, is shown in Figure 4.19.

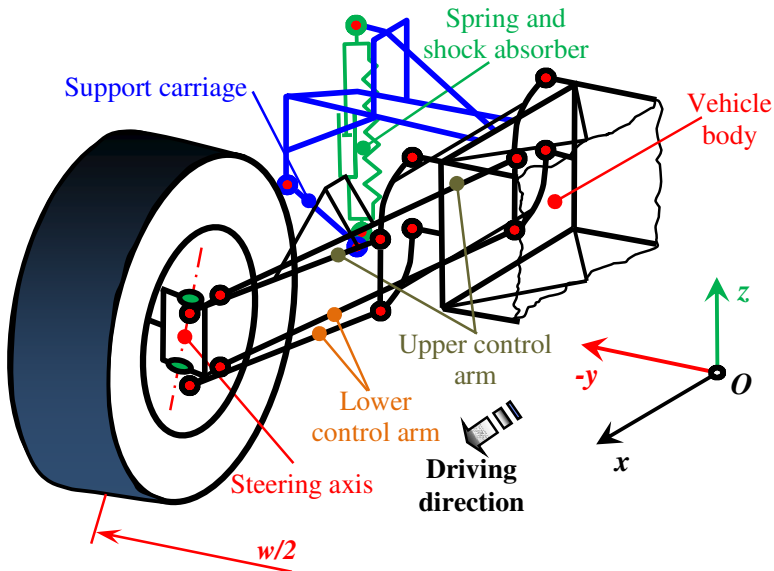


Figure 4.18: Final design of the 3D quarter suspension system for the terrain vehicle

Design of the quarter suspension system in 2D (y and z - axis) with necessary parameters is shown in Figure 4.19.

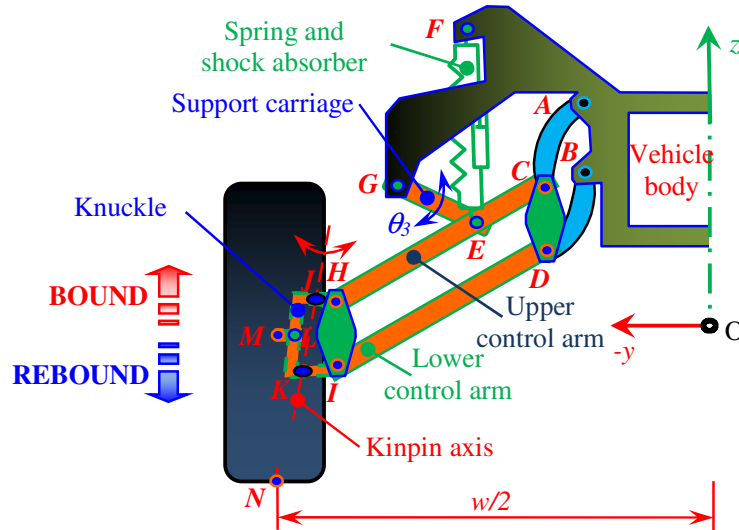


Figure 4.19: Front view of 2D quarter suspension system for terrain vehicle

Point O is centre of coordinative system $-yOz$ with coordinates O (0, 0). Axis $-yO$ go through centre of the wheel (rest position), while Oz is centers of vehicle-front view. For evaluation of the performance that provides this suspension system is necessary to make geometric modeling. The joints position and other necessary data for geometry modeling are given in Table 4.5. This data help to analyze performance that provides that system.

Table 4.5: Joint points and main lengths of the suspension mechanism links

Axis	Joint positions and length of links [mm]											
	A	B	C	D	E	F	G	H	\overline{AC}	\overline{BD}	\overline{AB}	\overline{CD}
y_i	-273	-273	-351	-351	-517	-554	-708	-876	220	220	170	170
z_i	317	147	111	-59	19	501	107	-181				
Axis	I	J	K	L	M	N	\overline{CE}	\overline{EH}	\overline{GE}	\overline{DI}	\overline{HI}	\overline{ML}
y_i	-876	-913	-950	-930	-1017.5	-1017.5	190	410	210	600	170	325
z_i	-351	-176	-344	-250	-250	-650						

Modeling of the quarter suspension system for terrain vehicle is performed in Working Model environments. All simulations are making with fixing vehicle body and wheel motion in boundary position, bound and rebound is ensured by using a hydraulic actuator. Simulation results are presented by diagrams.

Figure 4.20 presents path of wheel for both double wishbone with longer equal length and final design of the suspension systems.

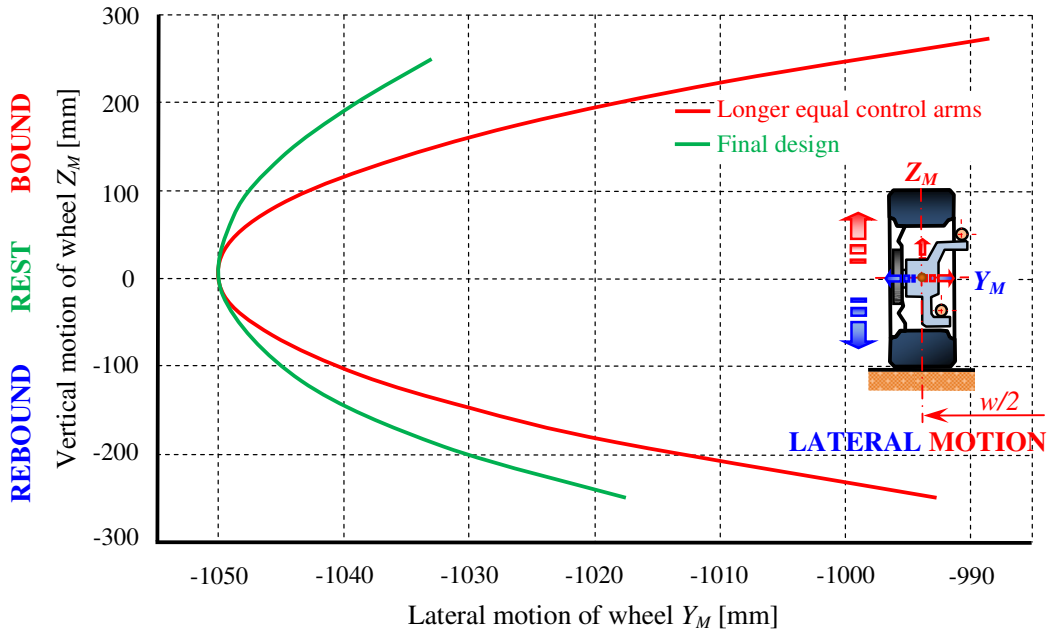


Figure 4.20: Path of wheel for the suspension system with double wishbone longer equal control arms and final design

Figure 4.21 introduces the changing of the camber angle for both double wishbones with longer equal length, and final design of the suspension system as a function of the vertical wheel motion (bound and rebound). In the following chapters present, in great detail, the final design of the terrain vehicle's suspension system which successfully fulfilled the design requirements given by the check list.

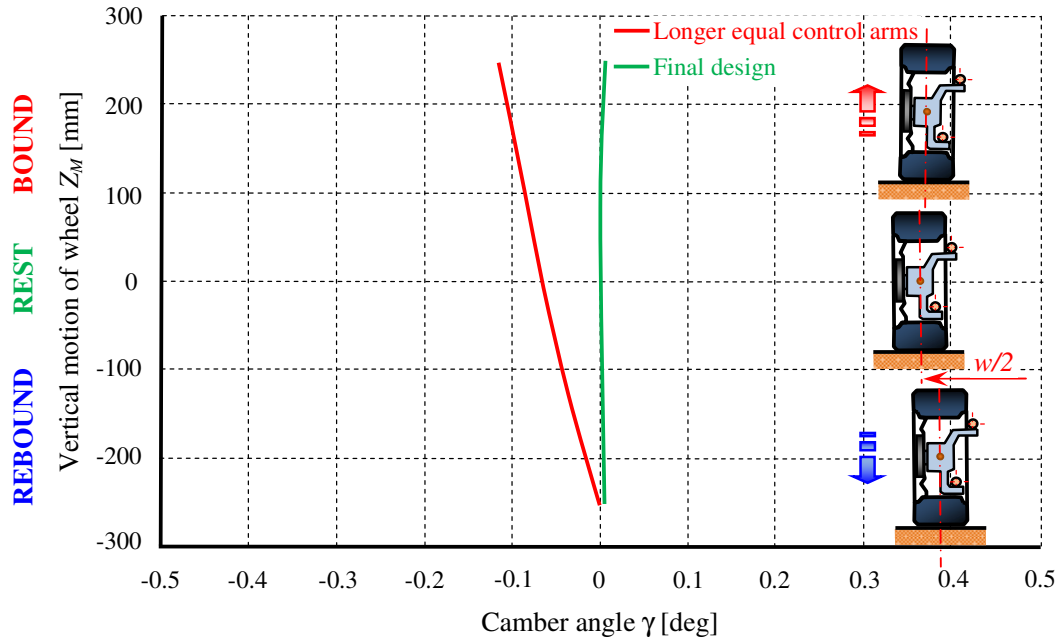
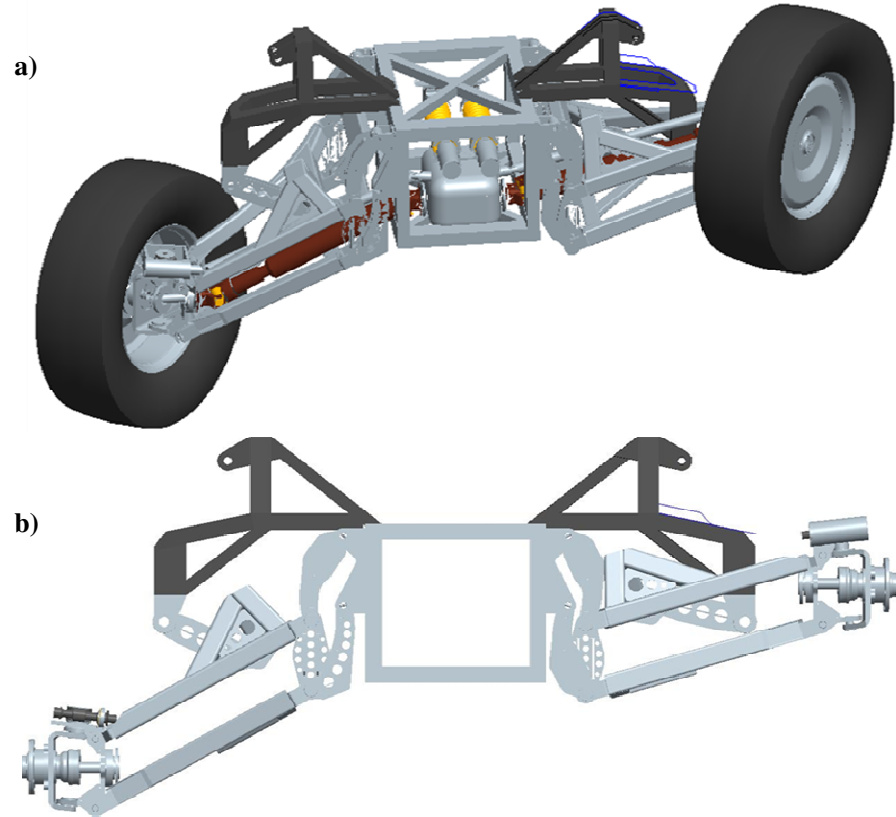


Figure 4.21: Vertical motion of the wheel as a function of the camber angle for the suspension system with double wishbone longer equal control arms and final design

Figure 4.22 show a model of the final design of the terrain vehicle suspension system performed within the Pro/ENGINEER environment (3D view, frontal view and plane view).



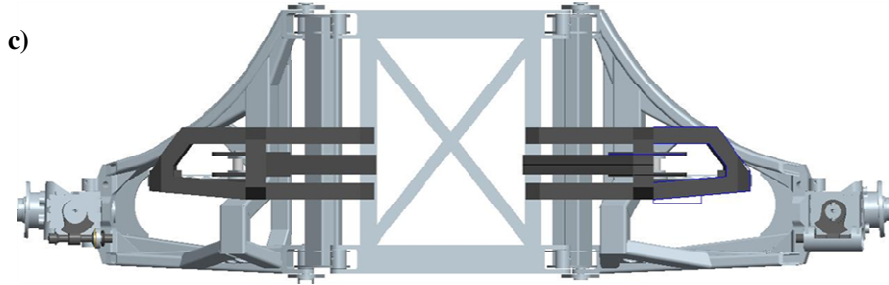


Figure 4.22: Final design of the terrain vehicle suspension system; [6]

a) 3D view, b) front view, and c) plane view

4.4 Discussing of the results

From Figure 4.20, it can be observed that when the wheel moves from its rest position to a rebound position (0 ... – 250 mm), the final design of the suspension system provides 45 % less lateral displacement of the wheel. When the wheel moves from the rest to the bound position (0 ... +250 mm) the obtained results display better behavior by ensuring 72.6 % less displacements compared with the suspension system with double wishbone longer equal control arms.

Therefore, the final design provides relatively small values for lateral displacements thus effectively improving the life-expectancy of the tire, reducing the additional load on the suspension mechanism and improving the stability of the vehicle when driving over various terrains.

Figure 4.21 show that the change of camber angle in the final design of the suspension system provides zero camber angles, thus causing better quality contact of the tire with the ground surface. In this case, the tire acts perpendicularly with the ground surface. Improving the quality contact has had an influence on improving the stability of the vehicle's movement when cornering, accelerating or braking.

Due to experiences, the vehicle suspension system mostly operates from rest to the bound direction as a result of ground excitation. The final design regarding the boundary position provides lateral wheel displacements of up to 17 mm. Such displacements in other systems are considered to be relatively larger.

5 MODELING, SIMULATION AND OPTIMIZATION OF THE SUSPENSION MECHANISM FOR A TERRAIN VEHICLE

Many centuries ago mechanisms found great application in various fields of mechanical engineering especially when required to transfer one type of motion into another (e.g. from displacements to rotational motion). A suitable methodology for analyzing mechanism behavior during the development process is more than necessary in order to obtain functionality and predefined motion. In this contest, the suspension mechanism is a spatial mechanism and would be difficult to analyze without an effective computer program. Their analyses are going to be more complicated when involving a greater number of rubber bushes which have influences on the suspension mechanism links by giving variable length. Despite these complications it is possible to gain appreciation of the suspension mechanism by neglecting rubber bush and concentrating on their basic motion.

The objective of this chapter is the modeling, simulation, and optimization of the suspension mechanism for a terrain vehicle. Based on the specific requirement given in the check list, the suspension mechanism will ensure that during all vertical motion of the wheels (± 250 mm bound and rebound), the camber angle should be zero. Except camber angle it is necessary that the lateral motion of the wheels is as small as possible when vehicle wheels moves upward or downward, in order to improve vehicle stability.

In order to estimate these requirements, it is necessary to have a powerful tool to compute those motions and forces that act in suspension mechanism as a result of the ground excitation. To speed this procedure it is helpful to have an effective program that simulates the suspension mechanism's behavior by employing appropriate essential parameters. One of the well-established ways of explaining mechanism performance is the modeling of the quarter of it. The developing of computer programs for solving equations of motion is performed in MathCAD environment for a quarter of it. Solutions are mainly based on the kinematic and dynamic behaviors which determine the motions and loads that affect the suspension mechanism, Werff [55]. To verify the reliability of the developed model, a comparison with one of the simple commercial Working Model Software [56], is carried out. In order to have an as small as possible lateral motion of the wheels, an optimization procedure is done for getting optimal lengths of suspension mechanism links.

5.1 Kinematic modeling and analysis of the suspension mechanism

The kinematic analyses for the terrain vehicle suspension mechanism are estimated according geometric modeling data shown in the final design for the suspension mechanism (chapter 4). By these data are estimating the mechanism's behavior. For kinematic analysis it is necessary to check the geometric variations of the components of the suspension mechanism over the operating range, spring and shock absorber relative motion along the vertical motion of the wheels. Notwithstanding the apparent complexities of some types of suspension systems, a basic understanding of their kinematic behavior can be derived from a two – dimensional analysis, by considering the motion of it only within a vertical plane (y , z – axis), Happian-Smith [57].

Determining the kinematic expressions for the suspension mechanism will enable simulation of the vertical displacement, velocity, and acceleration of the mechanism links for different positions of the wheel, for which expressions are usually inconvenient. Solving of the kinematic relations is performed in MathCAD and MATLAB environments.

5.1.1 Displacement analysis of the suspension mechanism

Terrain vehicle suspension mechanism for displacement analysis is shown in Figure 5.1.

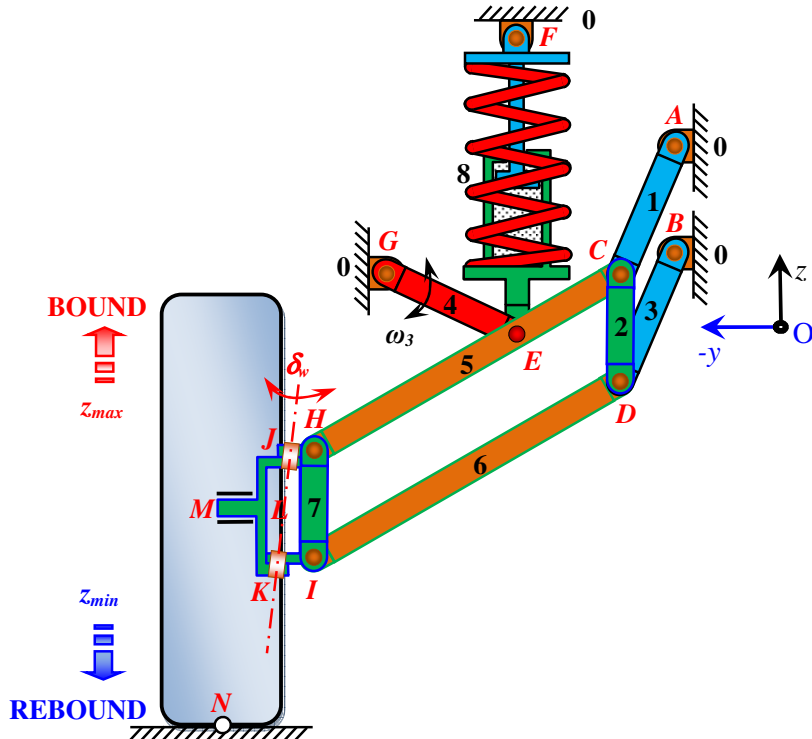


Figure 5.1: Kinematic linkages of the terrain vehicle suspension mechanism

The mechanism presented in Figure 5.1, has **nine links**, such as: 0, 1, 2, 4, 5, 6, 7 and 8 links. The motions of each link is in the vertical plane (y , z – axis). To derive expressions for computing displacement of the suspension mechanism it is necessary to employ methodology for the projection of the vector position defined by the vector loops. Each link of the mechanism is represented by a vector position. In followers are treated as vector loops and the equations of motion for the suspension mechanism is shown in Figure 5.1.

5.1.1.1 Vector loops and vector position

Based on the design task, the suspension mechanism should allow the wheel to move in a downward direction from the rest position (rebound) for displacement $z_{min} = -250$ mm where input angular displacement of links EG is $\theta_{3min} = 335.18$ deg. When the wheel moves upwards vertically from the rest position (bound), the maximal displacement is $z_{max} = 250$ mm and input angles of link \overline{EG} is $\theta_{3max} = 378.22$ deg. So, input angular displacement θ_3 of the link \overline{EG} is when considering primary variable by range from 335.18 to 378.22 deg. In order to determine the vertical motion of the wheel (point M) is necessary for determining unknown angular displacement such as $\theta_1(\theta_3)$, $\theta_2(\theta_3)$, $\theta_3(\theta_3)$ and relative length of spring and shock absorber $L_s(\theta_3)$ as a function of *input angular displacement* θ_3 . The vector positions of the suspension mechanism are: \mathbf{R}_1 , \mathbf{R}_2 , \mathbf{R}_3 , \mathbf{R}_4 , \mathbf{R}_5 , \mathbf{R}_6 , \mathbf{R}_7 , \mathbf{R}_8 , and \mathbf{R}_9 . The direction of each vector is arbitrary, however the angle is associated with the vectors direction measured using the positive direction of the y – axis. The unknown angular displacement and vectors position are shown in Figure 5.2, Figure 5.5 and Figure 5.8.

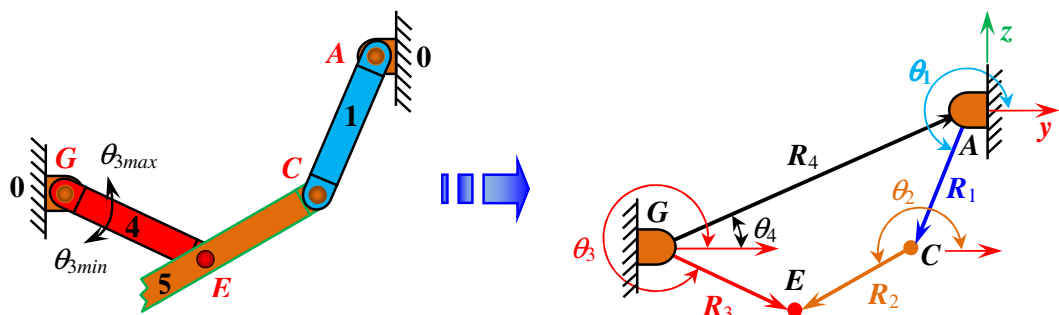


Figure 5.2: Vector loops of four-bar links derived from the suspension mechanism

A closed vector loop (four-bar links) is formed from the vector loops: \mathbf{R}_1 , \mathbf{R}_2 , \mathbf{R}_3 , and \mathbf{R}_4 , Figure 5.2. Link \overline{AG} is formed by the vector position \mathbf{R}_4 called the ground link which is fixed in the vehicle's body at an angular displacement θ_4 . Link \overline{EG} is the vector position \mathbf{R}_3 which is considered as the *input link* and is controlled by the *input angular displacement* θ_3 . Link \overline{CE} forms vector position \mathbf{R}_2 as a coupler link with angular displacement θ_2 and connects

the input and output links. Link \overline{AC} introduces vector position \mathbf{R}_1 which is the *output link* with angular displacement θ_1 . The *output angular displacement* θ_1 and *coupler angular displacement* θ_2 are functions of the links length and *input angular displacement* θ_3 . The vector loops of the four-bar links and data for links are shown in Figure 5.2 and Table 5.1.

Table 5.1 Vector representation of the four-bar linkages shown in Figure 5.2

Links	Name	Vector	Length [mm]	Angular angle [deg]	Variable
\overline{AC}	<i>Output</i>	\mathbf{R}_1	$r_1 = 220$	θ_1	$\rightarrow YES$
\overline{CE}	<i>Coupler</i>	\mathbf{R}_2	$r_2 = 190$	θ_2	$\rightarrow YES$
\overline{GE}	<i>Input</i>	\mathbf{R}_3	$r_3 = 210$	$\theta_3 \sim 335\ldots378$	$\rightarrow YES$
\overline{GA}	<i>Ground</i>	\mathbf{R}_4	$r_4 = 483.04$	θ_4	$\rightarrow NO$

Each vectors position \mathbf{R}_i is described by length r_i and angular displacement θ_i . The vector loop for four bar linkages (links: \overline{AC} , \overline{CE} , \overline{EG} and \overline{AG}) in global coordinate is:

$$\mathbf{R}_1 + \mathbf{R}_2 - \mathbf{R}_3 + \mathbf{R}_4 = 0, \quad (5.1)$$

where,

$$\mathbf{R}_{1\pm 4} = R_{x1\pm 4}\mathbf{i} + R_{y1\pm 4}\mathbf{j} = r_{1\pm 4} \cdot (\cos \theta_{1\pm 4}\mathbf{i} + \sin \theta_{1\pm 4}\mathbf{j}). \quad (5.2)$$

The horizontal and vertical components for each vector loop's equation is required the sum to be identically zero at all times in order to satisfy the physical assembly of the links. Substituting the Cartesian expression for the planar vector in equation (5.1), the result in:

$$\begin{aligned} r_1 \cdot \cos \theta_1 + r_2 \cdot \cos \theta_2 - r_3 \cdot \cos \theta_3 + r_4 \cdot \cos \theta_4 &= 0, \\ r_1 \cdot \sin \theta_1 + r_2 \cdot \sin \theta_2 - r_3 \cdot \sin \theta_3 + r_4 \cdot \sin \theta_4 &= 0, \end{aligned} \quad (5.3)$$

after regulation of expression (5.3), we get expressions:

$$\begin{aligned} r_2 \cdot \cos \theta_2 &= r_3 \cdot \cos \theta_3 - r_1 \cdot \cos \theta_1 - r_4 \cdot \cos \theta_4, \\ r_2 \cdot \sin \theta_2 &= r_3 \cdot \sin \theta_3 - r_1 \cdot \sin \theta_1 - r_4 \cdot \sin \theta_4. \end{aligned} \quad (5.4)$$

To derive the relationship between the *input* θ_3 and *output angular displacement* θ_1 , it is necessary to eliminate the *coupler angular displacement* θ_2 by some mathematical operation between equation (5.3) and (5.4). By squaring both sides, providing the following equations:

$$(r_2 \cdot \cos \theta_2)^2 = (r_3 \cdot \cos \theta_3 - r_1 \cdot \cos \theta_1 - r_4 \cdot \cos \theta_4)^2, \quad (5.5)$$

$$(r_2 \cdot \sin \theta_2)^2 = (r_3 \cdot \sin \theta_3 - r_1 \cdot \sin \theta_1 - r_4 \cdot \sin \theta_4)^2. \quad (5.6)$$

After some mathematic operation, expressions (5.5) and (5.6) are written as follow:

$$\begin{aligned} (r_2 \cdot \cos \theta_2)^2 &= r_1^2 \cdot \cos^2 \theta_1 + r_3^2 \cdot \cos^2 \theta_3 + r_4^2 \cdot \cos^2 \theta_4 + \dots \\ &\quad + 2 \cdot [r_1 \cdot \cos \theta_1 (r_4 \cdot \cos \theta_4 - r_3 \cdot \cos \theta_3) - r_3 \cdot r_4 \cdot \cos \theta_3 \cdot \cos \theta_4], \end{aligned} \quad (5.7)$$

$$(r_2 \cdot \sin \theta_2)^2 = r_1^2 \cdot \sin^2 \theta_1 + r_3^2 \cdot \sin^2 \theta_3 + r_4^2 \cdot \sin^2 \theta_4 + \dots \\ + 2 \cdot [r_1 \cdot \sin \theta_1 (r_4 \cdot \sin \theta_4 - r_3 \cdot \sin \theta_3) - r_3 \cdot r_4 \cdot \sin \theta_3 \cdot \sin \theta_4]. \quad (5.8)$$

By adding equation (5.7) and (5.8), generates the following expression:

$$\cos \theta_1 \cdot (r_4 \cdot \cos \theta_4 - r_3 \cdot \cos \theta_3) + \sin \theta_1 \cdot (r_4 \cdot \sin \theta_4 - r_3 \cdot \sin \theta_3) = \\ = \frac{r_2^2 - r_1^2 - r_3^2 - r_4^2}{2 \cdot r_1} + \frac{r_3 \cdot r_4 \cdot (\cos \theta_3 \cdot \cos \theta_4 + \sin \theta_3 \cdot \sin \theta_4)}{r_1}. \quad (5.9)$$

By substitution of the trigonometric function $\cos(\alpha\beta)$, equation (5.9) is written as follow:

$$r_4 \cdot \cos(\theta_1 - \theta_4) - r_3 \cdot \cos(\theta_1 - \theta_3) = \frac{r_2^2 - r_1^2 - r_3^2 - r_4^2}{2 \cdot r_1} + \frac{r_3 \cdot r_4}{r_1} \cdot \cos(\theta_3 - \theta_4). \quad (5.10)$$

Equation (5.14) is called as *Freudenstein's Equation*. From equation (5.10), it is difficult to determine the value of *output* θ_1 for the given value of *input angular displacement* θ_3 therefore it is necessary to simplify this equation by using trigonometrically expressions:

$$\sin \theta_1 = \frac{2 \cdot \tan(\theta_1 / 2)}{1 + \tan^2(\theta_1 / 2)}; \quad \cos \theta_1 = \frac{1 - \tan^2(\theta_1 / 2)}{1 + \tan^2(\theta_1 / 2)}. \quad (5.11)$$

Substituting $\sin \theta_1$, $\cos \theta_1$, and some other mathematical operation in order to simplify the relation between the *inputs angles* θ_3 and the *output angles* θ_1 , obtains the more practical expression given below:

$$A(\theta_3) \cdot \tan^2\left(\frac{\theta_1}{2}\right) + B(\theta_3) \cdot \tan\left(\frac{\theta_1}{2}\right) + C(\theta_3) = 0, \quad (5.12)$$

where substitution constants $A(\theta_3)$, $B(\theta_3)$ and $C(\theta_3)$ are in a function of *the input variable angular displacement* θ_3 , written by the following expressions:

$$A(\theta_3) = r_4 \cdot \cos \theta_4 - r_3 \cdot \cos \theta_3 + \frac{r_2^2 - r_1^2 - r_3^2 - r_4^2}{2 \cdot r_1} + \frac{r_3 \cdot r_4}{r_1} \cdot \cos(\theta_3 - \theta_4), \quad (5.13)$$

$$B(\theta_3) = 2 \cdot (r_3 \cdot \sin \theta_3 - r_4 \cdot \sin \theta_4), \quad (5.14)$$

$$C(\theta_3) = \frac{r_2^2 - r_1^2 - r_3^2 - r_4^2}{2 \cdot r_1} + \frac{r_3 \cdot r_4}{r_1} \cdot \cos(\theta_3 - \theta_4) - (r_4 \cdot \cos \theta_4 - r_3 \cdot \cos \theta_3). \quad (5.15)$$

As shown equation (5.12) is a quadratic function in $\tan(\theta_1/2)$ and their solution for finding the *output angular displacement* θ_1 are written as follow:

$$\tan\left(\frac{\theta_1}{2}\right) = \frac{-B(\theta_3) \pm \sqrt{B^2(\theta_3) - 4 \cdot A(\theta_3) \cdot C(\theta_3)}}{2 \cdot A(\theta_3)}. \quad (5.16)$$

Finally *output angular displacement* θ_1 , may be calculated by expression:

$$\theta_1(\theta_3) = 2 \cdot \tan^{-1} \left[\frac{-B(\theta_3) \pm \sqrt{B^2(\theta_3) - 4 \cdot A(\theta_3) \cdot C(\theta_3)}}{2 \cdot A(\theta_3)} \right]. \quad (5.17)$$

The *input angular displacement* θ_3 of the link \overline{EG} rotates for small angles to satisfy the vertical motion of the wheel. The data for determining the *output angular displacement* θ_1 are shown in Table 4.5 & Table 5.1. Obtained results are performed in the MathCAD [58] environment and exported in Microsoft Excel graphic presentation, Figure 5.3.

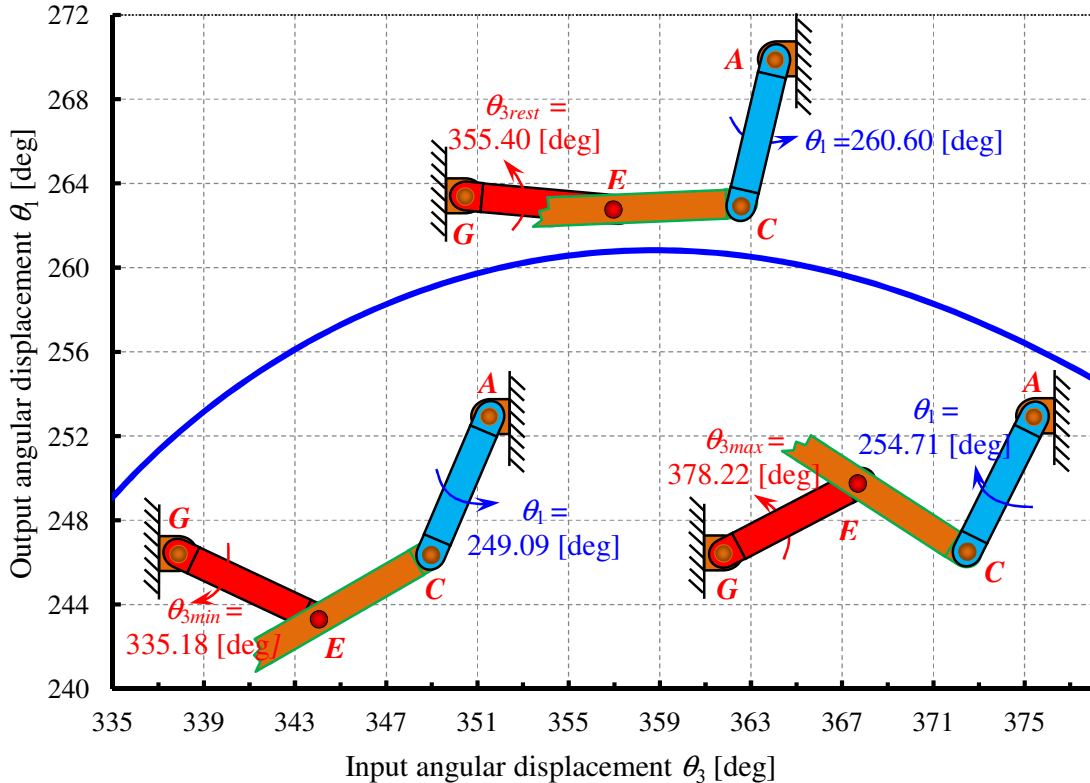


Figure 5.3: Output angular displacement θ_1 as a function of input angular displacement θ_3

To find the *coupler angular displacement* θ_2 it is necessary to eliminate *output angular displacement* θ_1 from equation (5.3). So, by squaring both sides and simplifying the expression by using trigonometric transformation, equation (5.3) now is:

$$r_4 \cdot \cos(\theta_2 - \theta_4) - r_3 \cdot \cos(\theta_2 - \theta_3) = \frac{r_1^2 - r_2^2 - r_3^2 - r_4^2}{2 \cdot r_2} + \frac{r_3 \cdot r_4}{r_2} \cdot \cos(\theta_3 - \theta_4). \quad (5.18)$$

Similar to previously, equation (5.18) is unsuitable for obtaining the *coupler angular displacement* θ_2 and it is necessary to transform in a more favorable form such as:

$$D(\theta_3) \cdot \tan^2\left(\frac{\theta_2}{2}\right) + E(\theta_3) \cdot \tan\left(\frac{\theta_2}{2}\right) + F(\theta_3) = 0, \quad (5.19)$$

where the substitution constants $D(\theta_3)$, $E(\theta_3)$ and $F(\theta_3)$ are as a function of the *input variable angular displacement* θ_3 , determined by the following expressions:

$$D(\theta_3) = r_4 \cdot \cos \theta_4 - r_3 \cdot \cos \theta_3 + \frac{r_1^2 - r_2^2 - r_3^2 - r_4^2}{2 \cdot r_2} + \frac{r_3 \cdot r_4}{r_2} \cdot \cos(\theta_3 - \theta_4), \quad (5.20)$$

$$E(\theta_3) = 2 \cdot (r_3 \cdot \sin \theta_3 - r_4 \cdot \sin \theta_4), \quad (5.21)$$

$$F(\theta_3) = \frac{r_1^2 - r_2^2 - r_3^2 - r_4^2}{2 \cdot r_2} + \frac{r_3 \cdot r_4}{r_2} \cdot \cos(\theta_3 - \theta_4) - (r_4 \cdot \cos \theta_4 - r_3 \cdot \cos \theta_3). \quad (5.22)$$

Equation (5.19) is a quadratic function in $\tan(\theta_2/2)$ and is used to find the *coupler angular displacement* θ_2 , through the following expressions:

$$\theta_2(\theta_3) = 2 \cdot \tan^{-1} \left[\frac{-E(\theta_3) \pm \sqrt{E^2(\theta_3) - 4 \cdot D(\theta_3) \cdot F(\theta_3)}}{2 \cdot D(\theta_3)} \right]. \quad (5.23)$$

By using the equations (5.17) and (5.23), the *output* θ_1 and *coupler* θ_2 are defined as a function of the *input angular displacement* θ_3 , by data given in Table 5.1.

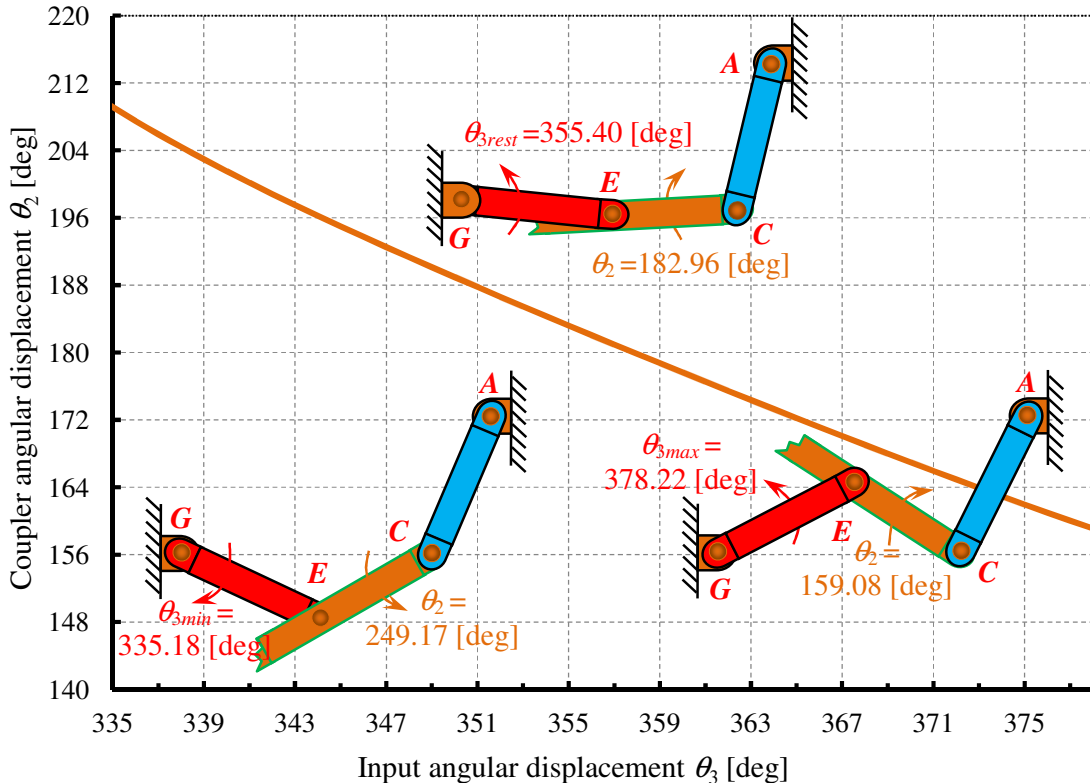


Figure 5.4: Coupler angular displacement θ_2 as a function of input angular displacement θ_3

The piston rod of the shock absorber known as the *slider mechanism* is fixed in the vehicle's body by a revolute joint F . The bottom of the spring & shock absorber is connected

by revolute joint E and single arm - link \overline{GE} which is connected to the upper control arm of the suspension mechanism. The link \overline{GE} is also fixed in the vehicle's body by a revolute joint G . The vector loops of this configuration are shown in Figure 5.5.

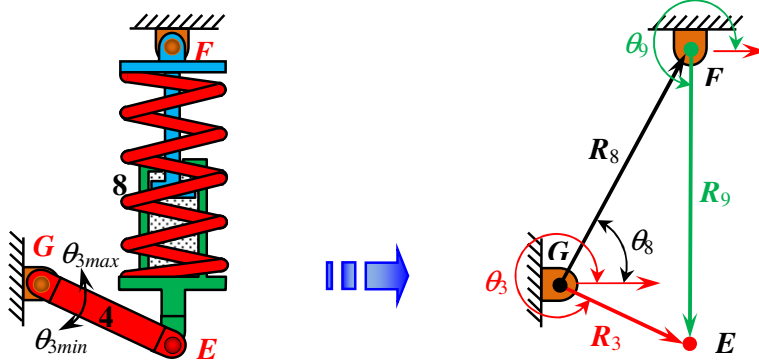


Figure 5.5: Vector loops of three-bar links derived from the suspension mechanism

Vector loops are formed from vectors position such as loops: \mathbf{R}_3 , \mathbf{R}_8 and \mathbf{R}_9 . The direction of each vector is arbitrary. The vector position - link \overline{GF} is \mathbf{R}_8 known as ground fixed link in a vehicle body defined by angular displacement θ_8 . The other position vector - link \overline{GE} is \mathbf{R}_3 considered as an *input link* for the suspension mechanism which is controlled by the *input angular displacement* θ_3 . Link \overline{FE} is the slider link (stroke of the sprig & shock absorber) which produced variables vector position \mathbf{R}_9 with angular displacement θ_9 . The slider link \overline{FE} is considered as *output link* L_s which connects both the input and output links. The *slider link* L_s and *angular displacement* θ_9 are in the function of the *input variables angular displacement* θ_3 . For the vector position that connects ground link r_8 and input link r_3 will remain constant value. The *slider link* L_s and *angular displacement* θ_9 will change as the results of the wheel motion caused from the suspension mechanism motion. The vector loop is written as follows:

$$\mathbf{R}_8 + \mathbf{R}_9 - \mathbf{R}_3 = 0, \quad (5.24)$$

where,

$$\mathbf{R}_{3,8,9} = R_{x3,8,9}\mathbf{i} + R_{y1\div 4}\mathbf{j} = r_{3,8,9} \cdot (\cos \theta_{3,8,9}\mathbf{i} + \cos \theta_{3,8,9}\mathbf{j}). \quad (5.25)$$

By decomposition the vector loop equation (5.24) into $\sin \theta_i$ and $\cos \theta_i$, obtains this expression:

$$r_8 \cdot \cos \theta_8 + L_s \cdot \cos \theta_9 - r_3 \cdot \cos \theta_3 = 0, \quad (5.26)$$

$$r_8 \cdot \sin \theta_8 + L_s \cdot \sin \theta_9 - r_3 \cdot \sin \theta_3 = 0. \quad (5.27)$$

To derive at the relation between the *input* θ_3 , *output length* L_s and *angular displacement* θ_9 , it is necessary to eliminate the *output angular displacement* θ_9 by some mathematical rearrangements between equations (5.26) and (5.27), written as follows:

$$L_s(\theta_3) = \sqrt{r_3^2 + r_8^2 - 2 \cdot r_3^2 \cdot r_8^2 \cdot \cos(\theta_3 - \theta_9)}. \quad (5.28)$$

Figure 5.6 presents the *slider length* s of the spring & shock absorber in the function of the *input angular displacement* θ_3 determined from equation (5.28). The vector representation for the three bar links with necessary data for suspension mechanism is shown in Table 5.2.

Table 5.2 Vector representation of the three-bar linkages shown in Figure 5.5

Links	Name	Vector	Length	Angular displacements	Variable
\overline{GE}	<i>Input</i>	\mathbf{R}_3	$r_3 = 210$	θ_3	$\rightarrow YES$
\overline{GF}	<i>Ground</i>	\mathbf{R}_8	$r_8 = 423.03$	$\theta_8 = 68.65$	$\rightarrow NO$
\overline{FE}	<i>Output</i>	\mathbf{R}_9	L_s	θ_9	$\rightarrow YES$

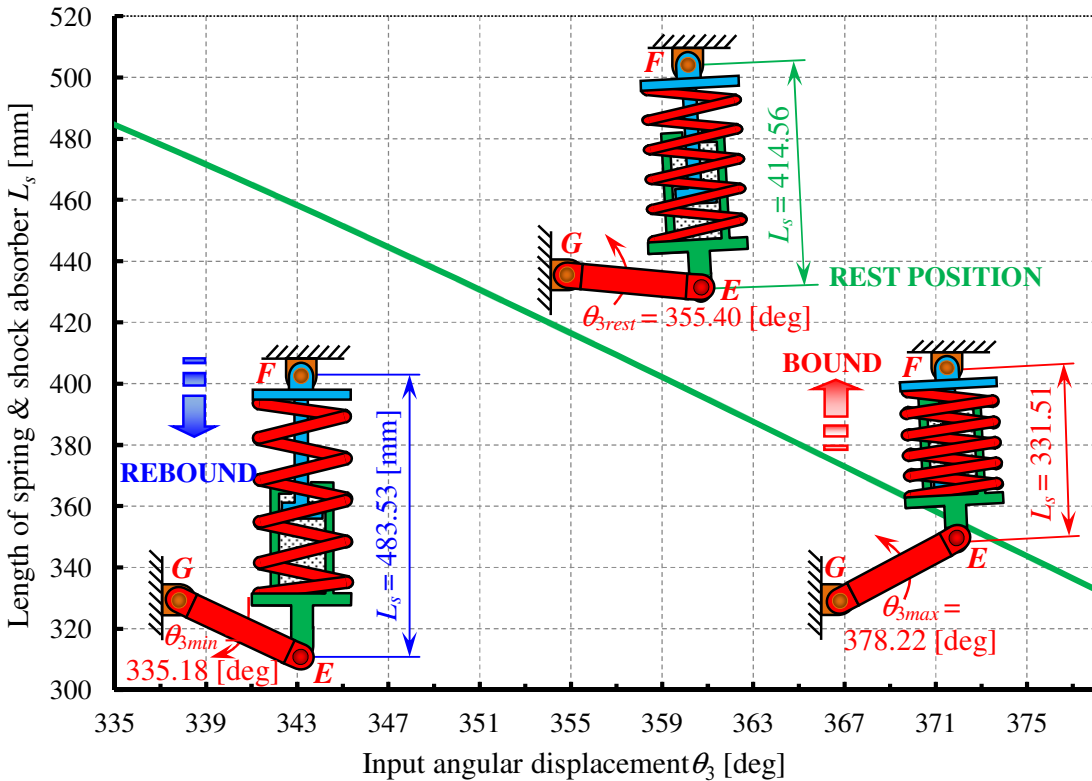


Figure 5.6: Length of spring-shock absorber L_s as a function of input angular displacement θ_3

The relation between *output angular displacement* θ_9 and *input angular displacement* θ_3 is determined after some mathematical arrangement into equations (5.26), (5.27) and (5.28). The *output angular displacement* θ_9 is defined by the following expression:

$$\theta_9(\theta_3) = \frac{r_3 \cdot \cos \theta_3 - r_8 \cdot \cos \theta_8}{\sqrt{r_3^2 + r_8^2 - 2 \cdot r_3^2 \cdot r_8^2 \cdot \cos(\theta_3 - \theta_9)}}. \quad (5.29)$$

The equations (5.28) and (5.29) determine the variable output *length* L_s (Figure 5.6) and *angular displacement* θ_9 of the slider link as functions of the *input angular displacement* θ_3 .

Figure 5.7 presents the *output* θ_9 as a function of the *input angular displacement* θ_3 .

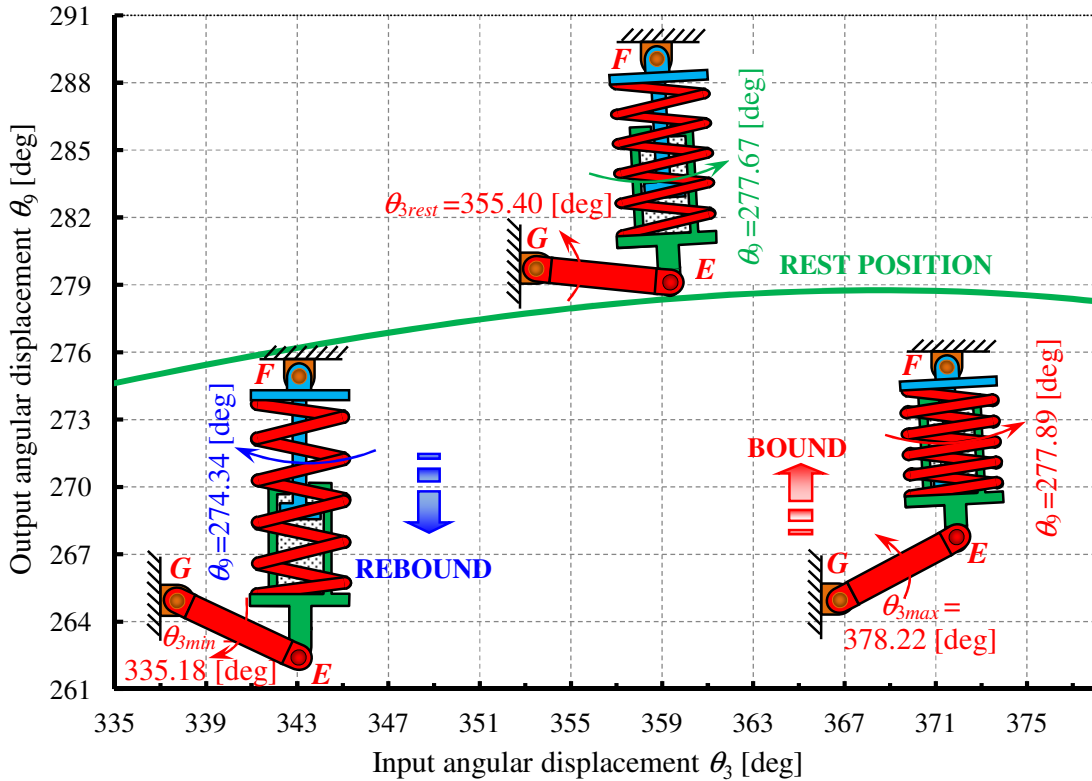


Figure 5.7: Output θ_9 as a function of input angular displacement θ_3

Figure 5.8 shows closed-loops for four-bar linkages. It is formed by vectors position: R_1 , R_5 , R_6 and R_7 . Link \overline{AB} is formed by vector position R_7 called a ground link fixed in the vehicle's body at angular displacement θ_7 . Link \overline{AC} is described with vector position R_1 considered as *input link* respectively *output link* (Figure 5.2) and is controlled from *input angular displacement* θ_3 . Link \overline{CD} determines vector position R_5 known as coupler link with angular displacement θ_5 that connect both input and output links. Link \overline{BD} introduces vector position R_6 considered as the *output link* with *angular displacement* θ_6 .

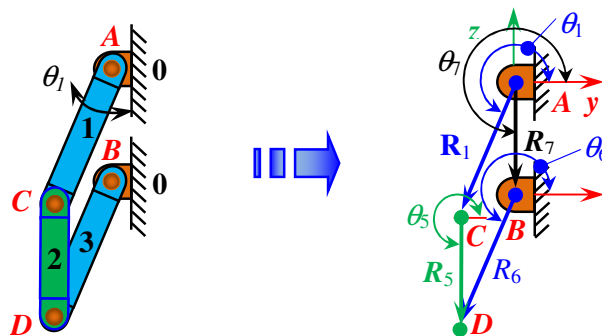


Figure 5.8: Vector loops of four-bar links derived from the suspension mechanism

The vector representation for the four-bar links with necessary data for suspension mechanism is shown in Table 5.3.

Table 5.3 Vector representation of the four-bar linkages shown in Figure 5.8

Links	Name	Vector	Length [mm]	Angular displacement [deg]	Variable
\overline{AC}	<i>Input (Output)</i>	R_1	$r_1 = 220$	θ_1	$\rightarrow YES$
\overline{CD}	<i>Coupler</i>	R_5	$r_5 = 170$	$\theta_5 = 270$	$\rightarrow NO$
\overline{BD}	<i>Output</i>	R_6	$r_6 = 220$	$\theta_6 = \theta_1$	$\rightarrow YES$
\overline{AB}	<i>Ground</i>	R_7	$r_7 = 170$	$\theta_7 = 270$	$\rightarrow NO$

Table 5.3 shown that the lengths of links: r_1+r_5 are equal with r_6+r_7 then by using Grashof's criterion of movability, the four bar mechanism can be classified into a parallelogram mechanism as a double crank mechanism. This means that by changing the *input* θ_1 of link \overline{AC} also *output angular displacement* θ_6 of link \overline{BD} has same angles $\theta_1=\theta_6$. The *angular displacement* θ_5 of link \overline{CD} don't change during its motion because *link* \overline{CD} and *ground link* \overline{AB} are equal and parallel and has the same values as *ground angular displacement* θ_7 .

By using such a mechanism as an additional part of the suspension mechanism makes it possible that the orientation of the coupler angular displacement does not change during all the motion. Maintaining the parallelism is an important thing due to the fact that the vehicle suspension mechanism must maintain the chamber angle at zero.

5.1.1.2 Determining of the wheel path and other characteristic of the suspension mechanism
By determining the angular displacement and lengths of each link defined previously is possibility of determining the positions of each link in the y and z axes of the suspension mechanism, respectively the positions of each joint. Specific interest in this approach is determining the positions of the center M and the bottom N of the wheel, defined as follows:

$$\begin{aligned} Y_E(\theta_3) &= y_A + r_1 \cdot \cos(\theta_1) + r_2 \cdot \cos(\theta_2), \\ Z_E(\theta_3) &= z_A + r_1 \cdot \sin(\theta_1) + r_2 \cdot \sin(\theta_2), \end{aligned} \quad (5.30)$$

$$\begin{aligned} Y_M(\theta_3) &= y_A + r_1 \cdot \cos(\theta_1) + r_2 \cdot \cos(\theta_2) + \overline{EH} \cdot \cos(\theta_2) + (y_M - y_H), \\ Z_M(\theta_3) &= z_A + r_1 \cdot \sin(\theta_1) + r_2 \cdot \sin(\theta_2) + \overline{EH} \cdot \sin(\theta_2) + (z_M - z_H), \end{aligned} \quad (5.30)$$

$$\begin{aligned} Y_N(\theta_3) &= y_B + r_6 \cdot \cos(\theta_6) + \overline{DI} \cdot \cos(\theta_{10}) + (y_N - y_I), \\ Z_N(\theta_3) &= z_B + r_6 \cdot \sin(\theta_6) + \overline{DI} \cdot \sin(\theta_{10}) + (z_N - z_I). \end{aligned} \quad (5.31)$$

Expression (5.30) determines the *paths* or *motions* at the center of wheel ($Y_M(\theta_3)$ and $Z_M(\theta_3)$) as a function of the *input angular displacement* θ_3 . The essential data for determining the *paths of the center of wheel* ($Y_M(\theta_3)$, $Z_M(\theta_3)$) and $Z_M = f(Y_M)$ are given in Table 4.5, Table 5.1 and Table 5.3. Figures 5.9 to 5.11 presents motion of the center of wheel.

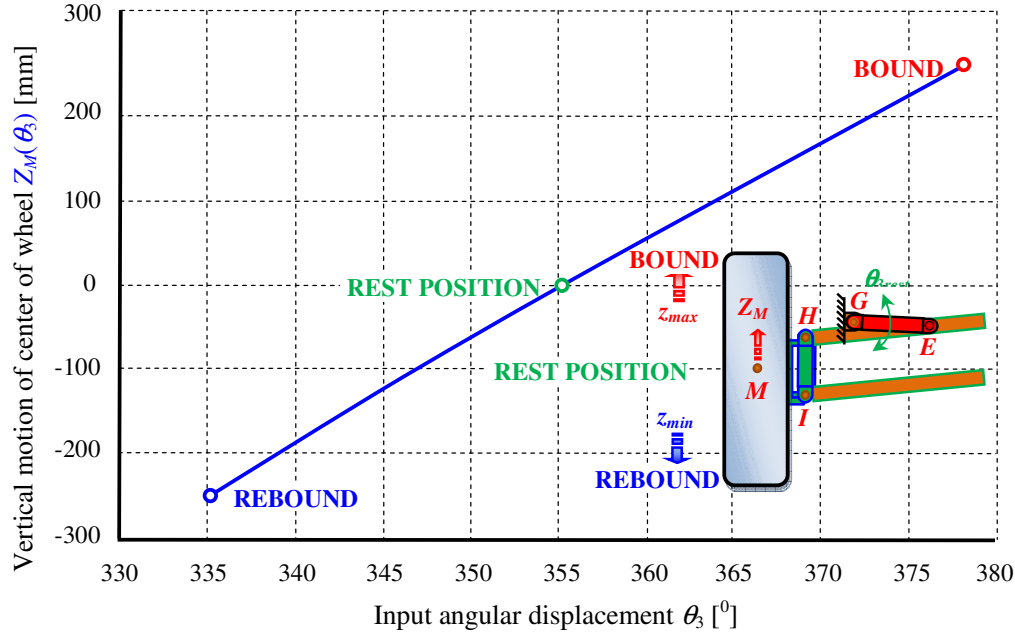


Figure 5.9: Vertical motion of center of wheel as a function of input angular displacement θ_3

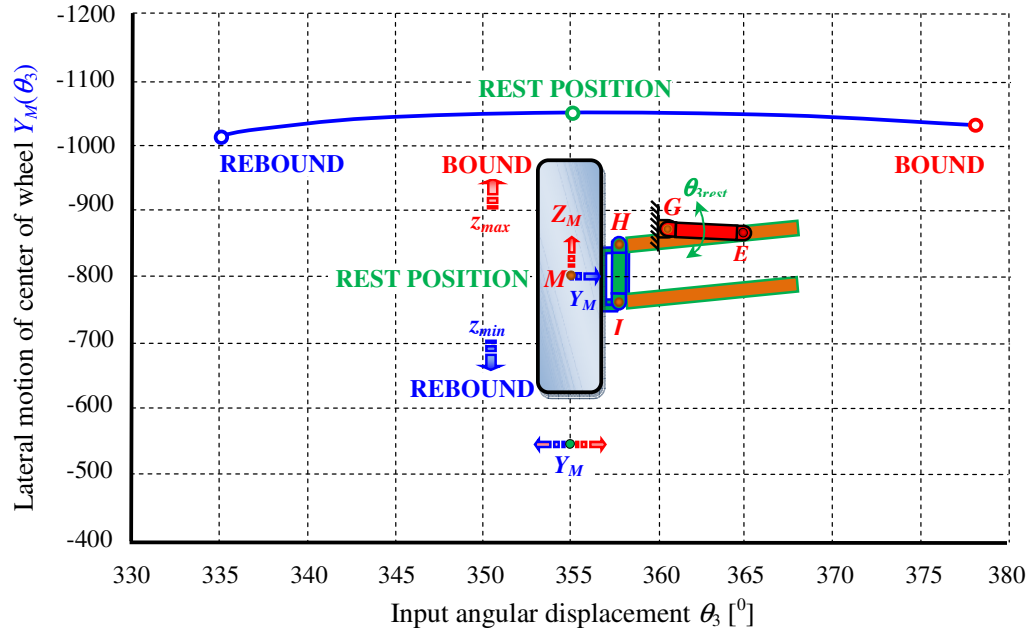


Figure 5.10: Lateral motion of center of wheel as a function of input angular displacement θ_3

The expression for the determining *kingpin inclination angle* (σ) of the suspension mechanism, is written as follow:

$$\sigma = a \tan \left[\frac{(y_K - y_I) - (y_J - y_H)}{(z_I - z_H)} \right], \text{ [deg]} \quad (5.32)$$

By substitution of known values, *kingpin inclination angle* is: $\sigma = 12.28$ [deg].

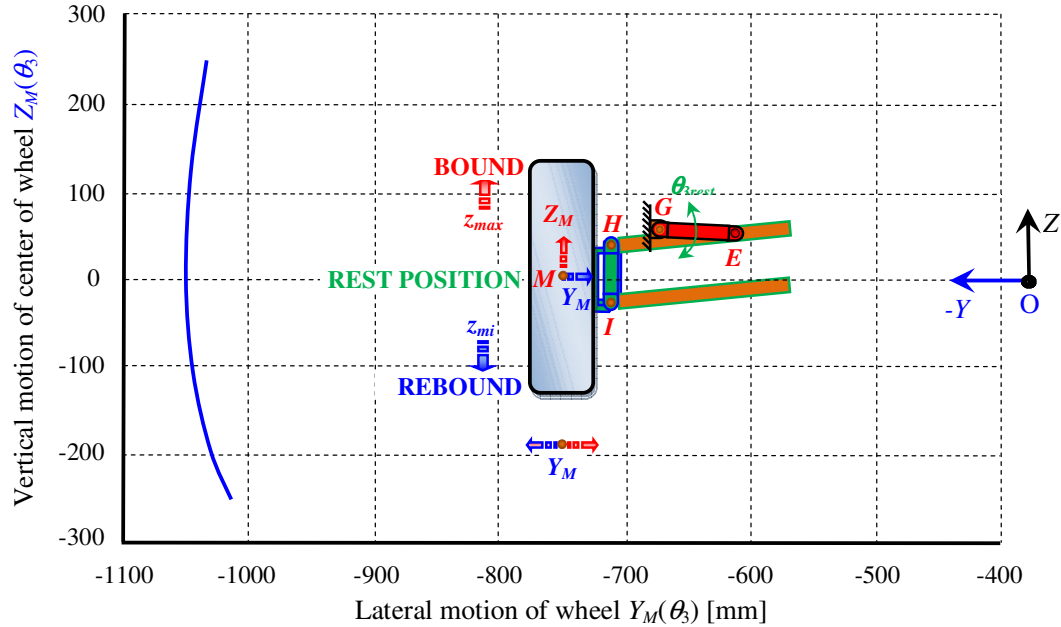


Figure 5.11: Path of the center of wheel of the suspension mechanism

The expression for determining the *kingpin offset* is written as follows:

$$\text{Kingpin offset} = [y_M - y_K + (z_M - z_K - r_d) \cdot \tan \sigma], [\text{mm}] \quad (5.33)$$

By substitution of known values, *kingpin offset* is: $\text{Kingpin offset} = 0.9$ [mm].

Whilst the expression for the determining of camber angle γ is derived from expressions (5.30) and (5.31) as a function of the input angular displacement θ_3 , is written as follow:

$$\gamma(\theta_3) = a \tan \left[\frac{Y_M(\theta_3) - Y_N(\theta_3)}{Z_M(\theta_3) - Z_N(\theta_3)} \right], [\text{deg}] \quad (5.34)$$

By the substitution of known values, the camber angle during all vertical motion of the wheel is zero: $\gamma(\theta_3) = 0$ [deg].

5.1.1.3 Comparison of the obtained results between developed program and the commercial Working Model Software

To be sure when developing the mathematical model performed in MathCAD environments, in Working Model software [53] the numerical simulations are performed for the same known geometric data of the suspension mechanism. Simulation results are shown for wheel path and other significant characteristic of the suspension mechanism. Table 5.4 presents the results obtained by two ways in order to compare the accuracy of the developed model. Result are presented when the wheels of the terrain vehicle are in rebound $Z_{Mmin} = -250$ mm, rest $Z_{Mrest} = 0$ and bound position $Z_{Mmax} = 250$ mm.

Table 5.4: Comparison of the obtained result between the developed programs performed in MathCAD and the simply commercial Working Model Software

Input angle [deg]	Angular displacement and camber angle [deg]				Wheel motion and displacement of the joint E and slider length s [mm]					
	$\theta_1(\theta_3)$	$\theta_2(\theta_3)$	$\theta_9(\theta_3)$	$\gamma(\theta_3)$	$Y_M(\theta_3)$	$Z_M(\theta_3)$	$Y_E(\theta_3)$	$Z_E(\theta_3)$	$s(\theta_3)$	
Theory	$\theta_{3\min} =$ 335.18	249.09	209.18	274.34	0.00	1017.50	250.05	517.40	18.85	483.54
	$\theta_{3\text{rest}} =$ 355.40	260.60	182.96	277.67	0.00	1050.00	0.00	498.68	90.153	414.56
	$\theta_{3\max} =$ 378.22	254.71	159.08	277.89	0.00	1033.00	250.05	508.52	172.64	331.49
Working Model	$\theta_{3\min} =$ 335.18	249.11	209.14	274.34	0.00	1017.50	250.00	517.40	18.93	483.45
	$\theta_{3\text{rest}} =$ 355.40	260.60	182.95	277.67	0.00	1050.14	0.21	498.68	90.17	414.54
	$\theta_{3\max} =$ 378.22	254.70	159.08	277.89	0.00	1033.51	249.72	508.52	172.62	331.52

Figure 5.12 shown the obtained results within the Working Model environment when the wheel of the terrain vehicle is in the rest position. The same results are tabulated in Table 5.4.

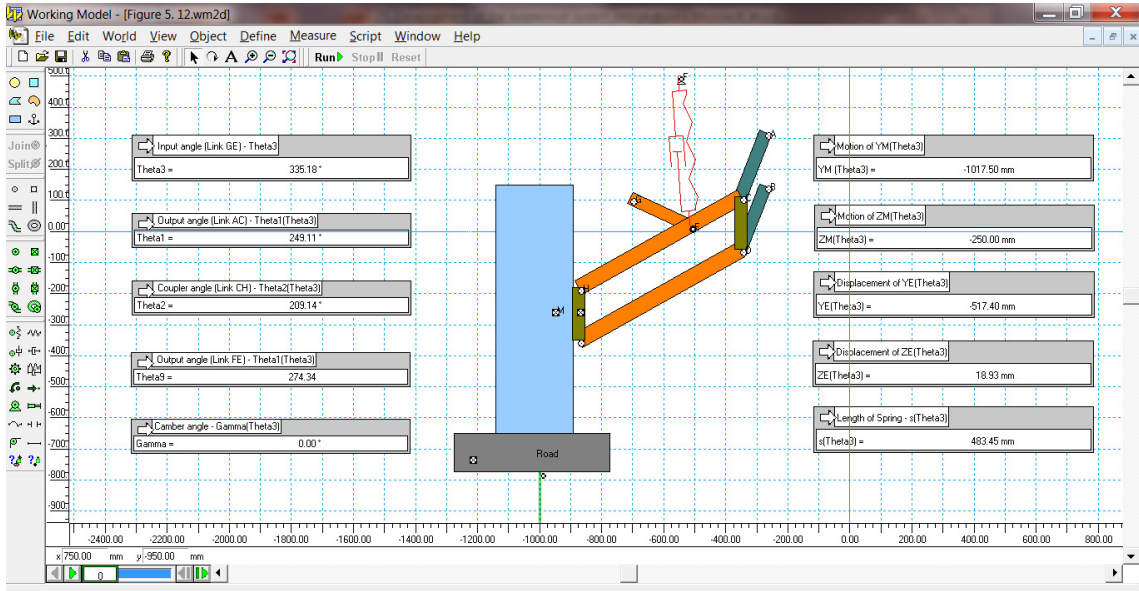


Figure 5.12: Modeling of the suspension mechanism in WM environment

From Table 5.4, it can be observed that the obtained results from the developed program in the MathCAD environment coincides very well with the results performed by commercial Working Model software. Consequently, it can be concluded that, the developed program is suitable for further analysis of the terrain vehicle suspension mechanism.

5.1.2 Velocities analysis of the suspension mechanism

Assuming that the input variable angular displacement θ_3 and angular velocity $\omega_3(t)$ are predefined and angles and length $\theta_1(\theta_3)$, $\theta_2(\theta_3)$, $\theta_9(\theta_3)$ and $L_s(\theta_3)$ are determined by equations (5.17), (5.23), (5.29), and (5.28). Therefore, the angular velocities $\omega_1(t)$, $\omega_2(t)$ and $\omega_9(t)$ may be found by differentiating equations (5.3), (5.26) and (5.27) with respect to time and after some mathematical operation, can be obtain by the following expressions:

$$\omega_1(t) = \frac{r_3}{r_1} \cdot \frac{\sin(\theta_2 - \theta_3)}{\sin(\theta_2 - \theta_1)} \cdot \omega_3(t), \quad (5.35)$$

$$\omega_2(t) = \frac{r_3}{r_2} \cdot \frac{\sin(\theta_1 - \theta_3)}{\sin(\theta_1 - \theta_2)} \cdot \omega_3(t), \quad (5.36)$$

$$\omega_9(t) = \frac{r_3 \cdot \cos(\theta_3 - \theta_9)}{\sqrt{r_3^2 + r_8^2 - 2 \cdot r_3^2 \cdot r_8^2 \cdot \cos(\theta_3 - \theta_9)}} \cdot \omega_3(t), \quad (5.37)$$

$$v_{Ls}(t) = r_3 \cdot \sin(\theta_9 - \theta_3) \cdot \omega_3(t), \quad (5.38)$$

when are:

$$\omega_1(t) = \frac{d\theta_1}{dt} = \dot{\theta}_1; \quad \omega_2(t) = \frac{d\theta_2}{dt} = \dot{\theta}_2 \text{- Angular velocity of the link } \overline{AC} \text{ and } \overline{CE}$$

$$\omega_3(t) = \frac{d\theta_3}{dt} = \dot{\theta}_3; \quad \omega_9(t) = \frac{d\theta_9}{dt} = \dot{\theta}_9 \text{- Angular velocity of the link } \overline{GE} \text{ and } \overline{EF}$$

$$v_{Ls}(t) = \frac{dL_s}{dt} = \dot{L}_s \text{- Relative velocity of the shock absorber-slider link } \overline{EF}$$

By determining the values derived from equations (5.35) to (5.38), results can be obtained for the velocities of each link and joint of the suspension mechanism. Particular interest is shown in finding the velocity at the center of wheel $v_M(t)$, determined by the following expression:

$$v_M(t) = \sqrt{[v_{MY}(t)]^2 + [v_{MZ}(t)]^2}, \quad (5.39)$$

when $v_{MY}(t)$ denotes the component of velocity in y , whilst $v_{MZ}(t)$ is component of velocity in z -axis, determined by deriving equation (5.30) with respect to time, given as follow:

$$v_{MY}(t) = \frac{dY_M(\theta_3)}{dt} = -[r_1 \cdot \sin(\theta_1) \cdot \omega_1(t) + (r_2 + \overline{EH}) \cdot \cos(\theta_2) \cdot \omega_2(t)], \quad (5.40)$$

$$v_{MZ}(t) = \frac{dZ_M(\theta_3)}{dt} = r_1 \cdot \cos(\theta_1) \cdot \omega_1(t) + (r_2 + \overline{EH}) \cdot \sin(\theta_2) \cdot \omega_2(t). \quad (5.41)$$

Equation (5.39) determines absolute velocity of the center wheel $v_M(t)$. This velocity will be obtained when the vehicle body is fixed and the wheel moves relatively around its

positions throughout the suspension mechanism. The situation is completely different when the vehicle's body and wheels moves at the same time, caused by ground excitation. This case is treated in the next chapter.

5.1.3 Accelerations analysis of the suspension mechanism

Assuming that, the angular displacement θ_3 , angular velocity $\omega_3(t)$ and angular acceleration $\varepsilon_3(t)$ are predefined as the kinematic of the input link \overline{GE} . Then the angles and lengths $\theta_1(\theta_3)$, $\theta_2(\theta_3)$, $\theta_9(\theta_3)$ and $L_s(\theta_3)$ are determined by equations (5.17), (5.23), (5.29), and (5.28), as well as $\omega_1(t)$, $\omega_2(t)$, $\omega_9(t)$ and $v_{Ls}(t)$ being determined by equations (5.35) to (5.38). Therefore, the angular acceleration $\varepsilon_1(t)$, $\varepsilon_2(t)$, $\varepsilon_9(t)$ respectively linear acceleration $a_{Ls}(t)$, may be found by a second differentiation of the equations (5.3), (5.26) and (5.27) with respect to time and after some mathematical regulation can be obtained by the following expressions:

$$\varepsilon_1(t) = \frac{r_1 \cdot \omega_1^2 \cdot \cos(\theta_1 - \theta_2) + r_2 \cdot \omega_2^2 - r_3 \cdot \omega_3^2 \cdot \cos(\theta_2 - \theta_3)}{r_1 \cdot \sin(\theta_2 - \theta_1)} - \frac{r_3 \cdot \sin(\theta_3 - \theta_2)}{r_1 \cdot \sin(\theta_2 - \theta_1)} \cdot \varepsilon_3(t), \quad (5.42)$$

$$\varepsilon_2(t) = \frac{r_1 \cdot \omega_1^2 + r_2 \cdot \omega_2^2 \cdot \cos(\theta_1 - \theta_2) - r_3 \cdot \omega_3^2 \cdot \cos(\theta_1 - \theta_3)}{r_2 \cdot \sin(\theta_1 - \theta_2)} - \frac{r_3 \cdot \sin(\theta_3 - \theta_1)}{r_2 \cdot \sin(\theta_1 - \theta_2)} \cdot \varepsilon_3(t), \quad (5.43)$$

$$\varepsilon_9(t) = \frac{r_3 \cdot \sin(\theta_3 + \theta_9) \cdot \omega_3^2 - 2 \cdot v_s \cdot \omega_9}{s} - \frac{r_3 \cdot \cos(\theta_3 + \theta_9)}{s} \cdot \varepsilon_3(t), \quad (5.44)$$

$$a_{Ls}(t) = \ddot{L}_s(t) = L_s \cdot \omega_9 - r_3 \cdot \omega_3^2 \cdot \cos(\theta_3 - \theta_9) - r_3 \cdot \sin(\theta_3 - \theta_9) \cdot \varepsilon_3(t). \quad (5.45)$$

when are:

$$\varepsilon_1(t) = \frac{d\omega_1}{dt} = \ddot{\theta}_1; \quad \varepsilon_2(t) = \frac{d\omega_2}{dt} = \ddot{\theta}_2 - \text{Angular acceleration of the link } \overline{AC} \text{ and } \overline{CE}$$

$$\varepsilon_3(t) = \frac{d\omega_3}{dt} = \ddot{\theta}_3; \quad \varepsilon_9(t) = \frac{d\omega_9}{dt} = \ddot{\theta}_9 - \text{Angular acceleration of the link } \overline{GE} \text{ and } \overline{EF}$$

$$a_{Ls}(t) = \frac{dv_{Ls}}{dt} = \frac{d^2 L_s}{dt^2} = \ddot{L}_s(t) - \text{Relative acceleration of the spring & shock absorber}$$

By the simulation of the equations (5.42) to (5.45) the results of acceleration can be found for each links and joints of the suspension mechanism. Let us now try to find an equation for determining the acceleration at the center of wheel $a_M(t)$, determined by the following expression:

$$a_M(t) = \sqrt{[a_{MY}(t)]^2 + [a_{MZ}(t)]^2} \quad (5.46)$$

when $a_{MY}(t)$ denotes the component of acceleration in y - axis, whilst $a_{MZ}(t)$ is the component of acceleration in z - axis, performed by deriving equations (5.40) and (5.41) with respect to time, generate by the following expressions:

$$a_{MY}(t) = \frac{dv_{MY}(t)}{dt} = (r_2 + \overline{EH}) \cdot [\sin(\theta_2) \cdot \omega_2^2(t) - \cos(\theta_2) \cdot \varepsilon_2(t)] - \dots \\ - r_1 \cdot [\cos(\theta_1) \cdot \omega_1^2(t) + \sin(\theta_1) \cdot \varepsilon_1(t)], \quad (5.47)$$

$$a_{MZ}(t) = \frac{dv_{MZ}(t)}{dt} = (r_2 + \overline{EH}) \cdot [\cos(\theta_2) \cdot \omega_2^2(t) + \sin(\theta_2) \cdot \varepsilon_2(t)] - \dots \\ - r_1 \cdot [\sin(\theta_1) \cdot \omega_1^2(t) - \cos(\theta_1) \cdot \varepsilon_1(t)]. \quad (5.48)$$

Equation (5.46) determines the absolute acceleration at the center of wheel $a_M(t)$. This case is valid when the vehicle's body is fixed and the wheel moves relatively around its positions.

5.2 Dynamic modeling of forces that acts on the suspension mechanism

There are two fundamental forms of forces that act on the suspension mechanism of the vehicle. The first type of force is **internal force** such as the reactions forces of joints F_i , spring forces F_s and shock absorber damper forces F_{sh} . The *reaction forces* are as a result of the joints of two bodies (connection between two links). Due to the principle of the third Newton's law, these forces are often called action-reaction forces $\mathbf{F}_{12} = -\mathbf{F}_{21}$, as shown in Figure below:



The *spring force* F_s is a force that act along the spring axis (axis between joints E and F), schematically shown in Figure 5.13.

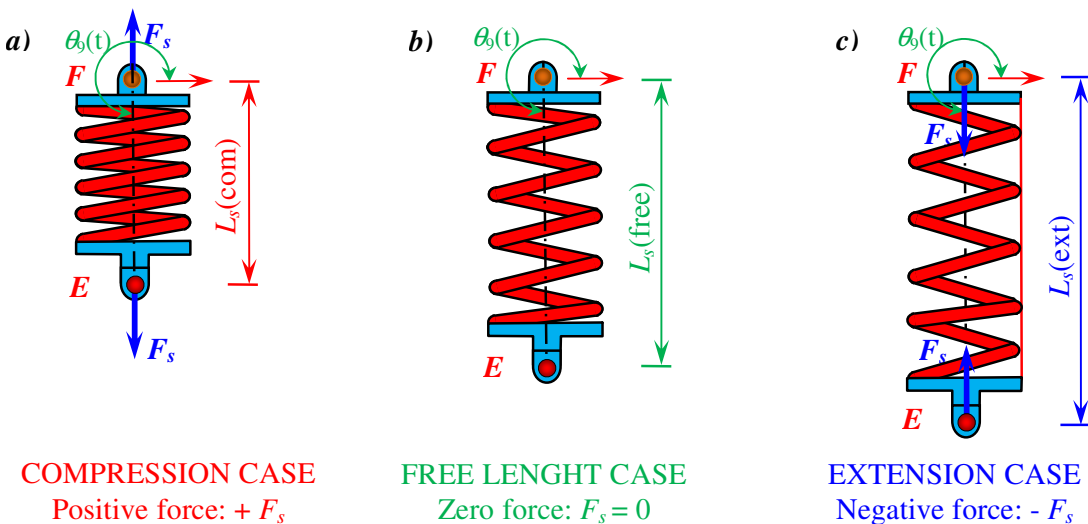


Figure 5.13: Working principles of the spring; a) compression, b) free and c) extension

The forces that act between joints E and F are equal but in opposite directions. Determining the spring force is based on the assumption that the spring force is linear in nature. The spring force is a function of the spring length L_s and spring stiffness k_s . Therefore, the spring force is determined by Hooke's law, defined by the following expression:

$$F_s = k_s \cdot [L_s - L_s(\text{def})], [\text{N}] \quad (5.49)$$

where L_s denotes free length of the spring at zero force, whilst $L_s(\text{def})$ is the length of the spring in compression or extension cases (working length) when force is applied.

From equation (5.49) it seems that the spring force will be positive when the spring is in compression case, zero when the length of spring is free, whilst negative when it is in extension case. A presentation of the spring forces F_s is shown in Figure 5.14. The convention sign used for spring force is positive $+F_s$ when the spring is in compression case, whereas negative $-F_s$ when in extension case. This convention sign is opposite to the convention used for stress analysis and finite element analyses programs, Blundell and Harty [59].

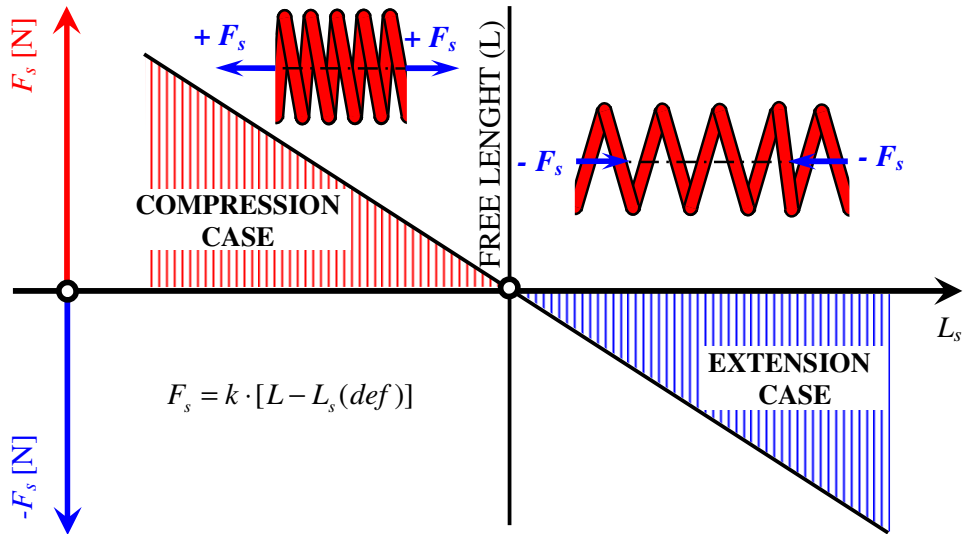


Figure 5.14: Convention sign used for a linear spring force as a function of spring length

The *shock absorber damping force* F_{sh} is a function of relative velocity of piston v_{Ls} and shock absorber damping coefficient c_{sh} . Therefore, the shock absorber damping force is determined by the following expression:

$$F_{sh} = -c_{sh} \cdot v_{Ls}, [\text{N}] \quad (5.50)$$

So, the force generated in the shock absorber is related to the relative velocity acting along the shock absorber axis (axis between joints F and E). The shock absorber damping force is positive $+F_{sh}$ when the shock absorber is in compression case (bound motion) and negative $-F_{sh}$ when in extension case (rebound motion), graphically shown in Figure 5.15.

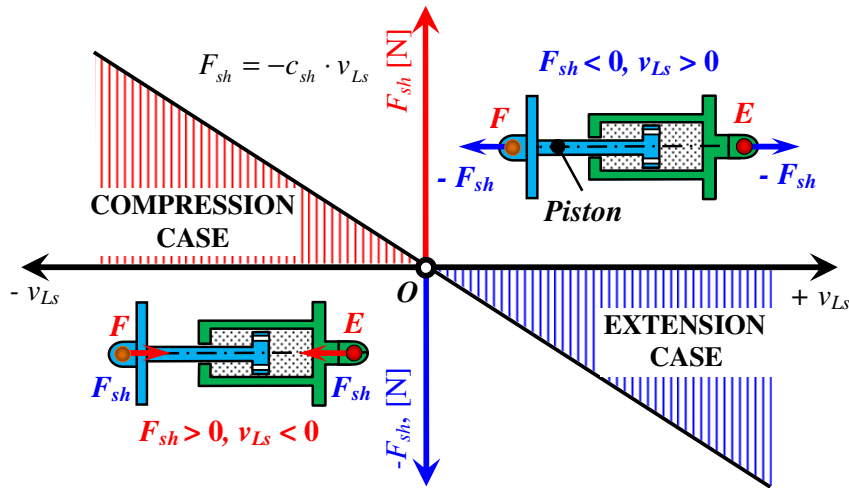


Figure 5.15: Convention sign used for a linear damper force as a function of piston velocity

The shock absorber damping force is assumed to have linear characteristics whilst most of the shock absorbers exhibit non-linear relations between force and relative velocity. The shock absorber damping force is not only non-linear but also asymmetric, having different characteristics in bound and rebound motions, Blundell and Harty [59]. Spring and shock absorbers are usually mounted in parallel and will be used in the passive suspension system.

The second types of forces applied on the suspension mechanism are **external forces**. External forces are: gravitational forces and other forces caused from wheel loads, generated forces by uneven road, cornering, braking of vehicle, which act in the tire and after them follow through the wheel centers into the vehicle suspension mechanism.

Wheel loads may be in these directions: longitudinal (acceleration and breaking forces), lateral (cornering forces) and vertical (gravity force caused from weight of vehicle, generated forces by uneven road). In order to determine wheel loads it is necessary to make some assumptions such as the chassis of the vehicle being rigid, the vehicle is driven on flat roads (no slope), constant speed cornering, constant longitudinal acceleration, Figure 5.16 shows the wheel loads applied on the front and rear axles for a vehicle during a braking case.

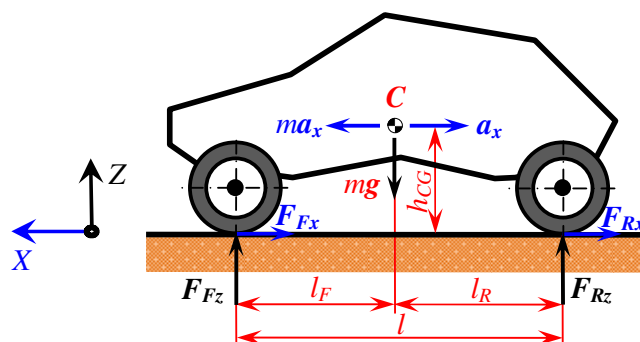


Figure 5.16: Free - body diagram of a vehicle during braking (longitudinal weight transfer)

The loads applied on the front and rear axles are determined by using Figure 5.16 and an equation of static equilibrium:

$$\sum X_i = 0; \Rightarrow F_{Fx} + F_{Rx} = m \cdot a_x, \quad (5.51)$$

$$\sum Z_i = 0; \Rightarrow F_{Fz} + F_{Rz} - m \cdot g = 0, \quad (5.52)$$

$$\sum M_{CG} = 0; \Rightarrow F_{Fz} \cdot l_F - F_{Rz} \cdot l_R - (F_{Fx} + F_{Rx}) \cdot h_{CG} = 0. \quad (5.53)$$

After some mathematical substitutions, the obtain expressions for determining vertical loads applied into the front F_{Fz} and rear axles F_{Rz} are determined by the following expression:

$$F_{Fz} = \frac{m \cdot g \cdot l_R}{l} + \frac{m \cdot a_x \cdot h_{CG}}{l}, \quad (5.54)$$

$$F_{Rz} = \frac{m \cdot g \cdot l_F}{l} - \frac{m \cdot a_x \cdot h_{CG}}{l}. \quad (5.55)$$

The first term on the right sides of the equations (5.54) and (5.55) is the static load, whilst the second term increases the loads at the front axle, respectively decrease the loads at the rear axle, due to braking process.

The vertical's tire forces acting on the left or right of the front and rear axles when the vehicle is at the rest state, are derived from expression (5.54) and (5.55):

$$F_{FW} = \frac{m \cdot g \cdot l_R}{2 \cdot l}; \quad F_{RW} = \frac{m \cdot g \cdot l_F}{2 \cdot l}. \quad (5.56)$$

Determining of the longitudinal braking force F_{Fx} and F_{Rx} from equation (5.51) and (5.53) is impossible because we have a case of indeterminacy with four unknown forces and there are only three equations of static equilibrium. The solution is found by the relation between the braking and vertical loads. It is assumed that the braking system has been designed to give same braking effort in the front and rear tires given through the coefficient of friction μ between tire and road surface, determined by the following expressions:

$$F_{Fx} = \left(\frac{m \cdot g \cdot l_R}{l} + \frac{m \cdot a_x \cdot h_{CG}}{l} \right) \cdot \mu \quad (5.57)$$

$$F_{Rx} = \left(\frac{m \cdot g \cdot l_F}{l} - \frac{m \cdot a_x \cdot h_{CG}}{l} \right) \cdot \mu$$

where F_{Fx} , F_{Rx} denotes the braking force in the front and rear tires, F_{Fz} , F_{Rz} are the vertical forces acting in the front and rear tires, F_{FW} F_{RW} introduces the vertical static forces acting in one tire in the front and rear tires, whilst a_x is termed longitudinal vehicle acceleration.

Blundell and Harty [59] and Popa [60] provide some reference values for dynamic loads that receive tires during different driving condition of the vehicle. In fact, dynamic loads are

very difficult to quantifying exists to standardize what quantifies these loads. Therefore, some manufacturers implement their own procedures for quantifying dynamic loads. Reference values for dynamic load are given in Table 5.5, Blundell and Harty [59].

Table 5.5: Dynamic load for different driving condition, Blundell and Harty [59]

Dynamic load case	Dynamic loads on a wheel of the terrain vehicle		
	Longitudinal F_x [N]	Lateral F_y [N]	Vertical F_z [N]
1g rest (static) position	0	0	2820
3g bound movement	0	0	8461
2g rebound movement	0	0	- 5641
0.75g cornering (outer wheel) cases	0	1)	1)
0.75g cornering (inner wheel) cases	0	1)	1)
1g braking	1)	0	1)

From Table 5.5 it can be observed that, the large value of the dynamic force that the tire receives and then transmits the suspension mechanism, is when the vehicle moves through uneven road (bump movement) and takes values up to $3g^2$. Therefore, the suspension mechanism for a terrain vehicle must withstand these dynamic loads.

5.2.1 Dynamic equation of the free bodies

For each free body the dynamic equation of motion can be written independently from other bodies, once applied forces are known. The dynamic equations of the free body are written corresponding to its degrees of freedom. The total applied force on the body ($\Sigma \mathbf{F}_i$), is given by inertial frame ($m_i \mathbf{a}_i = \Sigma \mathbf{F}_i$). Its components along Y_i and Z_i are determined as F_{yi} and F_{zi} . So, for each free body of planar mechanism, there are three dynamic equations of motion, defined by the following expressions:

$$m_i \cdot a_{yi} = \sum Y_i = \sum F_{yi}, \quad (5.58)$$

$$m_i \cdot a_{zi} = \sum Z_i = \sum F_{zi}, \quad (5.59)$$

$$J_{ci} \cdot \epsilon_i = \sum^{+CG} M_{ci} = \sum^{+CG} M_{xi}. \quad (5.60)$$

Whilst in matrix form, the equations of motion determined by equations (5.58) to (5.60), are:

¹⁾ Dynamic loads are dependent from driving condition of the vehicle such as vehicle speed, turning radius, road slope, road surface, and vehicle height from gravity centre and vehicle acceleration;

²⁾ $g = 9.806 \text{ [m/s}^2\text{]}$ – gravitational acceleration.

$$\begin{bmatrix} m_i & 0 & 0 \\ 0 & m_i & 0 \\ 0 & 0 & J_{ci} \end{bmatrix} \cdot \begin{bmatrix} a_{yi} \\ a_{zi} \\ \varepsilon_i \end{bmatrix} = \begin{bmatrix} \sum F_{yi} \\ \sum F_{zi} \\ \sum M_{xi} \end{bmatrix}, \quad (5.61)$$

where m_i is the mass of each free body, a_{yi} , a_{zi} denote the component of acceleration along y_i and z_i axes, $\sum F_{yi}$, $\sum F_{zi}$ introduces the sums of the components of internal and external forces along y_i and z_i axes, ε_i is the angular acceleration for i body, J_{ci} is mass moments of inertia for i body, and $\sum M_{xi}$ is the sum of moments acting on i body of the suspension mechanism.

The expressions (5.58) to (5.61) indicates that for dynamic analyses the physical properties of the suspension components should be known, such as, mass m_i , mass moments of inertia J_{ci} , mass center location $C_i(y_i, z_i)$, etc. In appendix A are presents free body diagram, of forces that act in components of mechanisms as well as expressions for determining reaction forces in all joints by employing kinematic modeling of the suspension mechanism.

5.3 Simulation of the terrain vehicle suspension mechanism

In order to determine forces that act on the components of suspension mechanism as a result ground excitation is started by the assumption that the ground configuration will change over time. The ground configuration is selected in such a way that the center of the wheel reaches the limits of the vertical motion, such as *rebound* $z_{min} = -250$ mm, *rest* $z_{rest} = 0$ and *bound* $z_{max} = +250$ mm, referring to the z – axis, Figure 5.17.

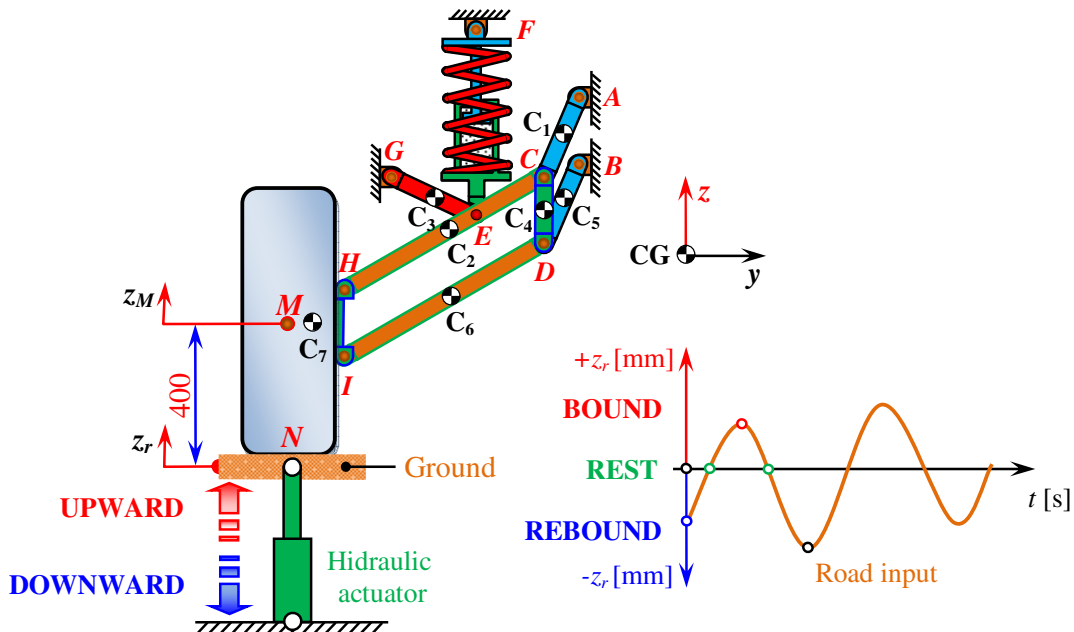


Figure 5.17: Simulation of ground configuration by using a hydraulic actuator

Simulation of the ground configuration is done by installation of a hydraulic actuator at the bottom of the tire. The tire is assumed to be rigid and moves vertically and parallel to the z -axis of the ground reference frame as schematically shown in Figure 5.17. The hydraulic actuator expects to perform vertical motion of the wheel to also produce adequate driving force which ensures the defining of kinematic and dynamic characteristics of the suspension mechanism. The vertical displacement produced by a hydraulic actuator which represents the configuration of the ground excitation is written by the following expression:

$$z_r(t) = -400 - 250 \cdot \cos(t), \quad (5.62)$$

where $z_r(t)$ denotes ground excitation (road), whilst t is the termed times.

Simulation of ground configuration is done for periods of time starting from $t = 0 \dots 2\pi$ s. For time $t = 0 \& 2\pi$ s, the position of the center of wheel reaches the *rebound* position $z_{min} = -250$ mm, for time $t = \frac{1}{2}\pi \& \frac{3}{4}\pi$ s, the position of the center of wheel is in the *rest* position $z_{rest} = 0$ mm, whilst for time $t = \pi$ s, the position of the center of the wheel reaches the *bound* position: $z_{max} = 250$ mm. Figure 5.18 illustrates ground excitation (terrain configuration) performed by the expression (5.62) and vertical motions at the center of the wheel as a function of time.

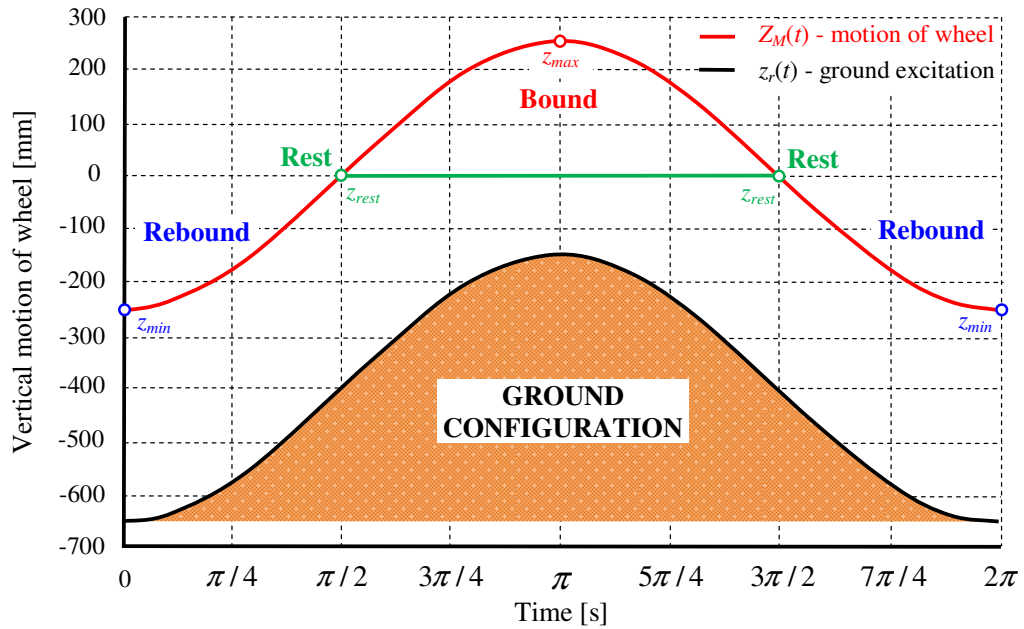


Figure 5.18: Ground excitation $z_r(t)$ and motion of wheel $Z_M(t)$ as a function of time

In order to obtain kinematic and dynamic results for the suspension mechanism previously known data and other characteristics for it. Table 5.6 shows the necessary data for simulation of the terrain vehicle suspension mechanism.

Table 5.6: Data for simulation of the suspension mechanism

Nr.	Characteristics	Value	Unit	Nr.	Characteristics	Value	Unit
1.	Length of link \overline{AC}	220	[mm]	15.	Mass of link \overline{CD} - m_4	2	[kg]
2.	Length of joints \overline{AB}	170	[mm]	16.	Mass of link \overline{BD} - m_5	4	[kg]
3.	Length of link \overline{BD}	220	[mm]	17.	Mass of link \overline{DI} - m_6	6	[kg]
4.	Length of link \overline{CD}	170	[mm]	18.	Mass of knuckle - m_7	35	[kg]
5.	Length of link \overline{CE}	190	[mm]	19.	Mass of inertia - J_{C1}	16670	[kgmm ²]
6.	Length of link \overline{DI}	600	[mm]	20.	Mass of inertia - J_{C2}	182000	[kgmm ²]
7.	Length of link \overline{EG}	210	[mm]	21.	Mass of inertia - J_{C3}	15230	[kgmm ²]
8.	Length of joints \overline{HI}	170	[mm]	22.	Mass of inertia - J_{C4}	5083	[kgmm ²]
9.	Length of link \overline{CH}	600	[mm]	23.	Mass of inertia - J_{C5}	16670	[kgmm ²]
10.	Distance $\overline{H'M}$	141.5	[mm]	24.	Mass of inertia - J_{C6}	182000	[kgmm ²]
11.	Distance \overline{MN}	400	[mm]	25.	Mass of inertia - J_{C7}	143000	[kgmm ²]
12.	Mass of link \overline{AC} - m_1	4	[kg]	26.	Spring stiffness - k_s	141.40	[N/mm]
13.	Mass of link \overline{CH} - m_2	6	[kg]	27.	Damping coeff. - c_{sh}	14.14	[Ns/mm]
14.	Mass of link \overline{EG} - m_3	4	[kg]				

To determine forces that act on the suspension mechanism, it is firstly necessary to predefine the kinematic characteristics. By using the given data in Table 5.6 the positions, velocities and acceleration of each joint and points of the suspension mechanism will be determined. Besides these characteristics, the angular displacement, angular velocities and angular acceleration all of that as a function of time, can also be determined. There are large numbers of kinematic characteristic that can be obtained through expressions developed previously. Therefore, we can present larger numbers of diagrams. The best presentation of the result would be through tables for wheel center positions when in *rebound*, *rest*, and *bound*. The same tables give the kinematic values obtained from numerical simulation realized in Working Model environment. Table 5.7, Table 5.8 and Table 5.9 present the results obtained by two ways (developed program & commercial Working Model Software) in order to compare the accuracy of the developed model.

Table 5.7: Results comparison for angular displacement, velocities & accelerations obtained by the developed program performed in MathCAD and Working Model Software

Body centers	Wheel position	Angular: displacement, velocities, and accelerations					
		Developed program			Working Model Software		
		$\theta(t)$ [deg]	$\omega(t)$ [s ⁻¹]	$\varepsilon(t)$ [s ⁻²]	$\theta(t)$ [deg]	$\omega(t)$ [s ⁻¹]	$\varepsilon(t)$ [s ⁻²]
C_1	$z_{Mmin}(t = 0 \text{ s})$	249.097	0.000	21.390	249.109	0.000	20.535
	$z_{Mrest}(t = \pi/2 \text{ s})$	260.600	2.744	-16.495	260.600	2.748	-16.494
	$z_{Mmax}(t = \pi \text{ s})$	254.704	0.000	15.645	254.711	0.006	15.633
C_2	$z_{Mmin}(t = 0 \text{ s})$	209.174	0.000	-30.547	209.156	0.000	-29.540
	$z_{Mrest}(t = \pi/2 \text{ s})$	182.957	-24.070	1.559	182.963	-24.070	1.565
	$z_{Mmax}(t = \pi \text{ s})$	159.083	0.000	23.937	159.094	0.010	23.935

C_3	$z_{Mmin}(t = 0 \text{ s})$	335.184	0.000	17.778	335.195	0.000	17.413
	$z_{Mrest}(t = \pi/2 \text{ s})$	355.398	21.348	1.388	355.393	21.347	1.383
	$z_{Mmax}(t = \pi \text{ s})$	378.210	0.000	-25.849	378.198	-0.011	-25.841
C_4	$z_{Mmin}(t = 0 \text{ s})$	270.000	0.000	0.000	270.000	0.000	0.000
	$z_{Mrest}(t = \pi/2 \text{ s})$	270.000	0.000	0.000	270.000	0.000	0.000
	$z_{Mmax}(t = \pi \text{ s})$	270.000	0.000	0.000	270.000	0.000	0.000
C_5	$z_{Mmin}(t = 0)$	249.097	0.000	21.390	249.109	0.000	20.535
	$z_{Mrest}(t = \pi/2 \text{ s})$	260.600	2.744	-16.495	260.600	2.748	-16.494
	$z_{Mmax}(t = \pi \text{ s})$	254.704	0.000	15.645	254.711	0.006	15.633
C_6	$z_{Mmin}(t = 0 \text{ s})$	209.174	0.000	-30.547	209.156	0.000	-29.540
	$z_{Mrest}(t = \pi/2 \text{ s})$	182.957	-24.070	1.559	182.963	-24.070	1.565
	$z_{Mmax}(t = \pi \text{ s})$	159.083	0.000	23.937	159.094	0.010	23.936
C_7	$z_{Mmin}(t = 0 \text{ s})$	270.000	0.000	0.000	270.000	0.000	0.000
	$z_{Mrest}(t = \pi/2 \text{ s})$	270.000	0.000	0.000	270.000	0.000	0.000
	$z_{Mmax}(t = \pi \text{ s})$	270.000	0.000	0.000	270.000	0.000	0.000

Table 5.8: Results comparison for length, relative velocity & acceleration of the spring & shock absorber, obtained by developed program and Working Model Software

Body	Wheel position	Length, relative velocity & acceleration of spring & damper					
		Developed program			Working Model Software		
		$L_s(t)$ [mm]	$v_{Ls}(t)$ [mms ⁻¹]	$a_{Ls}(t)$ [mms ⁻²]	$L_s(t)$ [mm]	$v_{Ls}(t)$ [mms ⁻¹]	$a_{Ls}(t)$ [mms ⁻²]
Spring & shock absorber	$z_{Mmin}(t = 0 \text{ s})$	483.527	0.000	-56.902	483.492	0.000	-55.826
	$z_{Mrest}(t = \pi/2 \text{ s})$	414.556	-76.455	-10.499	414.576	-76.453	-10.483
	$z_{Mmax}(t = \pi \text{ s})$	331.509	0.000	93.207	331.552	0.038	93.182

Table 5.9: Results comparison for total and projection in y and z-axis of velocities for mechanism components, obtained by developed program and Working Model Software

Body centers	Wheel position	Velocities of the components of the suspension mechanism					
		Developed program			Working Model Software		
		$v_y(t)$ [mms ⁻¹]	$v_z(t)$ [mms ⁻¹]	$v(t)$ [mms ⁻¹]	$v_y(t)$ [mms ⁻¹]	$v_z(t)$ [mms ⁻¹]	$v(t)$ [mms ⁻¹]
C_1	$z_{Mmin}(t = 0 \text{ s})$	0.000	0.000	0.000	0.000	0.000	0.000
	$z_{Mrest}(t = \pi/2 \text{ s})$	5.198	-0.860	5.268	5.206	-0.862	5.276
	$z_{Mmax}(t = \pi \text{ s})$	0.000	0.000	0.000	0.012	-0.003	0.012
C_2	$z_{Mmin}(t = 0 \text{ s})$	0.000	0.000	0.000	0.000	0.000	0.000
	$z_{Mrest}(t = \pi/2 \text{ s})$	3.893	124.140	124.201	3.896	124.138	124.138
	$z_{Mmax}(t = \pi \text{ s})$	0.000	0.000	0.000	0.005	-0.054	0.054
C_3	$z_{Mmin}(t = 0 \text{ s})$	0.000	0.000	0.000	0.000	0.000	0.000
	$z_{Mrest}(t = \pi/2 \text{ s})$	3.139	38.995	39.121	3.142	38.994	39.121
	$z_{Mmax}(t = \pi \text{ s})$	0.000	0.000	0.000	0.006	-0.018	0.019
C_4	$z_{Mmin}(t = 0 \text{ s})$	0.000	0.000	0.000	0.000	0.000	0.000
	$z_{Mrest}(t = \pi/2 \text{ s})$	10.395	-1.721	10.537	10.411	-1.724	10.553
	$z_{Mmax}(t = \pi \text{ s})$	0.000	0.000	0.000	0.024	-0.006	0.019
C_5	$z_{Mmin}(t = 0 \text{ s})$	0.000	0.000	0.000	0.000	0.000	0.000
	$z_{Mrest}(t = \pi/2 \text{ s})$	5.198	-0.860	5.268	5.206	-0.862	5.276
	$z_{Mmax}(t = \pi \text{ s})$	0.000	0.000	0.000	0.012	-0.003	0.012
C_6	$z_{Mmin}(t = 0 \text{ s})$	0.000	0.000	0.000	0.000	0.000	0.000
	$z_{Mrest}(t = \pi/2 \text{ s})$	3.893	124.140	124.201	3.896	124.138	124.199

	$z_{Mmax}(t = \pi \text{ s})$	0.000	0.000	0.000	0.005	-0.054	0.054
	$z_{Mmin}(t = 0 \text{ s})$	0.000	0.000	0.000	0.000	0.000	0.000
7 C_7	$z_{Mrest}(t = \pi/2 \text{ s})$	-2.608	250.000	250.014	-2.620	250.000	250.014
	$z_{Mmax}(t = \pi \text{ s})$	0.000	0.000	0.000	-0.013	-0.102	0.103

Table 5.10: Results comparison for total and projection in y and z -axis of acceleration for mechanism components, obtained by developed program and Working Model Software

Body centers	Wheel position	Acceleration of the components of the suspension mechanism					
		Developed program			Working Model Software		
		$a_y(t)$ [mms^{-2}]	$a_z(t)$ [mms^{-2}]	$a(t)$ [mms^{-2}]	$a_y(t)$ [mms^{-2}]	$a_z(t)$ [mms^{-2}]	$a(t)$ [mms^{-2}]
1 C_1	$z_{Mmin}(t = 0 \text{ s})$	38.363	-14.652	41.066	36.891	-13.902	39.424
	$z_{Mrest}(t = \pi/2 \text{ s})$	-31.202	5.421	31.669	-31.199	5.422	31.667
	$z_{Mmax}(t = \pi \text{ s})$	28.973	-7.924	30.037	28.951	-7.914	30.013
2 C_2	$z_{Mmin}(t = 0 \text{ s})$	-1.240	110.348	110.355	-0.757	107.721	107.724
	$z_{Mrest}(t = \pi/2 \text{ s})$	-9.109	5.421	10.600	-9.106	5.396	10.585
	$z_{Mmax}(t = \pi \text{ s})$	13.200	-132.924	133.578	13.182	-132.901	133.553
3 C_3	$z_{Mmin}(t = 0 \text{ s})$	13.674	29.571	32.579	13.287	29.014	31.912
	$z_{Mrest}(t = \pi/2 \text{ s})$	-14.325	3.704	14.796	-14.323	3.697	14.793
	$z_{Mmax}(t = \pi \text{ s})$	14.803	-44.998	47.371	14.789	-44.987	47.356
4 C_4	$z_{Mmin}(t = 0 \text{ s})$	76.726	-29.304	82.132	73.782	-27.804	78.847
	$z_{Mrest}(t = \pi/2 \text{ s})$	-62.403	10.842	63.338	-62.399	10.843	63.334
	$z_{Mmax}(t = \pi \text{ s})$	57.946	-15.848	60.074	57.901	-15.828	60.026
5 C_5	$z_{Mmin}(t = 0 \text{ s})$	38.363	-14.652	41.066	36.891	-13.902	39.424
	$z_{Mrest}(t = \pi/2 \text{ s})$	-31.202	5.421	31.669	-31.199	5.422	31.667
	$z_{Mmax}(t = \pi \text{ s})$	28.973	-7.924	30.037	28.951	-7.914	30.013
6 C_6	$z_{Mmin}(t = 0 \text{ s})$	-1.240	110.348	110.355	-0.757	107.721	107.724
	$z_{Mrest}(t = \pi/2 \text{ s})$	-9.109	5.421	10.600	-9.106	5.396	10.585
	$z_{Mmax}(t = \pi \text{ s})$	13.200	-132.924	133.578	13.182	-132.901	133.553
7 C_7	$z_{Mmin}(t = 0 \text{ s})$	-79.206	250.000	262.247	-75.296	243.247	254.634
	$z_{Mrest}(t = \pi/2 \text{ s})$	44.185	0.000	44.185	44.187	-0.051	44.187
	$z_{Mmax}(t = \pi \text{ s})$	-31.546	-250.000	251.982	-31.537	-249.974	251.955

From Tables 5.7 to 5.10 for the three position of motion at the center of the wheel *rebound*, *rest* and *bound*, it can be observed that, the obtained results by commercial Working Model Software coincided very well with results obtained by the developed program performed in MathCAD environments. The results are practically identical. This verifies the reliability of the developed kinematic modeling of the suspension mechanism.

Figure 5.19 presents the kinematic results obtained by Working Model Software when the center of the wheel is in rest position or let us say when the vehicle is in a static position.

After setting all necessary kinematic characteristic for the suspension mechanism, now it is possible to determine the unknown reaction forces in each joint of the suspension mechanism by employing expression (A.33). It is supposed that, the maximal tire loads for one wheel during bump motion will be up to $3g$ according to authors Blundell and Harty [59].

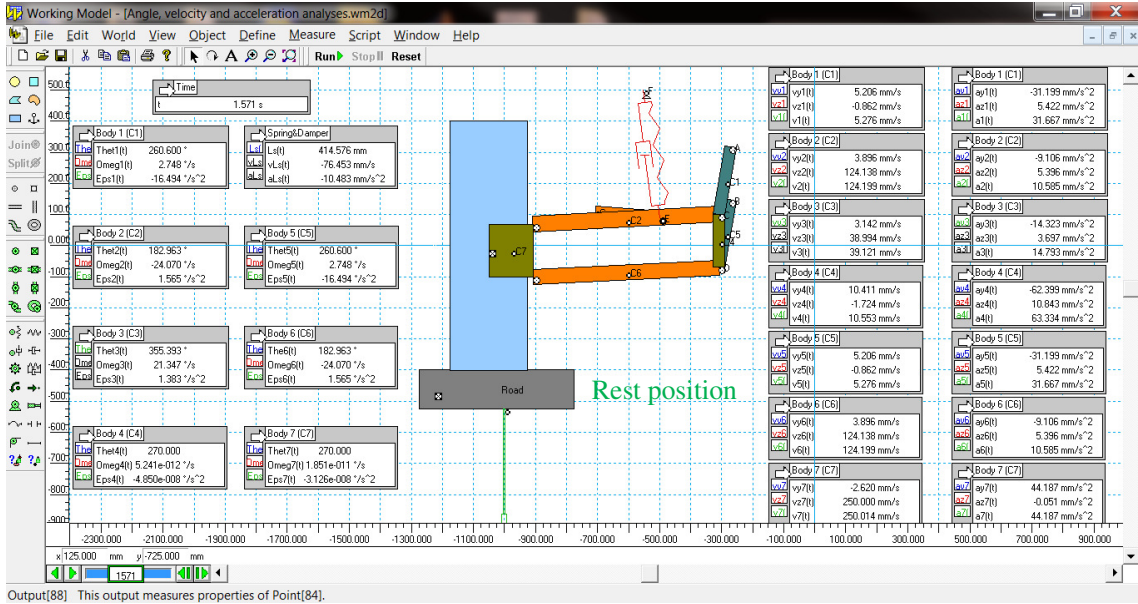


Figure 5.19: Kinematic results obtained in Working Model Software

According to these authors, the maximal tire force that acts on one wheel in vertical direction is $F_w = 8\,461$ N, whilst forces in other direction are considerably smaller. By employing force $F_w = 8\,461$ N and the necessary data tabulated in Table 5.6, the spring force $F_s(t)$, the shock absorber damping force $F_{sh}(t)$ and reaction forces $F_j(t)$ for joints; A, B, C₂, C₄, D₄, D₆, E, F, G, H and I are presented by the diagrams in Figures A.4 to A.14 as a function of times.

5.4 Optimization of the suspension mechanism

The final design of the suspension mechanism was obtained from the initial design concept because it is clearly evident that this design ensures suitable performance for the developed terrain vehicle. Therefore, some of the dimensions of the mechanism can be still changed. The idea is to determine optimal dimensions of mechanism in order for the suspension mechanism to reduce as much as possible the lateral displacement of the wheels known as track changes. This optimization of the dimensions of the terrain vehicle suspension mechanism will improve the stability of the vehicle when is driven around corners and on uneven road.

5.4.1 The problem of optimum design

Over past years, optimization of mechanical systems has become almost an obligatory part of the design process. During design processing, the difficulties of the optimization process may vary over a wider range. On the one hand, there are the simplest problems with linear response, where it is necessary to optimize only a few simple parameters. In the other hand,

complex problems exist with highly non-linear responses that require lots of effort. The optimization of the mechanical systems is often based on the non-linear mathematical programming problem F , determined by the following form:

$$\min f_0(\mathbf{b}, \mathbf{u}), \quad (5.63)$$

subjected to the constraint:

$$h_j(\mathbf{b}, \mathbf{u}) \leq 0; \quad j = 1, \dots, i, \quad (5.64)$$

where the scalar functions f_0 and h_j are termed the objective and constraint function, respectively. The vector $\mathbf{b} \in R^n$ denotes design variables, whilst $\mathbf{u} \in R^m$ is the vector of the response variables, usually presenting displacement and rotation of the mechanical systems, discrete by finite elements (Figure 5.20). The symbol n denotes the number of design variables, m is the number of response variables, and i is the number of constraints. The objective function is related to the quality of the design, whilst the constraint function usually reflects the nodal displacement or rotation, design variable limits, technological limitations and so on, Lenart [52], Kegel et al. [61], Pehan et al. [62], Kegl et al. [63], Kegl and Antes [64], Kegl and Brank [65] and Zidarič [66].

Therefore, in such an optimization problem the objective and constraint functions are assumed to be continuous design variables and problem F can be solved efficiently by utilizing one of the gradient methods which is based on the mathematical programming. Therefore, the solution procedure for solving the non-linear problem F is an iterative process and can be described by the following steps:

Step 1: Determining initial values ($k = 0$) of the design variables $\mathbf{b}^{(k)} = \mathbf{b}^{(0)}$,

Step 2: Computing f_0 and $h_j, j = 0, \dots, i$ at $\mathbf{b}^{(k)}$ (response analysis),

Step 3: Computing $df_0/d\mathbf{b}$ and $dh_j/d\mathbf{b}, j = 0, \dots, i$ at $\mathbf{b}^{(k)}$ (sensitivity analysis),

Step 4: Submission of the calculated values to the optimization algorithm, in order to obtain some improvement in design variables $\Delta\mathbf{b}^{(k)}$ and computing improved design variables $\mathbf{b}^{(k+1)} = \mathbf{b}^{(k)} + \Delta\mathbf{b}^{(k)}$,

Step 5: Check convergence criteria - if it fulfilled exit, otherwise go back to *step 2*.

Objective function f_0 and constraint function h_j are in relation to design \mathbf{b} and response variables \mathbf{u} . However, before any optimization process is determined the response variable \mathbf{u} at given design variable \mathbf{b} needs to be dealt with. In other words, the dependency $\mathbf{u} = \mathbf{u}(\mathbf{b})$ is established implicitly by using the equilibrium equation of the structure in general form, as:

$$\mathbf{F} - \mathbf{R} = 0, \quad (5.65)$$

where \mathbf{F} and \mathbf{R} denote the vectors of the structural internal and external forces, respectively. The response variable $\mathbf{u}^{(k)}$ is obtained from equilibrium equation (5.65), whilst $(d\mathbf{u}/db)^{(k)}$ has to be determined from the sensitive equation (more detail is given in literature [65]). These derivatives are commonly expressed by differentiation of the equation (5.65) with respect to design variables \mathbf{b} :

$$\frac{\partial \mathbf{F}}{\partial \mathbf{u}} \cdot \frac{d\mathbf{u}}{db} + \frac{\partial \mathbf{F}}{\partial \mathbf{b}} - \left(\frac{\partial \mathbf{R}}{\partial \mathbf{u}} \cdot \frac{d\mathbf{u}}{db} + \frac{\partial \mathbf{R}}{\partial \mathbf{b}} \right) = 0, \text{ or} \quad (5.66)$$

$$\frac{d\mathbf{u}}{db} = \left[\frac{\partial \mathbf{F}}{\partial \mathbf{u}} - \frac{\partial \mathbf{R}}{\partial \mathbf{u}} \right]^{-1} \left(\frac{\partial \mathbf{R}}{\partial \mathbf{b}} - \frac{\partial \mathbf{F}}{\partial \mathbf{b}} \right). \quad (5.67)$$

The inverse matrix $[\partial \mathbf{F} / \partial \mathbf{u} - \partial \mathbf{R} / \partial \mathbf{u}]^{-1}$ is a tangential stiffness matrix of the structure. This matrix is already known from the response analyses. Equation (5.67) can be solved with a rather small additional computer effort: only partial design derivatives of internal and external forces ($\partial \mathbf{R} / \partial \mathbf{b} - \partial \mathbf{F} / \partial \mathbf{b}$) need to be computed.

5.4.2 The modeling of the suspension mechanism by finite elements

The full terrain vehicle suspension system for the front and rear axles are modeling by Finite Elements performed in *STAKx* [67] software presented in Figure 5.20.

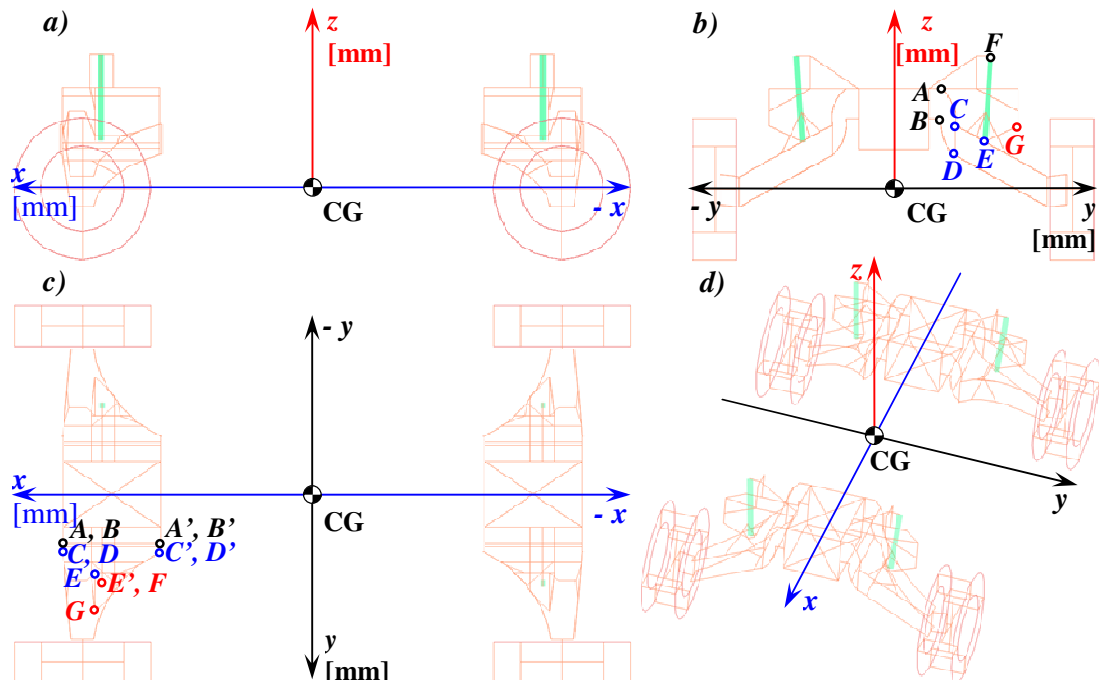


Figure 5.20: Modeling of terrain vehicle suspension system by Finite Elements in *STAKx* software; a) side view, b) front view, c) plane view, and d) 3D view

Figure 5.21 present the analyzing of the terrain vehicle suspension system when on the right wheels of the front and rear axles vertical tire force is applied by $F_w = 8461$ [N] causing bound position of wheel $Z_{Mmax} = 250$ [mm]. Whilst, the left wheel of the front and rear axles is in rebound position $Z_{Mmin} = -250$ [mm].

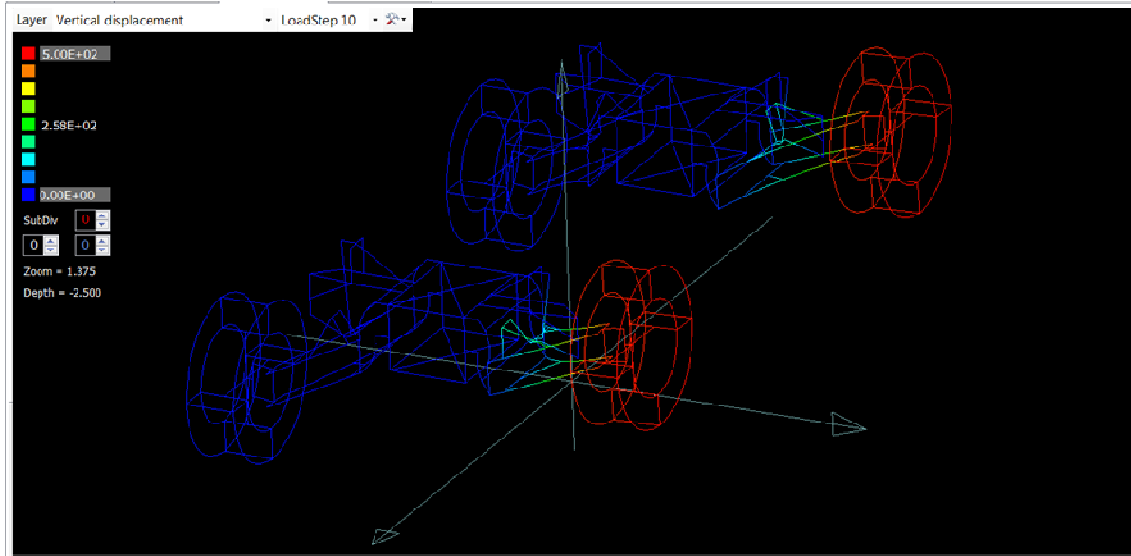


Figure 5.21: Analyzing of vertical wheel motion by Finite Elements in *STAKx* [67].

After modeling of the terrain vehicle suspension system in *STAKx*, the environments ensure conditions for the optimization of the suspension mechanism caused by applied forces.

5.4.3 The optimal design of the suspension mechanism

In order to obtain an optimal design of the suspension mechanism, the *iGOx* [68] optimization program was employed, as is shown in Figure 5.22. This is a separate (stand-alone) optimization program containing the approximation method described by Pehan et al. [62], Kegl et al. [63], Kegl and Antes [64], Kegl and Brank [65] and Zidarić [66].

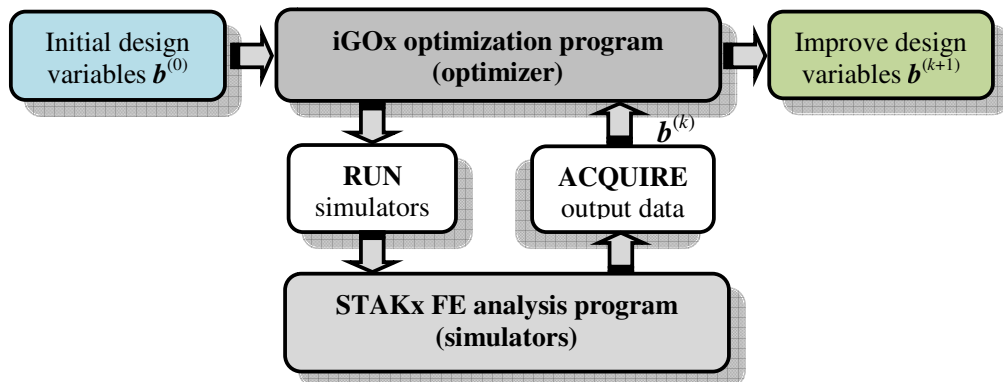


Figure 5.22: The optimization procedure for obtaining optimal design variables

Essentially, *iGOx* run simulators in order to get the values of the objective and constraint functions from the FEA program (simulators) called *STAKx*. After that it calls its own built-in optimization algorithm to improve the values of the design variables. This procedure is repeated in each cycle of the optimization process, as is presented in Figure 5.23.

The objective and constraint functions are derived in that way, the lateral displacement of the wheel during bound and rebound wheel motion to be as small as possible. The design variables are represented by joints position in y and z – axis. These positions of the joints connection are required to optimize. Table 5.11 presents the position of joints connection represented by design variables which present the distance of the joint shown in Figure 5.20.

Table 5.11: Position of joints connection and design variables

Joints point	x - axis	y - axis	z - axis
A	1515	$253 + 20b_1$	$297+20b_2$
B	1515	$253 + 20b_3$	$127+20b_4$
A'	945	$253 + 20b_5$	$297+20b_6$
B'	945	$253 + 20b_7$	$127+20b_8$
C	1515	$331 + 20b_9$	$91.5+20b_{10}$
D	1515	$331 + 20b_{11}$	$-78.5+20b_{12}$
C'	945	$331 + 20b_{13}$	$91.5+20b_{14}$
D'	945	$331 + 20b_{15}$	$-78.5+20b_{16}$
E	1326	$493 + 20b_{17}$	$-1 + 20b_{18}$
E'	1286	$493 + 20b_{19}$	$-1 + 20b_{20}$
G	1326	$688 + 20b_{21}$	$87 + 20b_{22}$
F	1286	$534 + 20b_{23}$	$481 + 20b_{24}$

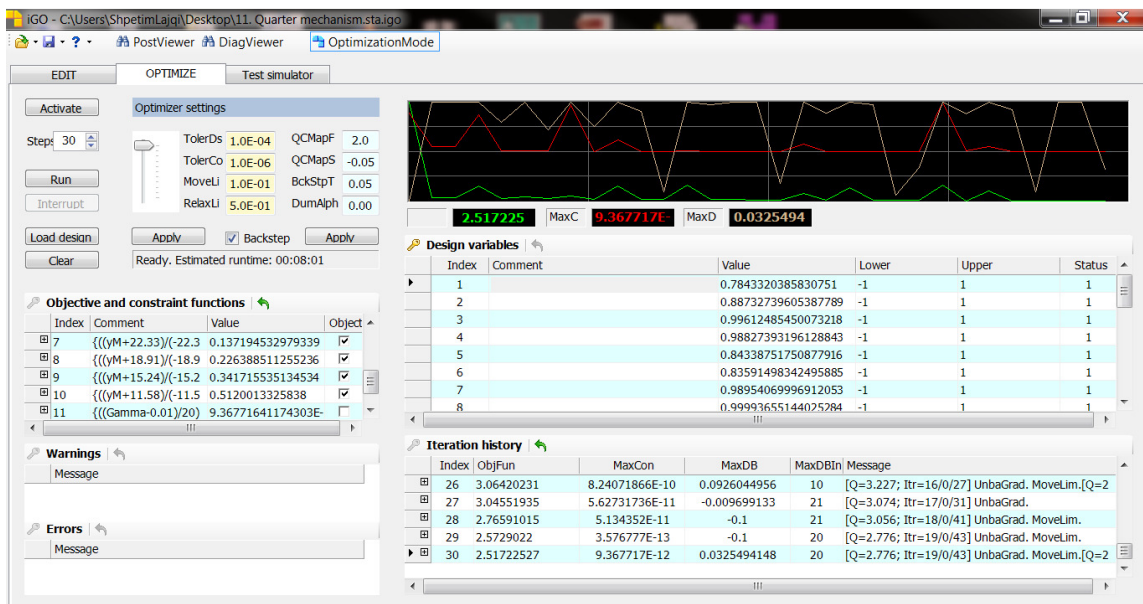


Figure 5.23: Optimization procedure performed in *iGOx* environment

Figure 5.23 shows the optimization process performed in *iGOx* environment. In Table 5.12 are tabulated the initial and optimal values of the design variables.

Table 5.12 Initial and optimal values of design variables

Index	Design variable	Initial	Optimal	Index	Design variable	Initial	Optimal
1.	b_1	1	0.78433204	13.	b_{13}	1	0.99150173
2.	b_2	1	0.88732740	14.	b_{14}	1	0.96843082
3.	b_3	1	0.99612486	15.	b_{15}	1	0.83479659
4.	b_4	1	0.98827393	16.	b_{16}	1	0.85650417
5.	b_5	1	0.84338752	17.	b_{17}	1	0.95183656
6.	b_6	1	0.83591498	18.	b_{18}	1	0.88955777
7.	b_7	1	0.98954070	19.	b_{19}	1	0.90502150
8.	b_8	1	0.99993655	20.	b_{20}	1	0.68099104
9.	b_9	1	0.95295080	21.	b_{21}	1	0.74739873
10.	b_{10}	1	0.98487951	22.	b_{22}	1	0.93353712
11.	b_{11}	1	0.88722175	23.	b_{23}	1	0.98966755
12.	b_{12}	1	0.89947748	24.	b_{24}	1	0.89172519

Figure 5.24 shows the wheel path for the initial and optimal design variables when the positions of the wheel are in bound and rebound resulting from applied forces in the wheel.

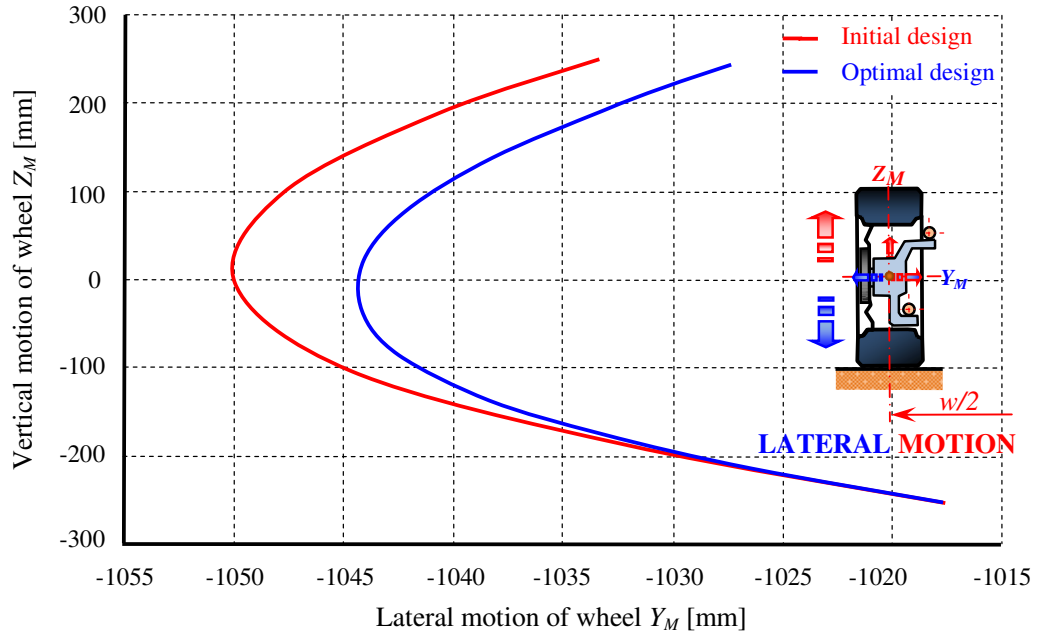


Figure 5.24: Path of wheel for initial and optimal design variables of the terrain vehicle suspension mechanism

5.5 Discussion of the results

Figures 5.9 and 5.10 show that for minimal input angle $\theta_{3min} = 335.18$ deg, the vertical and lateral motions of the wheel are $Z_M = -250$ mm and $Y_M = -1017.5$ mm - *rebound*, for rest input angle $\theta_{3rest} = 355.40$ deg are $Z_M = 0$ mm and $Y_M = -1050$ mm - *rest*, whilst for maximal input angle $\theta_{3max} = 378.22$ deg are $Z_M = +250$ mm and $Y_M = -1033$ mm - *bound*.

Simulation results performed in MathCAD environment stated that the *camber angle* during all vertical motions of the wheel (*bound* and *rebound*) was zero: $\gamma(\theta_3) = 0$ deg, *kingpin inclination angle* is $\sigma = 12.28$ deg, while *kingpin offset* is: 0.9 mm. These obtained results help for offering suitable space for fitting brakes, steering gears, and not provide turning moments in steering wheels during the braking or acceleration processes.

Tables 5.4 presented results for angular displacements of main links, chamber angle, and the position of the center of the wheel as a function of the input angles of the suspension mechanism. Tables 5.7 to 5.10 introduced the results for angular displacements, velocities and accelerations, as well as absolute and projection velocities and accelerations as a function of ground excitation for the main part of the suspension mechanism. The obtained results are taken by two ways in order to compare the accuracy of the developed model. One is from the developed program performed in MathCAD environments, whilst the other by simple commercial Working Model software. The results are practically identical and coincide very well with the two methods. This verifies the reliability of the developed kinematic modeling for the terrain vehicle suspension mechanism.

Appendix A shows the results by diagrams regarding unknown reaction forces for joints of the suspension mechanism for maximal tire force $F_w = 8461$ N that could be acts in one wheel. These reaction forces are obtained from the dynamic modeling of suspension mechanisms as a function of ground excitation which changes over time.

From Figure 5.24 it can be concluded that, the optimized suspension system offers 0% rebound, 18% rest and 37.5% bound less lateral wheel displacement when compared with the initial rebound position.

From discussing the results it can be concluded that, the developed suspension mechanism allows motion of wheel upwards and downward by providing optimal lateral wheel displacements and zero camber angle.

6 DESIGNS AND OPTIMIZATIONS OF PASSIVE, ACTIVE AND SEMI-ACTIVE SUSPENSION SYSTEMS FOR A TERRAIN VEHICLE

This chapter introduces designs and optimization procedures for passive, active, and semi-active linear and non-linear suspension systems regarding a terrain vehicle. Due to the specific requirements for a terrain vehicle such as large vertical motion of the wheels, comfort, and safety, the objective of this approach is the ability to design, optimize and analyze the vehicle's suspension performance. In this way it is possible to decide which kind of the suspension system resulting from passive, active or semi-active fulfills, as far as possible, the specific requirements for a terrain vehicle when designing it.

This vehicle's suspension system is first represented using mathematical modeling regarding a quarter of it, and the equations of motion are derived at and solved by using MATLAB/Simulink. In order to verify the reliability of the derived at computer program, a comparison is made between the measured experimental data. The decision parameters for passive linear suspension systems are optimized by applying the Multi-Objective Genetic Algorithms. On the other hand, the parameters for the active damping device are optimized by using the Hooke-Jeeves method, which is based on non-linear programming. The vehicle's suspension performance prior to development is evaluated using initial and optimal designs.

The applications of active and semi-active systems on a concrete terrain vehicle are presented and compared with the passive systems by evaluating results regarding the vehicle's body acceleration, velocity, displacement, and vertical tire force, namely those aspects that have a directly influence on *driving comfort*, and *driving safety*. The results are shown by diagrams that represent the sensitivities of responses depending on the ground excitation and other parameters. The *driving comfort* is related to the vehicle's vertical body acceleration. The *driving safety* is dependent on the quality of the contact between the tires and the ground surface, and so the wheels should remain in contact with the ground's surface as firmly as possible, Belingardi and Demic [69]. Designers always devote particular attention to the suspension systems in order to improve both characteristics; *comfort* and *safety*.

The vehicle suspension systems are categorized as passive, active, and semi-active systems. In this thesis attention is focused on the active and semi-active systems. These systems ensure better performances (driving comfort and driving safety) than passive

suspension systems. The key problem regarding the active and semi-active suspension systems is when determining the optimal active damping force. This force depends on the operational conditions that come from the sensors. The control programming unit (CPU) controls the actuator or variable shock-absorber for producing an adequate damping force. The actuator or variable shock-absorber needs to respond quickly and precisely. The focus of this approach is a mathematical model of the active damping force and its optimization. The optimization process for design variables is carried out by using the stochastic parametric optimization method, Pajaziti [23] and Demic et al. [70]. The optimal design parameters are obtained when the objective function obtains minimal values. One of the well-established models for understanding and explaining vehicle suspension is the so-called quarter vehicle model (QVM), Yu et al. [37] and Ram Mohan Rao et al. [71]. However, for more detailed analyses more complex models such as half and full vehicle models can also be used. QVM is comparatively easy to transform into a mathematical model that actually consists of two second-order differential equations that can be solved in numerical ways.

Due to simplicity it is assumed that the spring and tire stiffness coefficients remain at constant values. At this stage a powerful computing program is needed to calculate the suspension's behavior and its characteristics. It is supposed that considering only the vertical ground excitation provides usable results. Any eventual longitudinal and lateral excitations that may arise during vehicle movement are therefore neglected.

6.1 Mathematical modeling of the quarter vehicle suspension system

The quarter-vehicle model consists of two masses, two springs, one or two shock-absorbers, and probably an actuator, Figures 6.1 and 6.2. The lower mass is the un-sprung mass m_u , and the upper one is the sprung mass m_s . The un-sprung mass represents one wheel assembly mass, whilst the sprung mass represents approximately $\frac{1}{4}$ of the remaining total vehicle mass. The lower spring is described by the linear k_t or non-linear k_{t1}, k_{t2}, k_{t3} tire stiffness coefficients, whilst the shock absorber is by the c_t tire damping coefficient. The tire damping is often neglected due to its insignificant influence on the final results, Jazar [9]. The suspension system is completed when the spring and the shock absorber are inserted between two masses. The spring is defined by the linear k_s or non-linear k_{s1}, k_{s2} spring stiffness coefficients and the shock-absorber is determined by the linear c_{sh} or non-linear c_{sh1}, c_{sh2} shock absorber damping coefficients. The lower or un-sprung mass is excited by the ground surface z_r through the tires' contact. Forces that act within the suspension systems can be

described by linear or non-linear characteristics (Figures 6.1 and 6.2). Based on experience, the real behavior is better described using the non-linear characteristics. In the continuation the mathematic models are detailed for passive, active, and semi-active suspension systems.

6.1.1 Passive linear and non-linear suspension systems

The linear and non-linear models of the passive quarter-vehicle used for simulation of the terrain vehicle's suspension, are shown in Figure 6.1.

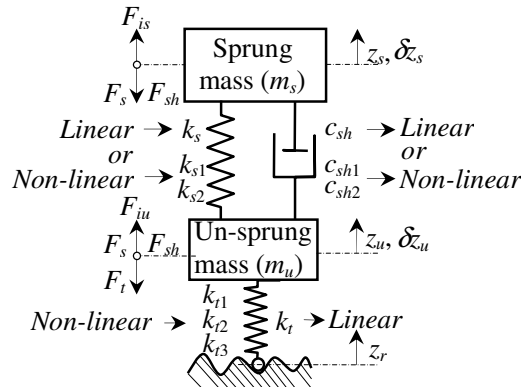


Figure 6.1: The passive linear and non-linear quarter-vehicle models

For the presented QVM the differential equations of the motion are determined by applying Lagrange's equations:

$$\frac{d}{dt} \left(\frac{\partial E_k}{\partial \dot{z}_s} \right) - \frac{\partial E_k}{\partial z_s} = \frac{\delta W}{\delta z_s}; \quad \frac{d}{dt} \left(\frac{\partial E_k}{\partial \dot{z}_u} \right) - \frac{\partial E_k}{\partial z_u} = \frac{\delta W}{\delta z_u}. \quad (6.1)$$

The kinetic energy E_k is defined by the following expression:

$$E_k = \frac{1}{2} \cdot m_s \cdot \dot{z}_s^2 + \frac{1}{2} \cdot m_u \cdot \dot{z}_u^2. \quad (6.2)$$

The derivatives of Lagrange's equations can be written as follow:

$$\frac{d}{dt} \left(\frac{\partial E_k}{\partial \dot{z}_s} \right) = m_s \cdot \ddot{z}_s, \frac{\partial E_k}{\partial z_s} = 0; \quad \frac{d}{dt} \left(\frac{\partial E_k}{\partial \dot{z}_u} \right) = m_u \cdot \ddot{z}_u, \frac{\partial E_k}{\partial z_u} = 0. \quad (6.3)$$

The elementary work δW is given by the following expression:

$$\delta W = -(F_{s-l or n} + F_{sh-l or n}) \cdot \delta z_s + (F_{s-l or n} + F_{sh-l or n} - F_{t-l or n}) \cdot \delta z_u. \quad (6.4)$$

The elementary work during virtual displacement of the sprung mass δz_s , and un-sprung mass δz_u , is expressed as:

$$\frac{\delta W}{\delta z_s} = -(F_{s-l or n} + F_{sh-l or n}), \quad \frac{\delta W}{\delta z_u} = F_{s-l or n} + F_{sh-l or n} - F_{t-l or n}. \quad (6.5)$$

The linear forces that act within the suspension system, such as; dynamic tire force F_{t-l} , spring force F_{s-l} , and shock-absorber damping force F_{sh-l} , are determined by the following expressions:

$$F_{t-l} = k_t \cdot (z_u - z_r), \quad (6.6)$$

$$F_{s-l} = k_s \cdot (z_s - z_u), \quad (6.7)$$

$$F_{sh-l} = c_{sh} \cdot (\dot{z}_s - \dot{z}_u). \quad (6.8)$$

With a few mathematical rearrangements, the Lagrange's equations of motion for passive linear suspension systems can be written as follows:

$$\begin{aligned} m_s \cdot \ddot{z}_s &= -k_s \cdot (z_s - z_u) - c_{sh} \cdot (\dot{z}_s - \dot{z}_u), \\ m_u \cdot \ddot{z}_u &= k_s \cdot (z_s - z_u) + c_{sh} \cdot (\dot{z}_s - \dot{z}_u) - k_t \cdot (z_u - z_r). \end{aligned} \quad (6.9)$$

In matrix form the equation (6.9) is written as follows:

$$\begin{bmatrix} m_s & 0 \\ 0 & m_u \end{bmatrix} \cdot \begin{Bmatrix} \ddot{z}_s \\ \ddot{z}_u \end{Bmatrix} = \begin{bmatrix} -c_{sh} & c_{sh} \\ c_{sh} & -c_{sh} \end{bmatrix} \cdot \begin{Bmatrix} \dot{z}_s \\ \dot{z}_u \end{Bmatrix} + \begin{bmatrix} -k_s & k_s \\ k_s & -(k_s + k_t) \end{bmatrix} \cdot \begin{Bmatrix} z_s \\ z_u \end{Bmatrix} + \begin{Bmatrix} 0 \\ k_t \end{Bmatrix} \cdot z_r. \quad (6.10)$$

The non-linear behaviors of those dynamic forces that act within the suspension are high-order polynomial functions. The non-linear dynamic tire force F_{t-n} is described as a third-order polynomial function, spring force F_{s-n} is given by a third-order polynomial function, whilst the shock-absorber damping force F_{sh-n} is modeled as a second-order polynomial function.

These forces are determined by the following expressions, Pajaziti [23] and Demic [72]:

$$F_{t-n} = k_{t1} \cdot (z_u - z_r) + k_{t2} \cdot (z_u - z_r)^2 - k_{t3} \cdot (z_u - z_r)^3, \quad (6.11)$$

$$F_{s-n} = k_{s1} \cdot (z_s - z_u) + k_{s2} \cdot (z_s - z_u)^3, \quad (6.12)$$

$$F_{sh-n} = c_{sh1} \cdot (\dot{z}_s - \dot{z}_u) + c_{sh2} \cdot (\dot{z}_s - \dot{z}_u)^2 \operatorname{sign}(\dot{z}_s - \dot{z}_u). \quad (6.13)$$

The differential equations of motion for the passive non-linear suspension systems are:

$$\begin{aligned} m_s \cdot \ddot{z}_s &= -k_{s1} \cdot (z_s - z_u) - k_{s2} \cdot (z_s - z_u)^3 - c_{sh1} \cdot (\dot{z}_s - \dot{z}_u) - c_{sh2} \cdot (\dot{z}_s - \dot{z}_u)^2 \operatorname{sign}(\dot{z}_s - \dot{z}_u), \\ m_u \cdot \ddot{z}_u &= k_{s1} \cdot (z_s - z_u) + k_{s2} \cdot (z_s - z_u)^3 + c_{sh1} \cdot (\dot{z}_s - \dot{z}_u) + c_{sh2} \cdot (\dot{z}_s - \dot{z}_u)^2 \operatorname{sign}(\dot{z}_s - \dot{z}_u) \dots \\ &\quad - k_{t1} \cdot (z_u - z_r) - k_{t2} \cdot (z_u - z_r)^2 + k_{t3} \cdot (z_u - z_r)^3, \end{aligned} \quad (6.14)$$

where \ddot{z}_s , \dot{z}_s , z_s and \ddot{z}_u , \dot{z}_u , z_u denote the acceleration, velocity, and displacement of the sprung and un-sprung masses, respectively. Whilst $(z_s - z_u)$, $(z_u - z_r)$ and $(\dot{z}_s - \dot{z}_u)$ represent the suspension travel, tire deflection, and relative velocity of the shock absorber.

Equations (6.9), (6.10) and (6.14) represent a system of second-order non-homogeneous linear differential equations regarding the motions for linear and non-linear passive suspension systems, respectively.

6.1.2 Active and semi-active non-linear suspension systems

Many attempts regarding control strategies on active and semi-active suspension systems have been performed over past years to improve driving comfort and driving safety. Several control strategies have been developed for the semi-active, such as on-off skyhook, on-off ground-hook, continuous skyhook, fuzzy logic control, Abramov et al. [73]. Consequently, a CPU-controlled active system for adjusting damping force has been implemented here.

The main problem concerning the already-mentioned control systems is to determine an adequate active damping force. Determination of this force is done by the addition of two virtual passive shock-absorbers. The first one is fixed on the sprung mass whilst the other one is fixed on the un-sprung mass. The second fixing-point for both shock-absorbers is fixed in the fictive hook on the sky. The damping force caused by the first virtual shock-absorber, always acts in the opposite direction to the velocity of the sprung mass, whereas the other damping force produced by the second virtual shock absorber, always acts in the same direction as the velocity of the un-sprung mass. In reality, any addition of the skyhook approach is impossible because hooking the shock-absorber onto the sky is also impossible.

The real implementation of the skyhook approach is possible by using an active actuator installed between the sprung and un-sprung masses, Figure 6.2, Lajqi and Pehan [2].

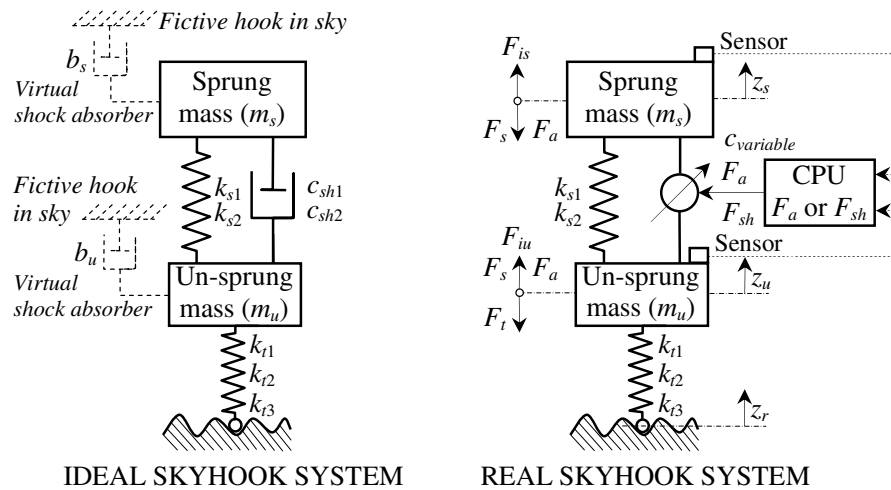


Figure 6.2: Skyhook concept for active and semi-active non-linear suspension systems

In this case the active damping force is described by the expression:

$$F_a = -b_s \cdot \dot{z}_s + b_u \cdot \dot{z}_u, \quad (6.15)$$

where b_s and b_u denote the damping coefficients of both virtual shock-absorbers. The adequate damping coefficients b_s and b_u are determined by an optimization process.

The active damping force F_a given by equation (6.15) can be re-written as follows:

$$F_a = b_u \cdot (\dot{z}_u - \dot{z}_s) - b_s \left(1 - \frac{b_u}{b_s} \right) \cdot \dot{z}_s, \quad (6.16)$$

where the first member, $(\dot{z}_u - \dot{z}_s)$ of the equation (6.16) relates to the relative velocity of the active actuator, whilst the second member relates to the absolute velocity of the sprung mass.

In order to fulfill, as far as possible, the specific requirements given in this thesis dealing with active suspension systems, the priority is dedicated to hydraulic active actuators. For a semi-active suspension system dealing with variable shock-absorber, regulation of the damping characteristic by using servo-valve will be considered.

The dynamic equations of motion for the active non-linear suspension system derived from Figure 6.2, are written as follow:

$$\begin{aligned} m_s \cdot \ddot{z}_s &= -k_{s1} \cdot (z_s - z_u) - k_{s2} \cdot (z_s - z_u)^3 + b_s \cdot \dot{z}_s - b_u \cdot \dot{z}_u, \\ m_u \cdot \ddot{z}_u &= k_{s1} \cdot (z_s - z_u) + k_{s2} \cdot (z_s - z_u)^3 - b_s \cdot \dot{z}_s + b_u \cdot \dot{z}_u \dots \\ &\quad - k_{t1} \cdot (z_u - z_r) - k_{t2} \cdot (z_u - z_r)^2 + k_{t3} \cdot (z_u - z_r)^3. \end{aligned} \quad (6.17)$$

The dynamic equations of motion for the semi-active non-linear suspension systems determined from Figure 6.2, generate the following form:

$$\begin{aligned} m_s \cdot \ddot{z}_s &= -k_{s1} \cdot (z_s - z_u) - k_{s2} \cdot (z_s - z_u)^3 + b_s \cdot \dot{z}_s - b_u \cdot \dot{z}_u, \\ m_u \cdot \ddot{z}_u &= k_{s1} \cdot (z_s - z_u) + k_{s2} \cdot (z_s - z_u)^3 - b_s \cdot \dot{z}_s + b_u \cdot \dot{z}_u \dots \\ &\quad - k_{t1} \cdot (z_u - z_r) - k_{t2} \cdot (z_u - z_r)^2 + k_{t3} \cdot (z_u - z_r)^3. \end{aligned} \quad \left. \right\} IF(F_a \cdot F_{sh}) \leq 0 - ON \quad (6.18)$$

$$\begin{aligned} m_s \cdot \ddot{z}_s &= -k_{s1} \cdot (z_s - z_u) - k_{s2} \cdot (z_s - z_u)^3 - c_{sh1} \cdot (\dot{z}_s - \dot{z}_u) \dots \\ &\quad - c_{sh2} \cdot (\dot{z}_s - \dot{z}_u)^2 sign(\dot{z}_s - \dot{z}_u), \\ m_u \cdot \ddot{z}_u &= k_{s1} \cdot (z_s - z_u) + k_{s2} \cdot (z_s - z_u)^3 + c_{sh1} \cdot (\dot{z}_s - \dot{z}_u) \dots \\ &\quad + c_{sh2} \cdot (\dot{z}_s - \dot{z}_u)^2 sign(\dot{z}_s - \dot{z}_u) \\ &\quad - k_{t1} \cdot (z_u - z_r) - k_{t2} \cdot (z_u - z_r)^2 + k_{t3} \cdot (z_u - z_r)^3. \end{aligned} \quad \left. \right\} IF(F_a \cdot F_{sh}) > 0 - OFF$$

Forces that act within active and semi-active suspension systems are taken for non-linear behavior, as determined by equations (6.11), (6.12), and (6.13).

The *ON-OFF* skyhook control given in equation (6.18) presents an effective vibration control strategy. The CPU-respond $IF(F_a \cdot F_{sh} \leq 0)$ causes shock-absorber adjustment in the high-damping state. The CPU-respond $IF(F_a \cdot F_{sh} > 0)$ causes the shock absorber adjustment

in the low-damping state. Adjusting the shock-absorber within high or low states depends on the product regarding the relative speed of the shock-absorber ($\dot{z}_s - \dot{z}_u$) and the absolute speeds of the sprung and un-sprung masses (\dot{z}_s and \dot{z}_u). If this product is zero or negative, the shock-absorber is adjusted to a higher-damping state, otherwise it is set to a low-damping state.

Equations (6.17) and (6.18) represent a system of second-order non-homogeneous, non-linear differential equations regarding the motions for non-linear active and semi-active suspension systems, respectively.

6.2 Simulations of vehicle suspension by numerical methods

In order to solve the differential equations of motion for the general case of ground excitation, it is more than necessary to have an efficient tool to speed-up the numerical procedures. Numerical simulations have been developed for all the presented suspension systems. A methodology is presented for solving differential equations of motion for passive, linear, and semi-active non-linear suspension systems. Whereas for other systems the procedure is the same, here only the output results are presented, as obtained from simulation. In order to speed-up the numerical procedures, the differential equations of motion need to be transformed into more suitable forms.

Equation (6.9) is transformed into the state variables equation by simplifying the second order differential equations into first-order differential equations. It is supposed that the state variables are given by the following expressions:

$$\begin{aligned} x_1 &= z_s, & x_2 &= z_u, & x_3 &= \dot{z}_s, & x_4 &= \dot{z}_u, \\ dx_1 &= x_3 = \ddot{z}_s, & dx_2 &= x_4 = \ddot{z}_u, & dx_3 &= \ddot{z}_s, & dx_4 &= \ddot{z}_u. \end{aligned} \quad (6.19)$$

Substituting equation (6.19) into equation (6.9), the state variables equation is written as follows:

$$\begin{bmatrix} dx_1 \\ dx_2 \\ dx_3 \\ dx_4 \end{bmatrix} = \begin{bmatrix} 0 & 0 & 1 & 0 \\ 0 & 0 & 0 & 1 \\ -k_s/m_s & k_s/m_s & -c_{sh}/m_s & c_{sh}/m_s \\ k_s/m_u & -(k_s+k_t)/m_u & c_{sh}/m_u & -c_{sh}/m_u \end{bmatrix} \cdot \begin{bmatrix} x_1 \\ x_2 \\ x_3 \\ x_4 \end{bmatrix} + \begin{bmatrix} 0 \\ 0 \\ 0 \\ k_t/m_u \end{bmatrix} \cdot \{z_r\}. \quad (6.20)$$

The state variables for the semi-active non-linear suspension system derived from equation (6.19), are expressed as follow:

$$\begin{aligned}
dx_1 &= x_3 = \dot{z}_s, \\
dx_2 &= x_4 = \dot{z}_u, \\
\text{If } (F_a \cdot F_{sh}) \leq 0 - \text{ON} &\quad (\text{ACTIVE-HIGH STATE}) \\
dx_3 &= \ddot{z}_s = (1/m_s) \cdot \{-k_{s1} \cdot (x_1 - x_2) - k_{s2} \cdot (x_1 - x_2)^3 + b_s \cdot x_3 - b_u \cdot x_4\}, \\
dx_4 &= \ddot{z}_u = (1/m_u) \cdot \{k_{s1} \cdot (x_1 - x_2) + k_{s2} \cdot (x_1 - x_2)^3 - b_s \cdot x_3 + b_u \cdot x_4 \dots \\
&\quad - k_{t1} \cdot (x_2 - z_r) - k_{t2} \cdot (x_2 - z_r)^2 + k_{t3} \cdot (x_2 - z_r)\}.
\end{aligned} \tag{6.21}$$

$$\begin{aligned}
\text{If } (F_a \cdot F_{sh}) > 0 - \text{OFF} &\quad (\text{PASSIVE-LOW STATE}) \\
dx_3 &= \ddot{z}_s = (1/m_s) \cdot \{-k_{s1} \cdot (x_1 - x_2) - k_{s2} \cdot (x_1 - x_2)^3 - c_{sh1} \cdot (x_3 - x_4) - c_{sh2} \cdot (x_3 - x_4)^2 \text{sign}(x_3 - x_4)\}, \\
dx_4 &= \ddot{z}_u = (1/m_u) \cdot \{k_{s1} \cdot (x_1 - x_2) + k_{s2} \cdot (x_1 - x_2)^3 + c_{sh1} \cdot (x_3 - x_4) \dots \\
&\quad + c_{sh2} \cdot (x_3 - x_4)^2 \text{sign}(x_3 - x_4) - k_{t1} \cdot (x_2 - z_r) - k_{t2} \cdot (x_2 - z_r)^2 + k_{t3} \cdot (x_2 - z_r)^3\}.
\end{aligned}$$

Equation (6.20) represents the general form of the state variables equation for passive linear suspension system in matrix form, whilst equation (6.21) defines the state variables equation for a semi-active, non-linear suspension system.

The flowchart diagram for solving differential equations of motion is shown in Figure 6.3. The program starts by reading the suspension parameters, ground excitation, number of input and output variables, the initial conditions, and the number of iterations (time). Then the program continues to solve differential equations of motion by applying the solver ode45 in a MATLAB/Simulink environment. The program stops when the iteration condition is fulfilled. The results are presented through diagrams. The output results, depending on time, are the accelerations, velocities, and displacements of the sprung mass. The program also computes the vertical tire forces, which act between the ground's surface and the tire. The output results are within the function of ground excitation that represents road profile or so-called road bumps. In this thesis the ground excitation is demonstrated by two repeated smooth obstacles on a flat road, which is approximated by a smooth function, such as the cosine function shown in Figure 6.4.

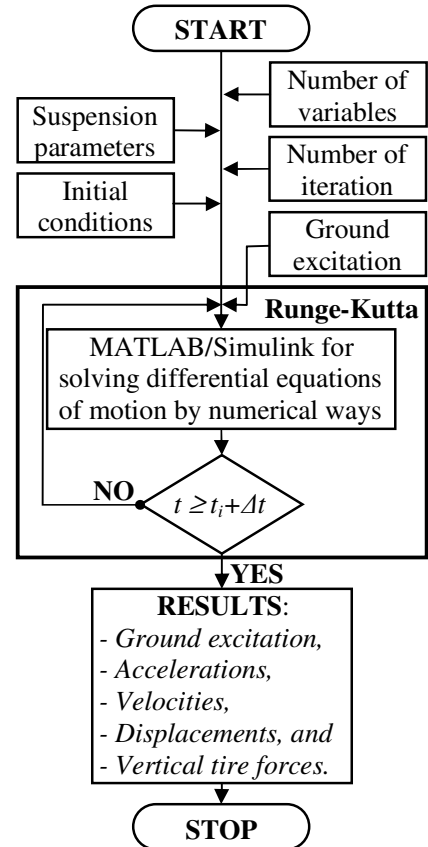


Figure 6.3: Flowchart diagram for solving differential equations of motion

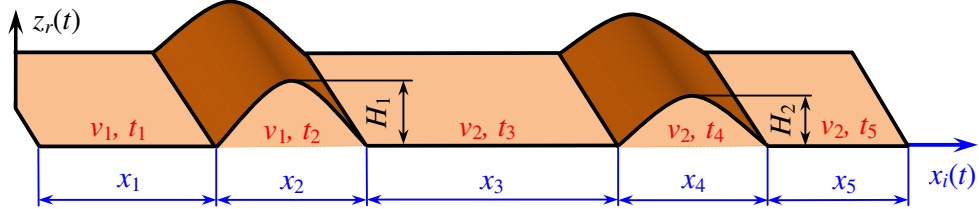


Figure 6.4: Ground excitation represented by double cosine road bumps

The ground excitation $z_r(t)$ is written, as follow:

$$z_r(t) = \begin{cases} 0.5 \cdot H_1 \cdot [1 - \cos(8\pi \cdot t)] & \text{if } t_1 \leq t \leq t_2 \\ 0.5 \cdot H_2 \cdot [1 - \cos(4\pi \cdot t)] & \text{if } t_3 \leq t \leq t_4 \\ 0 & \text{else} \end{cases}, \quad (6.22)$$

where H_1, H_2 are amplitudes of the first and second bumps, v_1, v_2 denotes vehicle speed, x_i define each part of road, and t_i is the termed time for passing each part of road. Table 6.1 gives the appropriate data for simulation of the ground excitation computed by expression (6.22).

Table 6.1: Description data for road bumps when the vehicle passed over them

Road data		Amplitudes of the road bumps: $H_1 = 0.05$ [m], $H_2 = 0.1$ [m]	
i	x_i [m]	for $v_1 = 20$ [kmh $^{-1}$], $t_i = x_i/v_1$ [s]	for $v_2 = 10$ [kmh $^{-1}$], $t_i = x_i/v_2$ [s]
1	2.78	0.50	-
2	1.39	0.25	-
3	3.47	-	1.25
4	1.39	-	0.50
5	4.17	-	1.50

A few authors such as Rill [4] and Sam and Osman [74] have used similar functions for ground excitation, as described here. Therefore, road bumps introduced by cosine functions, can be considered as one of the complex ground excitation inputs.

6.3 Verifying the reliability of the developed program

In order to verify the presented computer program, the results are compared to those done in an experimental ways. The input data are: $m_s = 320$ kg, $k_s = 15450.42$ Nm $^{-1}$, $c_{sh} = 1544.94$ Nsm $^{-1}$, whilst $m_u = 25$ kg and $k_t = 400000$ Nm $^{-1}$, are adopted. These data are obtained from experimental methods for a passive suspension system within an *Opel Vectra 1.8i* passenger car. The experiment is performed at Graz of University Technology, Vehicle Safety Institute (VSI), Figure 6.5. More details regarding the performed experiment are given in reference Lajqi et al. [18].

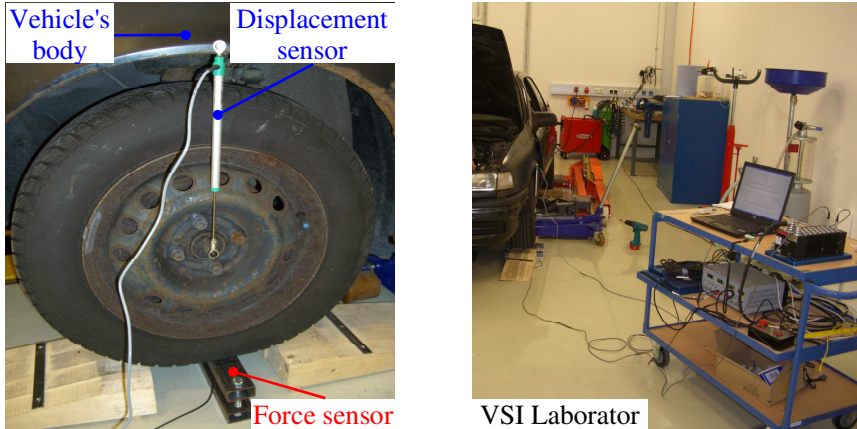


Figure 6.5: Laboratory devices for determining suspension characteristics, Lajqi et al. [18]

In order to verify the reliability of the developed program, ground excitation and other decision parameters are used that corresponded to the one explained above. The ground excitation is theoretically simulated by step bump as a function of time, Figure 6.6.a. Only the passive linear suspension system is considered for comparison.

Figure 6.6 show the results in the form of ground excitation and displacements that correspond to the vehicle's body (sprung mass), depending on time. These results are obtained by experimental and simulation methods, respectively. Finally, the displacements of the vehicle's body are compared, as obtained by different approaches.

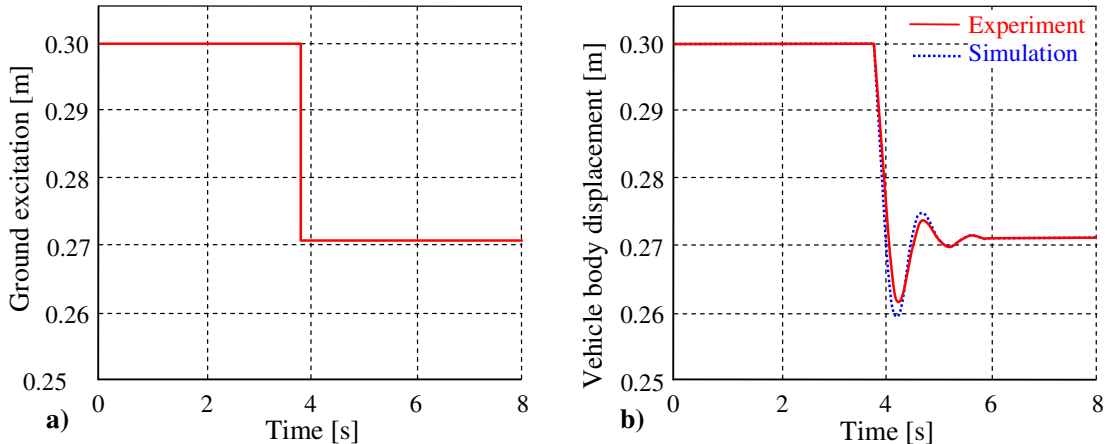


Figure 6.6: a) Ground excitation, and b) vertical vehicle body displacements, Lajqi et al. [18]

From Figure 6.6.b it is observed that, the simulation results performed in MATLAB environment generates sufficient and reliable results when compared to those produced by the experimental method. Consequentially, it can be concluded that the developed program is suitable for use during further analysis of the vehicle's suspension behavior.

6.4 Optimization of the suspension parameters for passive, active, and semi-active suspension systems

6.4.1 Optimization of the suspension parameters for a passive linear suspension system

In order to ensure the optimal suspension parameters for a terrain vehicle equipped with a passive linear suspension system, *driving comfort* and *driving safety* as design criteria are taken into consideration. The *driving comfort* is evaluated by computing the standard deviation of the vehicle's body acceleration - $\sigma_{\ddot{z}_s}$, where greater values are undesired. The *driving safety* is estimated by the standard deviation of the dynamic tire forces acting between the ground's surface and the tires - σ_{F_t} . If the tire forces oscillate too much then the contact between the ground surface and the tire is weak. Consequentially the vehicle's maneuverability and steering would be in question. In order to obtain optimal suspension design parameters regarding driving comfort and driving safety, according to Gobbi and Mastinu [34], Mastinu et al. [46] Lajqi et al. [75], and Popp and Schiehlen [76], the following expressions are used:

- a. The standard deviation of the vehicle's body acceleration ($\sigma_{\ddot{z}_s}$ - *driving comfort*):

$$\sigma_{\ddot{z}_s} = \left\{ \frac{A_b \cdot v}{2} \cdot \left(\frac{m_s}{c_{sh} \cdot m_s^2} \cdot k_s^2 + \frac{m_u}{c_{sh} \cdot m_s^2} \cdot k_s^2 + \frac{c_{sh}}{m_s^2} \cdot k_t \right) \right\}^{\frac{1}{2}}. \quad (6.23)$$

- b. The standard deviation of the dynamic tire forces (σ_{F_t} - *driving safety*):

$$\begin{aligned} \sigma_{F_t} = & \left\{ \frac{A_b \cdot v}{2} \cdot \left(\frac{(m_s + m_u)^3}{c_{sh} \cdot m_s^2} \cdot k_s^2 + \frac{c_{sh} \cdot (m_s + m_u)^2}{m_s^2} \cdot k_t + \dots \right. \right. \\ & \left. \left. + \frac{m_u \cdot k_t^2 - 2 \cdot m_u \cdot (m_s + m_u) \cdot k_s \cdot k_t}{c_{sh} \cdot m_s} \right) \right\}^{\frac{1}{2}}. \end{aligned} \quad (6.24)$$

where A_b denotes the road roughness parameter, whilst v is the vehicle speed.

The equations (6.23) and (6.24) define the design criteria (driving comfort and driving safety) used as objective functions for optimizing the passive linear suspension parameters.

An optimization technique is used for determining the optimal suspension parameters for the passive linear suspension system --- the Multi-Objective Genetic Algorithms (MOGAs) method. In order to explain the optimization procedure by employing MOGAs, the Genetic Algorithms process is first introduced.

6.4.1.1 Genetic Algorithms

The genetic algorithms (GAs) are well-known as methods for the global optimization of highly complex problems, which were invented by Professor John Holland at the University of Michigan in the 1970s, Alkhatib et al. [36]. GAs is a stochastic global search and optimization method that mimics the metaphor of natural biological evolution and is developed based on Darwin's theory of evolution "survivor of the fittest". Figure 6.7 shows a flowchart of the evolutionary process as performed by GAs.

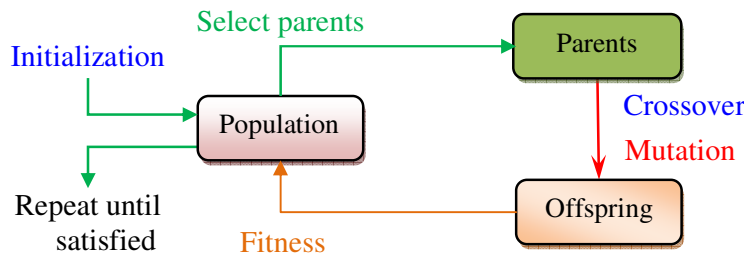


Figure 6.7: GAs evaluation process

The GAs does not use gradient information but rather perform stochastic searches of the design in order to minimize the values of the objective functions. The objective functions are not required to be continuous, neither do they need information about their derivates; therefore they can handle problems with discrete solution spaces. Evaluation of the objective functions and constraints is performed by fitness. In several aspects, GAs differs from traditional optimization techniques, Yu and Yu [37] and Zhang [77]. Some of these differences are summarized as follows:

- GAs are able to solve complex problems using non-convex solution space, where traditional methods usually fail,
- GAs searching mechanisms are stochastic in nature, which makes them capable of searching entire solution space with more probability of finding the global solution,
- GAs solutions search from a population, not from a single solution,
- GAs allow design variables to be mixed (continuous and discrete variables),
- GAs use probabilistic transition rules not deterministic rules. This characteristic makes GAs uniquely suited to MOGAs optimization.

All these described differences make the GAs superior over classic optimization methods in some real world applications, particularly for complex and sophisticated engineering problems. The basic procedure of the GAs consists of the following steps Senthil kumar [19], Yu and Yu [37], and Zhang [77]:

Step 1#: Initial population

GAs start iterations with an initial population (design solution). The initial population of chromosomes is created rather and consists of a set of design solutions. Each chromosome is used to express a sequence of genes from the binary digits (0 and 1). Hence, real expressions are used to represent chromosome for objective functions when considering optimization. The chromosomes exist within the architecture regarding the design variable's representation by the spring and tire stiffness coefficients, shock absorber damping coefficient, and the sprung and un-sprung masses.

Step 2#: Fitness function

The fitness function evaluates all the chromosomes. The target of the fitness function is to numerically encode the performance of the chromosomes. The fitness function for the treated problem consists of an objective function that enables minimization of the vehicle's body acceleration and dynamic tire forces.

Step 3#: Selection function

The selection function is one of the key procedures in order to produce successive generations. It determines which chromosomes (individuals) will be represented and continue on to the next generation. Selection starts from the old population to the new population based on the fitness's of the chromosomes, as given by the evaluation function. Chromosomes with the greater fitness rates are selected whilst chromosomes with lower fitness rates are removed from the population. There are several methods for selecting chromosomes, which have been reported in the literature [78], such as: tournament selection, roulette-wheel selection, ranking selection, etc.

The *tournament selection method*, selects each parent by choosing individuals at random, by a specified number of turnamnet size, and then choosing the best individual out of that set to be a parent. Thus the tournament selection method will be used as the selection function during the optimization process.

Step 4#: Genetic operators (crossover and mutation)

Generally speaking, there are two types of genetic operators: *crossover* and *mutation*. The *crossover* process allows for an exchange of genes (design solution) between individuals in the population. Crossover takes two individuals (chromosomes) and produces two new individuals whereas *mutation* directs an individual to produce a single new solution. If the parents are allowed to mate, a combination operator is used to exchange genes between the

two parents in order to produce children. If they aren't allowed to mate, the parents are placed unchanged into the next generation. Figure 6.8 shows the genetic operators.

The best *crossover rate* is between 0.80 and 0.95, whilst the best mutation rate for most applications is between 0.001 and 0.1.

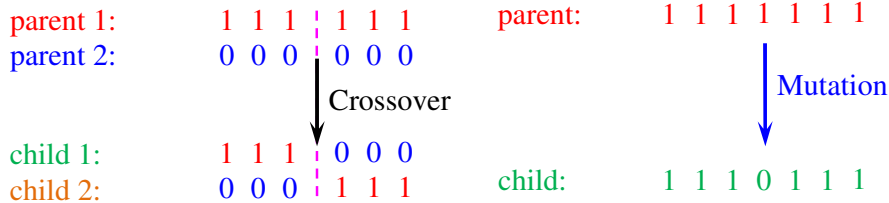


Figure 6.8: Genetic operators (crossover and mutation)

Step 5#: Evaluation function

The evaluation function is used to evaluate the fitness rates of the chromosomes, i.e. the quality of the solution, within a population. A better solution obtains a higher score. That function directs the population towards progress because a good solution with a high score will be selected during the selection process, and a poor solution removed.

Step 6#: Repeated steps 3 - 5

If the termination criterion has not been met, the process of selection, crossover and mutation (steps 3-5) should be repeated again in order to obtain an optimal design solution.

6.4.1.2 Multi-objective optimization process by using the Genetic Algorithms

In several cases regarding real problems, the multi-objective optimization problem involves multiple and conflicting objective function. So, optimizing of the design variables with respect to a single objective function often results in unacceptable results with respect to the other objective functions. Therefore, a perfect multi-objective solution that simultaneously optimizes each objective function is almost impossible in many cases, Konak et al. [33]. A reasonable solution to a multi-objective problem is to investigate a set of solutions. Each set of solutions should satisfy the objective functions at an acceptable level without being dominated by any other solution.

GA is one of the suitable techniques for solving multi-objective optimization problems. The first practical MOGAs, called vector evaluated GAs, was proposed by Schaffer [79]. Afterwards several multi-objective evolutionary algorithms were developed including MOGAs, Mastinu et al. [46], Fonseca and Fleming [80].

The multi-objective optimization problems are usually written in the following form:

$$\min f(x) = \begin{Bmatrix} f_1(x) \\ f_2(x) \\ \vdots \\ f_{n_{obj}}(x) \end{Bmatrix}, \quad (6.25)$$

$$x = \{x_1 \ x_2 \ \dots \ x_n\}^T \leq 0.$$

Subjected to the constraints:

$$h(x) = \{h_1(x) \ h_2(x) \ \dots \ h_{n_c}(x)\}^T \leq 0, \quad (6.26)$$

where, $f(x)$ is a termed multi-objective function, $h(x)$ denotes the constraint function, vector x describes the design variables, $n_{obj} \geq 2$ gives the number of objective functions, n presents the number of design variables, whereas n_c is the number of constrains.

6.4.1.3 Optimization of the passive linear suspension design parameters

In order to obtain an optimal suspension design for a terrain vehicle with passive linear suspension system, two design criteria are taken: *driving comfort* and *driving safety*. The driving comfort is presented by the standard deviation of the vehicle's body acceleration – $\sigma_{\ddot{z}_s}$. The driving safety is determined by the standard deviation of the dynamic tire forces – σ_{F_t} . There are five design variables employed during the optimization process such as spring stiffness coefficient k_s , shock-absorber damping coefficient c_{sh} , tire stiffness coefficient k_t , sprung m_s , and un-sprung mass m_u . The objective functions and design variables limits are written as follows:

$$\min f(x) = \begin{Bmatrix} \left\{ \frac{A_b \cdot v}{2} \cdot \left(\frac{m_s}{c_{sh} \cdot m_s^2} \cdot k_s^2 + \frac{m_u}{c_{sh} \cdot m_s^2} \cdot k_s^2 + \frac{c_{sh}}{m_s^2} \cdot k_t \right) \right\}^{\frac{1}{2}} \\ \left\{ \frac{A_b \cdot v}{2} \cdot \left(\frac{(m_s + m_u)^3}{c_{sh} \cdot m_s^2} \cdot k_s^2 + \frac{c_{sh} \cdot (m_s + m_u)^2}{m_s^2} \cdot k_t + \dots \right. \right. \\ \left. \left. + \frac{m_u \cdot k_t^2 - 2 \cdot m_u \cdot (m_s + m_u)}{c_{sh}} \cdot k_s \cdot k_t \right) \right\}^{\frac{1}{2}} \end{Bmatrix} \quad (6.27)$$

Subjected to the design variables limit:

$$\begin{aligned} 50000 \text{ N/m} &\leq k_s \leq 200000 \text{ N/m}, \\ 5000 \text{ Ns/m} &\leq c_{sh} \leq 20000 \text{ Ns/m}, \\ 200000 \text{ N/m} &\leq k_t \leq 500000 \text{ N/m}, \\ 280 \text{ kg} &\leq m_s \leq 300 \text{ kg}, \\ 35 \text{ kg} &\leq m_u \leq 70 \text{ kg}. \end{aligned} \quad (6.28)$$

The lower and upper limits of the design variables are selected based on previous studies. The initial populations of the design variables are selected to be of medium value between the lower and upper limits. Optimization of the design variables is carried out by employing MOGAs within the MATLAB environment. In Table 6.2 the used parameters in MOGAs optimizing process are shown. The optimization process starts by reading the design variables limit and initial population of the design variables. Then, the design variables pass for simulation of the differential equations of motion for the passive linear suspension system.

Table 6.2: The MOGAs parameters performed in the MATLAB GAs toolbox

GAs step	GAs parameters	Values
<i>Design variables limits</i>	Design variables (constraints)	
	Lower limits:	[50000 5000 200000 280 35]
	Upper limits:	[200000 20000 500000 300 70]
<i>Step 1#</i>	Population	
	Population type:	Double vector
	Population size:	100
	Creation function:	Uniform
	Initial population:	[125000 12500 350000 290 50]
<i>Step 2#</i>	Problem	
	Fitness function:	$\sigma_{\dot{z}_s}, \sigma_{F_t}$
	Number of variables:	5
<i>Step 3#</i>	Selection	
	Selection function:	Tournament
<i>Step 4#</i>	Reproduction	
	Crossover fraction:	0.8
	Mutation	
	Mutation technique:	Uniform
	Mutation rate:	0.01
<i>Step 5#</i>	Crossover	
	Crossover function:	Heuristic
	Crossover rate:	0.8
	Stopping criteria	
	Number of generation:	1000
	Fitness limit:	$-\infty$
	Evaluation function (tolerance)	$5 \cdot 10^{-5}$

After these steps, the design variables are followed within the MOGAs process to calculate the fitness function. The optimization process will be stopped when the design variables have been improved and the design criteria is fulfilled, otherwise the optimization process will be repeated again and stopped whenever the optimal design solution is obtained. The already described optimization process performed in MOGAs is summarized in the flowchart diagram shown in Figure B.5. The initial and optimal values of the design variables

for four independent runs by utilizing MOGAs for two objective functions are shown in Table 6.3.

This table gives the values of the objective functions and the number of iterations for vehicle speed $v = 20 \text{ kmh}^{-1}$. During each run the number of iterations is plotted automatically by computer. It can be observed that, for each new run, significantly similar results for the design variables are found. The small differences are a result of two conflicting objective functions, which try to fulfill driving comfort and diving safety at the same time. These smaller differences can also be noticed in Figure 6.9.b, from the plotting of family points.

Table 6.3: Initial and optimal suspension design parameters

Suspension parameters	Initial	Optimal			
		Run 1	Run 2	Run 3	Run 4
$k_s [\text{Ns}^{-1}]$	125000	57008	54872	50700	52686
$c_{sh} [\text{kg}]$	12500	5686	5360	5170	5073
$k_t [\text{Ns}^{-1}]$	350000	202180	207330	208055	204520
$m_s [\text{kg}]$	290	298	299	300	295
$m_u [\text{kg}]$	50	36	37	35	35
$\sigma_{\dot{z}_s} [\text{ms}^{-2}]$	23.56	12.11	11.87	11.59	11.59
$\sigma_{F_t} [\text{N}]$	8057	4158	4139	4049.07	3998
Iteration number	-	102	102	102	107

The best design is obtained after the fourth runs, when the evaluation function has met the design criteria. In this case, the objectives function has reached the minimal values. Figure 6.9, illustrates the convergence of the four runs, by plotting objectives function with single points, and the average distance between individuals that corresponds to the design variables.

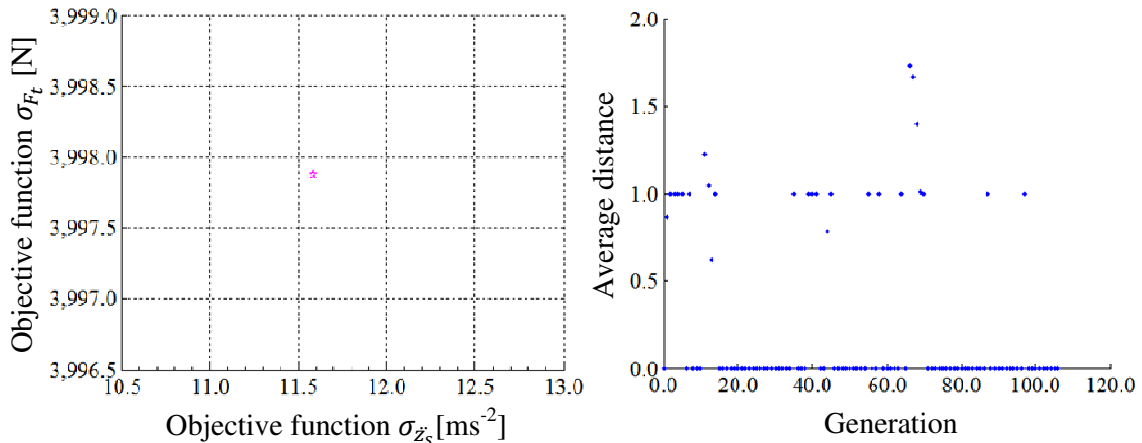


Figure 6.9: Optimization process; a) Single point between two objective functions, and b) average distance between individuals as a function of generation

The percentage of generation which met the design criteria (10.7% of 100%) is shown in Figure 6.10. The optimal design values for five suspension design parameters are consistently near their lower limit, except for the sprung mass which is near to the upper limit. These optimized design variables provide a “soft suspension performance” regarding driving safety, thus ensuring suitable forces to keep the tire in contact with the ground’s surface, whilst on other hand providing better driving comfort.

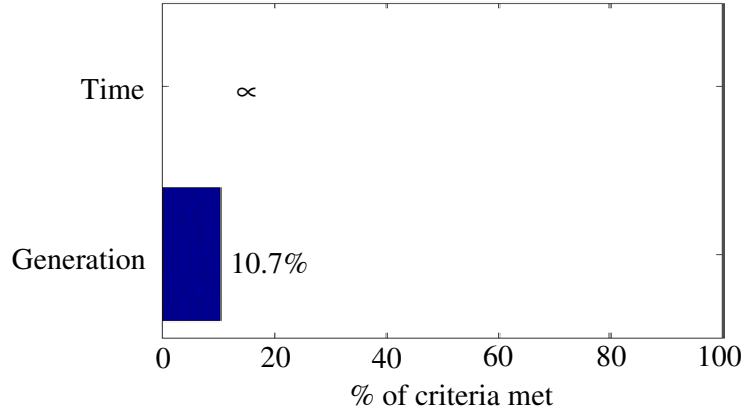


Figure 6.10: Percentage of generation as a function of criteria met over the fourth runs

Figure 6.11 introduces the initial and optimal design variables substituted into objective functions regarding the standard deviation of the vehicle’s body acceleration - $\sigma_{\ddot{z}_s}$, and dynamic tire forces - σ_{F_t} as a function of the vehicle velocity. It can be observed that the reduction of the vehicle’s body acceleration is 50.79%, whilst for the dynamic tire forces it is 53.01%, compared to the initial design of the passive linear suspension system, respectively.

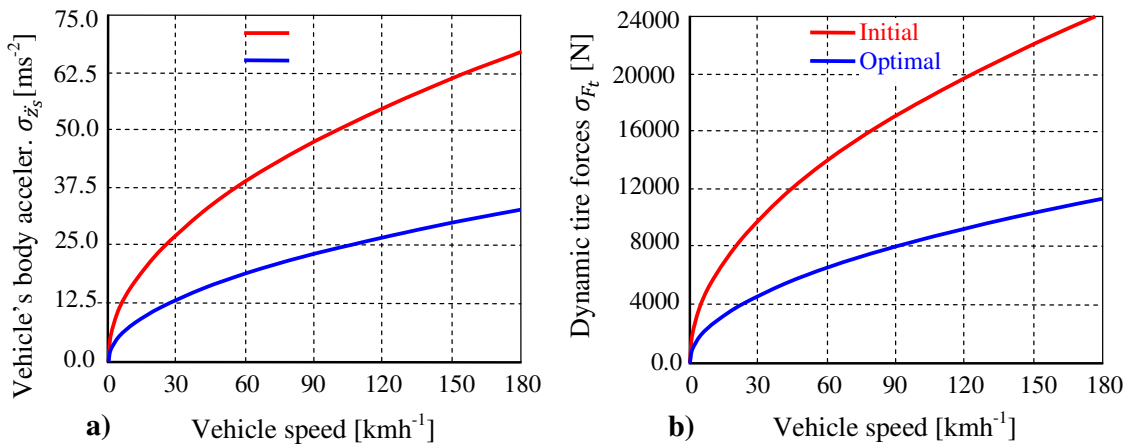


Figure 6.11: Initial and optimal values for the objective functions, as functions of vehicle speed; a) Vehicle’s body acceleration - $\sigma_{\ddot{z}_s}$, and b) Dynamic tire forces - σ_{F_t}

6.4.2 Optimization of the design parameters for the active and semi-active non-linear suspension systems

The stochastic parametric optimization method is applied to ensure the optimal active damping force. This method is based on non-linear programming, by using the Hooke-Jeeves method. The optimization procedures are carried out in this order:

- definition of the input data and limit values of the design variables,
- definition of the objective function,
- simulation of the ground excitation, and
- simulations of the different equations of motion.

A flowchart diagram of the optimization process is shown in Figure 6.12. Simulations of the differential equations of motion are performed by equations (6.17) and (6.18), and the vehicle's suspension parameters tabulated in Table 6.4, Pajaziti [23], Lajqi and Pehan [2].

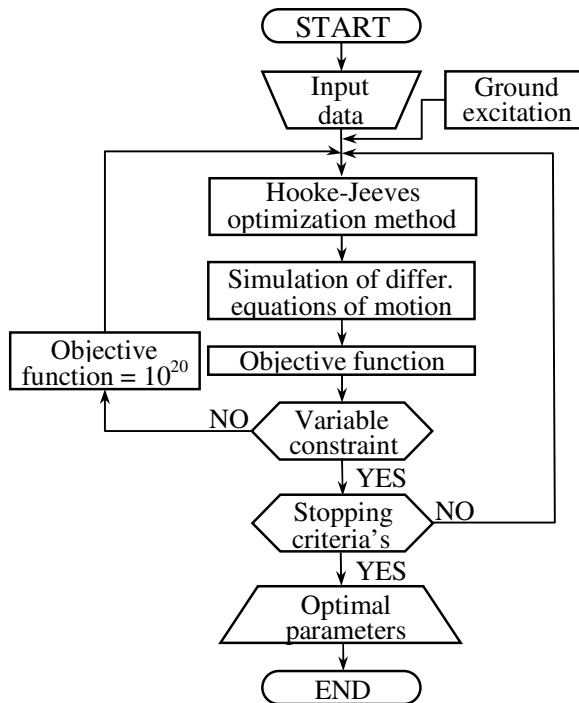


Figure 6.12: Flowchart diagram for optimization design variables for damping force

The objective function that enables minimization of the vertical vehicle's acceleration regarding the sprung and un-sprung masses is written as follows:

$$\min f(x) = \ddot{z}_s^2 + \alpha_1 \cdot \ddot{z}_u^2, \quad (6.29)$$

where $\alpha_1=5$ is the weight coefficient that describes the influence ranking of the corresponding ground excitation (equation (6.23)) on the objective function “f(x)”.

Table 6.4: Suspension parameters used for optimization of the active damping-force

Suspension parameters	Symbol	Unit	Value
Sprung mass	m_s	[kg]	295
Un-sprung mass	m_u	[kg]	35
Shock absorber non-linear damping coefficient	c_{sh1}	[Nsm ⁻¹]	3482
Shock absorber non-linear square damping coefficient	c_{sh2}	[Ns ² m ⁻²]	580
Spring stiffness non-linear coefficient	k_{s1}	[Nm ⁻¹]	15302
Spring stiffness non-linear square coefficient	k_{s2}	[Nm ⁻²]	2728
Tire stiffness non-linear coefficient	k_{t1}	[Nm ⁻¹]	60063
Tire stiffness non-linear square coefficient	k_{t2}	[Nm ⁻²]	42509
Tire stiffness non-linear cube coefficient	k_{t3}	[Nm ⁻³]	22875

The design variables' limits are, Pajaziti [67], Lajqi and Pehan [72]:

$$\begin{aligned} 0.0 \text{ Ns/m} &\leq b_s \leq 5000 \text{ Ns/m}, \\ 0.0 \text{ Ns/m} &\leq b_u \leq 2800 \text{ Ns/m}. \end{aligned} \quad (6.30)$$

The optimization procedure starts by employing three initial values of the design variables. The optimal values are reached when the difference between the two adjacent values of the objective function reaches 10^{-9} . Table 6.5 gives the initial and optimal design variables. The best results for active damping force F_a regarding *driving comfort* and *driving safety* were achieved by the 2nd iteration process and are $b_s = 841 \text{ Nsm}^{-1}$ and $b_u = 2512 \text{ Nsm}^{-1}$.

Table 6.5: Initial and optimal design variables for the active damping force

Parameters	1 st option	2 nd option	3 rd option
Initial design variables:			
b_s^* [Nsm ⁻¹]	0.00	2500	5000
b_u^* [Nsm ⁻¹]	0.00	1400	2800
Optimal design variables:			
b_s [Nsm ⁻¹]	1895	841	1198
b_u [Nsm ⁻¹]	2181	2512	2607
Objective function: $f(x)$	5.162995814·E-01	4.5684816·E-01	5.04968724·E-01
Number of iteration:	232	221	201

6.5 Simulation of the vehicle's suspension by using MATLAB/Simulink

The flowchart diagram for simulations of the terrain vehicle's suspension behavior is performed in MATLAB/Simulink environments, Figure 6.13 and Figure 6.14. Figure 6.13 shows a flowchart diagram for the initial and optimal design parameters for the passive linear suspension system. Figure 6.14 present a flowchart diagram for passive, active, and semi-active non-linear suspension systems.

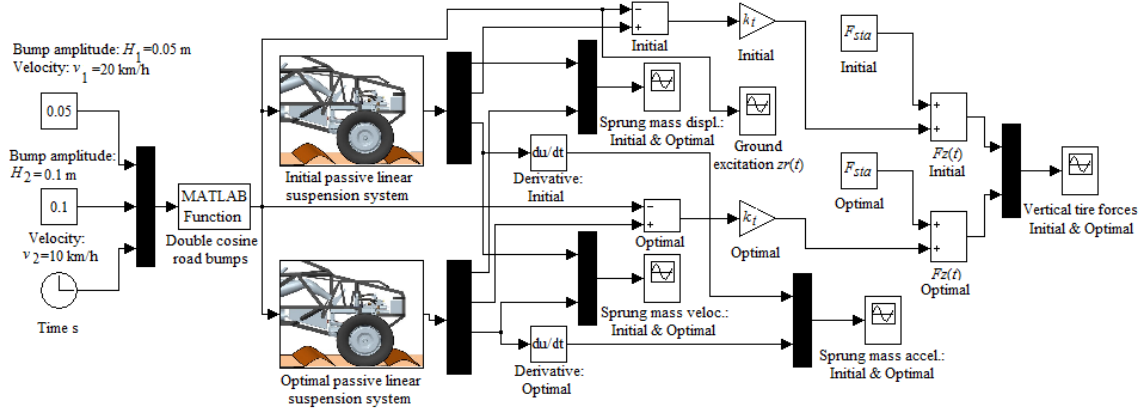


Figure 6.13: Flowchart diagram for simulation ground excitation, the vehicle's body accelerations, velocities, displacements, and tire forces as functions of time for initial and optimal design parameters of the passive linear suspension system

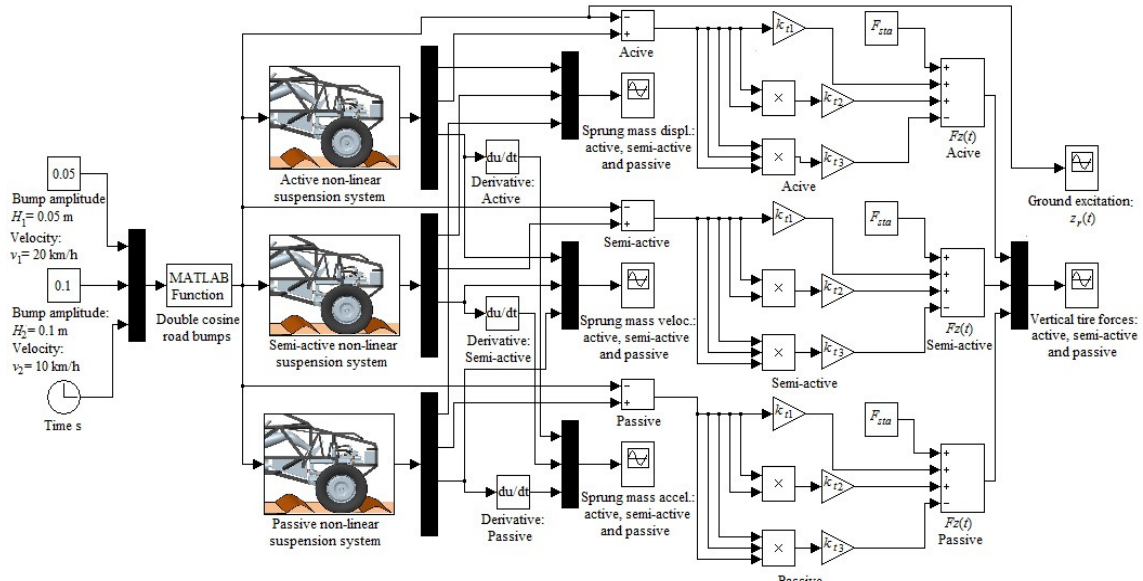


Figure 6.14: Flowchart diagram for simulation ground excitation, vehicle's body accelerations, velocities, displacements, and vertical tire forces as functions of time for non-linear active, semi-active, and passive suspension systems

These flowchart diagrams simulate the vehicle's accelerations, velocities, displacements, and forces powered by ground excitation, depending on time. The excitation is represented by repeated cosine road bumps. The driving comfort is represented by the vehicle's body acceleration (Figures 6.16 and 6.20), Mastinu et al. [46], Lajqi et al. [75], Popp and Schiehlen [76], where the greater values are undesirable. The driving safety relates to the vertical tire forces acting between the ground surface and the tire (Figures 6.19 and Figures 6.23), where it is necessary to be as stable as possible, Belingardi and Demic [69]. If

the vertical tire forces oscillate too much then the contact between the tire and ground surface will be weak. The vertical tire forces are strictly related to *active safety*, Mastinu et al. [46].

The linear $F_{z-l}(t)$ and non-linear $F_{z-n}(t)$ vertical tire forces are composed from static F_{sta} and linear $F_{dyn-l}(t)$, and non-linear $F_{dyn-n}(t)$ dynamic ones, given by the following expression:

$$\begin{aligned} F_{z-l}(t) &= F_{sta} + F_{dyn-l}(t) = g \cdot (m_s + m_u) + k_t \cdot [z_u(t) - z_r(t)], \\ F_{z-n}(t) &= F_{sta} + F_{dyn-n}(t) = g \cdot (m_s + m_u) + k_{t1} \cdot [z_u(t) - z_r(t)] + k_{t2} \cdot [z_u(t) - z_r(t)]^2 \dots \\ &\quad - k_{t3} \cdot [z_u(t) - z_r(t)]^3. \end{aligned} \quad (6.31)$$

In order to describe the vehicle's behavior as it runs over road bumps, the ground excitation is simulated by equation (6.22) and the data given in Table 6.1. The vehicle passed over the first bump at a speed of 20 kmh^{-1} and the second bump at a lower speed of 10 kmh^{-1} .

Figure 6.15 shows the ground excitation derived from a cosine function with amplitudes $H_1 = 0.05 \text{ m}$ and $H_2 = 0.1 \text{ m}$ for two different vehicle speeds ($v_1 = 20$ and $v_2 = 10 \text{ kmh}^{-1}$).

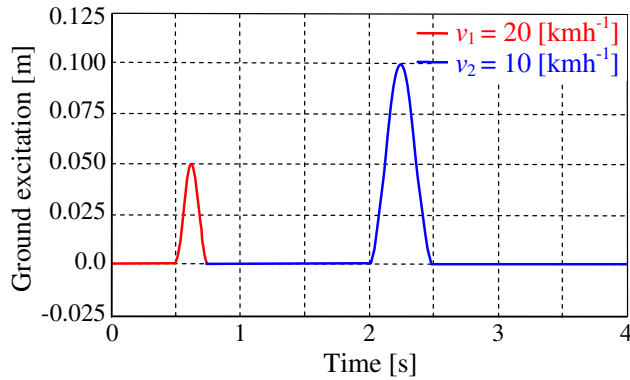


Figure 6.15: Ground excitation as a function of time

Figures 6.16, 6.17 and 6.18 shows the accelerations, velocities, and displacements of the vehicle's body, depending on time caused from double cosine road bumps for initial and optimal design parameters of the passive linear suspension systems.

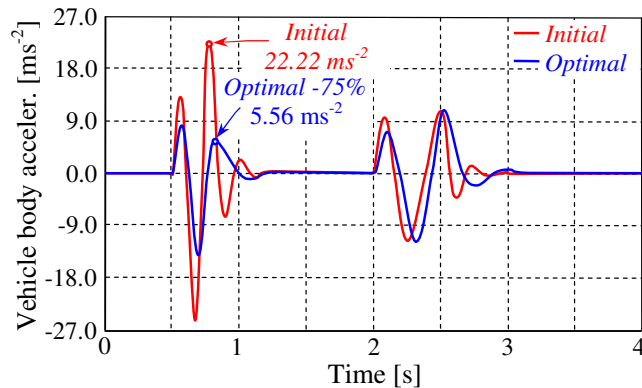


Figure 6.16: Vehicle's body accelerations as a function of time for passive linear system

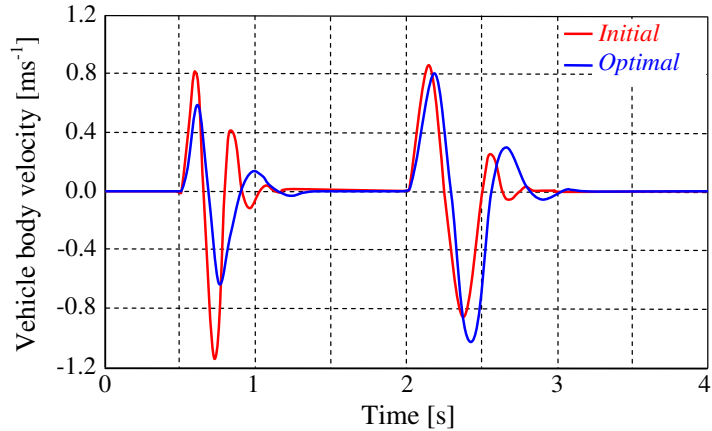


Figure 6.17: Vehicle's body velocities as a function of time for passive linear system

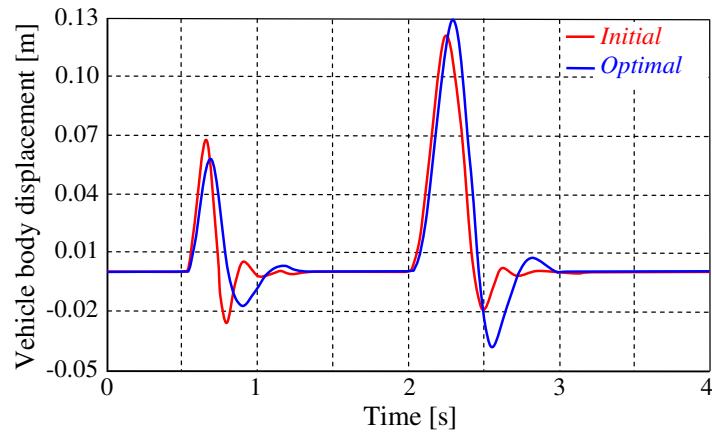


Figure 6.18: Vehicle's body displacements as a function of time for passive linear system

Figure 6.19 shows the vertical tire forces depending on time, for the initial and optimal design parameters for passive linear suspension systems.

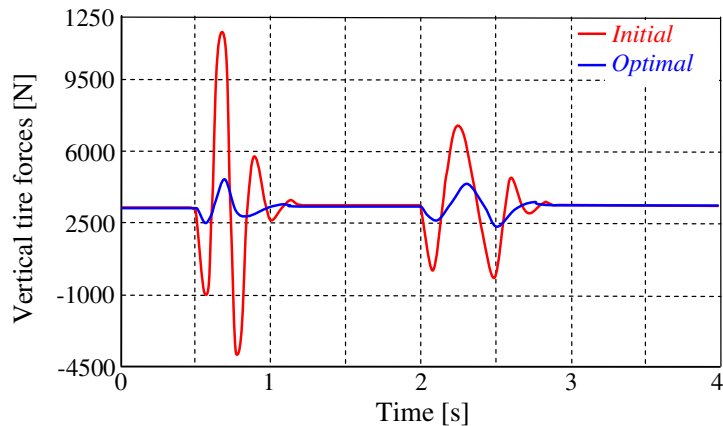


Figure 6.19: Vertical tire forces as a function of time for passive linear system

Figures 6.20, 6.21 and 6.22 show the accelerations, velocities, and displacements of the vehicle's body, depending on time, caused from double cosine road bumps for passive, active, and semi-active non-linear suspension systems.

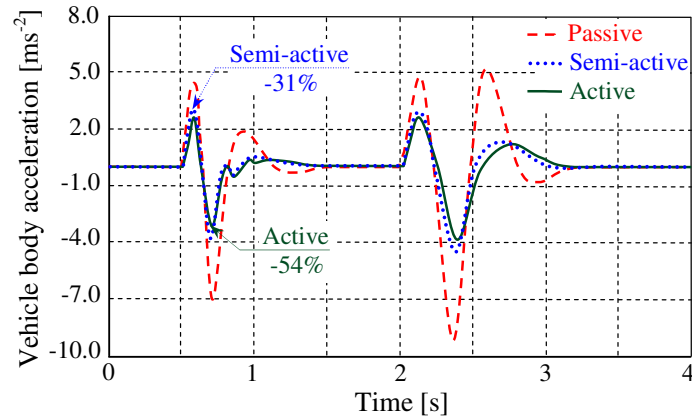


Figure 6.20: Vehicle's body accelerations as a function of time

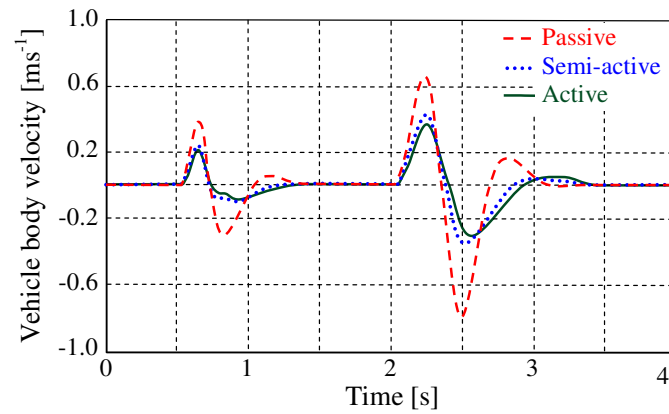


Figure 6.21: Vehicle's body velocities as a function of time

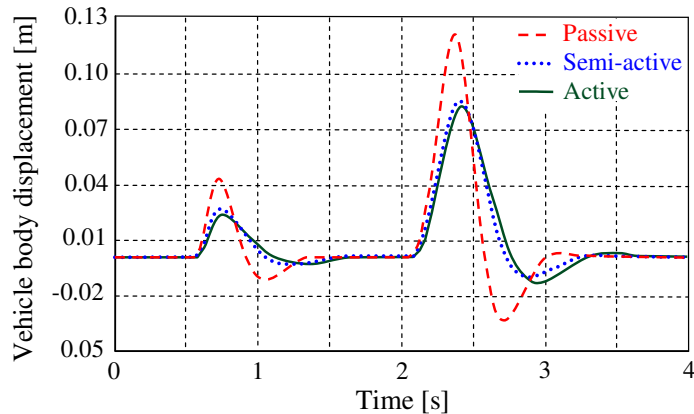


Figure 6.22: Vehicle's body displacements as a function of time

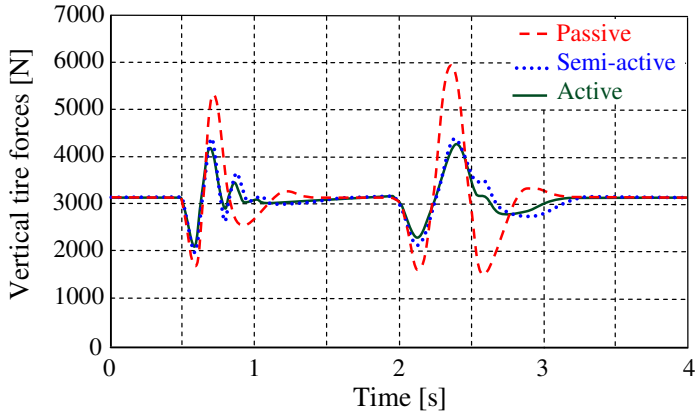


Figure 6.23: Vertical tire forces as a function of time

Figure 6.23 shows the vertical tire forces depending on time, for passive, active, and semi-active non-linear suspension systems.

6.6 Discussion of the results

Evaluation of a terrain vehicle's suspension system was performed by simulation of the double cosine road bumps. The vehicle passed over the first bump at an amplitude of 0.05 m and a speed of 20 kmh^{-1} , and the second bump at an amplitude of 0.1 m and a speed of 10 kmh^{-1} , Figure 6.15. This simplified form of the repeated road bumps with different amplitudes is used for better understanding of the appearances of the vehicle's body accelerations, velocities, displacements, and vertical tire forces for active, semi-active, and passive systems.

Figures 6.16, 6.17 and 6.18 introduce the accelerations, velocities, and displacements of the vehicle's body, as a function of time, for initial and optimal design parameters for passive linear suspension system. The references are for the initial design. When the vehicle passes over the first bump, the values for the vehicle's body: *accelerations* are reduced 37%, 45%, and 75%, *velocities* 28%, 45%, and 68%, and *displacements* 15%, 32% and 49% (depending on the location). The same explanation can also be found when the terrain vehicle passes over the second bump due to lower speed and higher amplitude. Figure 6.19 shows the vertical tire forces as a function of time, for initial and optimal designs of the passive linear suspension system. If the vehicle passes over the first bump, the vertical tire forces at maximal peaks is reduced by 84%, whilst at the second bump by 71% when is compared to the initial ones.

Figure 6.20 shows the vehicle's body accelerations for passive, active, and semi-active non-linear systems. The reference acceleration is the passive one. If the vehicle passes over the first bump the active system reduces it by 40%, 54%, and 81% (depending on the

location). The semi-active system reduces it by 31%, 46%, and 76% (depending on the location). Similar appearances were observed at the second bump, but the speed was lower and the amplitude higher. The same explanation for the second bump can also be found in Figures 6.21, 6.22 and 6.23. Figure 6.21 shows the vehicle's body velocities for passive, active, and semi-active non-linear systems. The reference velocity is the passive one. When passing over the first bump, the active suspension system reduced it by 44% and 81%. The semi-active system reduced it by 36% and 71%. Figure 6.22 shows the vehicle's body displacements for passive, active, and semi-active non-linear systems. The reference displacement is the passive one. When the vehicle passed over the first bump the active system reduced it by 43%. The semi-active system reduced it by 38%. Figure 6.23 shows the vertical tire forces for passive, active, and semi-active non-linear systems. The reference force is the passive one. When passing over the first bump the active system reduced it by 45% and 54%. The semi-active system reduced it by 22% and 49%.

If the terrain vehicle equipped with active or semi-active systems is driven over the road bumps at 10 and 20 km/h, the driving comfort ($\ddot{z}_s < 4 \text{ ms}^{-2}$) and the driving safety ($F_z < \pm 1.4 \text{ g}$), according Kuznestov et al. [81] are as yet within the acceptable zone. Although the passive linear system is optimized by MOGAs and the results are satisfactory compared with the initial design, the performances offered by this system are lower than the active or semi-actives suspension systems. If the terrain vehicle is equipped with a passive linear or non-linear system, the acceleration and dynamic tire forces, according to Kuznestov et al. [81], has exceeded the zone limit and consequence have negative influences on the driving comfort and driving safety.

Finally, it can be concluded that, the active system provides better performance in comparison with the passive system on account of better isolation of the vibration. Due to the damping capability, the semi-active systems were less effective than the active ones, as can be seen from the presented diagrams.

7 DEVELOPMENT OF THE FOUR WHEELS STEERING SYSTEM FOR THE 4x4 TERRAIN VEHICLE

This chapter introduces the development of the four/two wheels steering system intended to be used for 4x4 terrain vehicle. The four wheels steering (4WS) concept comes into consideration when the driver's steering wheel is able to turn both the front and rear wheels of the vehicle during the same steering input. In most cases the 4WS system operates using three modes, such as *counter steer*, *neutral steer*, and *same steer*, Figure 7.1.

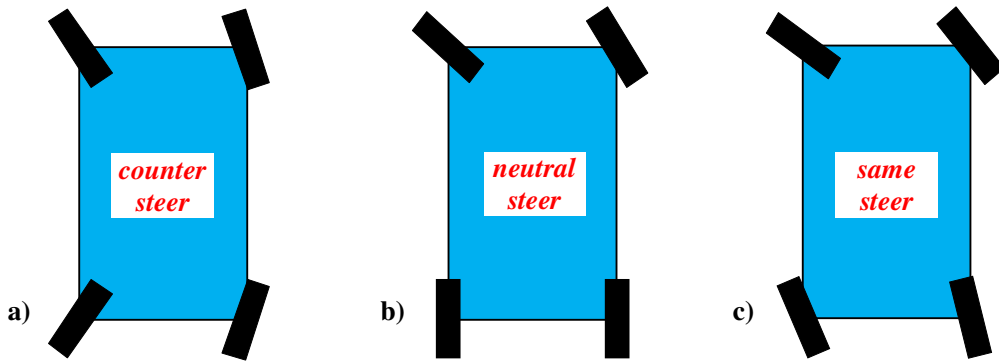


Figure 7.1: Operation modes of the 4WS; a) *counter steer*, b) *neutral steer*, and c) *same steer*

The *counter steer* mode is the case when the rear wheels are turned in the opposite direction to the front wheels. The *neutral steer* mode is a situation when the rear wheels are locked and the vehicle operates as an ordinary vehicle. The *same steer* mode comes into consideration when the rear wheels are turned in the same way as the front ones. The *counter steer* mode of the 4WS system is usually used at low vehicle speed, the *neutral steer* mode for average vehicle speed, whereas the *same steer* mode is for higher vehicle speed, Alter [40]. The main cause that affects the marketing limitations of vehicles with 4WS has been the vehicle's instability. On the one hand, the stability of the vehicle is one of the key issues for driving safety whilst, on the other hand, the requirements given by Council Directive 70/311/ECC and the latest supplement of the Commission Directive 1999/7/ECC regarding the steering system for vehicle's [82] has led the manufacturers of vehicles to limit the applications of 4WS.

The objective of this approach is to develop an effective steering system for 4x4 terrain vehicle, which offers high rates of the maneuverability when cornering, driving safely, and fulfilling the directives described previously. Based on the design task and operational

conditions, the steering mechanism for the terrain vehicle will be designed for two modes. One is to only steer the front wheels - 2WS and the other to steer all four wheels - 4WS, Figures 7.1.a and 7.1.b. The main target will be to design steering mechanisms that provide Ackermann steering geometry exactly. In order to actually utilize these types of steering system within terrain vehicles it is necessary to be clear that these systems do have some weaknesses especially where there is a question of stability. Main weakness has been shown to be bump steering as the result of significant vertical wheel motion. On the other hand, a terrain vehicle requires the vertical motion of its wheels to be very extensive due to vehicle rollover risk. Is it necessary to design a totally new concept? This approach is necessary in order to find a unique solution for the steering mechanism that exactly ensures the Ackermann conditions for the two modes. An adequate solution can be assumed by designing several pairs of gear transmissions such as bevel, planetary, and non-circular gears. Furthermore, when developing a 4WS system it must be in relation to the vehicle's kinematic behavior. Therefore, the following derives kinematic relations for two/four wheels steering system.

7.1 Kinematics of the two/four wheel steering system

For all vehicles to maneuver using it, it is necessary to have a steering mechanism in order to turn the steered wheels. The main task of this mechanism is to steer the vehicle and to follow an advance prescribed trajectory, Pehan et al. [1]. This should be done easily and safely by steering either the front or both the front and rear wheels. The kinematic behavior of the steering mechanism systems for 2WS and 4WS are given in the follow for a concrete terrain vehicle. Performances provided by terrain vehicles with 4WS will be evaluated by comparisons with the 2WS system.

7.1.1 Kinematic of the two-wheel steering system

The kinematic behavior of the 2WS system is determined when the rear wheels are not steered and the sideslip angle of the wheels is assumed to be negligible. This comes into consideration when the vehicle moves slowly, Spentzas et al. [41].

In order for all the wheels to turn freely on a curved road, the normal lines to the centers of each wheel must intersect at a common point, known as the vehicle turning center O. This is known as *Ackermann steering geometry*. Determining the correct steering geometry was a major problem in the early days the vehicles' manufacturers. Figure 7.2 illustrates the case when the terrain vehicle turns towards the left side using the 2WS system. The front steering angles for the left and right wheels are derived from the triangles ΔOAC and ΔOBD , such as:

$$\tan \delta_L = \frac{2 \cdot l}{2 \cdot R_{2WS} - w}, \quad (7.1)$$

$$\tan \delta_R = \frac{2 \cdot l}{2 \cdot R_{2WS} + w}, \quad (7.2)$$

where δ_L and δ_R denote the front steering angles for the left and right wheels, respectively.

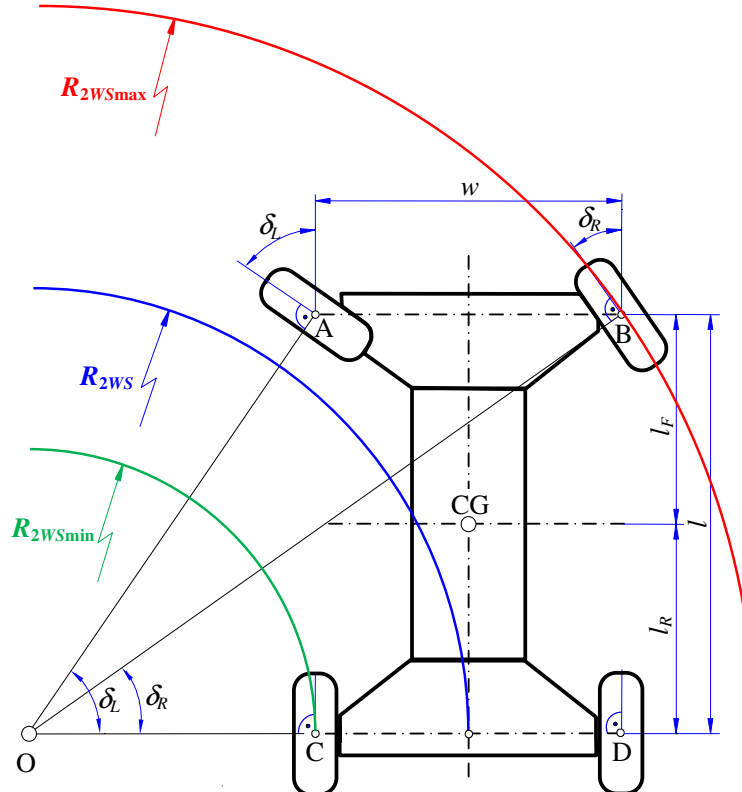


Figure 7.2: Turning of the terrain vehicle towards the left side using the 2WS system

The turning radii for the vehicle with 2WS presented in Figure 7.2 are determined by the following expressions:

$$R_{2WS} = \frac{l}{\tan \delta_L} + \frac{w}{2} = \frac{l}{\tan \delta_R} - \frac{w}{2}, \quad (7.3)$$

$$R_{2WS\min} = \frac{l}{\tan \delta_L} = \frac{a+b}{\tan \delta_L}, \quad (7.4)$$

$$R_{2WS\max} = \frac{l}{\sin \delta_R} = \frac{a+b}{\sin \delta_R}, \quad (7.5)$$

where R_{2WS} is the turning radius at the center of the rear axle, whilst $R_{2WS\min}$ and $R_{2WS\max}$ denote the minimal and maximal turning radius for the vehicle with 2WS, respectively.

After some mathematical arrangement in equation (7.3) it gets the *Ackermann steering condition* between the left and right wheel δ_L and δ_R , presented by the following expression:

$$\cot \delta_R - \cot \delta_L = \frac{w}{l}. \quad (7.6)$$

Equation (7.6) presents *Ackermann's steering geometry* or *Ackermann steering condition*. The *Ackermann steering geometry* is valid when the vehicle moves slowly and the sideslip angle is negligible.

7.1.2 Kinematic of the four-wheel steering system

The greater maneuverability of the terrain vehicle is one of the important issues whether it operates over the roughest terrain or in urban areas. A higher rate of the vehicle maneuverability is obtained when all the wheels (4WS) turn around their kingpin axes and the rear wheels are go in opposite directions to the front ones. Figure 7.3 presents situations when the front and rear wheels of the terrain vehicle go in opposite directions, known as *counter steer mode* that produces a higher maneuverability rate.

In order to determine expressions for estimating a vehicle's turning radius with four wheels steering (R_{4WS}), it is necessary to start by the assumption that the sideslip angle is zero. If the vehicle moves up to a 50 km/h or lower speed, the sideslip angle of the wheels may be negligible, Alter [40], Spentzas et al. [41].

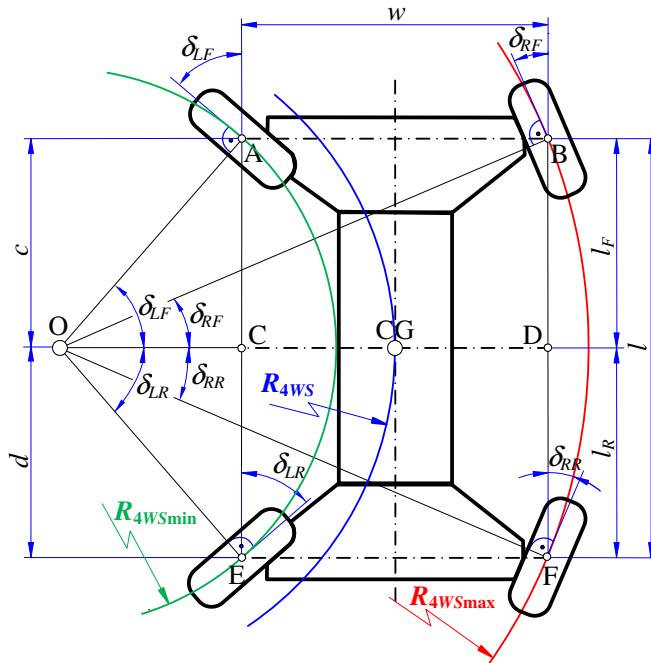


Figure 7.3: Turning of the terrain vehicle towards the left side using the 4WS system

In order to ensure that all the wheels of the vehicle can be turned freely on a curved road and fulfill the Ackermann steering geometry, the perpendicular lines of the centers of each wheel must intersect at a common point. The intersection point O is known as *the vehicle turning center*. The front steering angles for the left and right wheels δ_{LF} and δ_{RF} are derived from the triangles ΔOAC & ΔOBD . The rear steering angles for the left and right wheels δ_{LR} and δ_{RR} are determined from triangles ΔOCE & ΔODF . The expressions for determining the steering angles of the wheels are shown in Figure 7.3, and written as follow:

$$\tan \delta_{LF} = \frac{2 \cdot c}{2 \cdot R_{4WS} - w}, \quad (7.7)$$

$$\tan \delta_{RF} = \frac{2 \cdot c}{2 \cdot R_{4WS} + w}, \quad (7.8)$$

$$\tan \delta_{LR} = \frac{2 \cdot d}{2 \cdot R_{4WS} - w}, \quad (7.9)$$

$$\tan \delta_{RR} = \frac{2 \cdot d}{2 \cdot R_{4WS} + w}, \quad (7.10)$$

where δ_{LF} and δ_{RF} denote the front steering angles for the left and right wheels, and δ_{LR} and δ_{RR} the termed rear steering angles for the left and right wheels, respectively. The parameters c and d indicate the longitudinal distances between the turning centers of the front and rear wheels (point A or B and E or F) and the vehicle turning center O.

The turning radii for the vehicle with the 4WS system shown in Figure 7.3 are written by the following expressions:

$$R_{4WS} = \frac{c}{\tan \delta_{LF}} + \frac{w}{2} = \frac{c}{\tan \delta_{RF}} - \frac{w}{2}, \text{ or} \quad (7.11)$$

$$R_{4WS} = \frac{d}{\tan \delta_{LR}} + \frac{w}{2} = \frac{d}{\tan \delta_{RR}} - \frac{w}{2}, \quad (7.12)$$

$$R_{4WS \min} = \frac{c}{\sin \delta_{LF}} = \frac{d}{\sin \delta_{LR}}, \quad (7.13)$$

$$R_{4WS \max} = \frac{c}{\sin \delta_{RF}} = \frac{d}{\sin \delta_{RR}}, \quad (7.14)$$

where R_{4WS} is the turning radius at the center of gravity of the vehicle, whilst $R_{4WS\min}$ & $R_{4WS\max}$ denote the minimal and maximal turning radius for the vehicle with 4WS, respectively.

After several mathematical operations in equations (7.11) and (7.12), the kinematic condition between the left and right wheels on the front and rear axles was arrived at, written as follows:

$$\cot \delta_{RF} - \cot \delta_{LF} = \frac{w}{c}, \quad (7.15)$$

$$\cot \delta_{RR} - \cot \delta_{LR} = \frac{w}{d}. \quad (7.16)$$

Figure 7.3 indicates that, the longitudinal distances $c + d$ is given as follow:

$$c + d = l. \quad (7.17)$$

By combining equations (7.15) and (7.16), and substituting equation (7.17), the following expression is obtained:

$$\frac{(\cot \delta_{RR} - \cot \delta_{LR}) + (\cot \delta_{RF} - \cot \delta_{LF})}{(\cot \delta_{RF} - \cot \delta_{LF}) \cdot (\cot \delta_{RR} - \cot \delta_{LR})} = \frac{l}{w}. \quad (7.18)$$

Equations (7.18) present the kinematic relation between the steering angles of the front and rear wheels for a *counter steer* mode.

7.2 Steering system for a terrain vehicle

Terrain vehicle is designed to operate on flat roads as well as rough terrains, on the one hand, whilst on the other hand the main characteristics of terrain vehicles is their very extensive wheel movements due to the risk from rollover. For that reason it is required to have robust and effective steering system which provides as much as possible, maneuverability and suitable stability. In order to fulfill the predefined requirements, the steering system for a terrain vehicle is designed to work with two modes. The first mode is the 2WS introduced in Figure 7.2, whereas the second mode is 4WS, as represented in Figure 7.3.

7.2.1 Determining the steering wheel angles for the terrain vehicle in the 2WS mode

In order to fulfill the requirements given by the check list in Table 1.1, it is necessary to determine the maximal turning steering angles of the left and right wheels. These steering angles are determined by using equations (7.1) and (7.2), where it is written in matrix form:

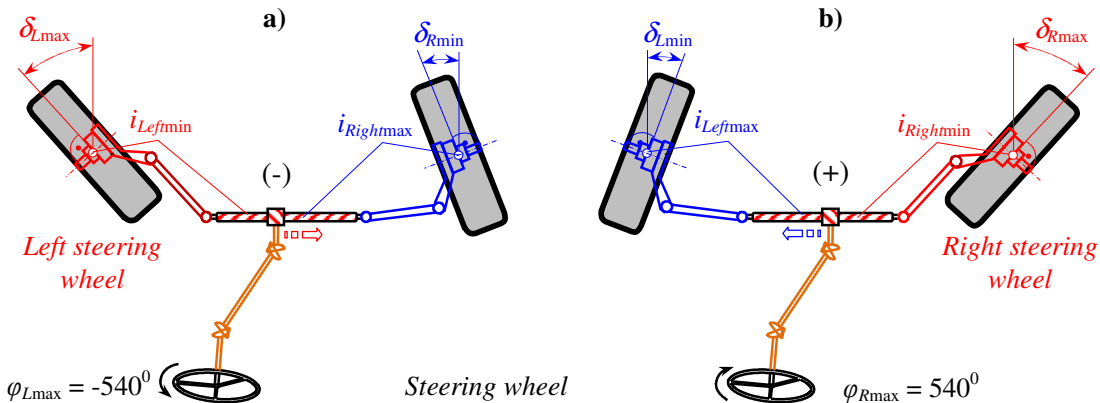
$$\begin{bmatrix} \delta_L \\ \delta_R \end{bmatrix} = \begin{bmatrix} 1 & 0 \\ 0 & 1 \end{bmatrix}^{-1} \cdot \begin{cases} a \tan \frac{2 \cdot l}{2 \cdot R_{2ws} - w} \\ a \tan \frac{2 \cdot l}{2 \cdot R_{2ws} + w} \end{cases}. \quad (7.19)$$

By substituting the geometric dimensions given in Table 1.1 into the equations (7.3) to (7.5) and (7.19) the results for the geometric characteristic of the steering system with 2WS are obtained, as shown in Table 7.1.

Table 7.1: The geometric characteristics of the steering system with 2WS

Parameters →	Turning radius for 2WS, [m]			Steering angles for 2WS, [°]			
	R_{2WSmin}	R_{2WS}	R_{2WSmax}	δ_{Lmax}	δ_{Rmin}	δ_{Lmin}	δ_{Rmax}
Values →	2.5	3.55	5.39	-48.24	-31.33	31.33	48.24

Figure 7.4.a presents the case where the front wheel of the vehicle turns towards the left side, and in Figure 7.4.b case when it turns towards the right side. The maximal turning radius on the left or right side from a straight-ahead position is ensured when the driver turns the steering wheel by $\varphi_{max} = \pm 540^0$ or 1.5 [rot] towards the left or right, Figure 7.4.

**Figure 7.4:** Turning of the vehicle with 2WS; a) on the left side, and b) on the right side

The conventional sign used for steering angles (δ_L and δ_R) will be negative (-) if the front wheels turn towards the left side, otherwise positive (+). The maximal steering angles of the left wheel when the vehicle is turning towards the left side is $\delta_{Lmax} = -48.24^0$, whilst the right wheel has minimal values $\delta_{Rmin} = -31.33^0$. Similar appearances were ensured when the vehicle turns towards the right side and the steering angles are $\delta_{Lmin} = 31.33^0$ & $\delta_{Rmax} = 48.24^0$.

According to the Ackermann steering geometry, the steering gear ratios are different for the left and right wheels. The steering gear ratio i is the steering wheel angle φ divided by the front steering angles of the wheels, written as follows:

$$i_{Left\ min} = i_{Right\ min} = \frac{\varphi_{Lmax}}{\delta_{Lmax}} = \frac{\varphi_{Rmax}}{\delta_{Rmax}} = 11.20, \quad (7.20)$$

$$i_{Left\ max} = i_{Right\ max} = \frac{\varphi_{Rmax}}{\delta_{Lmin}} = \frac{\varphi_{Lmax}}{\delta_{Rmin}} = 17.24. \quad (7.21)$$

Equations (7.20) and (7.21) show that the steering mechanism, in order to fulfill the Ackermann steering conditions, should be worked out as multiplication/reduction.

Figure 7.5 illustrates the Ackermann steering condition for the vehicle with 2WS, as computed by equation (7.6). The obtained results for the front steering angle of the right wheel δ_R when the vehicle turns towards the left or right sides are in dependence from the steering angle of the left wheel δ_L and on the function of the steering wheel angle φ . Figure 7.5 shows that the front steering angle of the right wheel δ_R displays non-linear behavior compared with the input linear steering angle of the left wheel δ_L .

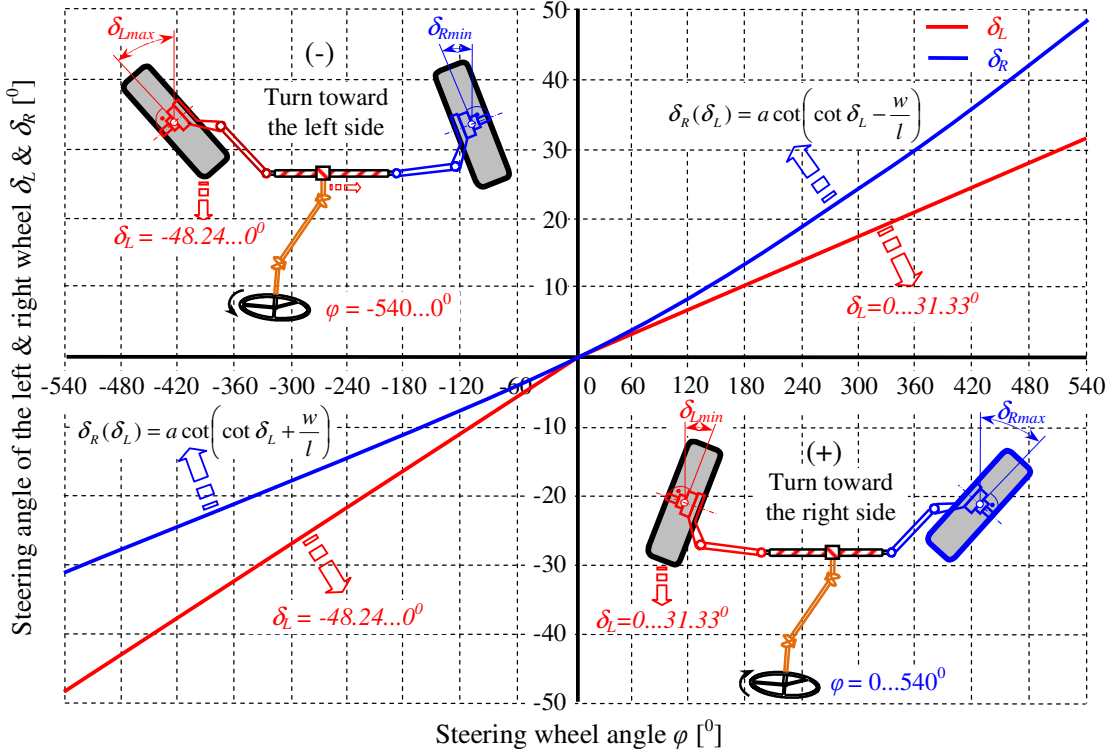


Figure 7.5: Steering angles for the front wheels as a function of the steering wheel angle φ

7.2.2 Determining of the steering wheel angles for the terrain vehicle in the 4WS mode

The maximal turning steering angles for the left and right wheels on the front and rear axles (δ_{LF} , δ_{RF} , δ_{LR} and δ_{RR}), as shown in Figure 7.3, are determined by employing equations (7.7) to (7.10), where in matrix form they are written as follows:

$$\begin{bmatrix} \delta_{LF} \\ \delta_{RF} \\ \delta_{LR} \\ \delta_{RR} \end{bmatrix} = \begin{bmatrix} 1 & 0 & 0 & 0 \\ 0 & 1 & 0 & 0 \\ 0 & 0 & 1 & 0 \\ 0 & 0 & 0 & 1 \end{bmatrix}^{-1} \cdot \begin{cases} a \tan\left(\frac{2 \cdot c}{2 \cdot R_{4ws} - w}\right) \\ a \tan\left(\frac{2 \cdot c}{2 \cdot R_{4ws} + w}\right) \\ a \tan\left(\frac{2 \cdot d}{2 \cdot R_{4ws} - w}\right) \\ a \tan\left(\frac{2 \cdot d}{2 \cdot R_{4ws} + w}\right) \end{cases}. \quad (7.22)$$

The decisional characteristics of the steering system with 4WS are determined by the substituting the geometric dimensions given in Table 1.1 into equations (7.11) to (7.14) and (7.22). The main geometric characteristic of the 4WS system is presented in Table 7.2.

Table 7.2: The main geometric characteristics of the steering system with 4WS

Parameters →	Turning radius of 4WS, [m]			Steering angles for 4WS, [$^{\circ}$]				
	R_{4WSmin}	R_{4WS}	R_{4WSmax}	δ_{LF}	δ_{RF}	δ_{LR}	δ_{RR}	
Values →	2.5	3.13	4.4	L R	-34 18.5	-18.5 34	34 -18.5	18.5 -34

Figure 7.6.a introduces steering angles of the wheels when vehicle is turning towards the left side, while Figure 7.6.b when vehicle is turning towards the right side.

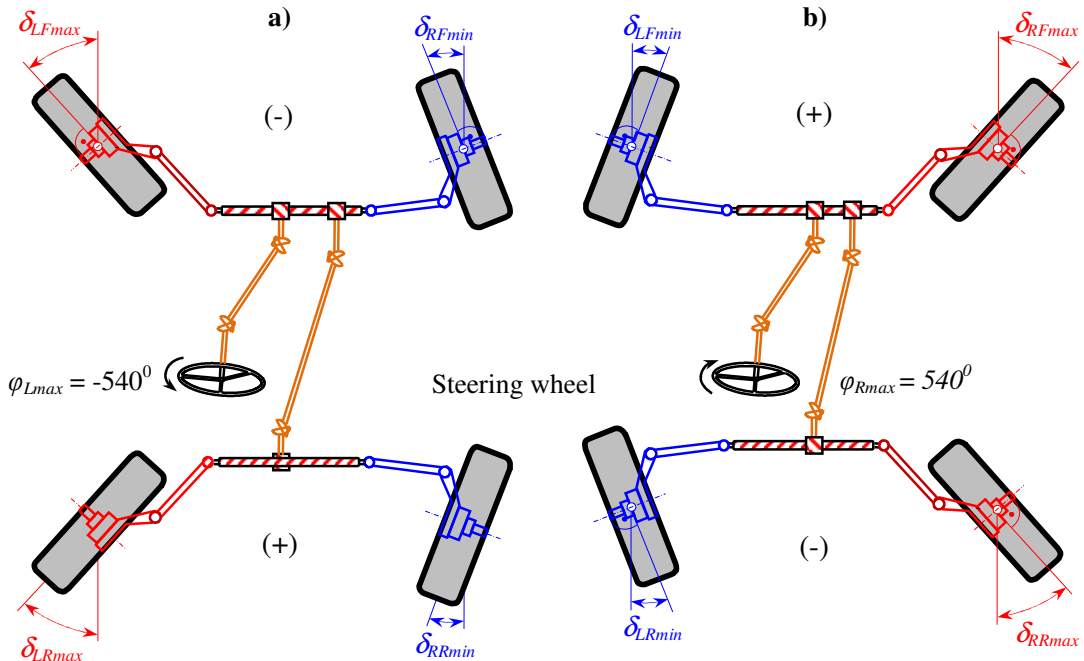


Figure 7.6: Turning of the 4WS system; a) towards the left side, and b) towards the right side

When the vehicle is turning towards the left side, the maximal steering angles of the left and right wheels for the front axle are $\delta_{LFmax} = -34^{\circ}$ and $\delta_{RFmin} = -18.5^{\circ}$, whilst for the rear axle they are $\delta_{LRmax} = 34^{\circ}$ and $\delta_{RRmin} = 18.5^{\circ}$. Similar appearances are ensured when the vehicle turns towards the right side and the steering angles are $\delta_{LFmin} = 18.5^{\circ}$, $\delta_{RFmax} = 34^{\circ}$, $\delta_{LRmin} = -18.5^{\circ}$ and $\delta_{RRmax} = -34^{\circ}$, Figure 7.6. The steering gear ratios i for the vehicle with 4WS are determined by the following expressions:

$$i_{F\min} = i_{R\min} = \frac{\varphi_{L\max}}{\delta_{LF\max}} = \frac{\varphi_{R\max}}{\delta_{RF\max}} = \frac{\varphi_{L\max}}{\delta_{LR\max}} = \frac{\varphi_{R\max}}{\delta_{RR\max}} = 15.88, \quad (7.23)$$

$$i_{F\max} = i_{R\max} = \frac{\varphi_{R\max}}{\delta_{LF\min}} = \frac{\varphi_{L\max}}{\delta_{RF\min}} = \frac{\varphi_{R\max}}{\delta_{LR\min}} = \frac{\varphi_{L\max}}{\delta_{RR\min}} = 29.19. \quad (7.24)$$

From equations (7.23) and (7.24) it is shown that, the steering mechanism in order to fulfill Ackermann steering condition should be worked out as multiplication/reduction.

Figure 7.7 illustrates the Ackermann steering condition for the vehicle with 4WS computed by equations (7.15) and (7.16). The obtained results of the steering angles for the front and rear right wheels δ_{RF} and δ_{RR} when the vehicle turns towards the left or right sides are dependent on the input steering angles of the front and rear left wheels δ_{LF} and δ_{FR} as a function of the steering wheel angle φ . From Figure 7.7, it can be observed that the steering angles for right wheels of the front and rear axles have non-linear behavior compared with the input linear steering angles for the left wheels on the front and rear axles.

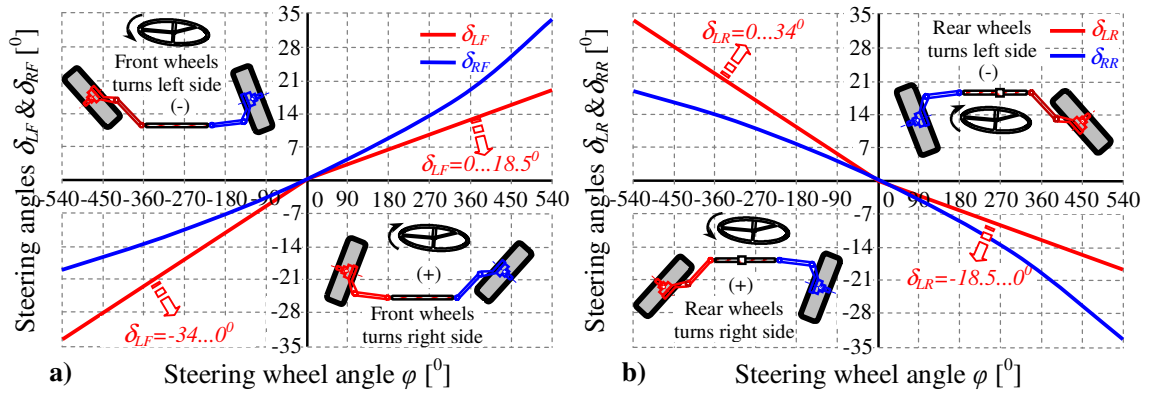


Figure 7.7: Steering angles for the front and rear wheels as a function of the steering wheel angle φ when vehicle with 4WS turns; a) towards the left side, and b) towards the right side

Figure 7.8 presents the cases when the terrain vehicle turns towards the left side and the steering systems operate as 2WS and 4WS modes. The vehicle turning radius is minimal when the steering wheel is rotated by $\varphi_{max} = -540^\circ$ and the vehicle provides higher maneuverability. When the terrain vehicle operates in 4WS mode, the turning radius is reduced by 34% compared with 2WS mode. This higher maneuverability only comes into consideration when the vehicle is moving at a slower speed.

Figure 7.9 shows the maximal vehicle turning radius R_{2WSmax} and R_{4WSmax} for both modes 2WS and 4WS as a function of the steering wheel angle φ . From the curves it can be observed that the vehicle's turning radius has smaller values when all the wheels are steered (4WS) thus ensuring a higher rate of maneuverability by the terrain vehicle. When the vehicle moves at a higher speed, the rear steered wheels are locked and steering system is in 2WS mode in order for the vehicle to provide better stability due to the increasing turning radius.

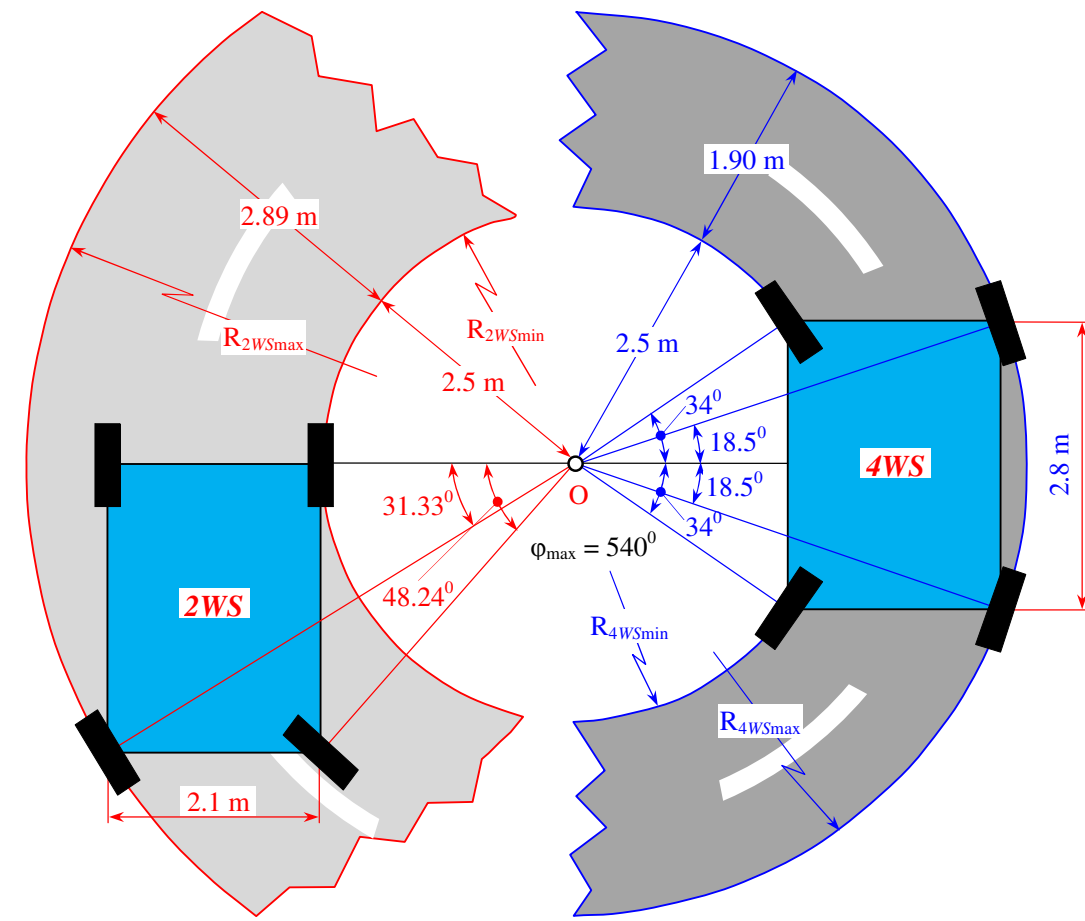


Figure 7.8: Terrain vehicle's turning radius when operates in the 2WS and 4WS modes

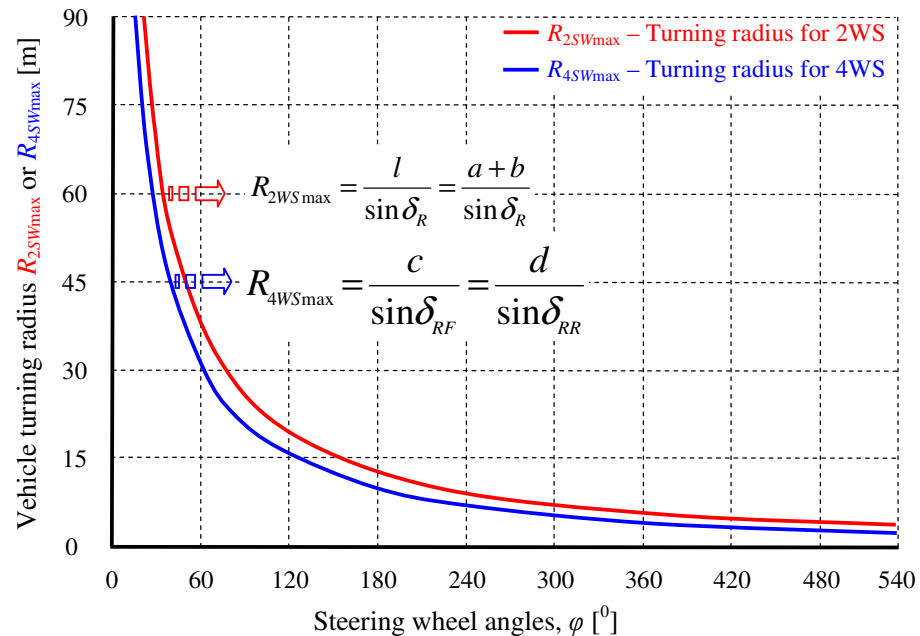


Figure 7.9: Vehicle turning radius as a function of steering wheel angle φ for 2WS and 4WS

7.3 Design of the steering mechanism for a terrain vehicle

There are devised many different designs for the steering mechanism. Even though they have the same basic components, each vehicle has some requirements that differ from others. For this reason a steering mechanism must be modeled and designed for each vehicle.

Each type vehicle has slightly different dimensions (length, width, etc.), different suspension systems and so on, which make it necessary to design new steering mechanisms. Even small changes in the dimension of the vehicles can drastically alter the steering performance, Leishman [83].

There are several types of steering mechanism used on road vehicles such as rack and pinion, lever arm, drag link, and the multi-link, Rill [4] and Jazar [9], Figure 7.10. Each of them has some advantages and disadvantages. Obviously the rack and pinion steering mechanism is the more widely used as a steering system within passenger vehicles, Figure 7.10.a. It is simple in design, has higher mechanical efficiency and lower price compared with other systems. The lever arm steering mechanism is used on tracks with large wheelbases and an independent suspension system at the front axle, Figure 7.10.b. The drag link steering mechanisms are usually used for trucks and buses with a front solid axle. By using such a steering mechanism the steering command is sent to only one wheel and connects the other one by a drag link, as shown in Figure 7.10.c.

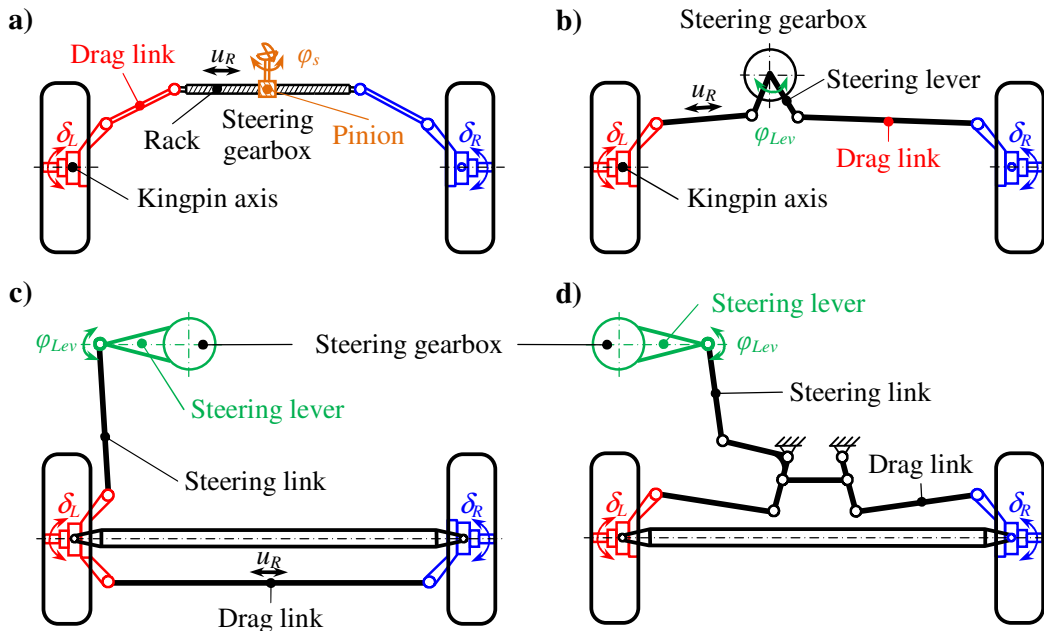


Figure 7.10: Road vehicle steering mechanism; a) rack and pinion, b) lever arm, c) drag link and d) multi-link

The multi-link steering mechanisms are used for busses and big trucks where it is necessary to have large steering angles at the front wheels in order to achieve higher maneuvering, Figure 7.10.d. Practically, it is impossible to build a simple steering mechanism in order to provide exactly the Ackermann steering condition. However, various steering mechanisms are used in practice, more or less satisfying the Ackermann steering conditions. Let us model one of the better known steering mechanisms which are used in almost all types of road vehicles, known as the trapezoidal steering mechanism.

7.3.1 Design of the trapezoid steering mechanism for front wheels steering

The Ackermann steering condition could be obtained if the trapezoidal steering mechanism were to be optimized. This mechanism would work closely to the Ackermann condition and would be exactly at a few angles, Figure 7.11. However, a trapezoidal mechanism is simple enough to produce in mass, and provides suitable accuracy for use in vehicles.

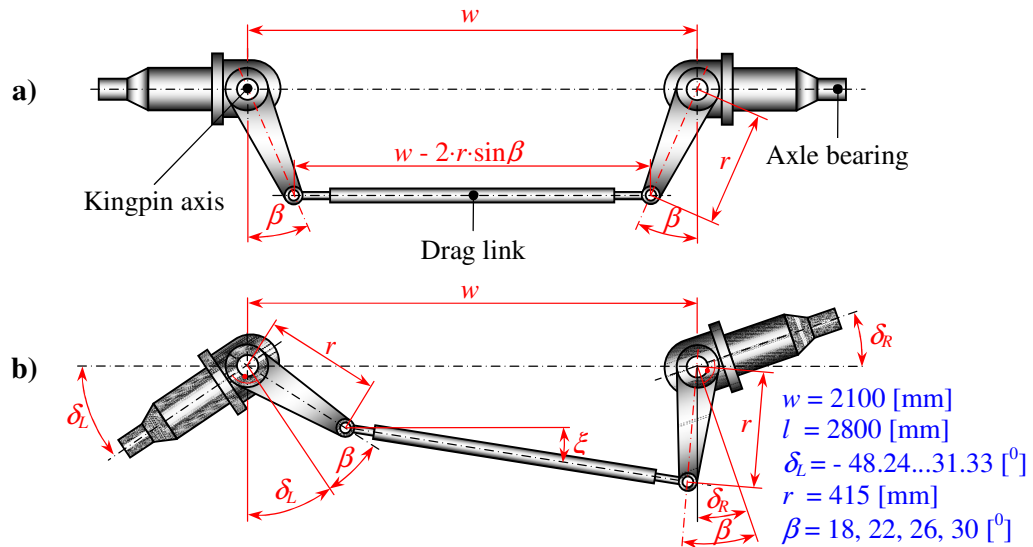


Figure 7.11: Trapezoidal steering mechanism;

a) straight-ahead position, b) turning toward the left side

Figure 7.11.a illustrates a trapezoidal steering mechanism in the straight-ahead position. Two characteristic parameters exist such as: angle β and the length of the offset arms r . Figure 7.11.b shows the steerable position as the trapezoidal mechanism turns towards the left side by the illustration of steer angles of the left and right wheels δ_L and δ_R and other parameters. In order to obtain a relation between the left and right steering angles ($\delta_L + \beta$) and ($\delta_R - \beta$) as shown in Figure 7.11.b, the projections of the Cartesian coordinative system in x and y axes are written as follows:

$$\begin{aligned} x: \quad & r \cdot \cos(\delta_L + \beta) + (w - 2 \cdot r \cdot \sin \beta) \cdot \cos \xi - r \cdot \cos(\delta_R - \beta) = 0, \\ y: \quad & r \cdot \sin(\delta_L + \beta) + (w - 2 \cdot r \cdot \sin \beta) \cdot \sin \xi - r \cdot \sin(\delta_R - \beta) = w. \end{aligned} \quad (7.25)$$

After some mathematical operation, the relationship between the left and right steer angles ($\delta_L + \beta$) and ($\delta_R - \beta$) now has got this form:

$$\sin(\delta_L + \beta) - \sin(\delta_R - \beta) + \frac{r}{w} \cdot \cos(\delta_R - \delta_L - 2 \cdot \beta) = \frac{r}{w} + 2 \cdot \sin \beta - 2 \cdot \frac{r}{w} + 2 \cdot \sin^2 \beta. \quad (7.26)$$

Equation (7.26) is known as the *Freudenstein's Equation*. The functionality of the trapezoid steering mechanism for a concrete terrain vehicle compared to the Ackermann steering condition is presented in Figure 7.12. It depicts that for the given parameters shown in Figure 7.11.b, a trapezoidal steering mechanism with $\beta \approx 22^\circ$ provides approximately the best Ackermann condition for the same input steer angles of the left wheel δ_L , Figure 7.12.

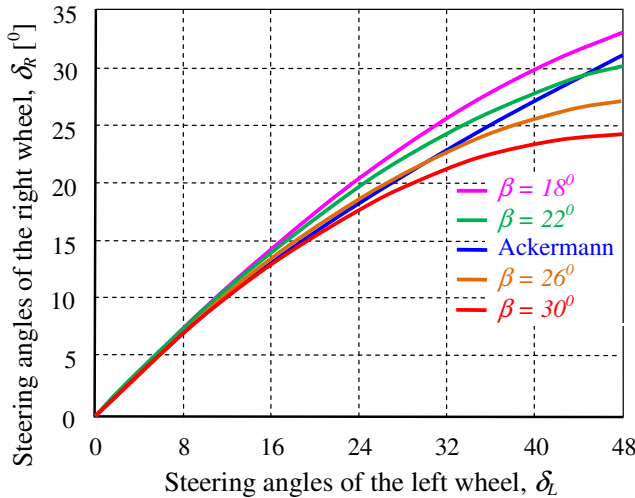


Figure 7.12: Comparison between functionality of the trapezoidal steering mechanism for different β angles and Ackermann steering condition

It is necessary to define in order to examine the performance that provides trapezoidal steering mechanism and compare it with the Ackermann steering condition as error parameters e . This error is the absolute difference between the steering angles of the right wheel δ_R defined by the trapezoidal steering mechanism and the Ackermann steering condition for the same input steering angles of the left wheel δ_L .

The error parameter e is determined by the following expression:

$$e = \Delta \delta_R = |\delta_{R,\text{trapezoid}} - \delta_{R,\text{Ackermann}}| \quad (7.27)$$

Figure 7.13 presents the values of the error parameter e steering mechanism that could be used for a terrain vehicle by using different β angles as a parameter. For different angles β

of the trapezoidal steering mechanism presented by the diagrams in Figures 7.12 and 7.13, it can be observed that for $\beta = 22^0$ and smaller input of steering angles $\delta_L = 0 \dots 10^0$, the error is minor. For $\delta_L = 28^0$ error has got maximal value $e = 1.3^0$, whilst for $\delta_L \approx 44^0$ the error is zero.

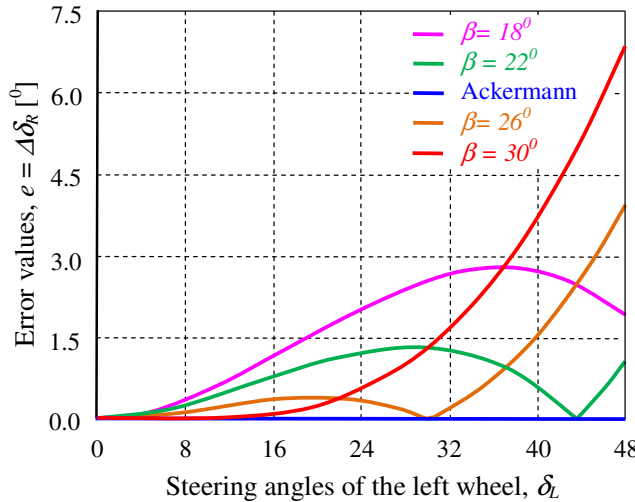


Figure 7.13: The error parameter e for concrete trapezoidal steering mechanism

If the terrain vehicle operates on the flat road by using such a mechanism, the vehicle will ensure sufficient Ackermann condition and at the same time provide suitable stability. The situation is totally different when the terrain vehicle operates over rough terrain. In this case, their wheels move extremely in a vertical direction in order for the vehicle to provide good performance and to be protected from rollover risk. On the other hand, the greater vertical motion of the wheels will cause so-called *bump steering*.

Bump steering will be appeared if during the vertical motion of the wheel, steerable wheels will be rotated for minor angles around the kingpin axle without the driver's steering input. In this case the vehicle moves along a different path which has not been selected by the driver and causes a reduction of vehicle stability, Figure 7.14. Bump steering is an undesired phenomenon and depends on the design of the suspension and steering mechanisms. To avoid this phenomenon requires the suspension and steering mechanisms to be rotated at the same centers during suspension travel. However, it is not that easy to design mechanisms which avoid bump steering, especially when the vertical movements of the wheels are greater? Perhaps as a proper solution to avoid bump steering would be the designing of the new steering mechanism by utilizing some kind of gear transmission. In this situation the steered wheels during vertical motion (bound and rebound) will stay in the straight-ahead position without minor rotation around the kingpin axis, such as presented in Figure 7.14.b.

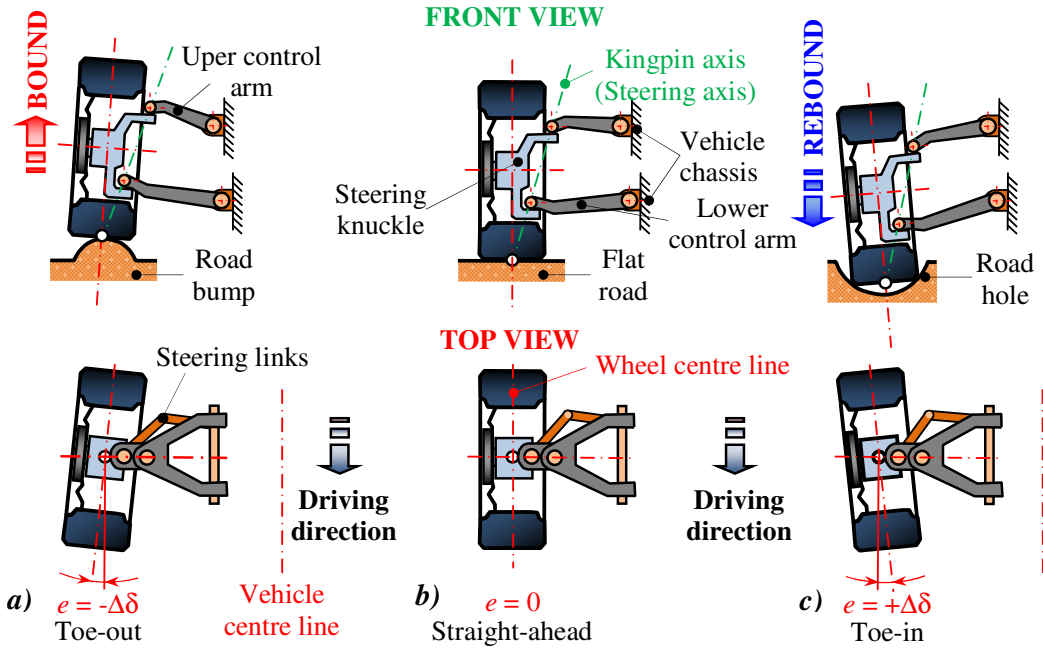


Figure 7.14: Cases of the bump steering; a) toe-out, b) straight-ahead direction and b) toe-in

Toe-out and *Toe-in* are undesired angles formed between the center line of the wheel and vehicle in longitudinal direction when the vehicle is viewed from above, Figure 7.14.

7.3.2 Design of a vehicle steering mechanism with 2WS by using non-circular gears

Design of the steering mechanism for terrain vehicle with 2WS is developed in such a way as to provide exactly the Ackermann steering conditions. By fulfilling this condition this ensures a reduction of the tire wear and improves the vehicle stability and maneuverability. On the other hand, vehicle stability would be improved if the steering bump is avoided during greater vertical motion of the steerable wheels.

However, the commonly used trapezoidal steering mechanism cannot exactly satisfy the Ackermann steering condition by avoiding steering bump. A perfect vehicle steering mechanism would be considered if the vehicle followed, as much as possible, the prescribed path determined by the driver and was unaffected steering bump when the vehicle moves over different terrains. The proper solution would be achieved by using pairs of non-circular gears. These pairs have non-circular pitch curves L_1 and L_2 which ensure variable gear ratios, Figure 7.15. Suitable design of the pairs of non-circular gears would fulfill exactly the Ackermann steering geometry. The non-circular gears are represented by two roll lines L_1 and L_2 , corresponding to pitch curves with two fixed rotation centers O_1 and O_2 , rolling together without slip. In general, the pitch curves L_1 and L_2 of the non-circular gears are described by using polar coordinates (r, δ) , Figure 7.15.b.

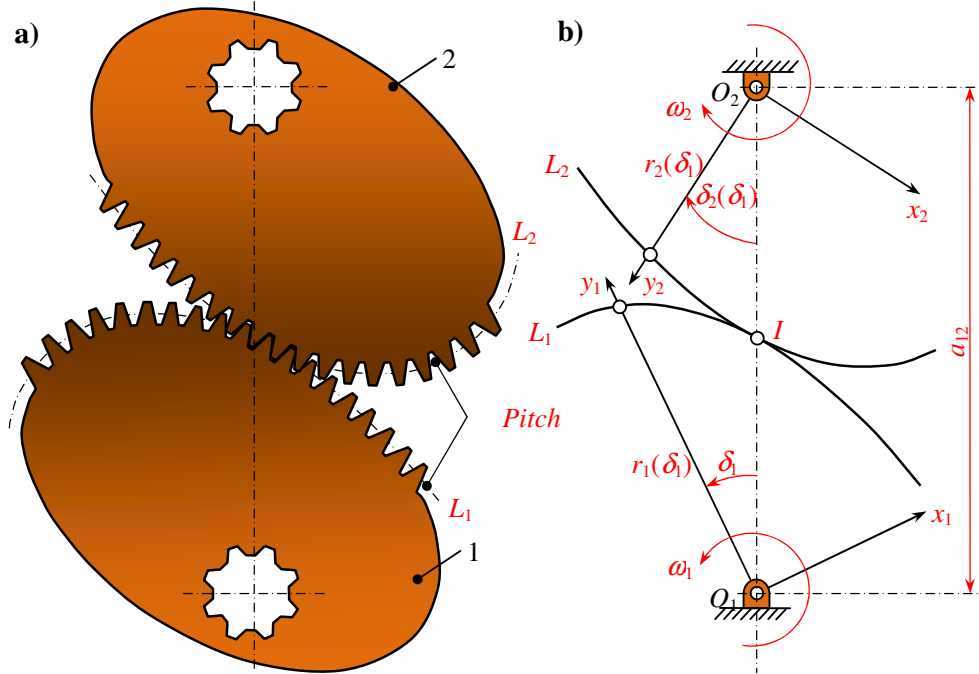


Figure 7.15: a) The non-circular gears, and b) pitch curves of the non-circular gears

The first pair of the non-circular gears is designed to rotate left front wheel, whilst the other pair to rotate the right front wheel, Figure 7.16. The angular displacements of the pair of non-circular gears δ_1 and δ_2 are written by the following expression:

$$\begin{aligned}\delta_1 &= \delta_R, \\ \delta_2 &= \delta_L,\end{aligned}\tag{7.28}$$

where δ_1 and δ_2 represents the angular displacements of the driving and driven non-circular gears 1 and 2, whilst δ_R and δ_L define front steering angles of the left and right wheels.

The angular displacement of the driving gear δ_1 is the input value. Table 7.1 presents the calculation values for the front steering angles that are substituted by angular displacement of the non-circular driving and driven gears $\delta_1 = \delta_R$ and $\delta_2 = \delta_L$. For the case when the angular displacement $\delta_2 = -\delta_L$ is counterclockwise then vehicle turns towards the left side, Figure 7.16.a. If the angular displacements are equal to zero then the vehicle goes in a straight-ahead direction, Figure 7.16.b. Whilst for the case when the angular displacement $\delta_2 = \delta_L$ is clockwise, the vehicle turns towards the right side, Figure 7.16.c.

The angular displacement of the non-circular driven gear δ_2 as a function of the driving gear δ_1 derived from Ackermann steering geometry, is determined as follow:

$$\delta_2(\delta_1) = \begin{cases} a \cot(\cot \delta_1 - w/l) & \text{if } -\delta_{1\min} \leq \delta_1 \leq 0, \\ a \cot(\cot \delta_1 + w/l) & \text{if } 0 \leq \delta_1 \leq \delta_{1\max}. \end{cases}\tag{7.29}$$

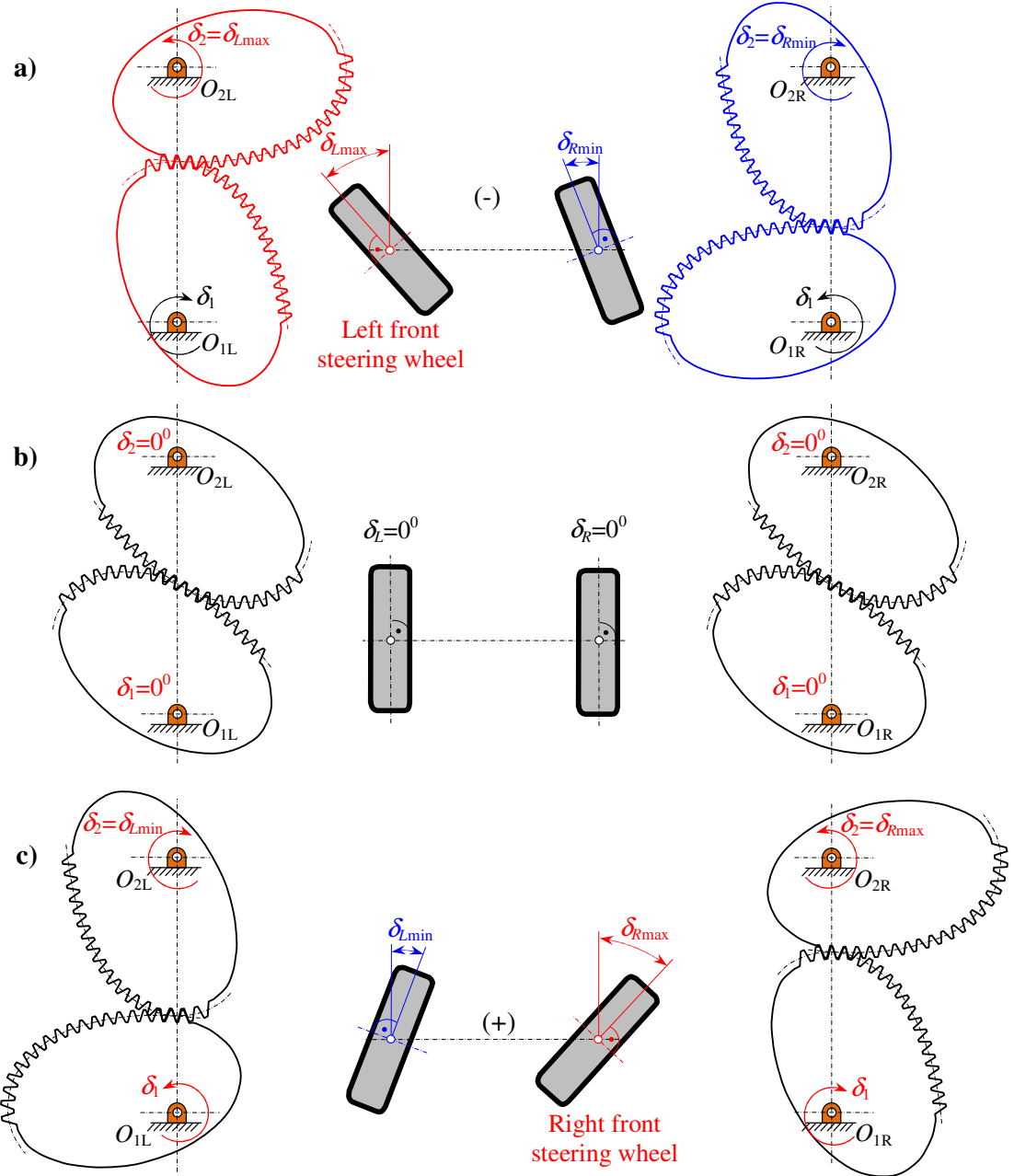


Figure 7.16: Working position of the two pair's non-circular gears when the front wheels of the terrain vehicle are turning towards the: a) left side, b) straight-ahead, and c) right side

The gear's ratio $i_{12}(\delta_1)$ for the driving gear to the driven gear of the non-circular gears is determined by the following expression:

$$i_{12}(\delta_1) = \frac{\omega_1(\delta_1)}{\omega_2(\delta_2)} = \frac{d\delta_1/dt}{d\delta_2/dt} = \frac{d\delta_1}{d\delta_2} = \frac{r_2(\delta_2(\delta_1))}{r_1(\delta_1)}, \quad (7.30)$$

where $\omega_1(\delta_1)$ and $\omega_2(\delta_2)$ denotes angular velocity, whilst $r_1(\delta_1)$ and $r_2(\delta_2(\delta_1))$ represents the radius of the pitch curves for the driving and driven non-circular gears, respectively.

The center distance a_{12} between the two fixed rotational centers O_1 and O_2 of the non-circular gears (Figure 7.15.b) always remains at a constant value and is determined as follow:

$$r_1(\delta_l) + r_2(\delta_2(\delta_l)) = a_{12} = \text{const}, \quad (7.31)$$

where a_{12} is distance between the rotation centers of the non-circular gears.

The radius of the pitch curves for driving gear $r_1(\delta_l)$ and driven gear $r_2(\delta_2(\delta_l))$ (Figures 7.15.b) are derived from equations (7.30) and (7.31), written as follow:

$$\begin{aligned} r_1(\delta_l) &= \frac{a_{12}}{1+i_{12}(\delta_l)} = \frac{a_{12}}{1+1/(d\delta_2/d\delta_l)}, \\ r_2(\delta_2(\delta_l)) &= \frac{i_{12}(\delta_l) \cdot a_{12}}{1+i_{12}(\delta_l)} = \frac{a_{12}/(d\delta_2/d\delta_l)}{1+1/(d\delta_2/d\delta_l)}, \end{aligned} \quad (7.32)$$

where the derivative function $d\delta_2/d\delta_l$ is defined from equation (7.29), and is written using the following expression:

$$\frac{d\delta_2(\delta_l)}{d\delta_l} = \begin{cases} 1/\sin^2 \delta_l \cdot [1 + (\cot \delta_l - w/l)^2] & \text{if } -\delta_{l\min} \leq \delta_l \leq 0, \\ 1/\sin^2 \delta_l \cdot [1 + (\cot \delta_l + w/l)^2] & \text{if } 0 \leq \delta_l \leq \delta_{l\max}. \end{cases} \quad (7.33)$$

For modeling of the non-circular gear in Table 7.3, the necessary parameters have to be given.

Table 7.3: Parameters for modeling non-circular gears for steering system with 2WS

Parameters →	Parameters for modeling non-circular gears				
	w [mm]	l [mm]	a_{12} [mm]	δ_l [$^\circ$]	m_{n12} [mm]
Values →	2100	2800	200	[-31.33, 31.33]	3

Figure 7.17 shows the modeling of the radius of the pitch curves for driving and driven non-circular gears $r_1(\delta_l)$ and $r_2(\delta_2(\delta_l))$ as a function of the angular displacement δ_l .

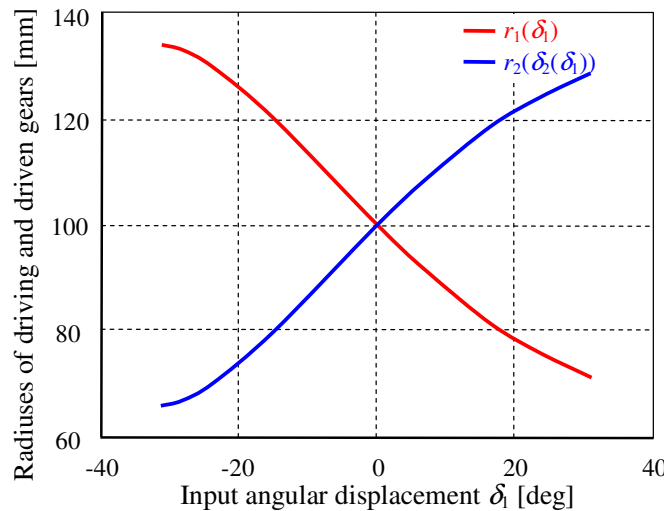


Figure 7.17: Radiiuses of the pitch curves as a function of input angular displacement δ_l

From Figure 7.17 it can be observed that, the radius of non-circular gears produce variable gear ratio ($i_{12}(\delta_l) \neq \text{const}$) and is depends on the input angular displacement δ_l . When the radius of the driving and driven gears have the same values (for $\delta_l = 0$), then the gear ratio is $i_{12}(\delta_l) = 1$ and the terrain vehicle moves in the straight-ahead direction.

In order to verify the reliability of equation (7.32) for determining the radius of the pitch curves $r_1(\delta_l)$ and $r_2(\delta_2(\delta_l))$, the angular displacement $\delta_2(\delta_l)$ of the non-circular gear 2 is determined from equations (7.30) and (7.31), written by the following expression:

$$\delta_2(\delta_l) = \int_0^{\delta_l} \frac{r_1(\delta_l)}{a_{12} - r_1(\delta_l)} d\delta_l. \quad (7.34)$$

The angular displacement $\delta_2(\delta_l)$ of the non-circular gear 2 determined with equation (7.34) should provide the same values as equation (7.29) in order to exactly follow the Ackermann steering geometry. Figure 7.18 introduces the angular displacement $\delta_2(\delta_l)$ of the driven non-circular gear 2 as a function of the input angular displacement δ_l of the driving non-circular gear 1. From Figure 7.18 it can be concluded that, the design of the pair of non-circular gears follows exactly the Ackermann steering geometry, and will be used for the steering mechanism of the terrain vehicle.

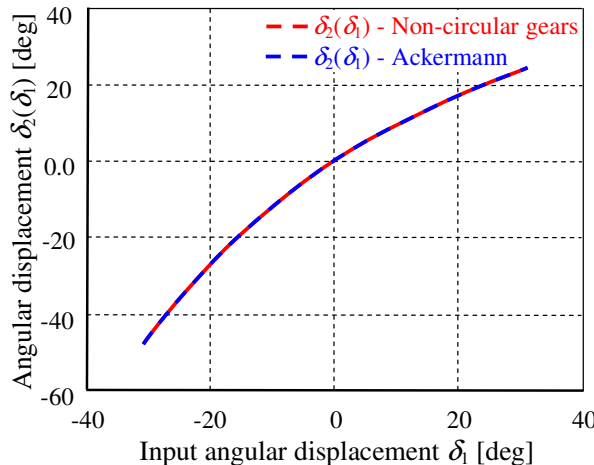


Figure 7.18: Angular displacements $\delta_2(\delta_l)$ obtained from the Ackermann steering geometry and the non-circular gears' as a function of angular displacement δ_l

Hence, the pitch curves of the driving $L_1(x_1, y_1)$ and driven $L_2(x_2, y_2)$ non-circular gears in their movable coordinate systems (x_i, y_i) are determined by the expressions:

$$\begin{aligned} x_1 &= r_1(\delta_l) \cdot \sin \delta_l, \\ y_1 &= r_1(\delta_l) \cdot \cos \delta_l. \end{aligned} \quad (7.35)$$

$$\begin{aligned}x_2(\delta_2(\delta_1)) &= r_2(\delta_2(\delta_1)) \cdot \sin(\delta_2(\delta_1)) \\y_2(\delta_2(\delta_1)) &= r_2(\delta_2(\delta_1)) \cdot \cos(\delta_2(\delta_1))\end{aligned}\quad (7.36)$$

With substitution of the parameters given in Table 7.3, the pitch curves of the driving and driven non-circular gears in the movable system (x_i, y_i) is shown in Figure 7.19. From Figure 7.19 it can be observed that, the distances between the rotation centers O_1 and O_2 of the non-circular gears remain constant values and when the movable axes x_1 and x_2 arise to 0, the axes y_1 and y_2 obtain the same values $y_i = 100$ mm, thus the vehicle moves straight-ahead.

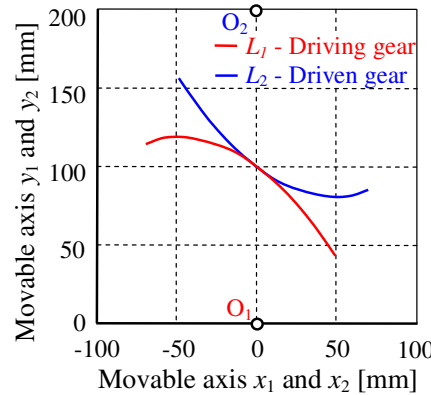


Figure 7.19: Pitch curves of the non-circular gear given by the movable coordinate system

7.3.2.1 Work principles of the steering mechanism with 2WS by using non-circular gears

After modeling the non-circular gears that follow exactly the Ackermann steering geometry, the design of the steering mechanism for the terrain vehicle with 2WS is developed in this way. The driver steering efforts transmit from the steering wheel to the steering gearbox through the steering shaft (propeller shaft).

The design of the steering gearbox consists of a planetary gear, a driving bevel gear, two driven bevel gears, and two pairs of the non-circular gears. The planetary gear has higher mechanical efficiency compared with other gear transmissions, and ensures a greater gear reduction ratio in order to provide drivers with a mechanical advantage for easy turning of the vehicle. The steering shaft is connected with the sun gear of planetary gear. The carrier of the planetary gear is connected to the driving bevel gear which splits the driver's command into left and right sides, and provides gear reduction. Two driven bevel gears transmit the driver's command into left and right driving non-circular gears and offers opposite rotational direction. This opposite direction of rotation allows for the using two of the same pairs of non-circular gears for left and right wheels. The driver commands from driving gears are then transmitted to the driven non-circular gears which precisely follow the Ackermann steering geometry specified by equation (7.6). The driven non-circular gears of the left and right sides

of the steering gearbox are connected via the propeller shafts to transmit driver command into bevel gears with ratio 1:1, fitted in the kingpin axle of the left and right steerable wheels. A typical working principle is shown in Figure 7.20.

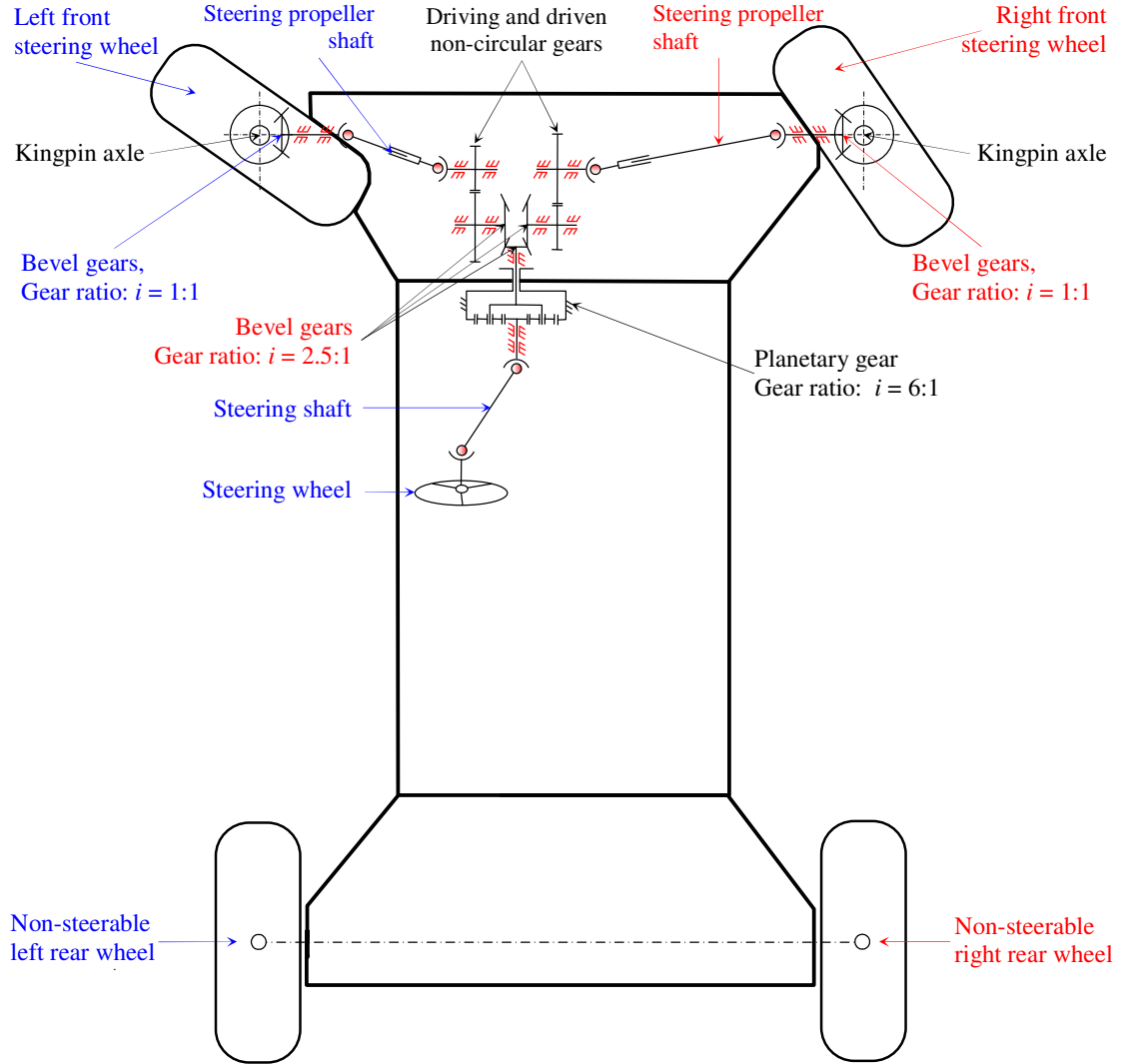


Figure 7.20: Steering mechanism for terrain vehicle with 2WS by using non-circular gears

7.3.3 Design of the vehicle's steering mechanism with 4WS by using non-circular gears

Designing of the steering mechanism for a terrain vehicle with 4WS is developed in same way as 2WS in order to exactly ensure the Ackermann steering geometry given by equations (7.15) and (7.16). The main goal of this steering mechanism is the designing of suitable pairs of the non-circular gears for front and rear steering wheels. The design principle is similar to that of vehicles with 2WS but with some substantial differences when determining the pitch curves of the non-circular gears. In the same ways are determines the angular displacements for the

front $\delta_{2F}(\delta_{1F})$ and rear $\delta_{2R}(\delta_{1R})$ driven non-circular gears as a function of angular displacements of the front δ_{1F} and rear δ_{1R} driving non-circular gears, written as:

$$\begin{aligned}\delta_{2F}(\delta_{1F}) &= \begin{cases} a \cot(\cot \delta_{1F} - w/c) & \text{if } -\delta_{1F\min} \leq \delta_{1F} \leq 0, \\ a \cot(\cot \delta_{1F} + w/c) & \text{if } 0 \leq \delta_{1F} \leq \delta_{1F\max}, \end{cases} \\ \delta_{2R}(\delta_{1R}) &= \begin{cases} a \cot(\cot \delta_{1R} - w/d) & \text{if } -\delta_{1R\min} \leq \delta_{1R} \leq 0, \\ a \cot(\cot \delta_{1R} + w/d) & \text{if } 0 \leq \delta_{1R} \leq \delta_{1R\max}. \end{cases}\end{aligned}\quad (7.38)$$

The gear's ratio for the front $i_{12F}(\delta_{1F})$ and rear $i_{12R}(\delta_{1R})$ for pairs of the non-circular gears is determined by the following expression:

$$\begin{aligned}i_{12F}(\delta_{1F}) &= \frac{\omega_{1F}(\delta_{1F})}{\omega_{2F}(\delta_{2F})} = \frac{d\delta_{1F}/dt}{d\delta_{2F}/dt} = \frac{d\delta_{1F}}{d\delta_{2F}} = \frac{r_{2F}(\delta_{2F}(\delta_{1F}))}{r_{1F}(\delta_{1F})}, \\ i_{12R}(\delta_{1R}) &= \frac{\omega_{1R}(\delta_{1R})}{\omega_{2R}(\delta_{2R})} = \frac{d\delta_{1R}/dt}{d\delta_{2R}/dt} = \frac{d\delta_{1R}}{d\delta_{2R}} = \frac{r_{2R}(\delta_{2R}(\delta_{1R}))}{r_{1R}(\delta_{1R})}.\end{aligned}\quad (7.39)$$

where $\omega_{1F}(\delta_{1F})$, $\omega_{2F}(\delta_{2F})$, $\omega_{1R}(\delta_{1R})$ and $\omega_{2R}(\delta_{2R})$ denotes the angular velocity, whilst $r_{1F}(\delta_{1F})$, $r_{2F}(\delta_{2F}(\delta_{1F}))$, $r_{1R}(\delta_{1R})$ and $r_{2R}(\delta_{2R}(\delta_{1R}))$ represent the radius of the pitch curves for front and rear driving and the driven non-circular gears, respectively.

The distance of the rotation center for the front a_{12F} and rear a_{12R} pairs of the non-circular gears always remains a constant value, and are determined as follow:

$$\begin{aligned}r_{1F}(\delta_{1F}) + r_{2F}(\delta_{2F}(\delta_{1F})) &= a_{12F} = \text{const}, \\ r_{1R}(\delta_{1R}) + r_{2R}(\delta_{2R}(\delta_{1R})) &= a_{12R} = \text{const}.\end{aligned}\quad (7.40)$$

The radius of the pitch curves front driving $r_{1F}(\delta_{1F})$ and driven $r_{2F}(\delta_{2F}(\delta_{1F}))$ gears and rear driving $r_{1R}(\delta_{1R})$ and driven $r_{2R}(\delta_{2R}(\delta_{1R}))$ gears, are written as follows:

$$\begin{aligned}r_{1F}(\delta_{1F}) &= \frac{a_{12F}}{1 + 1/(d\delta_{2F}/d\delta_{1F})}; & r_{1R}(\delta_{1R}) &= \frac{a_{12R}}{1 + 1/(d\delta_{2R}/d\delta_{1R})}, \\ r_{2F}(\delta_{2F}(\delta_{1F})) &= \frac{a_{12F} / (d\delta_{2F}/d\delta_{1F})}{1 + 1/(d\delta_{2F}/d\delta_{1F})}, & r_{2R}(\delta_{2R}(\delta_{1R})) &= \frac{a_{12R} / (d\delta_{2R}/d\delta_{1R})}{1 + 1/(d\delta_{2R}/d\delta_{1R})}.\end{aligned}\quad (7.41)$$

where the derivative functions $d\delta_{2F}/d\delta_{1F}$ and $d\delta_{2R}/d\delta_{1R}$ are defined from equation (7.38) and determined by the following expression:

$$\begin{aligned}\frac{d\delta_{2F}(\delta_{1F})}{d\delta_{1F}} &= \begin{cases} 1/\sin^2 \delta_{1F} \cdot [1 + (\cot \delta_{1F} - w/c)^2] & \text{if } -\delta_{1F\min} \leq \delta_{1F} \leq 0, \\ 1/\sin^2 \delta_{1F} \cdot [1 + (\cot \delta_{1F} + w/c)^2] & \text{if } 0 \leq \delta_{1F} \leq \delta_{1F\max}, \end{cases} \\ \frac{d\delta_{2R}(\delta_{1R})}{d\delta_{1R}} &= \begin{cases} 1/\sin^2 \delta_{1R} \cdot [1 + (\cot \delta_{1R} - w/d)^2] & \text{if } -\delta_{1R\min} \leq \delta_{1R} \leq 0, \\ 1/\sin^2 \delta_{1R} \cdot [1 + (\cot \delta_{1R} + w/d)^2] & \text{if } 0 \leq \delta_{1R} \leq \delta_{1R\max}, \end{cases}\end{aligned}\quad (7.42)$$

For the modeling of pairs of the non-circular gears for front and rear steering wheels in Table 7.4 are given necessary parameters.

Table 7.4: Parameters for modeling non-circular gears for steering system with 4WS

Parameters →	Parameters for modeling non-circular gears								
	w [mm]	c [mm]	d [mm]	a _{12F} [mm]	a _{12R} [mm]	δ _{1F} [°]	δ _{1R} [°]	m _{n12F} [mm]	m _{n12R} [mm]
Values →	2100	1400	1400	200	200	[-18.5;18.5]	[-18.5;18.5]	3	3

The angular displacements for front $\delta_{2F}(\delta_{1F})$ and rear $\delta_{2R}(\delta_{1R})$ driven non-circular gears are determined from equations (7.39) and (7.40), and are written as the following expression:

$$\delta_{2F}(\delta_{1F}) = \int_0^{\delta_{1F}} \frac{r_{1F}(\delta_{1F})}{a_{12F} - r_{1F}(\delta_{1F})} d\delta_{1F}; \quad \delta_{2R}(\delta_{1R}) = \int_0^{\delta_{1R}} \frac{r_{1R}(\delta_{1R})}{a_{12R} - r_{1R}(\delta_{1R})} d\delta_{1R}. \quad (7.43)$$

The angular displacement determined by equation (7.43) should provide the same values as equation (7.38) in order to follow exactly the Ackermann steering geometry. Figure 7.21.a introduces the angular displacement for the front and rear driven non-circular gears δ_{2ForR} as a function of the input angular displacement of the front and rear driving non-circular gears δ_{1ForR} . The front and rear pitch curves of the driving and driven non-circular gears in their movable coordinate systems (x_i, y_i) are determined by the expressions:

$$\begin{aligned} x_{1F} &= r_{1F}(\delta_{1F}) \cdot \sin \delta_{1F}; & x_{1R} &= r_{1R}(\delta_{1R}) \cdot \sin \delta_{1R}, \\ y_{1F} &= r_{1F}(\delta_{1F}) \cdot \cos \delta_{1F}; & y_{1R} &= r_{1R}(\delta_{1R}) \cdot \cos \delta_{1R}; \end{aligned} \quad (7.44)$$

$$\begin{aligned} x_{2F}(\delta_{2F}(\delta_{1F})) &= r_{2F}(\delta_{2F}(\delta_{1F})) \cdot \sin(\delta_{2F}(\delta_{1F})); & x_{2R}(\delta_{2R}(\delta_{1R})) &= r_{2R}(\delta_{2R}(\delta_{1R})) \cdot \sin(\delta_{2R}(\delta_{1R})) \\ y_{2F}(\delta_{2F}(\delta_{1F})) &= r_{2F}(\delta_{2F}(\delta_{1F})) \cdot \cos(\delta_{2F}(\delta_{1F})); & y_{2R}(\delta_{2R}(\delta_{1R})) &= r_{2R}(\delta_{2R}(\delta_{1R})) \cdot \cos(\delta_{2R}(\delta_{1R})) \end{aligned} \quad (7.45)$$

With the substitution parameters shown in Table 7.4, the front and rear pitch curves of the driving and driven non-circular gears in the (x_i, y_i) system, are presented in Figure 7.21.b.

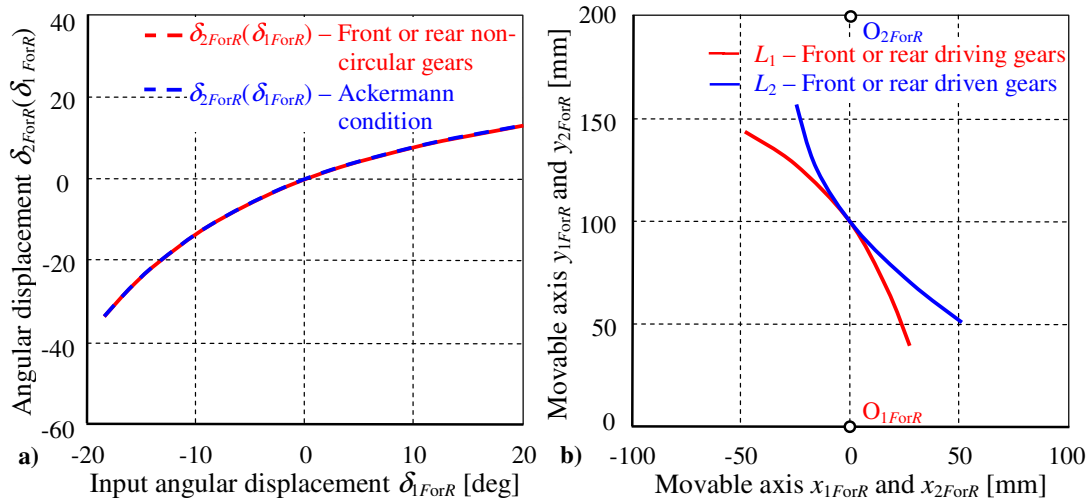


Figure 7.21: The front and rear; a) angular displacements $\delta_{2ForR}(\delta_{1ForR})$ of the driven non-circular gears and b) pitch curves in the (x_i, y_i) for driving and driven non-circular gears

From Figure 7.21 it can be observed that the characteristics for front and rear pairs of non-circular gears are the same. These are due to the center of rotation being at the middle of the terrain vehicle, and the longitudinal distances between the turning center of the front c and rear d are the same $c = d$. Furthermore, the pair of non-circular gears exactly follows the Ackermann steering geometry and is used for the steering mechanism of the terrain vehicle with 4WS, Figure 7.22.

7.3.3.1 Work principles of the steering mechanism with 4WS by using non-circular gears

After the modeling of the front and rear driving and driven non-circular gears, the steering mechanism for the terrain vehicle with 4WS conforms exactly to the Ackermann steering geometry, as illustrated in Figure 7.22. The working principles is the driver through the steering wheel transmit command to the front steering gearbox via the steering shaft.

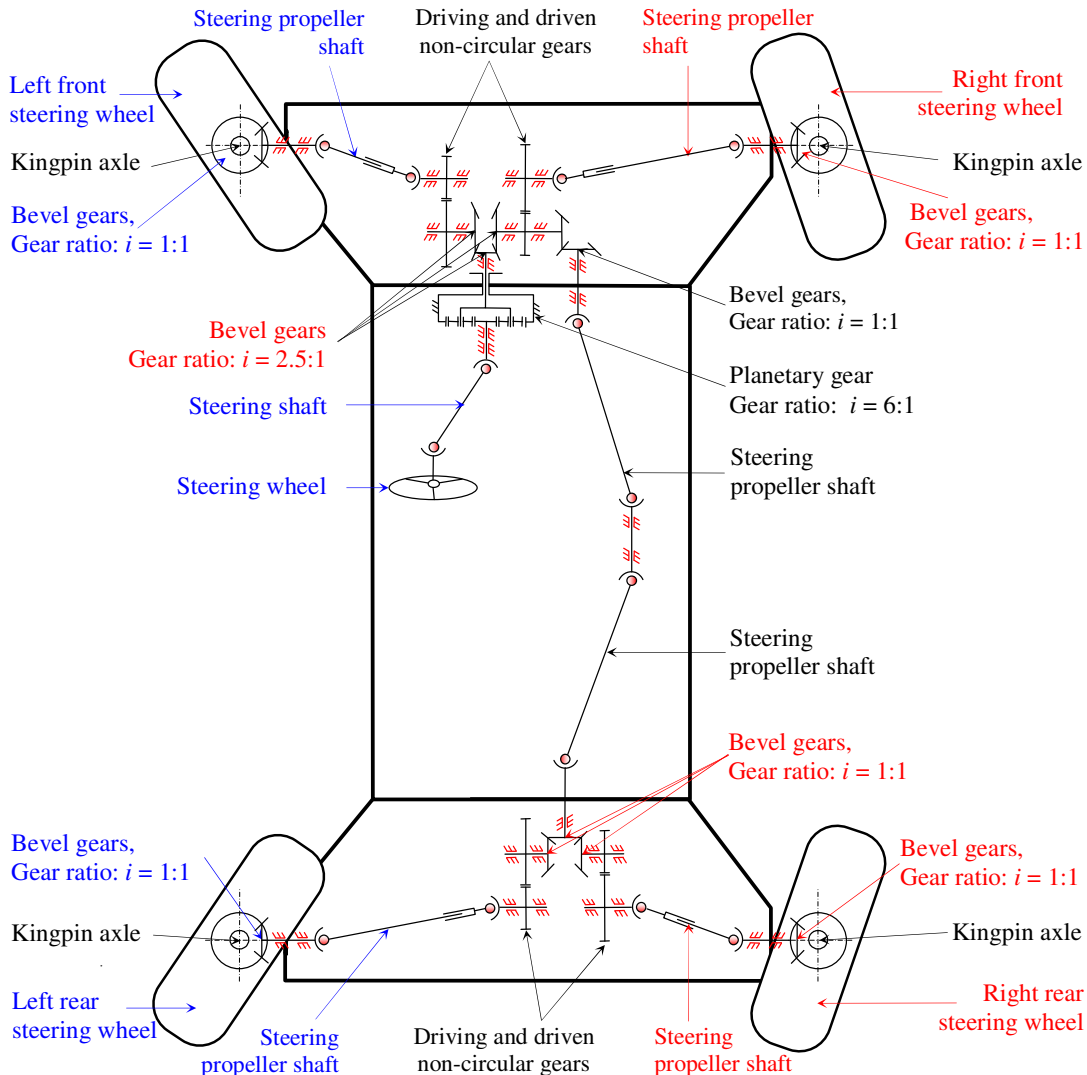


Figure 7.22: Steering mechanism for the terrain vehicle with 4WS

The design and working principles of the front steering gearbox are similar to the 2WS system. The substantial differences are in the radiiuses of the pitch curves for the pairs of non-circular gears and on the shaft of the driving non-circular gear a pair of bevel gears is added. The driver command from the front to the rear steering gearbox are transmitted through two pairs of bevel gears with gear ratio 1:1, and connected via the propeller shaft.

The rear steering gearbox consists of the driving bevel gear, two driven bevel gears, and two pairs of non-circular gears. The driving bevel gear with gear ratio 1:1 is activated and the steering command takes it from the front steering gearbox and split it to the left and right branches of the rear steering gearbox. The two driven bevel gears transmit the driver's parts of into the left and right driving non-circular gears. Then command is followed to the driven non-circular gears. The driven non-circular gears are connected through the propeller shafts into the bevel gears with gear ratio 1:1 which are fitted in the kingpin axle of the left and right rear steerable wheels. This way ensures the turning of the rear wheels in the opposite direction of the front steerable wheel. This form of steering allows the terrain vehicle to have a higher rate of maneuverability and successfully avoided the vehicle from steering bumps during greater vertical wheel motion.

7.3.4 Design of the steering mechanism with 2WS/4WS for terrain vehicle

After designing the steering mechanisms with 2WS and 4WS for terrain vehicles which exactly follow Ackermann steering geometry, it is necessary to design a steering mechanism in order that the terrain vehicle can have both systems. By using this steering mechanism a driver will have the opportunities of deciding whether to drive with the steering of only the front wheels (2WS - rear wheels are locked) or to steer all the wheels (4WS). The first option provides greater vehicle turning radius compared to the other option and could be used when vehicle is driven at higher speed by ensuring better stability of the vehicle. For better maneuvering in the city or when the vehicle moves over rough terrain, the vehicle's turning radius should be as small as possible. This would be ensured by the second option and would be used when the vehicle moves at lower speed.

7.3.4.1 Work principles of the steering mechanism with 2WS/4WS

The differences between 2WS/4WS and separate 2WS or 4WS are that, both systems are now fixed in the front steering gearbox. Front steering gearboxes, except gears that also have three joints fitted (A, B and C). The three joints are connected at the same time by motion towards the left or right direction by the lever, and don't have free positions, Figure 7.23. The joints

connect the front driven non-circular gears as 2WS or 4WS and the rear steering gearbox. Switch of joints could be done mechanically, hydraulically or in an electrical ways. The switching to 2WS or 4WS modes is selected by the driver and then fixed. Switching to 2WS or 4WS or reciprocally, depends on the driver's wish and can only change when the vehicle is stopped. This is for safety reasons. Figure 7.23 illustrate the unique design of the steering mechanism with 2WS/4WS modes for terrain vehicles.

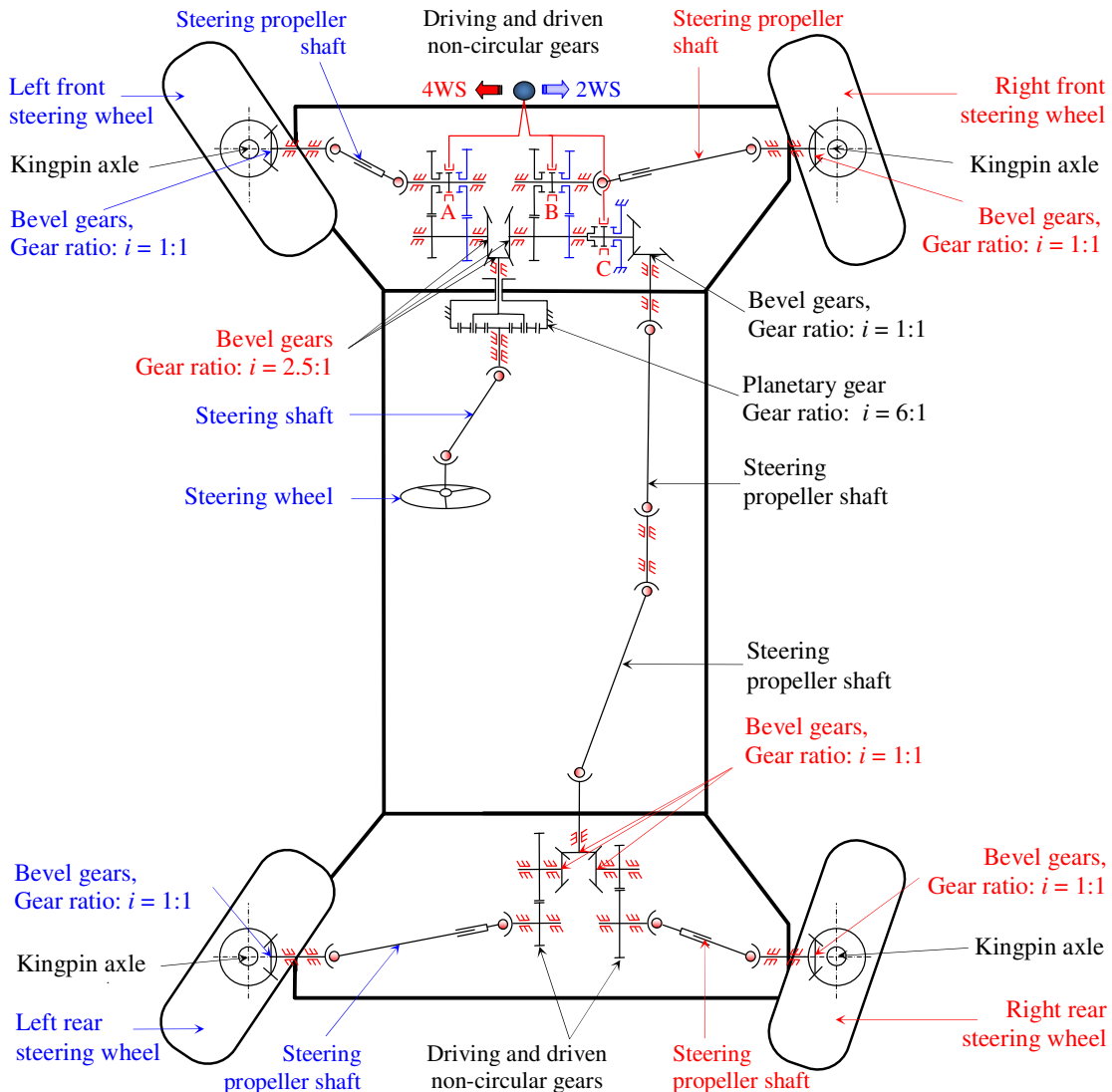


Figure 7.23: Steering mechanism of the terrain vehicle with 2WS/4WS

If the joints (A, B and C) moves in the left direction steering system provide 4WS mode, otherwise ensure 2WS mode.

7.4 Discussion of results

Designing a steering mechanism for terrain vehicles was done for front wheel steering and all wheel steering. Designs are in relation to all the requirements given in the check list. In all operation modes of the steering mechanism the target was a system to provide exactly the Ackermann steering geometry.

The trapezoid steering mechanism conforms closely to the Ackermann conditions by providing a steering error from $e = 1.3^0$. On the one hand, the characteristic of the terrain vehicle is largely vertical wheel movements due to protecting the vehicle from rollover risk. On the other hand, these movements cause so-called *bump steering* by cause a reduction in the vehicle stability. A better solution was thus sought. By employing a pair of non-circular gear modeled according to the Ackermann principle ensures the Ackermann steering geometry and avoids steering bumps. In this situation the steering wheels during all vertical motion will stay in the same position without minor rotation around its kingpin axis.

The design of this steering system with non-circular gears was done for three cases: 2WS, 4WS, and 2WS/4WS. All cases ensure Ackermann steering conditions. Differences in performance that provide 4WS compared with 2WS is the vehicle turning radius reduction of 34%. This means that by this system the terrain vehicle can demonstrate higher maneuverability when moving in city or over rough terrain. By utilizing 2WS/4WS vehicle performance significantly improves at both high and low speeds.

8 SUMMARY AND CONCLUSION

After the known research problems regarding the suspension and steering system were identified, three key elements became the main objectives of this research project.

The *first objective* was the developing of an optimal suspension mechanism for a terrain vehicle with four wheels-drive and four-wheels steering. The *second goal* was to design and optimize control strategies for a suspension system that would minimize undesired vibration that affects a vehicle's body caused by ground excitation, and provide better driving comfort. The *third topic* was to develop an effective steering system that would enable the provision of good maneuverability at lower speeds and efficient driving safety at higher speeds.

Obtaining these objectives was carried out by more or less comprehensive systems. The known suspension and steering systems are developed sufficiently enough for passenger cars but when a terrain vehicle is in question with greater wheel motions due to rollover risk, the situation is totally different.

The *first goal* is reached by designing a completely new suspension mechanism which was derived by improving a double wishbone with longer equal control arms. Mathematical modeling and solving of equations of motion had been developed by numerical methods for a quarter of it. In order to provide less lateral wheel motion, the Finite Element Methods were employed in order to optimize. The following summarizes the main features concerning the developed suspension mechanism:

- When the wheel moves from its rest position to the rebound direction, the suspension mechanism provides 45 % less lateral wheel motion, whilst when the wheel moves from the rest to the bound direction it obtains better behavior by ensuring 72.6 % less when compared with a predesigned suspension mechanism with double wishbone and a longer equal control arm,
- The suspension mechanism provides zero camber angles during all vertical wheel motion such as the rebound and bound directions, and
- Its optimized suspension mechanism provides up to 37.5% less lateral wheel motion when compared with the initially developed suspension mechanism.

The proposed suspension design provides relatively small lateral wheel motion, zero camber angles, and effectively absorbs the vibrations caused by ground excitation. These

features affect the improvement of tire life-expectancy, increasing the quality of the tire contact with the road surface, thus reducing the additional load in the suspension mechanism.

The *second objective* of this approach is obtained by design and optimization control strategies for active, semi-active, and passive suspension systems. A simplified quarter vehicle model was introduced, together with a suitably-created mathematical model for active, semi-active and passive systems. Solving of the differential equations of motion was carried out within a MATLAB/Simulink environment. The ground excitation was modeled using two repeated cosine bumps and flat lines. Optimal suspension parameters for a passive linear suspension system were optimized by using Multi Objective Genetics Algorithms. Whilst for optimal parameters for the active damping forces were determined by the stochastic parametric optimization method, which is based on non-linear programming, the suspension performances were optimized by maximizing the driving comfort and safety. The obtained results were gained by solving differential equations of motion for active, semi-active, and passive non-linear systems. The following features were identified concerning the developed control strategy:

- Vehicle's body acceleration for optimal design of the passive linear suspension system in some locations is reduced by 75%, whilst the vertical tire forces by 71% less compared with the initial design of the passive linear suspension system,
- Vehicle's body acceleration for optimal design of the active non-linear suspension system in some locations is reduced by 81%, whilst the vertical tire forces by 54% less compared with the passive non-linear suspension system, and
- Vehicle's body acceleration for optimal design of the semi-active non-linear suspension system in some locations is reduced by 76%, whilst the vertical tire forces by 49% less compared with the passive non-linear suspension system.

It is obvious that the active system provides better performances compared with the semi-active and passive ones.

The *third aim* has been to developing an effective steering system for terrain vehicle with four wheel steer. This steering mechanism is designed to work by two modes *steer such as all wheels steer* and *front wheels steer*. Proposed steering mechanism conform exactly the Ackermann steering geometry in all modes and situations.

The trapezoid steering mechanism conforms closely with the Ackermann law by providing 1.3° steering error in some steering angles. This error will probably not be a problem if the terrain vehicle moves over flat roads but problems will appear when it moves over bumps or rough terrain such as bump steering. Effective steering design consists of

special pairs of gears known as non-circular gears. The following features can be identified regarding the new steering mechanism:

- The vehicle turning radius for all wheel steering is reduced by 34% compared with only front wheel steering,
- The Ackermann steering condition is ensured 100%, and
- Bumps steering caused when the vehicle moves over rough terrain can be perfectly avoided.

So, the proposed steering system for the terrain vehicle demonstrates good maneuverability at low speed and provides suitable stability at higher speeds due to following Ackermann law.

Finally, on the basis of comprehensive analysis shown during this doctoral thesis, it can be concluded that the developed suspension and steering system for terrain vehicles with four wheel drives and four wheel steering can ensure efficient driving comfort, driving safety, and good maneuverability. In addition, this research project contributes to the state of knowledge for the designing of suspension and steering systems whilst building bridges between designers, manufacturers, researchers, and so one. Furthermore, this approach has already resulted in several academic publications given follows:

- [1] **Lajqi Shpetim**, Pehan Stanislav, Lajqi Naser, Gjelaj Afrim, Pšeničnik Jože, Sašo Emin. Design of Independent Suspension Mechanism for a Terrain Vehicle with Four Wheels Drive and Four Wheels Steering. *Annals of Faculty Engineering Hunedoara - International Journal of Engineering/Fascicule1* (2013), Fascicule1, Tome XI 2013, pp. 101-108.
- [2] **Lajqi Shpetim**, Stanislav Pehan. Designs and Optimizations of Active and Semi-Active Non-linear Suspension System for a Terrain Vehicle. *Strojniški vestnik - Journal of Mechanical Engineering* (2012), vol. 58, no.12, pp. 732-743.
- [3] **Lajqi Shpetim**, Gugler Jürgen, Lajqi Naser, Shala Ahmet, Likaj Ramë: Possibilities Experimental Method to Determine the Suspension Parameters in a Simplified Model of a Passenger Car. *Inter. Journal of Automotive Technology* (2012), vol. 13, no. 4, pp. 615-621.
- [4] **Lajqi Shpetim**, Pehan Stanislav, Lajqi Naser, Baxhaku Bashkim, Ymeri Besim. Influences of the Suspension Parameters on the Vehicle Suspension Performance for a Terrain Vehicle. *Journal of Mechanics Engineering and Automation* (2012), vol. 2, no. 9, pp. 550-554.
- [5] Pehan Stanislav, **Lajqi Shpetim**, Pšeničnik Jože, Flašker Jože. Modeling and Simulation of off Road Vehicle with Four Wheel Steering. The 7th International Scientific Conference, Research and Development of Mechanical Elements and Systems (2011), IRMES 2012 Conference Proceedings, pp. 77-83.
- [6] **Lajqi Shpetim**, Pehan Stanislav, Pšeničnik Jože, Lajqi Naser. Tracking the Prescribed Path Through an Autonomous Mobile Robot with Four Wheel Steering. The 3rd International Scientific Conference, *Management of Technology Step to Sustainable Production* (2011), MOTSP 2011 Conference proceedings, pp. 94-101.

LIST OF USED SOURCES

- [1] Pehan Stanislav, Lajqi Shpetim, Pšeničnik Jože, Flašker Jože. Modeling and simulation of off road vehicle with four wheel steering. *IRMES 2012 Conference Proceedings* (2011), pp. 77-83.
- [2] Lajqi Shpetim, Stanislav Pehan. Designs and Optimizations of Active and Semi-Active Non-linear Suspension System for a Terrain Vehicle. *Strojniški vestnik - Journal of Mechanical Engineering* (2012), vol. 58, no.12, pp. 732-743.
- [3] Lajqi Shpetim, Pehan Stanislav, Lajqi Naser, Gjelaj Afrim, Pšeničnik Jože, Sašo Emin. Design of Independent Suspension Mechanism for a Terrain Vehicle with Four Wheels Drive and Four Wheels Steering. *MOTSP 2012 Conference Proceedings* (2012), pp. 230-237.
- [4] Rill Georg. *Vehicle dynamics*. Regensburg University of Applied Science. Regensburg, 2009.
- [5] <http://www.interregs.com/spotlight.php?id=27> [17.08.2011].
- [6] RTC - Zavod za avtomobilsko industrijo (Razvojno Tehnološki Center) ([http://www.rtc.si](http://www rtc si)), Ceska k TAMU 7, Maribor, 2011&2012.
- [7] Genta Giancarlo, Morello Lorenzo. *The Automotive Chassis-Volume 1: Components Design*. Springer, Torino, 2009.
- [8] Dixon C. John. *Suspension Geometry and Computation*. John Wiley, New York, 2009.
- [9] Jazar Reza. *Vehicle dynamics: Theory and Application*. Springer, New York, 2009.
- [10] <http://www.daimler.com/dccom/0-5-1324882-49-1324893-1-0-0-1345593-0-0-135-0-0-0-0-0-0.html> [01.02.2012].
- [11] Mohd Zakaria Mohammad Nasir. Analysis of double wishbone suspension system (2008). Master dissertation in Automotive Engineering. Coventry University, School Engineering.
- [12] Gillespie Thomas. *Fundamental of Vehicle Dynamics*. Society of Automotive Engineering. Warrendale, 1992.
- [13] Duffy James, Krick Russell. Modern Automotive Technology-Suspension System Fundamental. Goodheart-Wilcox Publisher Co., Illinois, 2004, pp. 1280-1301.
- [14] Eslaminasab Nima. Development of a Semi-active Intelligent Suspension System for Heavy Vehicles (2008). Doctoral thesis, University of Waterloo, Waterloo.

- [15] Fisher, R., Gscheidle, R., Heider, U., Hohmann , B., Keil, W., Mann, J., Schlogl, B., Wimmer, A., Wormer, G. *Fachkunde Kraftfahrzeugtechnik*, Europa Lehrmittel, Germany, 2009.
- [16] Güler Duygu. Dynamic analyses of double wishbone suspension (2006). Master thesis. Izmir Institute of Technology, Izmir.
- [17] <http://www.autoevolution.com/news/how-multi-link-suspension-works-7804.html/> [28.01.2012].
- [18] Lajqi Shpetim, Gugler Jürgen, Lajqi Naser, Shala Ahmet, Likaj Ramë: Experimental possibilities for determination of suspension parameters by the simplified model of passenger car. *International Journal of Automotive Technology* (2012), vol. 13, no. 4, pp. 615-621.
- [19] Senthil kumar Mouleeswaran. Genetic Algorithm – Based Proportional Derivative Controller for the Development of Active Suspension System. *Information Technology and Control* (2007), vol. 36, No. 1, pp. 58-67.
- [20] Wong Jo Yung. *Theory of Ground Vehicle*. John Wiley & Sons, Inc., New York, 2001.
- [21] Nekoui A. Mohammad, Hadavi Parisa. Optimal Control of an Active Suspension System. *14th International Power Electronics and Motion Control Conference* (2010), T5-60-T5-63.
- [22] Karnopp D. C., Crosby M. J., Harwood R. A. Vibration Control Using Semi-Active Force Generators. *ASME Journal of Engineering for Industry* (1974), vol. 96, no. 2, pp. 619-626.
- [23] Pajaziti Agron. Contribution in the Parametric Optimization of the Shock Absorber Characteristic with Regulation in Aspect of the Vibration Impact in the Comfort and Stability to the Passenger Vehicles (1992). Doctoral thesis. University of Prishtina, Prishtina.
- [24] Lin Jung-Shan, Kanellakopoulos Ioannis. Nonlinear design of active suspensions. *IEEE Control Systems Magazines* (1997), vol. 17, no. 3, pp.45-59.
- [25] Yi Kyongsu, Song S. Byung. Observer Design for Semi-active Suspension Control, *Vehicle System Dynamics* (1999), vol. 32, pp. 129-148.
- [26] Hong, K. S., Sohn H. C., Hedrick J. K. Modified Skyhook Control of Semi-active Suspension: A New Model, Gain Scheduling, and Hardware-in-the Loop Tuning. *ASME Journal of Dynamics System, Measuring and Control* (2002), vol. 124, no. 1, pp. 158-167.
- [27] Turnip Arjon, Hong Keum-Shik, Park Seonghun. Control of a Semi-Active MR-

- Damper Suspension System: A New Polynomial Model. *Proceedings of the 17th Word Congress. The International Federation of Automatic Control* (2008). Seoul, Korea, pp. 4683-4688.
- [28] Erjavec Jack. *Automotive Technology-A systems Approach*: 5th Edition. Delmar, Cengage Learning, 2010.
- [29] Mokhlespour Esfahani Mohammad Iman, Mosayebi Masoud, Pourshams Mohammad, Keshavarzi Ahmad. Optimization of Double Wishbone Suspension System with Variable Camber Angle by Hydraulic Mechanism, *World Academy of Science, Engineering and Technology* (2010), vol. 61, pp. 299-306.
- [30] Allred M. Timothy. Compliant mechanism system (2003). Master thesis. Brigham Young University.
- [31] Heo J-H, Lee U-K, Lee S-H. Development of a method to compute the kingpin axis using screw axis theory based on suspension-parameter-measuring device data. *Proceeding of the Institution of Mechanical Engineers, Part D: Journal Automobile Engineering* (2009), vol. 223, no. 4, pp.: 519-531.
- [32] Maher Damien. Combined Time and Frequency Domain Approaches to the Operational Identification of Vehicle Suspension Systems (2011). Doctoral thesis. Dublin City University, School of Mechanical and Manufacturing Engineering, Dublin 9.
- [33] Bouazara Mohamed, Richard Marc. An optimization method designed to improve 3-D vehicle comfort and road holding capability through the use of active and semi-active suspension. *European Journal of Mechanic-A/Solids* (2001), vol. 20, no. 3, pp. 509-520.
- [34] Gobbi M., Mastinu G. Analytical description and optimization of the dynamic behavior of passively suspended road vehicles. *Journal of Sound and Vibration* (2001), vol. 245, no. 3, pp. 457-481.
- [35] Baumal A.E., McPhee J.J., Calamai P.H. Application of Genetic Algorithms to the Design Optimization of an Active Vehicle Suspension System. *Computer Methods in Applied Mechanics and Engineering* (1998), vol. 163, pp. 87-94.
- [36] Alkhatib R., Jazar G.N., Golnaraghi M.F. Optimal Design of Passive Linear Suspension Using Genetic Algorithm. *Journal of Sound and Vibration* (2004), vol. 275, pp. 665-691.
- [37] Yu Hong Biao, Yu Nan. Application of Genetic Algorithms to Vehicle Suspension Design (2003). The Pennsylvania State University, University Park, pp. 1-9.
- [38] Heisler Heinz. *Advanced Vehicle Technology*. Butterworth Heinemann, Woburn, 2002, pp. 654.

- [39] <http://www.scribd.com/doc/34677412/mechanical-four-wheels-steering> [22.11.2011].
- [40] Alter M. David. Transient and Steady-State Performance Comparison of Two-Wheel-Steer and Four-Wheel-Steer Vehicle Models. Department of Mechanical and Industrial Engineering, University of Illinois at Urbana Champaign, Illinois, 1989, pp. 787-792.
- [41] Spentzas K., Alkhazali I., Demic M. Kinematic of four-wheel-steering vehicles. *Forschung in Ingenieurwesen* 66 (2001), Springer-Verlang, pp. 211-216.
- [42] Brabec P., Maly M., Vozenilek R. Controls system of vehicle model with four wheel steering (4WS), *International Scientific Meeting Motor Vehicles & Engines, Kragujevac* (2004), pp. 7.
- [43] Lee Jong-Nyun. Design sensitivity analysis of multi-body system with special references to four wheel steering. Department of Aerospace and Mechanical Engineering, University of Arizona, 2002, pp. 159.
- [44] Emura Takashi, Arakawa Akira. A New Steering Mechanism Using Noncircular Gears, *JSME International Journal*, (1992), vol. 35, no. 3, pp. 604-610.
- [45] Pahl Gerhard, Beitz Wolfgang, Feldhusen Jörg, Grote Kark-Heinrich. *Engineering Design: A systematic Approach*. Springer – 3rd edition, Berlin, 2007.
- [46] Mastinu Giampiero, Gobbi Massimiliano, Miano Carlo. *Optimal design of complex Mechanical Systems: With Application to Vehicle Engineering*. Springer, London, Berlin, 2006.
- [47] Balič Jože. *Contribution to integrated manufacturing*. DAAAM Publishing series, Vienna, 1999.
- [48] Mecitoglu Zahit. *Finite Element Analysis in Structures*. Faculty of Aeronautics and Astronautics, Maslak, Istanbul, 2008.
- [49] Sorić Jurica. *Metoda Konačnih Elemenata*. Sveučilište u Zagrebu, Zagreb, 2004.
- [50] Mackerle Jaroslav. FEM and BEM in the context of information retrieval. *Computer and Structures* (2002), vol. 80, no. 20-21, pp. 1595-1604.
- [51] Roylance David. *Finite Element Analysis*. Massachusetts Institute of Technology, Cambridge, 2001, pp. 1-16.
- [52] Lenart Sašo. Optimiranje oblike nastavnih čeljusti ročnih klešč. Magistersko delo. Universa v Mariboru, Fakulteta za stroništvo, Maribor, 2009.
- [53] Likaj Ramë, Shala Ahmet, Bruqi Mirlind, Qelaj Mehmet. Optimal design of quarter car vehicle suspension system. *TMT 2010 Conference Proceedings* (2010), pp. 417-420.
- [54] Reimpell Jörsen, Stoll Helmut, Betzler Jürgen. *The automotive Chassis: Engineering Principles*. Butterworth-Heinemann, London, 2001.

- [55] Werff Klaas. Kinematic and dynamic analysis of mechanisms, a finite element approach. Technical University of Delft, Nederland, 1977.
- [56] <http://www.workingmodel.com> / Working Model Software.
- [57] Happian-Smith Julian. *An introduction to Modern Vehicle Design*. Butterworth – Heinemann, Woburn, 2002.
- [58] <http://www.ptc.com/go/mathsoft> / MathCAD Software
- [59] Blundell Mike, Harty Damian. *The Multibody Systems Approach to Vehicle Dynamics*. Elsevier Butterworth-Heinemann, UK, 2004.
- [60] Popa Elena Cristina. Steering System and Suspension Design for 2005 Formula SAE-A Racer Car. University of Southern Queensland - Faculty of Engineering and Surveying, Australia, 2005.
- [61] Kegel M., Butinar B., Kegel B. An efficient gradient – based optimization algorithm for mechanical systems. *Commun. Numer. Meth. Eng.* (2002), vol. 18, pp. 363-371.
- [62] Pehan Stanislav, Kegl Breda, Pogorevc Primož. Developing a Racing Car. *Journal of Mechanical Engineering* (2003), vol. 49-12, pp. 593-606.
- [63] Kegl Breda, Marko Kegl, Stanislav Pehan. Optimization of a Fuel Injection System for Diesel and Biodiesel Usage. *Energy & Fuel* (2008), 22, pp. 1046-1054.
- [64] Kegl M., Antes H. Shape optimal design of elastic space frames with non linear response. *Int. J. Numer. Meth. Eng.* (1998), vol. 43, pp. 93-110.
- [65] Kegl M., Brank B. Shape optimization of truss-stiffened shell structures with variable thickness. *Comput. Methods Appl. Mech. Eng.* (2006), vol. 195, pp. 2611-2634.
- [66] Zidarič Ivan. Numerično optimiranje nosilnega okvira dirkalnega vozila. Magistersko delo. Universa v Mariboru, Fakulteta za stroništvo, Maribor, 2003.
- [67] STAKx-Version 2009.09.16. Copyright © by: Marko Kegl, Boštjan Harl. Faculty of Mechanical Engineering, University of Maribor & Boštjan Brank, Matija Gams. Faculty of Civil and Geodetic Engineering, University of Ljubljana.
- [68] iGOx – Version 2009.09.16. Copyright © by: Marko Kegl, Boštjan Harl. Faculty of Mechanical Engineering, University of Maribor.
- [69] Belingardi Giovanni, Demic Miroslav. A Contribution to Shock Absorber Modeling by Using “Black Box” Method. *Scientific Bulletin of Faculty of Mechanical and Technology, Automotive series* (2009), vol. 19, no. B, pp. 1-15.
- [70] Demic M., Diligenksi D., Demic I., Demic M. A method of active suspension design. *Forsch Ingenieurwes* (2006), vol. 70, pp. 145-158.

- [71] Ram Mohan Rao T., Venkata Rao G., Sreenivasa Rao K., Purushottam A. Analysis of Passive and Semi-active Controlled Suspension Systems for Ride Comfort in an Omnibus Passing Over a Speed Bump. *International Journal of Research and Reviews in Applied Science* (2010), vol. 5, no. 1, pp. 7-17.
- [72] Demic M. Optimization of the Oscillation Systems in Motor Vehicles. Faculty of Mechanical Engineering, Kragujevac, 1997.
- [73] Abramov Sergey, Mannan Samjid, Durieux Olivier. Semi-Active Suspension System Simulation Using Simulink. *International Journal of Engineering System. Modeling and Simulation* (2009), vol. 1, no. 2/3, pp. 101-114.
- [74] Sam Y. M., Osman J. H. S., Ghani M. R.A. Active Suspension Control: Performance Comparison using Proportional Integral Sliding Mode and Linear Quadratic Regulator Methods. *IEEE* (2000), pp. 274-278.
- [75] Lajqi Shpetim, Pehan Stanislav, Lajqi Naser, Baxhaku Bashkim, Ymeri Besim. Influences of the Suspension Parameters on the Vehicle Suspension Performance for a Terrain Vehicle. *Journal of Mechanics Engineering and Automation* (2012), vol. 2, no. 9, pp. 550-554.
- [76] Popp Karl, Schiehlen Werner, *Ground Vehicle Dynamics*. Springer, Verlang, Berlin Heidelberg, 2010.
- [77] Zhang D. Kinetostatic analysis and optimization of parallel and hybrid architectures for machine tools (2000), Doctoral thesis, University of Laval Quebec.
- [78] *Fundamental of Genetic Algorithms: AI Course Lecture 39 – 40*, (2012) pp. 42, Available at http://www.myreaders.info/html/artificial_intelligence.html/25/04/12.
- [79] Schaffer JD. Multiple objective optimization with vector evaluated genetic algorithms. *Proceedings of the International Conference on Genetic Algorithm and their applications* (1985), pp. 93-100.
- [80] Fonseca CM., Fleming PJ. Multi-objective genetic algorithms. *The Institution of Electric Engineers, IEE* (1993), London, pp. 1-5.
- [81] Kuznestov Alexey, Mammadov Musa, Sultan Ibrahim, Hajilarov Eldar. Optimization of improved suspension system with inerter device of the quarter-car model in vibration analyses. *Archive of Applied Mechanics* (2011), vol. 81, no. 10, pp. 1427-1437.
- [82] <http://eur-lex.europa.eu/LexUriServ/LexUriServ.do?uri=CELEX:31999L0007:en:NOT> / [12.09.2012].

- [83] Leishman C. Robert. Application of Variations Analysis Methods to Automotive Mechanisms (2009), Master thesis, Brigham Young University.
- [84] Alanoly J., Sankar S. A new concept in semi-active vibration isolation. *American Society of Mechanical Engineers, Journal of Mechanics, Transmissions and Automation in Design* (1987), pp. 242-247.
- [85] Adam Theander. Design of a Suspension for Formula Student Race Car (2004). Master thesis. Vehicle Dynamic Aeronautic and Vehicle Engineering Royal Institute of Technology, Stockholm.
- [86] Lajqi Shpetim, Pehan Stanislav, Pšeničnik Jože, Lajqi Naser. Tracking the prescribed path through an autonomous mobile robot with four wheel steering. *MOTSP 2011 Conference Proceedings* (2011), pp. 94-101.
- [87] Khurmi R., Gupta J. *Theory of Machines*. S Chand & Co Ltd, India, 2005.
- [88] Dormand, J. R., Prince P. J. A family of embedded Runge-Kutta formulae. *Journal Computational Applied Mathematics* (1980), vol. 6, no. 1, pp. 19-26.
- [89] Lu Ya Yan. Numerical Methods for Differential Equations. Department of Mathematic, City University of Hong Kong, Kowloon, Hong Kong, 2011.
- [90] Konak Abdullah, Coit W. David, Smith E. Alice. Multi-objective optimization using genetic algorithms: A tutorial. *Reliability Engineering & System Safety* (2006), 91, pp. 992-1007.
- [91] Zhao Sheng, Zhao Jing-Shan, Feng Zhi-Jing. Design of a Pair of Noncircular Gears Meeting Ackermannn Steering Principle. *IEEE* (2011), pp. 604-610.
- [92] Guglielmino E, Sireteanu T., Stammers Ch., Ghita G., Giuclea M. *Semi – active Suspension Control-Improved Vehicle Ride and Road Friendliness*: Published by Springer. London, UK, 2008, pp. 294.
- [93] Ginsberg H. Jerry. *Advanced engineering dynamics*. Published by Harper & Row. Ney York, USA, 1988, pp. 432.
- [94] Grujicic M., Arakere G., Bell W.C., Marvi H., Yalavarthy H.V., Pandurangan B., Haque I., Fadel G.M. Reliability - Based Design Optimization for Durability of Ground Vehicle Suspension System Components. *Journal of Materials Engineering and Performance* (2010), vol. 19, pp. 301-313.
- [95] Hao W., Shaoping W., Mileta M. T. Suspension mechanism simulation and optimization considering multiple disciplines. *Journal of Mechanical Science and Technology* (2009), vol. 23, pp. 100-108.

- [96] Grujicic M., Bell C W., Arakere G. Haque. Finite element analysis of the effect of up-armoring on the off-road braking and sharp-turn performance of a high-mobility multi-purpose wheeled vehicle. *Journal Automobile Engineering* (2009), vol. 223, Part D, pp. 1419-1434.
- [97] Pfeffer P. E., Harrer M., Johnston D. N. Interaction of vehicle and steering system regarding on-centre handling. *Vehicle System Dynamics* (2008), vol. 46, no. 5, pp. 413-428.
- [98] Uys P.E., Els P.S., Thoresson M. Suspension settings for optimal ride comfort of off-road vehicles travelling on roads with different roughness and speeds, Department of Mechanical and Aeronautical Engineering, University of Pretoria, Pretoria, 2007.
- [99] Pehan S., Kegl B. Top race car development. V: DAŠIĆ, Predrag (ur.). RaDMI 2007: proceedings on CD-ROM. Kruševac: Institute IMK "14. October"; Trstenik: High Technical Mechanical School, 2007, str. 27-35.
- [100] Hiroyasu O., Masashi T., Nobuaki K., Akira I., Katsuya I. Control for Four – Wheel Individual Steering and Four – Wheel Driven Electronic Vehicle. *Electrical Engineering in Japan* (2005), vol. 153, no. 3, pp. 71-78.
- [101] Pehan S., Kegl M., Vipavc D. Optimizacija položaja zgibov zadnje obese kolesa. V: Fajdiga, Matija (ur.), Klemenc, Jernej (ur.), Kostanjevec, Andrej (ur.). 7. konferenca in razstava Inovativna avtomobilska tehnologija IAT'05 Bled (2005), Zbornik referatov, (IAT, Inovativna avtomobilska tehnologija). Ljubljana: ULJ-FS-LAVEK: ZSIS-SVM, 2005, str. 367-378.
- [102] Kegl B., Pehan S. Computer aided development of a racing car. V: Budin, Leo (ur.), Ribarić, Slobodan (ur.). *Computers in technical systems. Intelligent systems:* proceedings of the joint conferences CTS+CIS: zbornik radova zajedničkih savjetovanja CTS+CIS. Rijeka: Hrvatska udruga za mikroprocesorske, procesne i informacijske sustave, mikroelektroniku i elektroniku - MIPRO HU, 2004, str. 75-81.
- [103] Bian X. L., Song B. A., Walter R. Optimization of steering linkage and double-wishbone suspension via R-W multi-body dynamic analysis, *Forschung im Ingenieurwesen* (2004), vol. 69, Springer-Verlag, pp. 38-43.
- [104] Pehan S., Kegl B. The modern race car suspension. V: MVM 04. Kragujevac: [s.n.], 2004, str. 381-392, MVM04-A52.

- [105] João P. G., Jorge C. A.: Optimization of Vehicle Suspension Systems for Improved Comfort of Road Vehicles Using Flexible Multi body Dynamics, Nonlinear Dynamics 34: 2003. Kluwer Academic Publishers, Printed in the Netherlands, pp. 113-131.
- [106] Zidarič I., Pehan S., Kegl M.: Numerično optimiranje šasije dirkalnega vozila FS-03. V: Fajdiga, Matija (ur.), Klemenc, Jernej (ur.), Kostanjevec, Andrej (ur.), TRENC, Ferdinand (ur.). 6. konferenca IAT'03, Koper/Portorož, Slovenija, 24.-25. april 2003. Zbornik referatov, (IAT, Inovativna avtomobilska tehnologija). Ljubljana: ZSITS, SVM: Fakulteta za strojništvo, LAVEK, 2003, str. 387-394.
- [107] Pehan, Stanislav, Kegl, Breda, Pogorevc, Primož. Oblikovanje dirkalnika - Developing a racing car. *Stroj. vestn.* (2003), letn. 49, št. 12, str. 593-606.
- [108] Pehan S., Kegl B.: Design of formula student racer. V: Marjanović, Dorian (ur.). *Proceedings of the 6th International Design Conference DESIGN* (2000), Cavtat, Dubrovnik, Croatia, Zagreb: Centre of Technology Transfer: Faculty of Mechanical Engineering and Naval Architecture; Zürich: Workshop Design-Konstruktion, 2000, str. 483-488.
- [109] Madhusudan R.: Number and dimensional synthesis of independent suspension mechanisms. *Mech. Mach. Theory* (1996), vol. 31, no. 8, pp. 1141-1153.
- [110] Pehan S.: *Metodika konstruiranja*. Fakulteta za strojništvo, 2005. X, 218 str., graf. prikazi. ISBN 86-435-0710-5.
- [111] Tuan – Ahn N.: Application of Optimization Methods to Controller Design for Active Suspensions. Doctoral Thesis. Cottbus, Germany, 2006.
- [112] Michael J. Th.: Mathematical Optimization of the Suspension System of an Off Road Vehicle for Ride Comfort and Handling, University of Pretoria, November 2003, Master Thesis, pages 110.

Appendices

Appendix A: Free Body Diagrams and Forces That Act in Mechanism

The free body diagrams and forces that act in components of the suspension mechanism are presented in Figure A.1, Figure A.2 and Figure A.3.

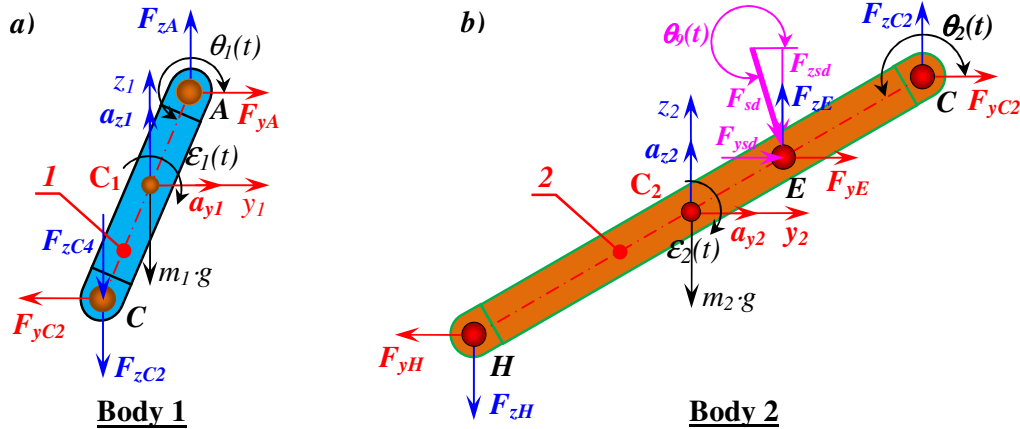


Figure A.1: Free - body diagram; a) Body 1, and b) Body 2

Dynamic equation of motion for **Body 1 – Revolute joints A & C** (Figure A.1.a):

$$m_1 \cdot a_{y1} = \sum F_{yi}; \Rightarrow m_1 \cdot a_{y1} = F_{yA} - F_{yC2}, \quad (\text{A.1})$$

$$m_1 \cdot a_{z1} = \sum F_{zi}; \Rightarrow m_1 \cdot a_{z1} = F_{zA} - F_{zC2} - F_{zC4} - m_1 \cdot g, \quad (\text{A.2})$$

$$J_{c1} \cdot \dot{\epsilon}_1 = \sum^{+CG} M_{xi}; \Rightarrow J_{c1} \cdot \dot{\epsilon}_1(t) = F_{yA} \cdot b_1 - F_{zA} \cdot b_2 + F_{yC2} \cdot b_1 - F_{zC2} \cdot b_2 - F_{zC4} \cdot b_2, \quad (\text{A.3})$$

when a_1 and a_2 are substitution by expressions:

$$b_1 = b_1(t) = \frac{\overline{AC}}{2} \cdot \sin(\theta_1(t)); \quad b_2 = b_2(t) = \frac{\overline{AC}}{2} \cdot \cos(\theta_1(t)). \quad (\text{A.4})$$

Dynamic equation of motion for **Body 2 – Revolute joints C, E & H** (Figure A.1.b):

$$m_2 \cdot a_{y2} = \sum F_{yi}; \Rightarrow m_2 \cdot a_{y2} = F_{yC2} + F_{yE} + F_{ysd} - F_{yH}, \quad (\text{A.5})$$

$$m_2 \cdot a_{z2} = \sum F_{zi}; \Rightarrow m_2 \cdot a_{z2} = F_{zC2} + F_{zE} - F_{zsd} - F_{zH} - m_2 \cdot g, \quad (\text{A.6})$$

$$J_{c2} \cdot \dot{\epsilon}_2 = \sum^{+CG} M_{xi}; \Rightarrow J_{c2} \cdot \dot{\epsilon}_2(t) = F_{yH} \cdot c_1 - F_{zH} \cdot c_2 + F_{yC2} \cdot c_1 \dots \\ - F_{zC2} \cdot c_2 + F_{yE} \cdot c_3 + F_{ysd} \cdot c_3 + F_{zsd} \cdot c_4 - F_{zE} \cdot c_4. \quad (\text{A.7})$$

when b_1, b_2, b_3 and b_4 are substitution by expressions:

$$c_1 = c_1(t) = \frac{\overline{CH}}{2} \cdot \sin(\theta_2(t)); \quad c_2 = c_2(t) = \frac{\overline{CH}}{2} \cdot \cos(\theta_2(t)), \quad (\text{A.8})$$

$$c_3 = c_3(t) = \left(\frac{\overline{CH}}{2} - \overline{CE} \right) \cdot \sin(\theta_2(t)); \quad c_4 = c_4(t) = \left(\frac{\overline{CH}}{2} - \overline{CE} \right) \cdot \cos(\theta_2(t)). \quad (\text{A.9})$$

Referring back to the discussion of spring & damper forces given by expressions in chapter 5, again remind that for a linear formulation based on the spring stiffness (k_s), length of spring (L_s) and the shock absorber damping coefficient (c_{sh}), can formulate the spring & damper forces (F_{sd}), which is given by expressions:

$$\begin{aligned} F_{ysd} &= F_{sd} \cdot \cos(\theta_9(t)) = \{k_s \cdot [L_s - L_s(\text{def})] - c_{sh} \cdot v_{Ls}\} \cdot \cos(\theta_9(t)), \\ F_{zsd} &= F_{sd} \cdot \sin(\theta_9(t)) = \{k_s \cdot [L_s - L_s(\text{def})] - c_{sh} \cdot v_{Ls}\} \cdot \sin(\theta_9(t)). \end{aligned} \quad (\text{A.10})$$

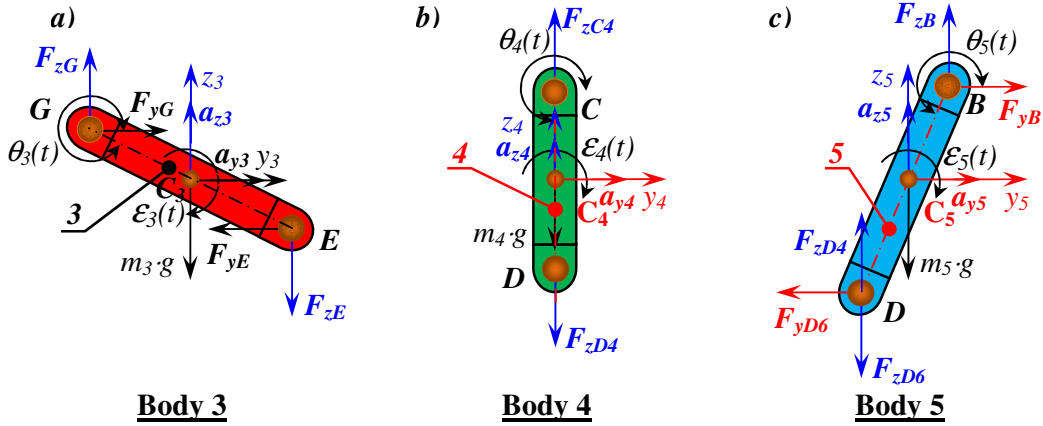


Figure A.2: Free - body diagram; a) Body 3, b) Body 4, and c) Body 5

Dynamic equation of motion for **Body 3 – Revolute joints E & G** (Figure A.2.a):

$$m_3 \cdot a_{y3} = \sum F_{yi}; \Rightarrow m_3 \cdot a_{y3} = F_{yG} - F_{yE}, \quad (\text{A.11})$$

$$m_3 \cdot a_{z3} = \sum F_{zi}; \Rightarrow m_3 \cdot a_{z3} = F_{zG} - F_{zE} - m_3 \cdot g, \quad (\text{A.12})$$

$$J_{c3} \cdot \boldsymbol{\varepsilon}_3 = \sum^{+CG} M_{x3}; \Rightarrow J_{c3} \cdot \boldsymbol{\varepsilon}_3(t) = F_{yG} \cdot d_1 + F_{zG} \cdot d_2 + F_{yE} \cdot d_1 + F_{zE} \cdot d_2. \quad (\text{A.13})$$

when c_1 and c_2 are substitution by expressions:

$$d_1 = d_1(t) = \frac{\overline{EG}}{2} \cdot \sin(\theta_3(t)); \quad d_2 = d_2(t) = \frac{\overline{EG}}{2} \cdot \cos(\theta_3(t)). \quad (\text{A.14})$$

Dynamic equation of motion for **Body 4 – Revolute joints C & D** (Figure A.2.b):

$$m_4 \cdot a_{y4} = \sum F_{yi}; \Rightarrow m_4 \cdot a_{y4} = 0, \quad (\text{A.15})$$

$$m_4 \cdot a_{z4} = \sum F_{zi}; \Rightarrow m_4 \cdot a_{z4} = F_{zC4} - F_{zD4} - m_4 \cdot g, \quad (\text{A.16})$$

$$J_{c4} \cdot \boldsymbol{\varepsilon}_4 = \sum^{+CG} M_{x4}; \Rightarrow J_{c4} \cdot \boldsymbol{\varepsilon}_4(t) = 0. \quad (\text{A.17})$$

when d_1 and d_2 are substitution by expressions:

$$e_1 = e_1(t) = \frac{\overline{CD}}{2} \cdot \sin(\theta_4(t)); \quad e_2 = e_2(t) = \frac{\overline{CD}}{2} \cdot \cos(\theta_4(t)). \quad (\text{A.18})$$

Dynamic equation of motion for **Body 5 – Revolute joints B & D** (Figure A.2.c):

$$m_5 \cdot a_{y5} = \sum F_{yi}; \Rightarrow m_5 \cdot a_{y5} = F_{yB} - F_{yD6}, \quad (\text{A.19})$$

$$m_5 \cdot a_{z5} = \sum F_{zi}; \Rightarrow m_5 \cdot a_{z5} = F_{zB} + F_{zD4} - F_{zD6} - m_5 \cdot g, \quad (\text{A.20})$$

$$J_{c5} \cdot \varepsilon_5 = \sum M_{xi}; \Rightarrow J_{c5} \cdot \varepsilon_5(t) = F_{yB} \cdot f_1 - F_{zB} \cdot f_2 + F_{yD6} \cdot f_1 - F_{zD6} \cdot f_2 + F_{zD4} \cdot f_2. \quad (\text{A.21})$$

when e_1 and e_2 are substitution by expressions:

$$f_1 = f_1(t) = \frac{\overline{BD}}{2} \cdot \sin(\theta_5(t)); \quad f_2 = f_2(t) = \frac{\overline{BD}}{2} \cdot \cos(\theta_5(t)). \quad (\text{A.22})$$

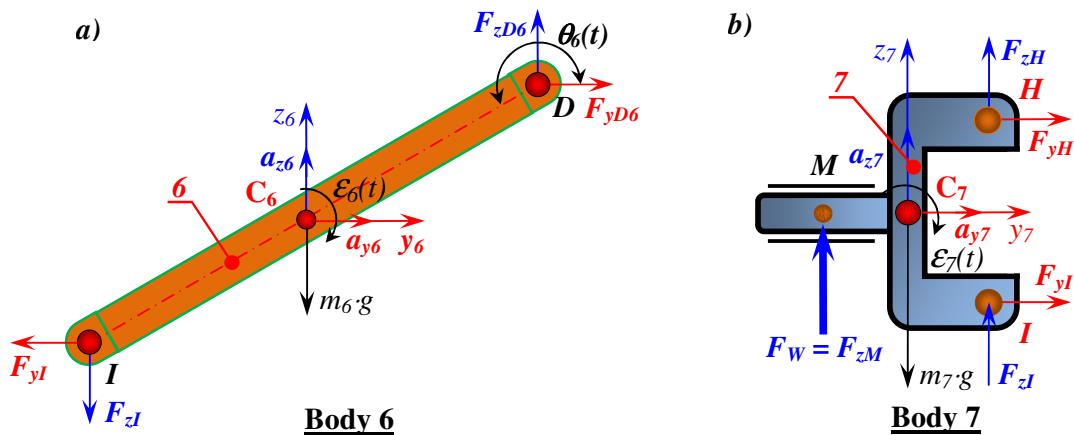


Figure A.3: Free - body diagram for dynamic analysis of the; a) Body 6, and b) Body 7

Dynamic equation of motion for **Body 6 – Revolute joints D & I** (Figure A.3.a):

$$m_6 \cdot a_{y6} = \sum F_{yi}; \Rightarrow m_6 \cdot a_{y6} = F_{yD6} - F_{yI}, \quad (\text{A.23})$$

$$m_6 \cdot a_{z6} = \sum F_{zi}; \Rightarrow m_6 \cdot a_{z6} = F_{zD6} - F_{zI} - m_6 \cdot g, \quad (\text{A.24})$$

$$J_{c6} \cdot \varepsilon_6 = \sum M_{xi}; \Rightarrow J_{c6} \cdot \varepsilon_6(t) = F_{yI} \cdot g_1 - F_{zI} \cdot g_2 + F_{yD6} \cdot g_1 - F_{zD6} \cdot g_2. \quad (\text{A.25})$$

when f_1 and f_2 are substitution by expressions:

$$g_1 = g_1(t) = \frac{\overline{DI}}{2} \cdot \sin(\theta_6(t)); \quad g_2 = g_2(t) = \frac{\overline{DI}}{2} \cdot \cos(\theta_6(t)). \quad (\text{A.26})$$

Dynamic equation of motion for **Body 7 – Revolute joints I & H** (Figure A.3.b):

$$m_7 \cdot a_{y7} = \sum F_{yi}; \Rightarrow m_7 \cdot a_{y7} = F_{yH} + F_{yI}, \quad (\text{A.27})$$

$$m_7 \cdot a_{z7} = \sum F_{zi}; \Rightarrow m_7 \cdot a_{z7} = F_{zH} + F_{zI} + F_w - m_7 \cdot g, \quad (\text{A.28})$$

$$J_{c7} \cdot \varepsilon_7 = \sum^{+CG} M_{x7}; \Rightarrow J_{c7} \cdot \varepsilon_7(t) = F_{yH} \cdot h_1 - F_{zH} \cdot h_2 + F_w \cdot h_1 - F_{yI} \cdot h_1 - F_{zI} \cdot h_2. \quad (\text{A.29})$$

when f_1 and f_2 are substitution by expressions:

$$h_1 = \frac{\overline{HI}}{2}; \quad h_2 = \frac{\overline{HM}}{2} \quad (\text{A.30})$$

So, we have 21 equations with 21 unknown. Suitable ways to solve these equations is their presentation in the matrix form, presented below:

$$A(t) \cdot X(t) = B(t) \quad (\text{A.31})$$

For finding unknowns reaction forces $X(t)$ it is required the equation (A.31) to transfer in matrix form, given by expression:

$$X(t) = [A(t)]^{-1} \cdot B(t) \quad (\text{A.32})$$

Equation (A.32) enables to find the unknowns reaction forces that act in suspension mechanism by using appropriate software such as MathCAD, MATLAB, etc. Elements in matrix $A(t)$ and $B(t)$ are parameters which are defined and are in function of the ground excitation by changing on the time. Therefore, unknown reactions forces are also in function of the time.

$$A(t) = \begin{bmatrix} 1 & 0 & 0 & 0 & -1 & 0 & 0 & 0 & 0 & 0 & 0 & 0 & 0 & 0 & 0 & 0 & 0 & 0 & 0 & 0 & 0 & 0 \\ 0 & 1 & 0 & 0 & 0 & -1 & 0 & -1 & 0 & 0 & 0 & 0 & 0 & 0 & 0 & 0 & 0 & 0 & 0 & 0 & 0 & 0 & 0 \\ b_1 & -b_2 & 0 & 0 & b_1 & -b_2 & 0 & -b_2 & 0 & 0 & 0 & 0 & 0 & 0 & 0 & 0 & 0 & 0 & 0 & 0 & 0 & 0 & 0 \\ 0 & 0 & 0 & 0 & 1 & 0 & 0 & 0 & 0 & 0 & 0 & 0 & 1 & 0 & 0 & 0 & 0 & -1 & 0 & 0 & 0 & 0 & 0 \\ 0 & 0 & 0 & 0 & 0 & 1 & 0 & 0 & 0 & 0 & 0 & 0 & 0 & 1 & 0 & 0 & 0 & -1 & 0 & 0 & 0 & 0 & 0 \\ 0 & 0 & 0 & 0 & c_1 & -c_2 & 0 & 0 & 0 & 0 & 0 & 0 & c_3 & -c_4 & 0 & 0 & c_1 & -c_2 & 0 & 0 & 0 & 0 & 0 \\ 0 & 0 & 0 & 0 & 0 & 0 & 0 & 0 & 0 & 0 & 0 & 0 & -1 & 0 & 1 & 0 & 0 & 0 & 0 & 0 & 0 & 0 & 0 \\ 0 & 0 & 0 & 0 & 0 & 0 & 0 & 0 & 0 & 0 & 0 & 0 & 0 & -1 & 0 & 1 & 0 & 0 & 0 & 0 & 0 & 0 & 0 \\ 0 & 0 & 0 & 0 & 0 & 0 & 0 & 0 & 0 & 0 & 0 & 0 & 0 & 0 & -1 & 0 & 1 & 0 & 0 & 0 & 0 & 0 & 0 \\ 0 & 0 & 0 & 0 & 0 & 0 & 0 & 0 & 0 & 0 & 0 & 0 & d_1 & d_2 & d_1 & d_2 & 0 & 0 & 0 & 0 & 0 & 0 & 0 \\ 0 & 0 \\ A(t) = & 0 & 0 & 0 & 0 & 0 & 0 & 0 & 1 & 0 & 1 & 0 & 0 & 0 & 0 & 0 & 0 & 0 & 0 & 0 & 0 & 0 & 0 & 0 \\ 0 & 0 \\ 0 & 0 & 0 & 1 & 0 & 0 & 0 & 0 & 0 & 0 & 0 & -1 & 0 & 0 & 0 & 0 & 0 & 0 & 0 & 0 & 0 & 0 & 0 & 0 \\ 0 & 0 & 0 & 0 & 1 & 0 & 0 & 0 & 0 & 0 & 1 & 0 & -1 & 0 & 0 & 0 & 0 & 0 & 0 & 0 & 0 & 0 & 0 & 0 \\ 0 & 0 & 0 & f_1 & -f_2 & 0 & 0 & 0 & 0 & f_2 & f_1 & -f_2 & 0 & 0 & 0 & 0 & 0 & 0 & 0 & 0 & 0 & 0 & 0 & 0 \\ 0 & 0 & 0 & 0 & 0 & 0 & 0 & 0 & 0 & 0 & 0 & 1 & 0 & 0 & 0 & 0 & 0 & 0 & 0 & 0 & -1 & 0 & 0 & 0 \\ 0 & 0 & 0 & 0 & 0 & 0 & 0 & 0 & 0 & 0 & 0 & 0 & 1 & 0 & 0 & 0 & 0 & 0 & 0 & 0 & 0 & 1 & 0 & 0 \\ 0 & 0 & 0 & 0 & 0 & 0 & 0 & 0 & 0 & 0 & 0 & g_1 & -g_2 & 0 & 0 & 0 & 0 & 0 & 0 & 0 & g_1 & -g_2 & 0 & 0 \\ 0 & 0 & 0 & 0 & 0 & 0 & 0 & 0 & 0 & 0 & 0 & 0 & 0 & 0 & 0 & 0 & 0 & 0 & 1 & 0 & 1 & 0 & 0 & 0 \\ 0 & 1 & 0 & 1 & 1 \\ 0 & h_1 & -h_2 & -h_1 & -h_2 & h_2 \end{bmatrix}$$

$$X(t) = \begin{bmatrix} F_{yA}(t) \\ F_{zA}(t) \\ F_{yB}(t) \\ F_{zB}(t) \\ F_{yC2}(t) \\ F_{zC2}(t) \\ F_{yC4}(t) \\ F_{zC4}(t) \\ F_{yD4}(t) \\ F_{zD4}(t) \\ F_{yD6}(t) \\ F_{zD6}(t) \\ F_{yE}(t) \\ F_{zE}(t) \\ F_{yG}(t) \\ F_{zG}(t) \\ F_{yH}(t) \\ F_{zH}(t) \\ F_{yI}(t) \\ F_{zI}(t) \\ F_w(t) \end{bmatrix} \quad B(t) = \begin{bmatrix} m_1 \cdot a_{y1}(t) \\ m_1 \cdot a_{z1}(t) + m_1 \cdot g \\ J_{c1} \cdot \varepsilon_1(t) \\ m_2 \cdot a_{y2}(t) - F_{ysd}(t) \\ m_2 \cdot a_{z2}(t) + m_2 \cdot g + F_{zs}(t) \\ J_{c2} \cdot \varepsilon_2(t) - F_{ysd}(t) \cdot b_3 - F_{zs}(t) \cdot b_4 \\ m_3 \cdot a_{y3}(t) \\ m_3 \cdot a_{z3}(t) + m_3 \cdot g \\ J_{c3} \cdot \varepsilon_3(t) \\ m_4 \cdot a_{y4}(t) \\ m_4 \cdot a_{z4}(t) + m_4 \cdot g \\ J_{c4} \cdot \varepsilon_4(t) \\ m_5 \cdot a_{y5}(t) \\ m_5 \cdot a_{z5}(t) + m_5 \cdot g \\ J_{c5} \cdot \varepsilon_5(t) \\ m_6 \cdot a_{y6}(t) \\ m_6 \cdot a_{z6}(t) + m_6 \cdot g \\ J_{c6} \cdot \varepsilon_6(t) \\ m_7 \cdot a_{y7}(t) \\ m_6 \cdot a_7(t) + m_7 \cdot g \\ J_{c7} \cdot \varepsilon_7(t) \end{bmatrix}$$

Determining of the projection of the reaction forces in x and y axis and total reaction forces in each joint of the suspension mechanism is written by the following expression:

$$F_j(t) = \sqrt{(F_{yj})^2 + (F_{zj})^2} \quad (\text{A.33})$$

where "j" are joint of suspension mechanism such as $A, B, C_2, C_4, D_4, D_6, E, F, G, H$ and I joint. Solution of the unknowns' reaction forces will be obtained in a function of time when wheels of the vehicle moves from minimal (-250 mm) to maximal (+250 mm) values as a consequence of the vertical wheel force act on the suspension mechanism. Other determined forces which act in the suspension mechanism except reaction forces are spring forces, damper forces and gravity forces of the mechanism linkages.

Following, in appropriate proportion are presented results of unknown reaction forces for parameters given in table 5.6 through the relevant diagrams in function of the time.

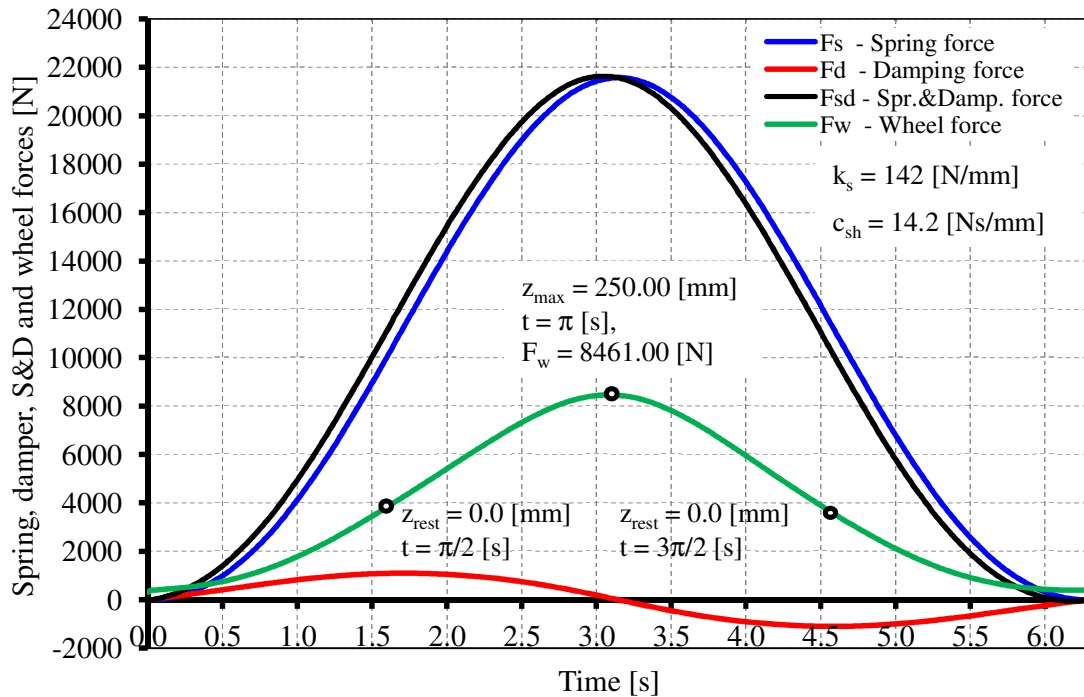


Figure A.4: Spring, damper, spring & damper and wheel forces as a function of time

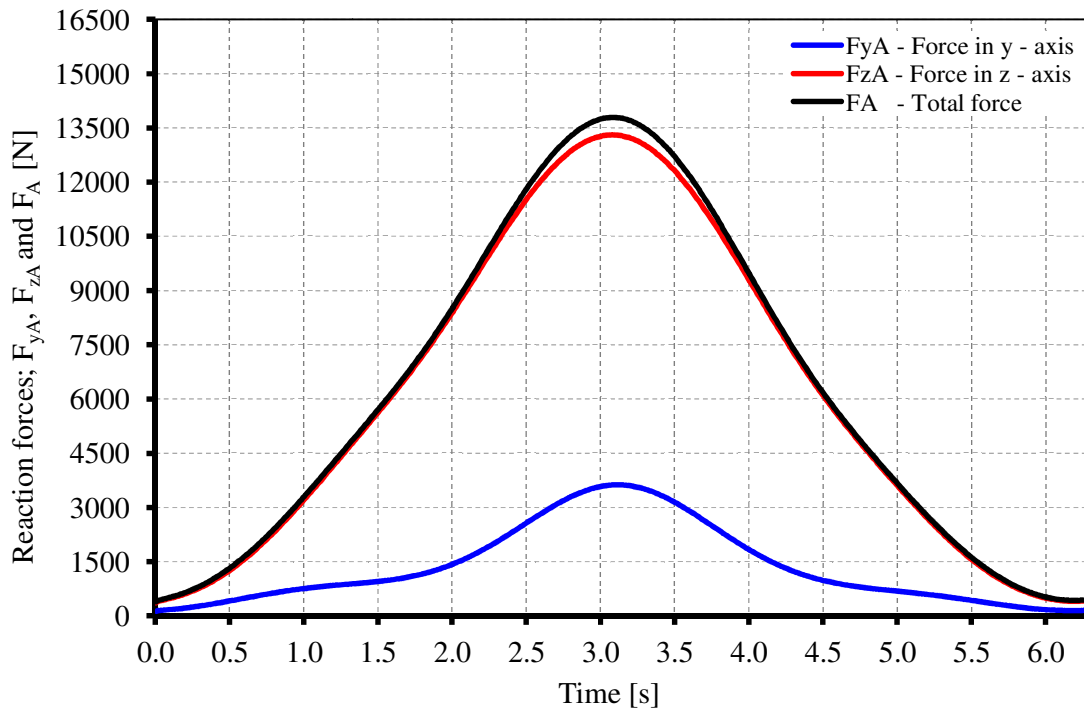
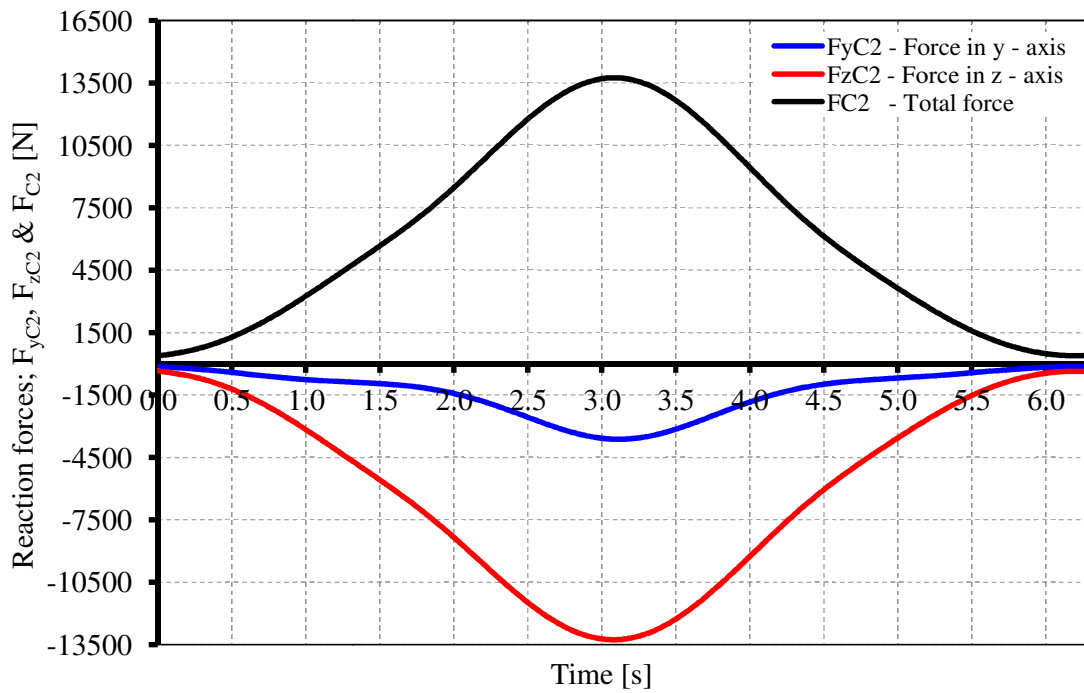
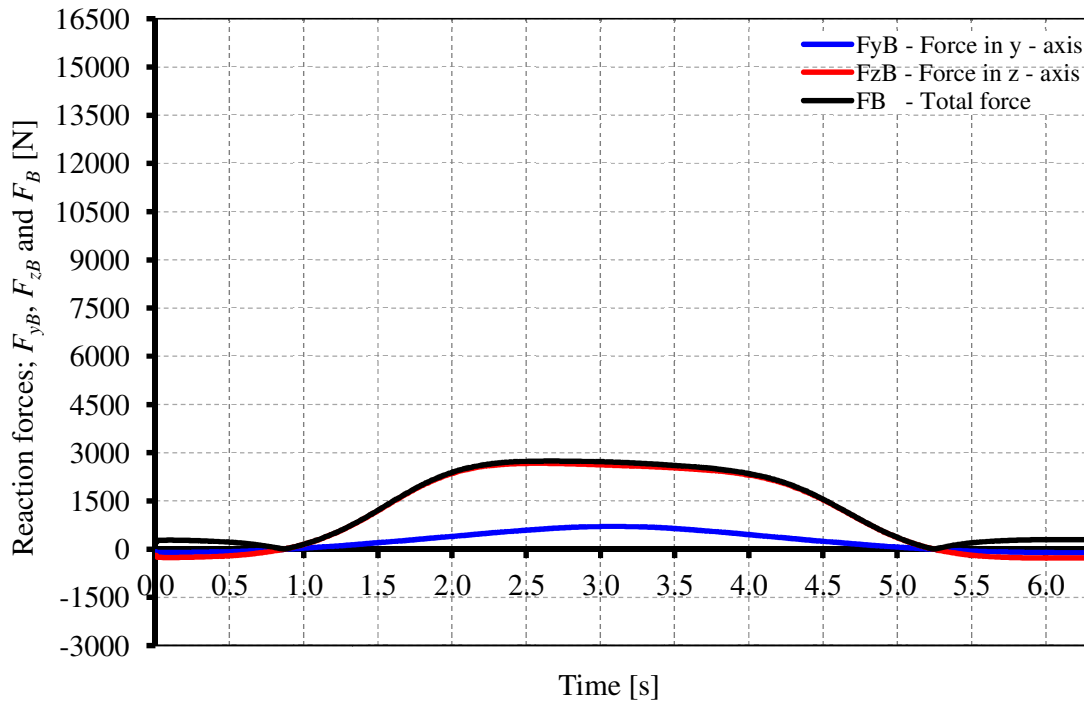


Figure A.5: Reaction forces in the joint A as a function of time

**Figure A.6:** Reaction forces in the joint C_2 as a function of the time**Figure A.7:** Reaction forces in the joint B as a function of time

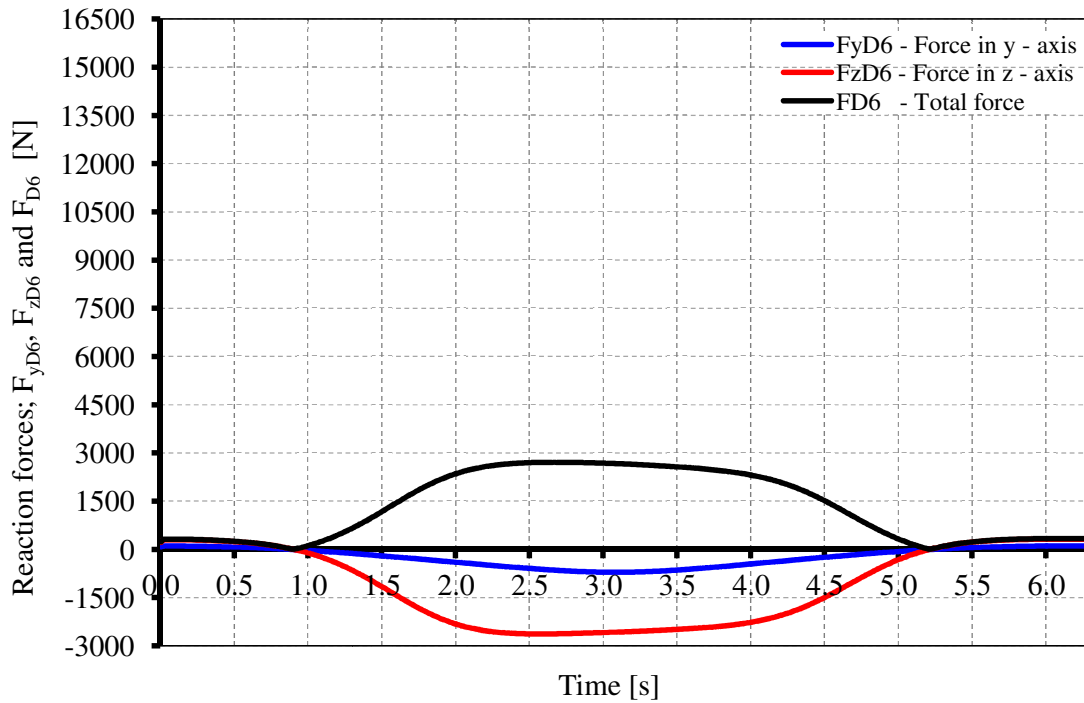


Figure A.8: Reaction forces in the joint D_6 as a function of time

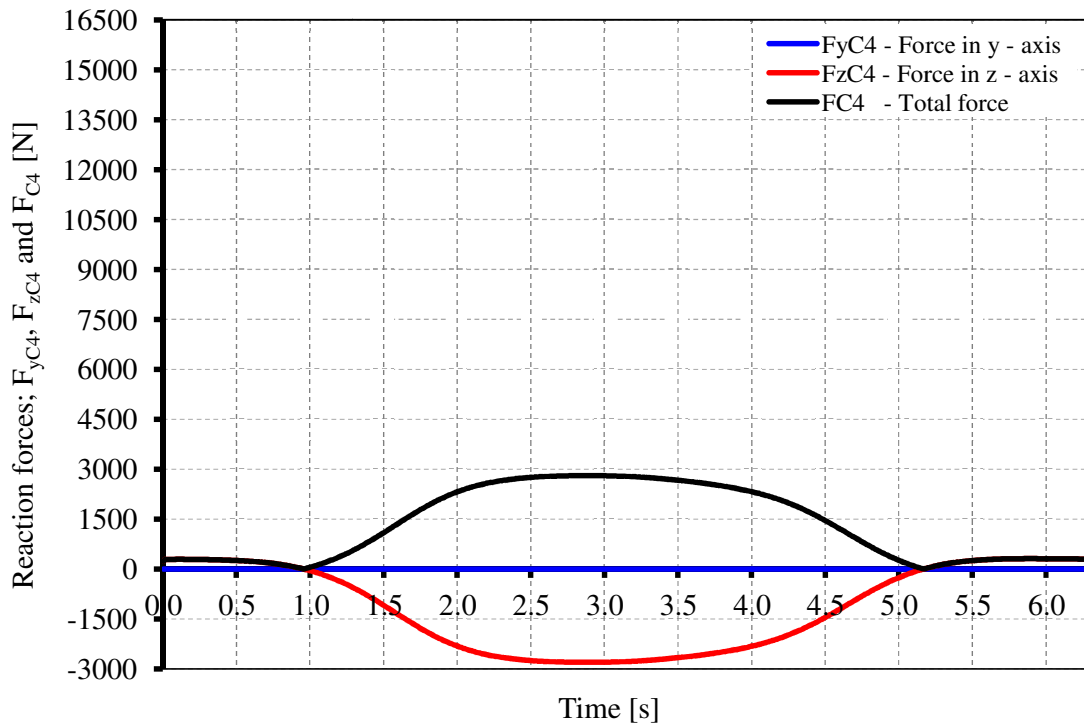


Figure A.9: Reaction forces in the joint C_4 as a function of time

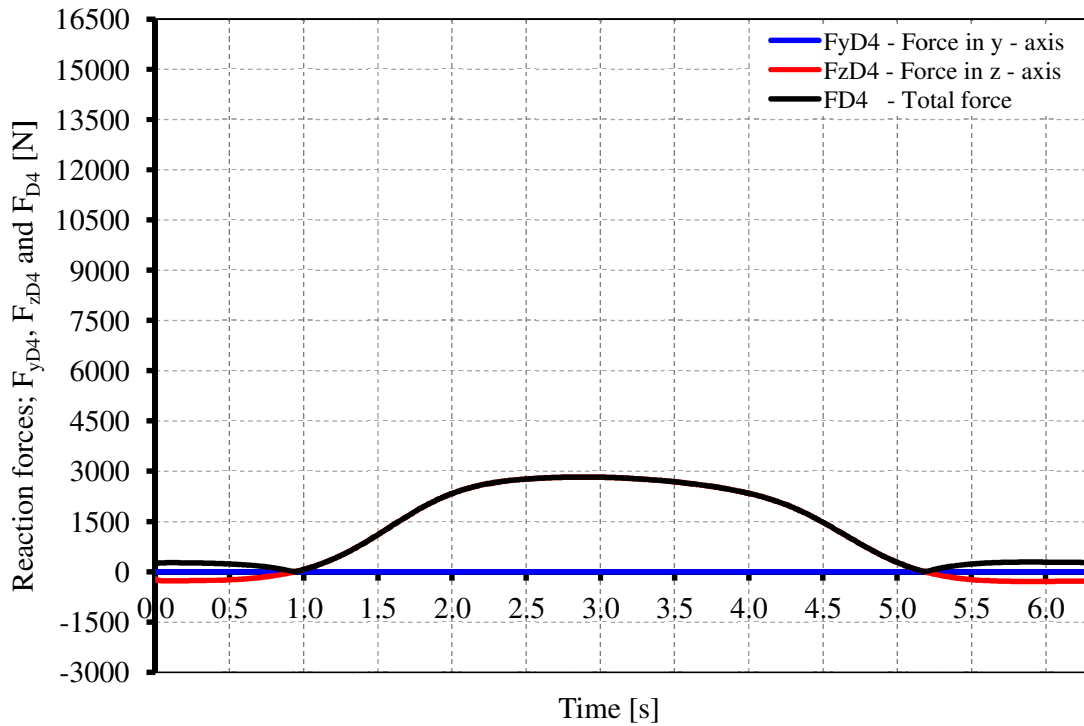


Figure A.10: Reaction forces in the joint D_4 as a function of time

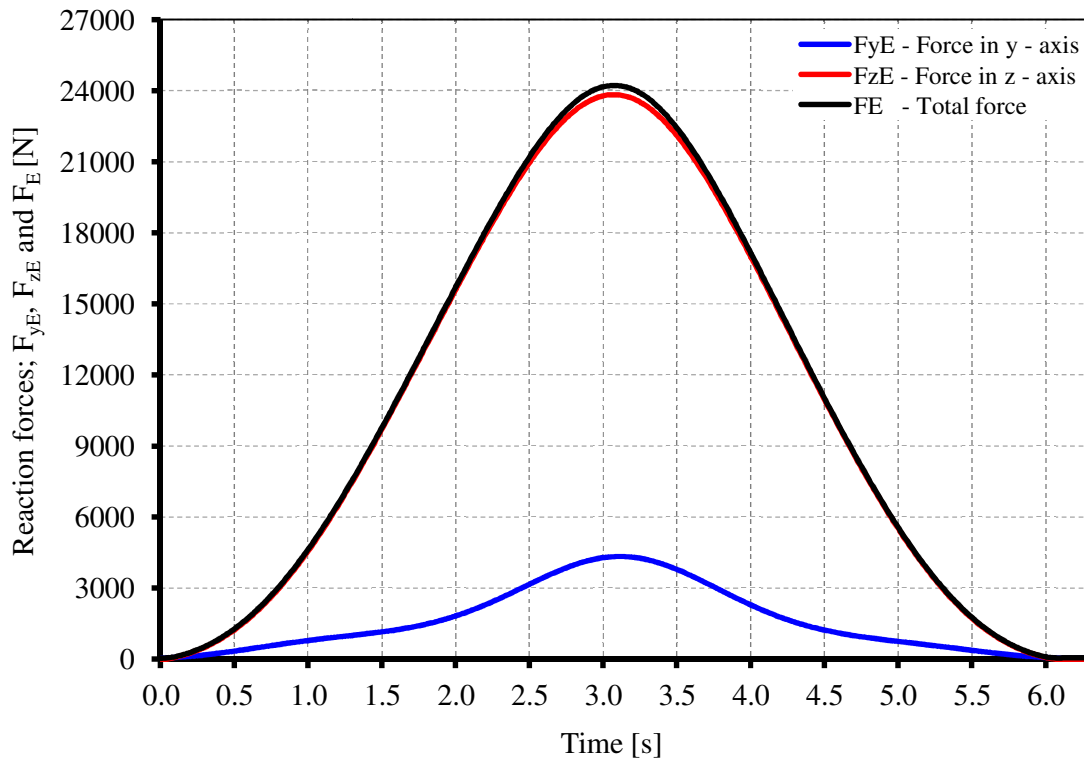
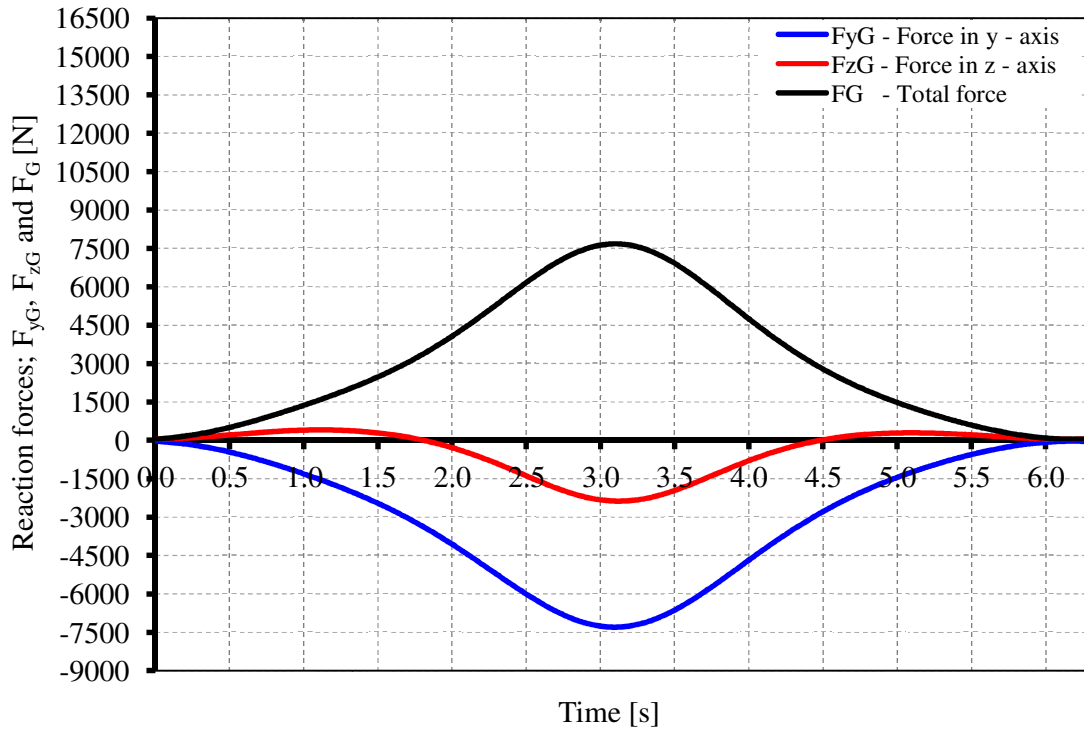
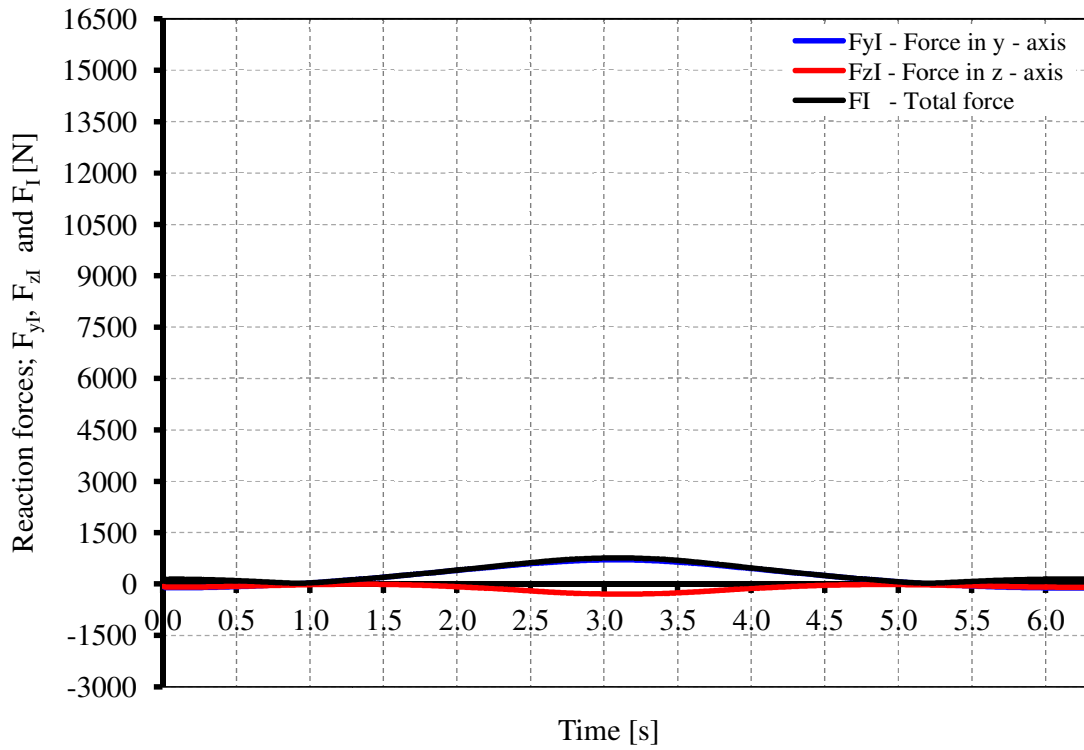


Figure A.11: Reaction forces in the joint E as a function of the time

**Figure A.12:** Reaction forces in the joint G as a function of time**Figure A.13:** Reaction forces in the joint I as a function of the time

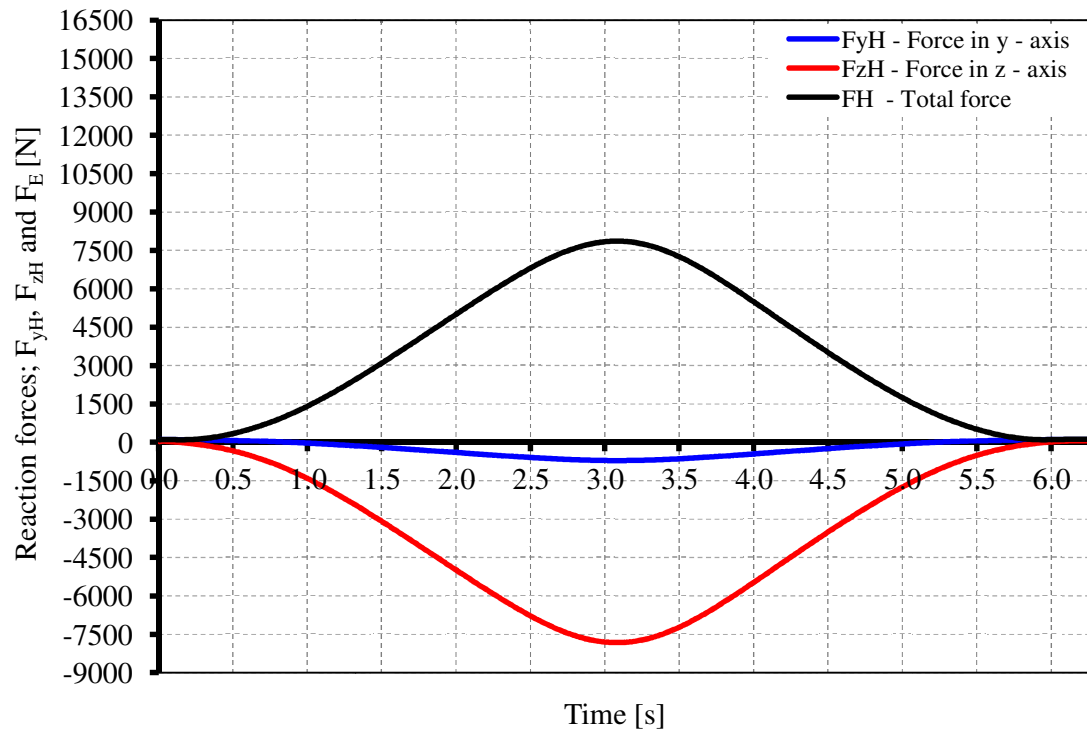
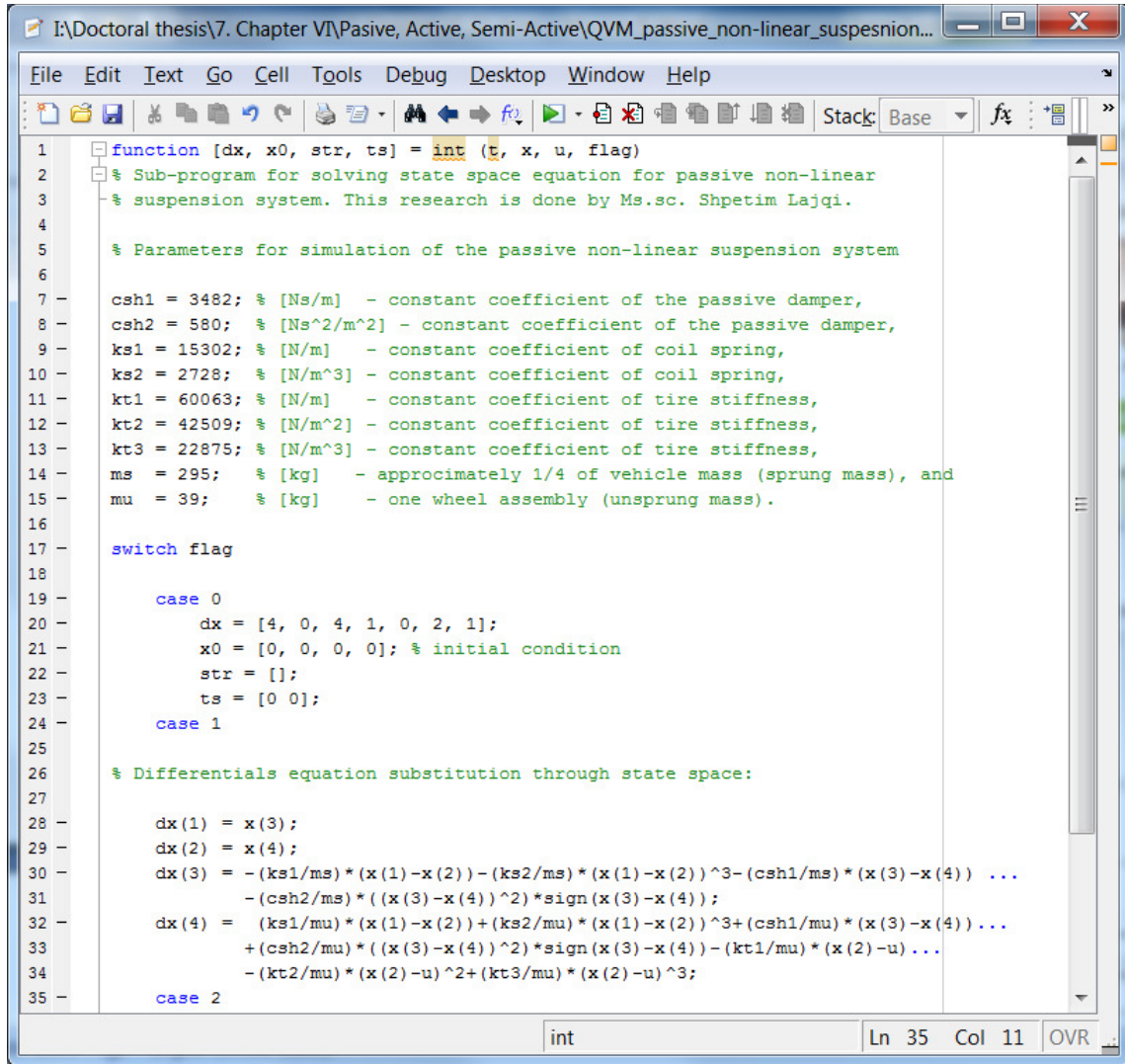


Figure A.14: Reaction forces in the joint H as a function of the time

Appendix B: Simulation and Optimization of the Suspension Parameters for Passive, Semi-active and Active System for a Terrain Vehicle



The screenshot shows a MATLAB code editor window with the following details:

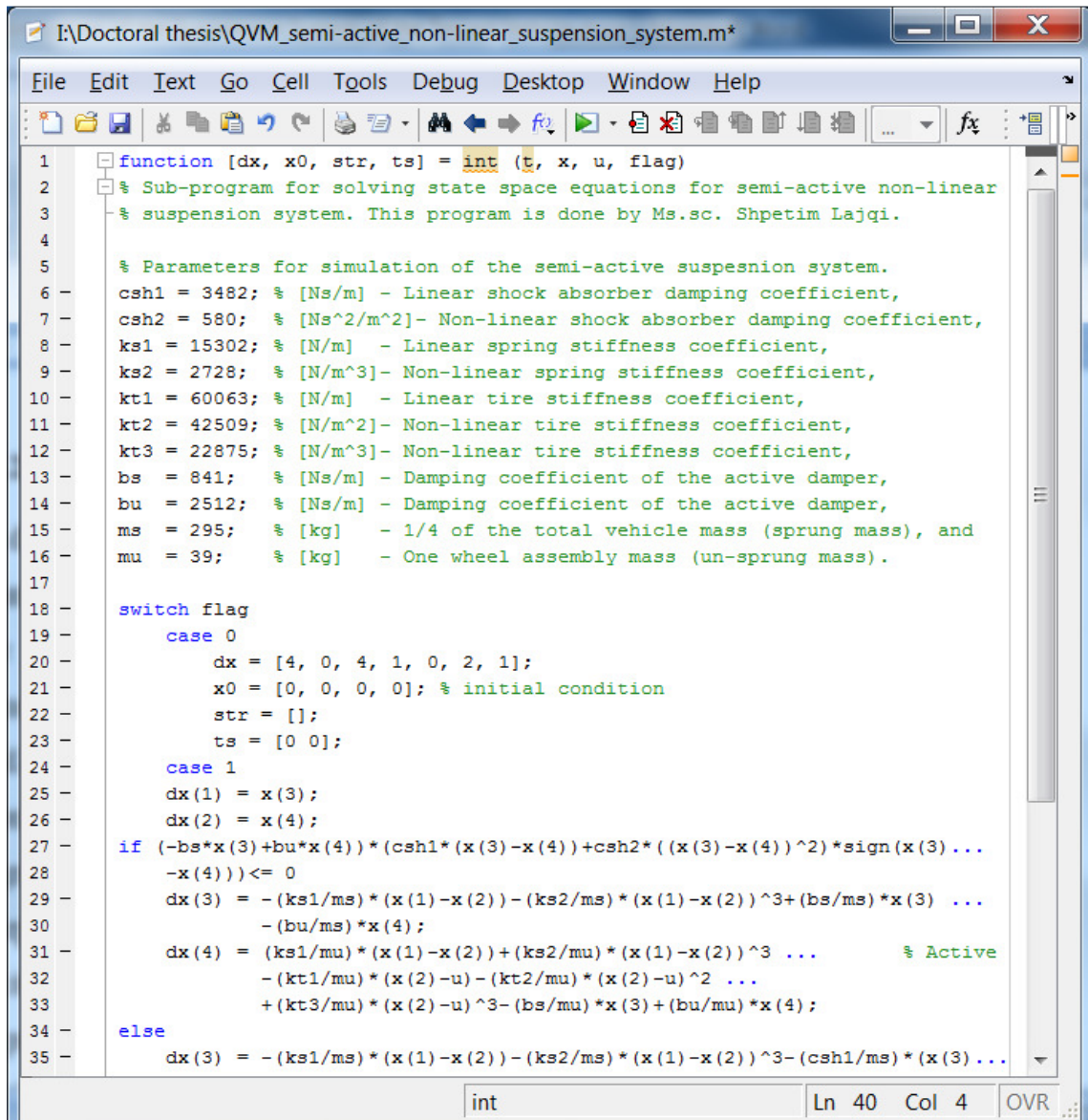
- Title Bar:** I:\Doctoral thesis\7. Chapter VI\Pasive, Active, Semi-Active\QVM_passive_non-linear_suspension...
- Menu Bar:** File, Edit, Text, Go, Cell, Tools, Debug, Desktop, Window, Help.
- Toolbar:** Standard MATLAB toolbar icons.
- Code Area:**

```

1 function [dx, x0, str, ts] = int(t, x, u, flag)
2 % Sub-program for solving state space equation for passive non-linear
3 % suspension system. This research is done by Ms.sc. Shpetim Lajqi.
4
5 % Parameters for simulation of the passive non-linear suspension system
6
7 csh1 = 3482; % [Ns/m] - constant coefficient of the passive damper,
8 csh2 = 580; % [Ns^2/m^2] - constant coefficient of the passive damper,
9 ks1 = 15302; % [N/m] - constant coefficient of coil spring,
10 ks2 = 2728; % [N/m^3] - constant coefficient of coil spring,
11 kt1 = 60063; % [N/m] - constant coefficient of tire stiffness,
12 kt2 = 42509; % [N/m^2] - constant coefficient of tire stiffness,
13 kt3 = 22875; % [N/m^3] - constant coefficient of tire stiffness,
14 ms = 295; % [kg] - approximately 1/4 of vehicle mass (sprung mass), and
15 mu = 39; % [kg] - one wheel assembly (unsprung mass).
16
17 switch flag
18
19 case 0
20     dx = [4, 0, 4, 1, 0, 2, 1];
21     x0 = [0, 0, 0, 0]; % initial condition
22     str = [];
23     ts = [0 0];
24 case 1
25
26 % Differential equation substitution through state space:
27
28 dx(1) = x(3);
29 dx(2) = x(4);
30 dx(3) = -(ks1/ms)*(x(1)-x(2))-(ks2/ms)*(x(1)-x(2))^3-(csh1/ms)*(x(3)-x(4)) ...
31     -(csh2/ms)*((x(3)-x(4))^2)*sign(x(3)-x(4));
32 dx(4) = (ks1/mu)*(x(1)-x(2))+(ks2/mu)*(x(1)-x(2))^3+(csh1/mu)*(x(3)-x(4)) ...
33     +(csh2/mu)*((x(3)-x(4))^2)*sign(x(3)-x(4))-(kt1/mu)*(x(2)-u) ...
34     -(kt2/mu)*(x(2)-u)^2+(kt3/mu)*(x(2)-u)^3;
35 case 2

```
- Status Bar:** int, Ln 35, Col 11, OVR

Figure B.1: Parts of the MATLAB codes for solving differential equations of motion for passive non-linear suspension system



The screenshot shows a MATLAB editor window with the following code:

```

1 function [dx, x0, str, ts] = int(t, x, u, flag)
2 % Sub-program for solving state space equations for semi-active non-linear
3 % suspension system. This program is done by Ms.sc. Shpetim Lajqi.
4
5 % Parameters for simulation of the semi-active suspesnion system.
6 csh1 = 3482; % [Ns/m] - Linear shock absorber damping coefficient,
7 csh2 = 580; % [Ns^2/m^2]- Non-linear shock absorber damping coefficient,
8 ks1 = 15302; % [N/m] - Linear spring stiffness coefficient,
9 ks2 = 2728; % [N/m^3]- Non-linear spring stiffness coefficient,
10 kt1 = 60063; % [N/m] - Linear tire stiffness coefficient,
11 kt2 = 42509; % [N/m^2]- Non-linear tire stiffness coefficient,
12 kt3 = 22875; % [N/m^3]- Non-linear tire stiffness coefficient,
13 bs = 841; % [Ns/m] - Damping coefficient of the active damper,
14 bu = 2512; % [Ns/m] - Damping coefficient of the active damper,
15 ms = 295; % [kg] - 1/4 of the total vehicle mass (sprung mass), and
16 mu = 39; % [kg] - One wheel assembly mass (un-sprung mass).
17
18 switch flag
19 case 0
20 dx = [4, 0, 4, 1, 0, 2, 1];
21 x0 = [0, 0, 0, 0]; % initial condition
22 str = [];
23 ts = [0 0];
24 case 1
25 dx(1) = x(3);
26 dx(2) = x(4);
27 if (-bs*x(3)+bu*x(4))*(csh1*(x(3)-x(4))+csh2*((x(3)-x(4))^2)*sign(x(3)...
28 -x(4)))<= 0
29 dx(3) = -(ks1/ms)*(x(1)-x(2))-(ks2/ms)*(x(1)-x(2))^3+(bs/ms)*x(3) ...
30 -(bu/ms)*x(4);
31 dx(4) = (ks1/mu)*(x(1)-x(2))+(ks2/mu)*(x(1)-x(2))^3 ... % Active
32 -(kt1/mu)*(x(2)-u)-(kt2/mu)*(x(2)-u)^2 ...
33 +(kt3/mu)*(x(2)-u)^3-(bs/mu)*x(3)+(bu/mu)*x(4);
34 else
35 dx(3) = -(ks1/ms)*(x(1)-x(2))-(ks2/ms)*(x(1)-x(2))^3-(csh1/ms)*(x(3) ...

```

The code defines a function `int` that takes parameters `t`, `x`, `u`, and `flag`. It sets up initial conditions and parameters for a semi-active suspension system, including linear and nonlinear shock absorber damping, linear and nonlinear spring stiffness, and linear and nonlinear tire stiffness. The code then handles two cases based on the `flag`: case 0 provides initial conditions, while case 1 solves the differential equations of motion using numerical methods involving state-space representation and piecewise linearization.

Figure B.2: Part of MATLAB codes for solving differential equations of motion for non-linear semi-active suspension system

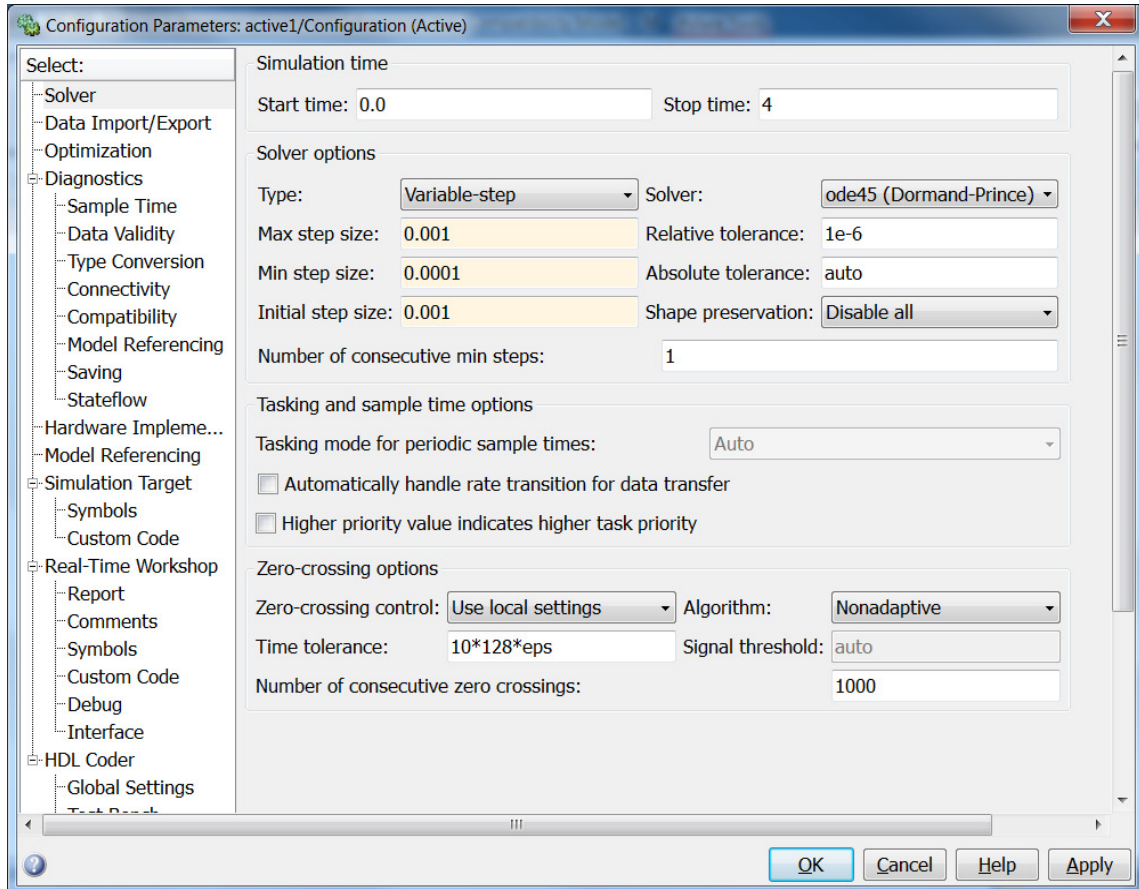


Figure B.3: Configuration MATLAB/Simulink parameters for solving the differential equations of motion

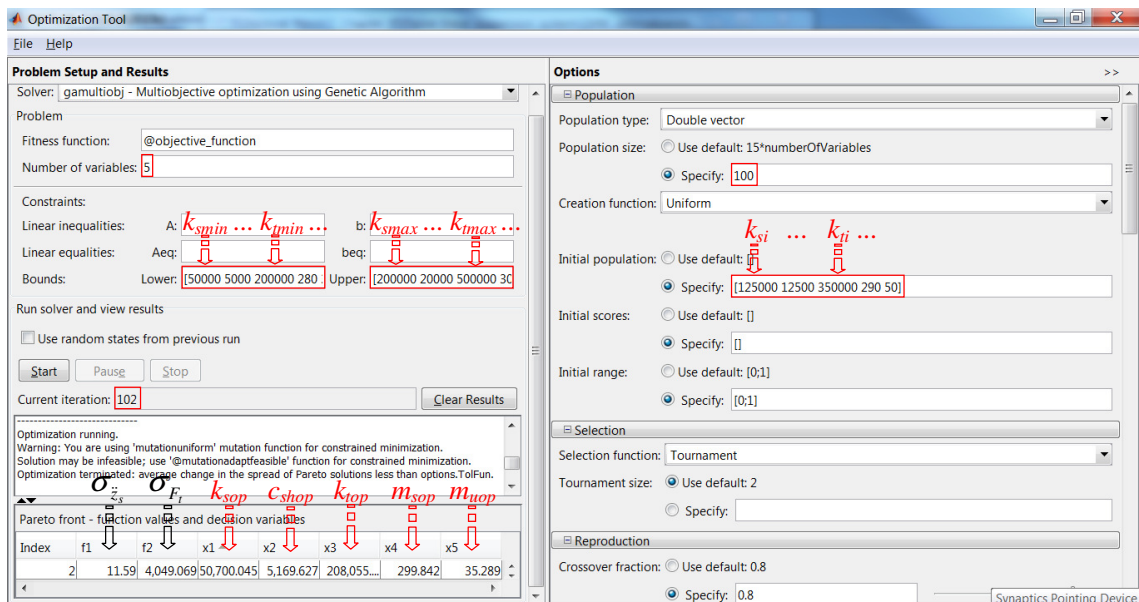


Figure B.4: Window of Multi Objective Genetic Algorithms performed in MATLAB Optimization Tool

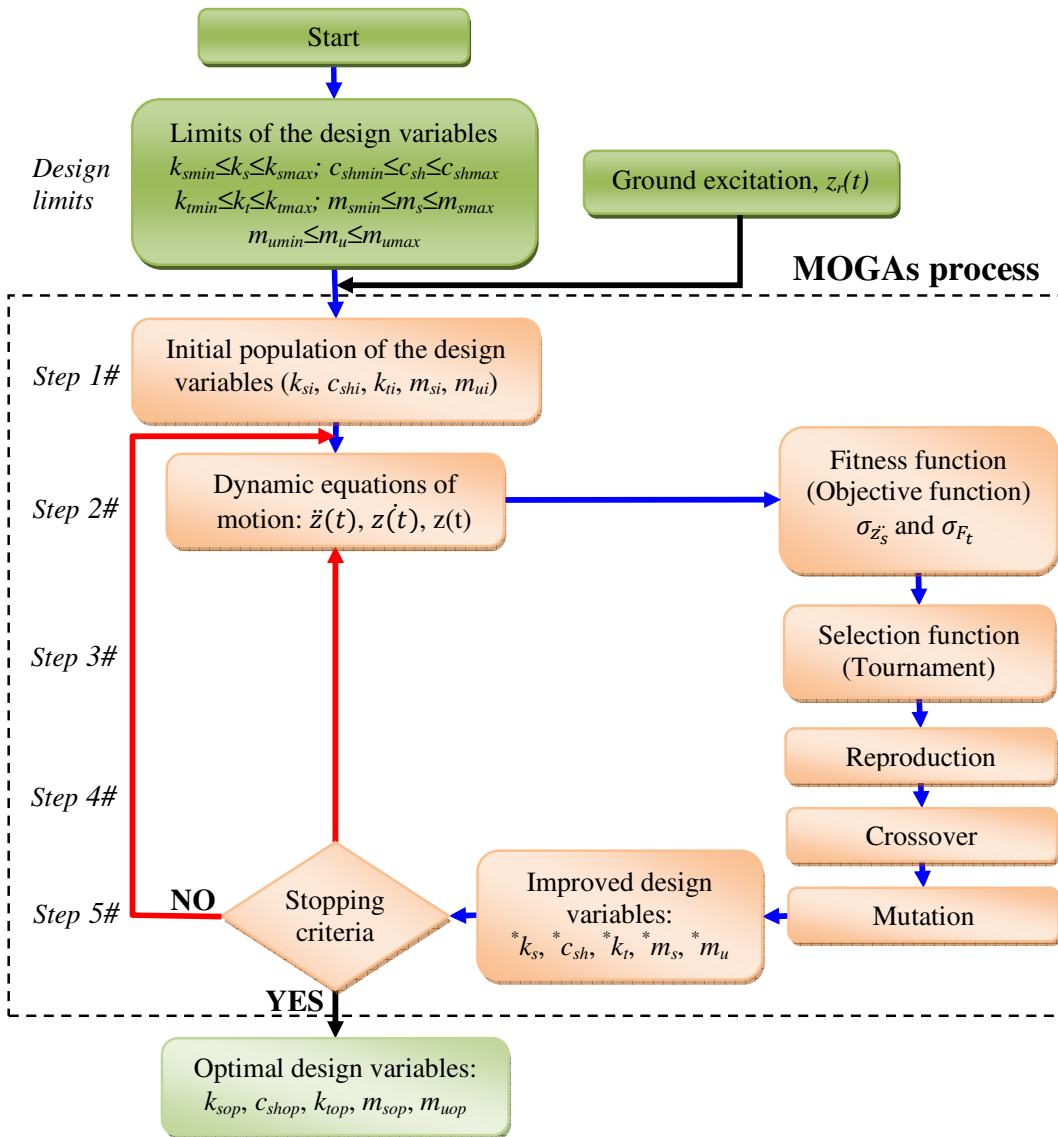


Figure B.5: Flowchart diagram of the optimization process utilized in MOGAs

Appendix C: Design of the Developed Terrain Vehicle

Figures C.1 introduces design of the terrain vehicle in 2D/3D with some main geometric dimension performed in Pro/ENGINEER environment.

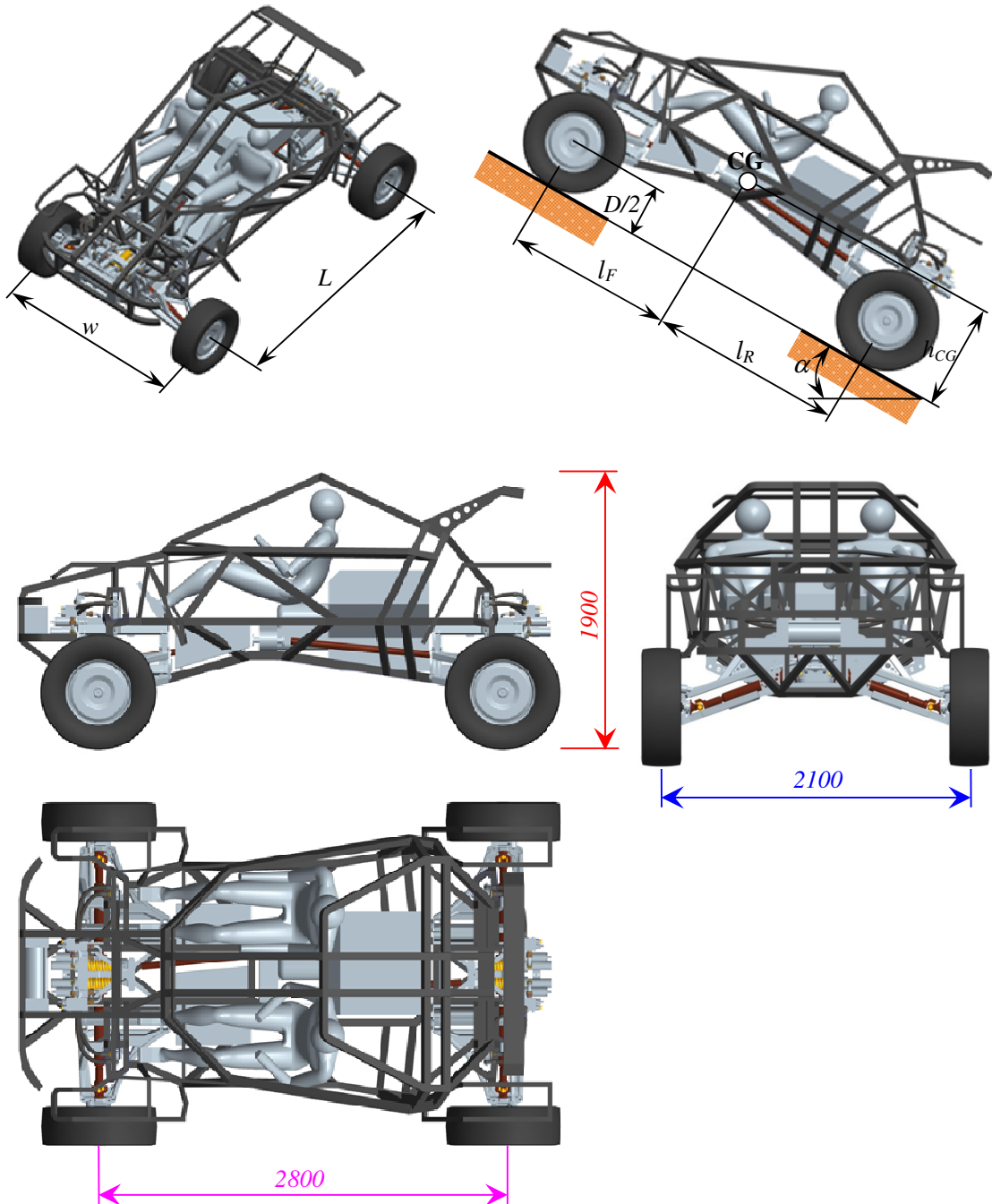


Figure C.1: 2D/3D modeling of the terrain vehicle with four wheels drive and four wheels steering performed in Pro/ENGINEER environment [6]

Figures C.2 and Figure C.3 3D present design of the front and rear mechanism and tires for terrain vehicle, performed in Pro/ENGINEER environment.

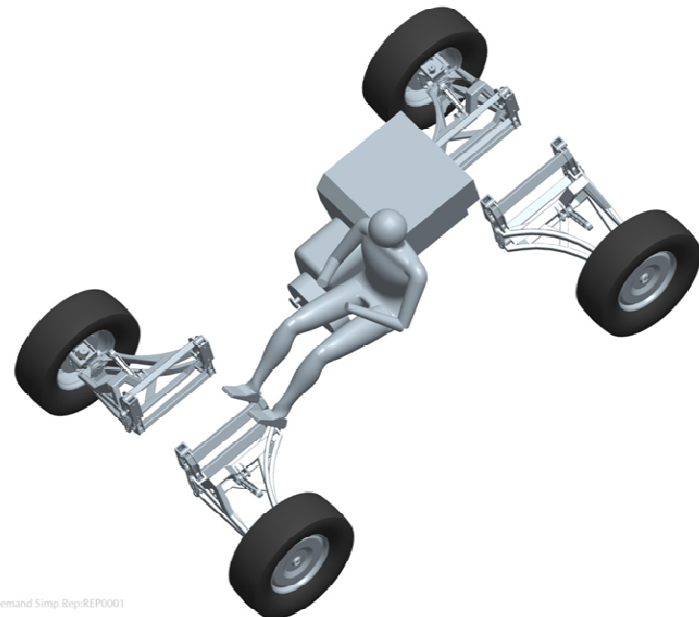


Figure C.2: 3D modeling of a front and rear suspension mechanism, engine and driver performed in Pro/ENGINEER environment [6]

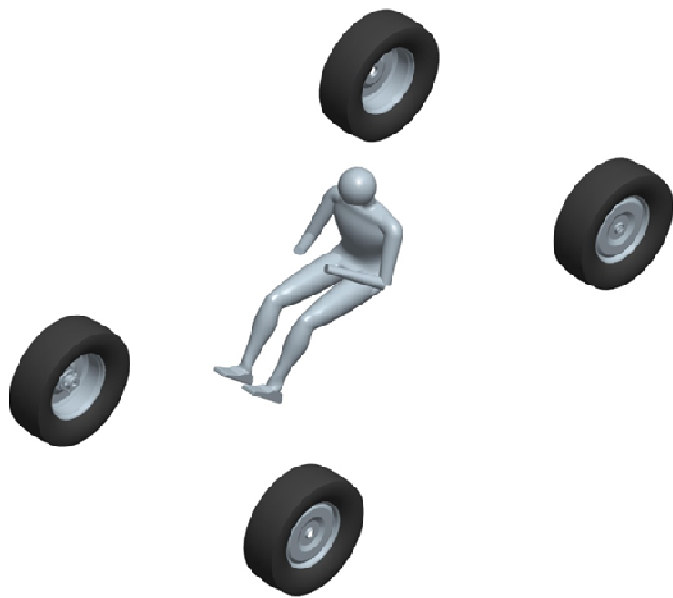


Figure C.3: 3D modeling of a front and rear wheels and driver performed in Pro/ENGINEER environment [6]

Appendix D: Bibliography of the Candidate

Personal bibliography for the period 2003 - 2013

ARTICLES AND OTHER COMPONENT PARTS

1.01 Original scientific article

- [1] Lajqi Shpetim, Pehan Stanislav, Lajqi Naser, Gjelaj Afrim, Pšeničnik Jože, Sašo Emin. Design of Independent Suspension Mechanism for a Terrain Vehicle with Four Wheels Drive and Four Wheels Steering. *Annals of Faculty Engineering Hunedoara – International Journal of Engineering* (2013), Fascicule1, Tome XI 2013, pp. 101-108. <http://annals.fih.upt.ro/pdf-full/2013/ANNALS-2013-1-12.pdf>.
- [2] Lajqi Shpetim, Gugler Jürgen, Lajqi Naser, Shala Ahmet, Likaj Ramë: Possibilities Experimental Method to Determine the Suspension Parameters in a Simplified Model of a Passenger Car. *International Journal of Automotive Technology* (2012), vol. 13, no. 4, pp. 615-621. <http://link.springer.com/article/10.1007%2Fs12239-012-0059-7>.
- [3] Lajqi Shpetim, Stanislav Pehan. Designs and Optimizations of Active and Semi-Active Non-linear Suspension System for a Terrain Vehicle. *Strojniški vestnik - Journal of Mechanical Engineering* (2012), vol. 58, no.12, pp. 732-743. DOI:10.5545/sv-jme.2012.776. <http://www.sv-jme.eu/archive/sv-jme-volume-2012/sv-jme-58-12-2012>.
- [4] Lajqi Shpetim, Pehan Stanislav, Lajqi Naser, Baxhaku Bashkim, Ymeri Besim. Influences of the Suspension Parameters on the Vehicle Suspension Performance for a Terrain Vehicle. *Journal of Mechanics Engineering and Automation* (2012), New York, vol. 2, no. 9, pp. 550-554. <http://www.davidpublishing.com/show.html?8218>.
- [5] Baxhaku Bashkim, Tytyri Hajredin, Lajqi Shpetim (2012): One of Scenarios for Reduction the Emission of Pollutant for Motor Vehicle in the Territory of the Republic of Kosovo, *Journal of Mechanics Engineering and Automation* (2012), New York, vol. 2, no. 5, pp. 321-326. <http://www.davidpublishing.com/show.html?7084>.
- [6] Mehmeti Xhemajl, Lajqi Naser, Baxhaku Bashkim, Lajqi Shpetim, Tytyri Hajredin. Preventive Maintenance of Passengers Cars Driving in the Territory of the Republic of

- Kosovo. *Journal of Mechanics Engineering and Automation* (2012), New York, vol. 2, no. 3, pp. 197-202. <http://www.davidpublishing.com/show.html?5582>.
- [7] Lajqi Naser, Lajqi Shpetim, Vataj Gjelosh, Avdiu Arben. The influence of Cavitations Phenomenon and Water Hammer in Pumping Station of Mitrovica. *Journal of Institute Alb-Shkenca – AKTET*, ISSN 2073-2244 (2011), vol. 4, no. 2, pp. 359-365. <http://alpa.mali-it.eu/journal/aktet//vol/?l=en>.
- [8] Lajqi Shpetim, Baxhaku Bashkim, Lajqi Naser. Influence of Planetary Gear in Improving Efficiency of Continuous Variable Transmission in Passenger Vehicle. *Journal of Institute Alb-Shkenca - AKTET*, ISSN 2073-2244 (2011), Tirana, vol. 4, no. 2, pp. 219-226. <http://alpa.mali-it.eu/journal/aktet//vol/?l=en>.

1.04 Professional article

- [9] Mehmeti Xhemail, Lajqi Naser, Lajqi Shpetim. Developing of the Model of the Functioning Vehicle Maintenance Which is Driven in Territory of the Republic of Kosova. *Annual Conference of Science - Science Week* (2012), Prishtina, Kosova.
- [10] Lajqi Shpetim, Elezaj Shaqir, Lajqi Naser. Possibility of Installing Micro Hydro – Generator in Territories with Hydraulic Potential of Water. *5th Conference of Albanian Association of Thermotechnics* (2010), Prishtina, Kosova.
- [11] Baxhaku Bashkim, Lajqi Naser, Lajqi Shpetim. Definitions of the Reaction in Main Support Bearing for Motor Perkins P-4 Massey-Ferguson. *Symposium of Mechanical Engineering* (2004), Prishtina, Kosova.
- [12] Fejzullahu Xhemajl, Lajqi Shpetim, Zhitia Ilir, Vataj Gjelosh. Analyzing of the Cavitations Phenomena in Main Pumping Station in Batllava. *Professional and Scientific Magazine* (2003), Ferizaj, Kosova.

1.08 Published scientific conference contribution

- [13] Lajqi Shpetim, Pehan Stanislav, Lajqi Naser, Gjelaj Afrim, Pšeničnik Jože, Emin Saso. Design of Independent Suspension Mechanism for Terrain Vehicle with Four Wheels Drive and Four Wheel Steering. *The 4th International Scientific Conference, Management of Technology Step to Sustainable Production* (2012), Zader, Croatia *MOTSP 2012 Conference proceeding*, pp. 230-237.

- [14] Lajqi Shpetim, Pehan Stanislav, Pšeničnik Jože, Lajqi Naser. Tracking the Prescribed Path Through an Autonomous Mobile Robot with Four Wheel Steering. *The 3rd International Scientific Conference, Management of Technology Step to Sustainable Production* (2011), *Bol, Croatia, MOTSP 2011 Conference proceedings*, pp. 94-101.
- [15] Pehan Stanislav, Lajqi Shpetim, Pšeničnik Jože, Flašker Jože. Modeling and Simulation of off Road Vehicle with Four Wheel Steering. *The 7th International Scientific Conference, Research and Development of Mechanical Elements and Systems* (2011), IRMES 2011, Conference Proceedings, pp. 77-83.
- [16] Baxhaku Bashkim, Lajqi Naser, Lajqi Shpetim, Tytyri Hajredin. Possibility of Reduction Emissions of Pollutants in Urban Areas. *1st International Scientific Conference on Engineering Manufacturing and Advanced Technologies* (2010), *Mostar, Bosnia and Herzegovina, MAT 2010 Conference proceedings*.
- [17] Baxhaku Bashkim, Lajqi Naser, Cakolli Heset, Lajqi Shpetim. Influence of motor vehicle in pollutant emission in urban environments. *14th International Research/Expert Conference, Trends in the Development of Machinery and Associated Technology* (2010), *Mediterranean Cruise, TMT 2010 Conference proceedings*, pp. 301 – 304. <http://www.tmt.unze.ba/proceedings2010.php>.
- [18] Baxhaku Bashkim, Lajqi Naser, Lajqi Shpetim. Ecology and road transport in Republic of Kosova. *14th International Research/Expert Conference, Trends in the Development of Machinery and Associated Technology* (2010), *Mediterranean Cruise, TMT 2010 Conference proceedings*, pp. 313 – 316. <http://www.tmt.unze.ba/proceedings2010.php>.
- [19] Lajqi Shpetim, Baxhaku Bashkim, Lajqi Naser. Influence of planetary gear in improving efficiency of continuous variable transmission in passenger vehicle. *International Annual Meeting of Alb-Science Institute* (2010), *Tirana, Albania*, pp. 462.
- [20] Lajqi Naser, Lajqi Shpetim, Vataj Gjelosh, Avdiu Arben. Influence of N.P.S.H. and water hammer in pumping station in Mitrovica. *International Annual Meeting of Alb-Science Institute* (2010), *Tirana, Albania*, pp. 463.
- [21] Lajqi Shpetim, Jürgen Gugler, Lajqi Naser, Shala Ahmet, Lika Ramë. Experimental Possibilities for Determination of Suspension Parameters by the Simplified Model of Passenger Car. *2nd International Scientific Conference, Management of Technology Step to Sustainable Production* (2010), *Rovinj, Croatia. MOTSP 2010 Conference proceedings*.
- [22] Lajqi Naser, Baxhaku Bashkim, Lajqi Shpetim. Effect of intercooler on turbocharged diesel engine performance. *13th International Research/Expert Conference Trends in the*

- Development of Machinery and Associated Technologies* (2009), Hammamet, Tunisia.
TMT 2009 Conference proceedings, pp. 437 – 440.
<http://www.tmt.unze.ba/proceedings2009.php>.
- [23] Lajqi Shpetim, Ibrahimi Nijazi, Baxhaku Bashkim, Lajqi Naser. Analyses of Powertrain System in a Passenger Vehicle with Using Planetary Gear Combine with Continuously Variable Transmission. *13th International Research/Expert Conference Trends in the Development of Machinery and Associated Technologies, 16-21 October 2009, Hammamet, Tunisia. TMT 2009 Conference proceedings*, pp. 641 – 644.
<http://www.tmt.unze.ba/proceedings2009.php>.
- [24] Lajqi Shpetim, Ibrahimi Nijazi, Baxhaku Bashkim, Lajqi Naser. Modelling of Continuous Variable Power Split Transmission in Hybrid Electric Vehicle. *6th Research/Expert Conference with International Participations* (2009), Neum, Bosnia and Herzegovina. *QUALITY 2009 Conference proceedings*, pp. 443 – 448.
<http://www.quality.unze.ba/zbornici/QUALITY%202009/index.php>.
- [25] Lajqi Naser, Baxhaku Bashkim, Lajqi Shpetim. Model of Coupling Turbocharger and Diesel Engine. *12th International Research/Expert Conference Trends in the Development of Machinery and Associated Technologies* (2008), Istanbul, Turkey. *TMT 2008 Conference proceedings*, pp. 685 – 688.
- [26] Lajqi Naser, Baxhaku Bashkim, Lajqi Shpetim. Model of Calculation of Characteristic Parameters for Marine Motors. *11th International Research/Expert Conference Trends in the Development of Machinery and Associated Technology* (2007), Hammamet, Tunisia. *TMT 2007 Conference proceedings*, pp. 1187 – 1190.

MONOGRAPHS AND OTHER COMPLETED WORKS

2.05 Other educational material

- [27] Lajqi Shpetim, Ramadani Riad. *Technical drawing with Descriptive Geometry*. Material for exercise, Faculty of Mechanical Engineering, 2010, Prishtina, Kosova.
- [28] Lajqi Shpetim. *Power transmitter*. Material for exercise, Faculty of Mechanical Engineering, 2010, Prishtina, Kosova.

2.09 Master's thesis

- [29] Lajqi Shpetim. *Planetary Transmissions Combined with Continuously Variable Transmission in Hybrid Electric Vehicle*. University of Prishtina, Faculty of Mechanical Engineering (2008), *Master Thesis*, Prishtina, Kosova, pp. 149.

2.11 Diploma thesis

- [30] Lajqi Shpetim. *Determining of the reactions and dimensioning of the crank shaft for Perkins Engine P-4 Massey-Ferguson*, University of Prishtina, Faculty of Mechanical Engineering (2002), *Diploma Thesis*, Prishtina, Kosova, pp. 150.

2.14 Project documentation (feasibility study, preliminary design, detail design)

- [31] Lajqi Shpetim, Vataj Gjelosh. Detail design of extension of water treatment plant in Mitrovica for water company "**MITROVICA sh.p.k.**", K.K. Mitrovicë, 2010.
- [32] Lajqi Shpetim, Vataj Gjelosh. Geomechanical & hydraulic study for alternate routing of slag granulation return channel, for enterprise "**NewCo FeroNickel L.L.C.**" sh.p.k., K.K. Drenas, 2010.
- [33] Bajraktari Musli, Lajqi Naser, Lajqi Shpetim, Vataj Gjelosh. Elaborate for periodically inspection and attesting of crane and elevators for enterprise "**NewCo FeroNickel L.L.C.**" sh.p.k., K.K. Drenas, 2006-2010.
- [34] Bajraktari Musli, Lajqi Naser, Lajqi Shpetim, Vataj Gjelosh. Detail design of technical – technologic project for dryer system for mineral production from Benard Company in Italy. Financing from enterprise "**NewCo FeroNickel L.L.C.**" sh.p.k., K.K. Drenas, 2010.
- [35] Bajraktari Musli, Lajqi Naser, Lajqi Shpetim, Vataj Gjelosh. Detail design of technical – technologic project for rock crusher & mobile separation of sand for private enterprise "**Alko-Impex-General Construction**" sh.p.k. in Vill. Dabishevc, K.K. Prishtinë, 2009.
- [36] Bajraktari Musli, Lajqi Naser, Lajqi Shpetim, Vataj Gjelosh. Detail design of technical – technologic project for mobile crusher for private enterprise "**I. SEFERI**", Suharekë, 2006.

-
- [37] Bajraktari Musli, Lajqi Naser, Lajqi Shpetim, Vataj Gjelosh. Detail design of technical – technologic project for base separation of sand for private enterprise "**BENITA COMPANY**", Klinë, 2005.
 - [38] Bajraktari Musli, Lajqi Naser, Lajqi Shpetim, Vataj Gjelosh. Detail design of technical – technologic project for concrete base for private enterprise "**BENITA COMPANY**", Klinë, 2005.
 - [39] Bajraktari Musli, Lajqi Naser, Lajqi Shpetim, Vataj Gjelosh. Detail design of technical – technologic project for concrete base for private enterprise "**GRANITI**" Istog, 2005.
 - [40] Bajraktari Musli, Lajqi Naser, Lajqi Shpetim, Vataj Gjelosh. Detail design of technical – technologic project for asphalt base for private enterprise "**GRANITI**" Istog, 2005.
 -
 - [51] Bajraktari Musli, Lajqi Naser, Lajqi Shpetim, Vataj Gjelosh. Detail design of technical – technologic project for asphalt base for private enterprise "**DRINI COMPANY**", Malishevë, 2005.

Appendix E: Curriculum Vitae

Name and surname: Shpetim LAJQI
Date and place of birth: 11.04.1977, Prapaqan
Permanent address: Rr. Rexhep Krasniqi p.n.
Lagja e Emshirit, Kulla 5, kati 3/3
10000 Prishtinë, Republika e Kosovës
Nationality: Kosovar
E-mail address: shpetim.lajqi@uni-pr.edu
Mobile phone: + 377 44 259 771
Driving licence: B1, B, C1, C, BE, C1E, CE, M, L, T

Education:

Postgraduates study:

Doctoral study: University of Maribor, Faculty of Mechanical Engineering, Maribor
Program/Institute: Mechanical Engineering/Institute for Structure and Machine Design
Date (from – to): 2010/11 – onward
Academic degree: Doctor of Science
Master study: University of Prishtina, Faculty of Mechanical Engineering, Prishtina
Program/Department: Mechanical Engineering/Department for Construction and Design
Title of thesis: Planetary Transmissions Combined with Continuously Variable
Transmission in Hybrid Electric Vehicles
Date (from – to): 2003/04 – 2007/08
Academic degree: Magister of Technical Science
Average score: 9.77

Graduate study: University of Prishtina, Faculty of Mechanical Engineering, Prishtina
Program/Department: Mechanical Engineering/Depart. Mech. Construction and Mechanism
Title of thesis: Determination of the Reactions and Dimensioning of the Crank Shaft
for Perkins Engine P-4 Massey - Ferguson
Date (from – to): 1995/96 – 2001/02
Academic degree: Graduate Mechanical Engineer
Average score: 9.20

Secondary school: Gymnasium “QAMO Vëllezërit Frashëri”, Deçan, Kosova

Date (from – to): 1991/92 – 1994/95

Degree: Diploma

Primary school: Primary school “Jusuf Gërvalla”, Prapaqan, Deçan, Kosova

Date (from – to): 1983/84 – 1990/91

Awards and Scholarships:

Awards: Diploma as the best student, issued from University of Prishtina
Diploma as the best student, issued from Faculty of Mechanical
Engineering, University of Prishtina,

Scholarship: Slovene human resource development and scholarship funds, Slovenia
JoinEU SEE, Austria
Austrian Exchange Service, Austria
University of Prishtina, Kosova
Municipality of Deçan, Kosova

Employment:

Institution: University of Prishtina, Faculty of Mechanical Engineering

Academic title: Assistant

Date (from – to): 2011– onward

Institution: University of Prishtina, Faculty of Mechanical Engineering

Academic title: New Assistant

Date (from – to): 2007– 2011

Institution: University of Prishtina, Faculty of Mechanical Engineering

Academic title: Teaching Assistant (collaborator)

Date (from – to): 2003 – 2007

Company: Regional Water Company “PRISHTINA”

Positions: Assistant Director, Maintenance Manager, Engineer, etc.

Date (from – to): 2002 – 2007

Training and some other activities:

Date (from – to)	Description of training and other activities
06 – 28 November 2007	Research in Austrian Universities, Graz University of Technology/Faculty of Mechanical Engineering, Vehicle Safety Institute, Graz, Austria,
15.10.07 – 02.11.07	Business Skills Training organized by the Business Start – Up Centre Kosovo, Prishtina, Kosova,
03.12.07 – 14.12.07	
16 – 20 May 2004	Regional Seminar from South - East Europe for preparation projects, Ohrid, Macedonia,
09 – 10 Mars 2004	Program for trainings of management,
17 December 2003	Investment plan and Business Plan,
19 – 26 May 2003	Study visit in “ <i>Helsinki Water Company</i> ” and “ <i>Tallinn Water Company</i> ”, Finland and Estonia.
24 – 25 April 2003	Study visit in “ <i>Water Company Essen</i> ”, Essen, Germany

UNIVERSITY OF MARIBOR
FACULTY OF MECHANICAL ENGINEERING

DECLARATION OF THE DOCTORAL CANDIDATE

The undersigned: **Shpetim LAJQI**, M. Sc., B. Sc. Mech. Eng. with enrolling nr. **95031843**

declare that,

the doctoral thesis entitled "**Suspension and Steering System Development of a Four Wheel Drive and Four Wheel Steered Terrain Vehicle**"

- present our results of the research works,
- submitted thesis in whole or part has not been submitted into any kind of academic programs in other faculties or universities,
- presented results are correctly specified, and
- I didn't breach copyright and other intellectual property.

Maribor, 04.03.2013

Signature: _____

